Expansion of Reductive Cross-Couplings: Reductive Arylation of Nitroarenes and Improved Methods for Nickel-Catalyzed Cross-Electrophile Coupling

by

Brett Daniel Akana-Schneider

A dissertation submitted in partial fulfillment of the

requirements for the degree of

Doctor of Philosophy

(Chemistry)

at the

UNIVERSITY OF WISCONSIN-MADISON

2024

Date of final oral examination: 7/31/2023

The dissertation is approved by the following members of the Final Oral Committee:

Daniel J. Weix, Professor, Organic Chemistry
Samuel H. Gellman, Professor, Chemical Biology
Jennifer M. Schomaker, Professor, Organic Chemistry
Shannon S. Stahl, Professor, Organic Chemistry

Dedication

To everyone who has supported and encouraged me along this journey. I never would have begun this journey without you, let alone finished it.

Table of Contents

Biographical Sketch

Brett D. Akana-Schneider was born in 1995 and raised in San Antonio, Texas, where he later graduated from East Central High School in 2013. He enrolled at St. Mary's University. There, he received a Bachelor of Science in Chemistry and a Bachelor of Arts in Mathematics in 2017, graduating summa cum laude with honors. In his sophomore year, Brett began researching under the supervision of Professor Jeff R. Schoonover, investigating mixed-metal oxide catalysts. After becoming a MARC U*STAR fellow, Brett gained experience in natural product isolation during a summer working with Professor John B. MacMillan at the University of Texas Southwestern Medical Center and built synthetic skills with Dr. William Bauta at Southwest Research Institute. During his final year of undergraduate schooling, Brett pursued organic methodology in the lab of Professor Oleg V. Larionov at The University of Texas at San Antonio, discovering his appreciation of methodology and the benefits of enabling more efficient synthetic sequences.

Following graduation in 2017, Brett began his graduate studies at the University of Wisconsin-Madison. He joined the laboratory of Professor Daniel J. Weix and was the recipient of the Pei Wang Fellowship (2017) and the ACS Division of Organic Chemistry Travel Award (2022). Brett received his Master of Science degree in 2022. During his graduate career, Brett was a member and co-chair of the Department of Chemistry Climate Survey Team, which worked to gauge and improve the experience of graduate and postdoctoral researchers in the Department of Chemistry.

The following publications were a result of work conducted during his doctoral study:

1. Akana-Schneider, B. D.; Weix, D. J. "Reductive Arylation of Nitroarenes with Chloroarenes: Reducing Conditions Enable New Reactivity from Palladium Catalysts" *J. Am. Chem. Soc.* **2023**. DOI: 10.1021/jacs.3c04647.
2. Akana, M. E.; Tcyrulnikov, S.; Akana-Schneider, B. D.; Reyes, G. P.; Monfette, S.; Sigman, M. S.; Hansen, E. C.; Weix, D. J. "Computational Methods Enable the Prediction of Improved Catalysts for Nickel-Catalyzed Cross-Electrophile Coupling" *J. Am. Chem. Soc*. **2023**. DOI: 10.1021/jacs.3c09554.

Acknowledgements

This achievement belongs not only to me, but to all of the people who have supported, educated, and encouraged me. I know that without you, this would not have been possible. For this I am truly grateful.

First, I want to thank my parents, Darryl and Sheri Schneider. Throughout my entire life, you have encouraged my curiosity and instilled in me the value of education. Additionally, I am forever grateful for the loving and supportive environment in which I was raised. The safety and opportunity to pursue your passion, even science, is incredibly valuable and unfortunately rare. At no point have I felt that this was not an option for me. I could not be the person I am today without the compassion, love, and support that you provide. Thank you to my brothers, Colton and Ethan Schneider, and Johnathan Hart. During this time of significant growth and change, you reminded me that I am loved, that there is a life outside of the lab, and that joy and fulfillment can be found in every moment and place. I am also grateful to my mother-in-law Marinella Akana. You have accepted me into your family and have been incredibly supportive and encouraging during this time in my life.

Thank you to everyone who encouraged me to pursue research and a graduate education. In particular, I would like to thank Professor Dmitriy Khon, who taught me organic chemistry. You pushed me—sometimes with an appropriately firm hand—to achieve excellence in my coursework, to seize opportunities when they present themselves, and to see the world beyond my current view. Without your expectations and encouragement, I would have never found my passion for research.

Thank you to my mentor, Professor Daniel J. Weix. Dan, you have guided me as I have grown into my role as a scientist. Beyond helping guide my research projects, you have taught me how to carefully design experiments, thoughtfully communicate my hypotheses and results, effectively navigate our highly collaborative field, and identify problems that actually need solving. You have also been a tenacious advocate for my science, character, and career. Your understanding and support throughout this process reminds me that science deals in facts, but is done by people. I'm glad that I got to work with one of the best ones. Additionally, I want to thank the other faculty and staff at UW-Madison who have impacted my education as a scientist. Thank you to Professor Tehshik P. Yoon for teaching me to find and appreciate the elegance of science, and for inspiring me to do better during a critical time in my graduate career. Thank you to Professor Zachary K. Wickens for teaching me to ask thoughtful questions when considering reaction mechanisms and that the only mechanism that matters is the operable one, not the one you want to find. I am also grateful for the guidance of my committee members, Professors Samuel H. Gellman and Shannon S. Stahl; in particular, thank you for teaching me to navigate the spectrum of experiments we run, experiments we discuss, and results that we publish.

Thank you to all my co-workers in the Weix group, past and present. You have all made this an incredible place to work for six years. No matter what was going on at the time, the unique culture and energy of the group made coming in to work an exciting part of my day. Beyond the outstanding scientific discussions we have had, I appreciate the times away from work, including game nights at Dr. Keywan Johnson, Dr. Kevin Garcia, and Daniel Enny's house, days at the lake with Dr. Michael Gilbert and Samantha

Gavin, porch time with Dr. Nathan Loud, or dinners together. I hope that going forward, I can take a small portion of your humor, compassion, and fun spirit with me.

I am eternally grateful to the friends that I have made during my time in graduate school; you have made this entire process possible. Your persistent kindness has helped me continue, even in the worst of times. I regret that our time together was interrupted so harshly by the pandemic, but it has made me even more appreciative of the times we have spent together, the effort needed to maintain a friendship, and the impact small moments together can have. In particular, the short walks and talks to get a coffee were deeply impactful during the most stressful times in my life. Thank you all.

Finally, I want to thank my partner, Michelle Akana. Michelle, your impact on me as my lab partner, co-worker, best friend, and constant companion has been immeasurable. The times spent with you in our garden, foraging in local parks, walking through museums, or just spending time together at home are some of the brightest memories that I carry with me. You inspire me to be a better scientist, a more thoughtful communicator, a more compassionate friend, and an overall better person. I am thankful every day that we have taken the steps that we have together, and I look forward to the next chapter of our life together.

Abstract

This dissertation will discuss the expansion of cross-electophile coupling reactions to allow for the formation of C–N bonds and the improvement of existing $C(sp^2)$–$C(sp^3)$ bond-forming reactions by the development of improved catalysts.

Chapter 1 will introduce the concepts of cross-electrophile coupling, compare and contrast them with redox-neutral cross-couplings, and identify key areas for improvement.

Chapter 2 describes the development of the reductive arylation of nitroarenes with aryl halides and the investigation into the mechanism of this transformation.

Chapter 3 translates computational and statistical methods to nickel-catalyzed cross-electophile coupling, allowing for the devleopment of improved 2,2′-bipyridine ligands, and describes their application to a variety of cross-electrophile coupling reactions.

Chapter 4 discusses the identification and initial survey of reactivity of 2,2′-bipyridine-6-carbonitrile ligands, and describes their similar yet distinct reactivity relative to their non-cyanated bpy analogues.

Contributors and Funding Sources

The author's thesis committee included Professors Daniel J. Weix, Samuel H. Gellman, Jennifer M. Schomaker, and Shannon S. Stahl from the University of Wisconsin-Madison Department of Chemistry. The author is responsible for all experimental procedures in this thesis unless specified below:

Chapter 2: This work was supported by the NIH (R01GM097243). Analytical data were obtained from the CENTC Elemental Analysis Facility at the University of Rochester, funded by NSF CHE-0650456. Dr. Jiang Wang assisted with initial experiments. Dr. Paige E. Piszel assisted with electrochemical measurements. Michelle E. Akana assisted with the preparation of charts and graphs.

Science is highly collaborative. As such—for Chapters 3 and 4—the generation of hypotheses, design of experiments, analysis of results, and discussion of findings was performed with the help of all authors, particularly Michelle E. Akana. The research detailed in these chapters was supported by the National Science Foundation (CHE-1900366) and Pfizer. DFT data was generated using computational resources managed and supported by the University of Wisconsin-Madison Department of Chemistry Phoenix cluster and the National Science Foundation award CHE-0840494.

Chapter 3: The initial high-throughput dataset used for modeling was gathered by Dr. Sergei Tcyrulnikov under the direction of Drs. Sebastien Monfette and Eric C. Hansen. Computations and statistical analyses were performed by Michelle E. Akana, with additional direction from Prof. Daniel J. Weix and Matthew S. Sigman. The production of charts and graphs are the result of a collaborative effort between Michelle E. Akana and the author.

Chapter 4: The initial data from which hypotheses were derived was gathered by Dr. Sergei Tcyrulnikov under the direction of Drs. Sebastien Monfette and Eric C. Hansen. Computations and statistical analyses were performed by Michelle E. Akana, with additional direction from Prof. Daniel J. Weix and Matthew S. Sigman. The production of charts and graphs are the result of a collaborative effort between Michelle E. Akana and the author.

All the work in this thesis was supported by the University of Wisconsin-Madison. In particular, mass spectroscopy and NMR data were obtained in the Paul Bender Chemistry Instrumentation Center. The purchase of the Thermo Scientific Q Exactive Plus in 2015 was funded by the NIH Award 1S10 OD020022-1 to the Department of Chemistry. The purchases of the Bruker Avance III 500 and 400 MHz instruments were funded by a generous gift from Paul J. and Margaret M. Bender in 2012 and NSF CHE-1048642 to the Department of Chemistry in 2010 respectively.

The author was funded by the University of Wisconsin-Madison Department of Chemistry, the donors of the Pei Wang Fellowship, the National Institute of Health (R01GM097243 to Daniel J. Weix), the National Science Foundation (1900366 to Daniel J. Weix), and the American Chemical Society Division of Organic Chemistry Travel Award.

List of Tables

List of Figures

List of Schemes

List of Symbols and Abbreviations

-	minus, negative, or hyphen
–	denotes a chemical bond or en dash
:	ratio
·	radical
%	percent
°	degrees
°C	degrees Celsius
±	racemic
×	times
~	about or approximately
^{13}C	carbon-13
$^{13}C\{^{1}H\}$	proton decoupled ^{13}C-NMR spectroscopy
^{19}F	fluorine-19
^{1}H	hydrogen-1
^{31}P	phosphorus-31
Ac	Acyl
ACS	American Chemical Society

Alk	alkyl
Ar	aryl
ARY	aryl
ASAP-MS	Atmospheric Solids Analysis Probe Mass Spectrometry
$B(OH)_2$	boro+B42nic acid
BINAP	(2,2′-bis(diphenylphosphino)-1,1′-binaphthyl)
bpp	2,6-bis(pyrazol-1-yl)pyridine
bpy	2,2'-bipyridine or derivative thereof
bpyCam	2,2′-bipyridine-6-carboxamidine
bpy^{CN}	2,2'-bipyridine-6-carbonitrile
Br	bromide
BrettPhos	2-(dicyclohexylphosphino)3,6-dimethoxy-2′,4′,6′-triisopropyl-1,1′-biphenyl
C	carbon
$C(sp^2)$	sp^2-hybridized carbon
$C(sp^3)$	sp^3-hybridized carbon
C_6D_6	benzene-d_6
calcd	calculated
CD_2Cl_2	dichloromethane-d_2

$CDCl_3$	chloroform-d
CENTC	Center for Enabling New Technologies Through Catalysis
CF_3	trifluoromethyl
CH_2Cl_2	dichloromethane
C_{ipso}	*ipso* carbon
Cl	chloride
cm	centimeter
CN	nitrile or cyano
CO_2	carbon dioxide
cod	1,5-cyclooctadiene
Cu	copper
CV	column volume(s) or cyclic voltammetry
d	d-orbital
dba	dibenzylideneacetone
DCM	dichloromethane
DFT	denisty functional theory
DI	deionized
DIPEA	*N*,*N*-diisopropylethylamine

DMA	*N*,*N*-dimethylacetamide
dme	dimethoxyethane
DMF	*N*,*N*-dimethylformamide
DMSO	dimethyl sulfoxide
DOI	digital object identifier
dppf	1,1′-ferrocenediyl-bis(diphenylphosphine)
DPV	differential pulse voltammetry
E	energy
$E_{1/2}$	half wave potential
$E_{DP,H}$	differential pulse height
$E_{DP,I}$	differential pulse increment
EDTA	ethylenediaminetetraacetic acid
equiv	equivalent(s)
ESI	electrospray ionization
Et	ethyl
EtOAc	ethyl acetate
EtOH	ethanol
F	fluoride

F1	F1 score
FAQ	frequently asked question(s)
Fc	ferrocene
Fc^+	ferrocenium
FG	functional group
FID	flame ionization detection
g	gram(s)
G3	3rd generation
GC	gas chromatography
GCMS	gas chromatography-mass spectrometry
h	hour(s)
H	hydrogen or proton
HAR	heteroaryl
HFIP	hexafluoroisopropanol
HOMO	highest occupied molecular orbital
HRMS	high-resolution mass spectrometry
HTE	high-throughput experimentation
Hz	hertz

I	iodide
i-Pr	isopropyl
ID	internal diameter
iPrOH	isopropanol
IR	infrared spectroscopy
IUPAC	International Union of Pure and Applied Chemistry
J	coupling constant
K	Kelvin
k_5-fold	five folds of k-fold cross-validation
kcal	kilocalorie(s)
L	ligand
L2	bidentate L-type ligand
L3	tridentate L-type ligand
Li	Lithium
LOO	leave-one-out cross-validation
LUMO	lowest unoccupied molecular orbital
M	molar (mol/L) or metal
m	meter(s)

m/z	mass-to-charge ratio
M^+	mass peak from organic cation in GCMS
MAE	mean absolute error
MARC	Maximizing Access to Research Careers
MCC	Matthews correlation coefficient
Me	methyl
MeCN	acetonitrile
MeOH	methanol
mg	milligram(s)
Mg	magnesium
MHz	megahertz
min	minute(s)
mL	mililiter(s)
mm	millimeter(s)
mmol	millimole
Mn	manganese
mol	mole
N	nitrogen

N	substituted position on nitrogen
NEt_2	diethylamino
NH_2	amine or amino
Ni	nickel
NIH	National Institutes of Health
nm	nanometer(s)
NMe_2	dimethylamino
NMP	*N*-methyl-2-pyrrolidone or 1-methyl-2-pyrrolidone
NMR	nuclear magnetic resonance
NO_2	nitro
NPA	Natural Population Analysis
NSF	National Science Foundation
O	oxygen
OAc	acetate
OEt	ethoxy
OMe	methoxy
P	phosphorus
P	substituted position on phosphorus

p	p-orbital
Pd	palladium
PDA	photo diode array
Ph	phenyl
phth	phthalimide
ppm	part(s) per million
$_{pred}R^2$	predicted R^2
PS	particle size
psi	pounds per square inch
PTFE	polytetrafluoroethylene
PyBCam	pyridine-2,6-bis(carboximidamide)
PyCam	pyridine-2-carboximidamide
Q^2	R^2 for leave-one-out cross-validation
Qda	Quadrupole Dalton mass detector
R	organic substructure or gas constant
R^2	coefficient of determination
rac	racemic
R_f	retention factor

rpm	revolutions per minute
rt	room temperature (~25 °C)
S	sulfur or total spin quantum number
s	s-orbital
SET	single-electron transfer
SFC	supercritical fluid chromatography
SMD	solvation model based on density
S_N2	bimolecular nucleophilic substitution
S_NAr	nucleophilic aromatic substitution
SP	single point
T	temperature
t	*tert* or tertiary
TBS	*tert*-butyldimethylsilyl
*t*Bu	*tert*-butyl
$T_{DP,P}$	differential pulse period
$T_{DP,POST}$	differential post-pulse width
$T_{DP,PRE}$	differential pre-pulse width
$T_{DP,W}$	differential pulse width

TFA	trifluoroacetic acid
TFE	2,2,2-trifluoroethanol
THF	tetrahydrofuran
THP	tetrahydropyran
TIPS	triisopropylsilyl
TLC	thin layer chromatography
TMS	tetramethylsilane
TMSCl	trimethylsilyl chloride
TMSCN	Trimethylsilyl cyanide
TMSI	trimethylsilyl iodide
tpy	terpyridine
U*STAR	Undergraduate Student Training in Academic Research
UPLC	ultra performance liquid chromatography
UV	ultraviolet
UW	The University of Wisconsin
V	volts
vs.	versus
wt%	weight percent

X	halide, pseudohalide, or numerical variable
XC	cross-coupling
XEC	cross-electrophile coupling
XPhos	2-dicyclohexylphosphino-2′,4′,6′-triisopropylbiphenyl
Y	numerical variable
Zn	zinc
β	beta
δ	delta or chemical shift
ΔE	difference in energies
$\Delta\Delta G^{‡}$	difference in transition state energies
η	eta or chemical hardness
μ	μ, micro, or chemical potential
μL	microliter(s)
μm	micrometer(s)
μmol	micromole(s)
σ^{m}	Hammett parameter for *meta* substituents
σ^{p}	Hammett parameter for *para* substituents

Chapter 1: Introduction to Reductive and Cross-Electrophile Couplings

1.1 Cross-Coupling Reactions

Transition metal-catalyzed C–C and C–N cross-coupling (XC) reactions are critical tools in modern synthetic organic chemistry. These reactions enable the construction of diverse structural features that were previously inaccessible or required multi-step synthetic sequences. The impact of these couplings—particularly palladium-catalyzed C(sp^2)–C(sp^2) and C(sp^2)–N bond formations—is seen in the prevalence of individual molecular features in synthetic small molecules. For example, the increased accessibility of biaryl cores via Suzuki cross-coupling has been cited as a driving force in the "flattening" of drug molecules after the reaction's adoption in medicinal chemistry.[1–3] Despite their utility, synthetic sequences employing these reactions are complicated by the low commercial availability, bench-stability, and functional group compatibility of requisite carbon and nitrogen nucleophiles. This dissertation focuses on the expansion of cross-electrophile coupling (XEC) reactions, which offer an alternative method to traditional redox-neutral cross-couplings. The two major goals of this work are: (1) applying the principles of cross-electrophile coupling to enable the formation of C–N bonds from abundant, stable nitroarenes, and (2) improving the selectivity and utility of cross-electrophile coupling reactions to match the best redox-neutral cross-couplings.

Studies of the reactivity of low-valent palladium(0) and arylpalladium(II) complexes have contributed to a robust mechanistic schema that informs the modification, improvement, and translation of cross-coupling strategies to diverse combinations of electrophiles and nucleophiles. Many C–C cross-coupling reactions proceed via a similar mechanism in which: an C(sp^2)–X electrophile—such as a

haloarene—is activated by oxidative addition of (L)Pd^0, transmetalation with an organometallic species (R–[M]) converts the resulting (L)Pd^{II}(Ar)X intermediate into (L)Pd^{II}(Ar)R, and reductive elimination forms the desired C–C bond–regenerating (L)Pd^0.[4] Informed by this knowledge, improved catalysts and reagents have expanded the utility of cross-couplings to allow for the formation of diverse—$C(sp^2)$–$C(sp^2)$, $C(sp^2)$–$C(sp^3)$, $C(sp^2)$–N, $C(sp^2)$–O, etc.—bonds. In particular, two major advances in the field of cross-coupling drove adoption in industrial applications: first, the development of organoboron nucleophiles, which display increased stability and functional group compatibility; and second, the identification of association-deprotonation pathways to allow for the arylation of nitrogen, oxygen, and sulfur nucleophiles.[5–10]

Scheme 1.1 Cross-Coupling Overview

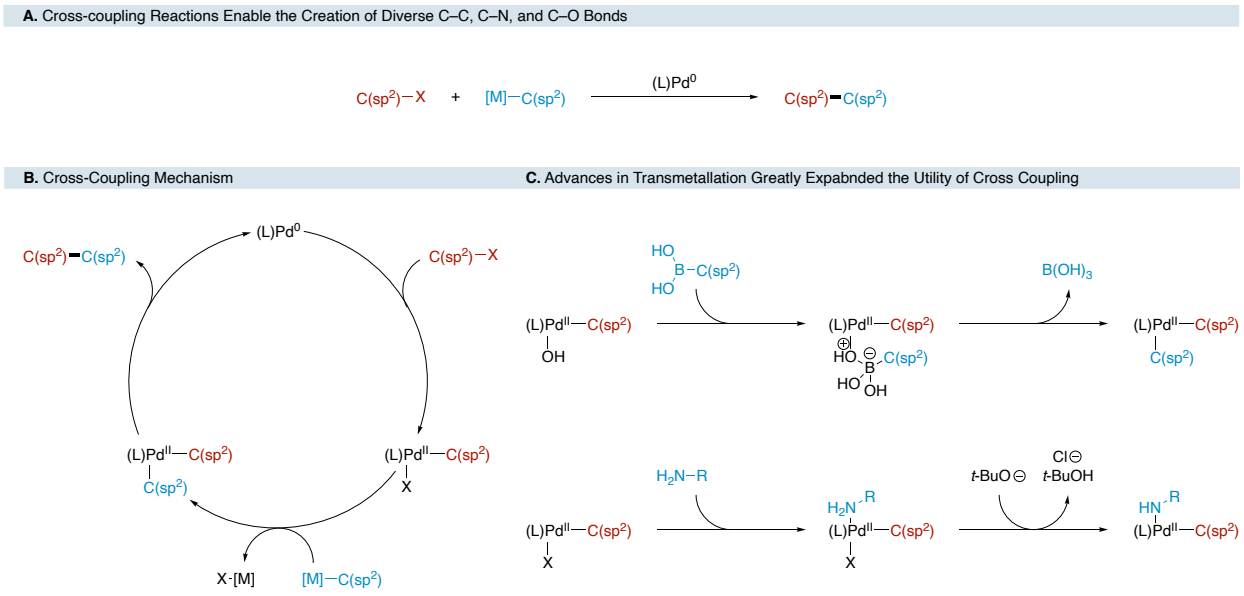

Suzuki-Miyaura cross-coupling—the cross-coupling of an organic electrophile with organoboron nucleophiles—is the most common cross-coupling reaction in medicinal chemistry.[5,11,12] Most often, Suzuki-Miyaura cross-coupling is employed to form to $C(sp^2)$–$C(sp^2)$ bonds. Despite demand for increased $C(sp^3)$ character in drug molecules, applications of this method to form $C(sp^2)$–$C(sp^3)$ bonds remain limited.[1,13–15]

The two possible strategies for the formation of C(sp^2)–C(sp^3) bonds via Suzuki-Miyaura—the coupling of an alkyl electrophile with an arylboron reagent or the coupling of an aryl electrophile with an alkylboron reagent—face a series of separate and shared challenges. First, oxidative addition of palladium(0) to alkyl halides is significantly slower than to aryl halides.[16,17] The resulting alkylpalladium is then prone to β-hydride elimination, leading to the formation of an undesired alkene.[18] This is amplified by slow C(sp^2)–C(sp^3) reductive elimination, which increases the propensity for off-cycle pathways from the intermediate (L)Pd^{II}(Ar)Alk complex.[19] Contrastingly, when an alkylboron reagent is used, the low availability and stability of alkylboron reagents negate many of the original benefits of Suzuki-Miyaura coupling.[20,21] As a result, despite its prevalence in C(sp^2)–C(sp^2) bond formation, Suzuki-Miyaura coupling does not enjoy a place of privilege in C(sp^2)–C(sp^3) cross-couplings. Instead, a variety of alternative methodologies are utilized, including palladium-, nickel-, and iron-catalyzed cross-couplings of organohalides with organoboron, organozinc, and organomagnesium reagents.[22]

Scheme 1.2 C(sp^3) Cross-Coupling Presents Several Obstacles

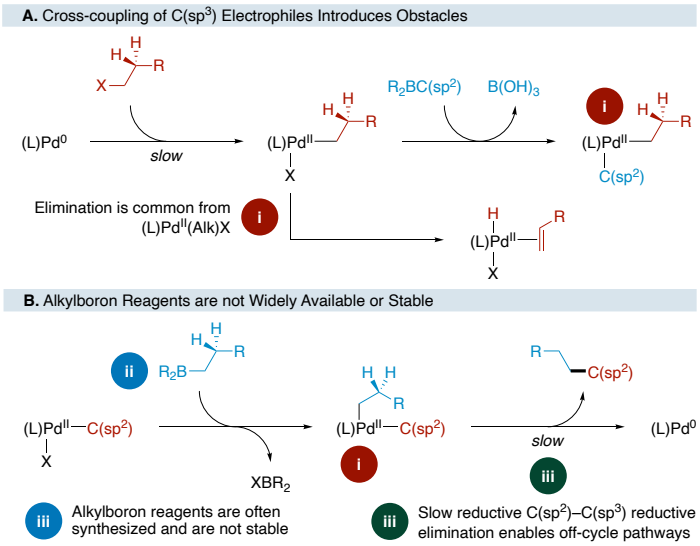

Amongst these methods, one enduring challenge is the low commercial availability, bench stability, and functional group tolerance of the requisite carbon nucleophile. As such, synthetic sequences employing these methods must incorporate a discrete C–H or C–X metalation step, as well as protection and deprotection steps to preserve sensitive functionalities, thereby lengthening and complicating the synthetic sequence.[22] While not discussed here, related obstacles exist in the field of palladium-catalyzed amine arylation (vide infra, Section 2.1). An ideal alternative would be the direct coupling of the organohalide precursor, circumventing many of these obstacles.

1.2 Cross-Electrophile Coupling Reactions

Nickel-catalyzed cross-electrophile coupling has emerged as a useful method for the formation of $C(sp^2)$–$C(sp^2)$[23] and $C(sp^2)$–$C(sp^3)$ bonds. These reactions utilize widely available, bench-stable carbon electrophiles in place of traditional carbon nucleophiles.[24] Most often, these reactions employ a $C(sp^2)$ electrophile, such as an aryl halide, and a $C(sp^3)$ electrophile, such as an alkyl halide. The reaction is balanced by the addition of a stoichiometric, terminal reductant—often zero-valent metals or organic reductants,[25–27]. Since the initial publications by the Weix,[28] Gong,[29] and Gosmini[30] groups, cross-electrophile coupling has grown to be a distinct reaction modality allowing for the incorporation of diverse $C(sp^2)$ and $C(sp^3)$ electrophiles.

Initial concerns about selectivity centered around the apparent similarities in reactivity between aryl and alkyl halides. Indeed, in palladium-catalyzed cross-coupling reactions, both classes of molecules undergo two-electron oxidative addition to form a $(L)Pd^{II}(R)X$ intermediate.[18,31] However, a shift in the type of reactivity—enabled by using first-row transition metals in concert with heterocycle-based L2 and L3 nitrogen ligands—of these two classes of electrophiles allows for differentiation by different

elementary steps. In a typical proposed mechanism for cross-electrophile coupling between an aryl and alkyl halide, (L)Ni^0 undergoes selective two-electron oxidative addition into the Ar–X bond despite the presence of the Alk–X coupling partner.[32] The resulting (L)Ni^{II}(Ar)X complex can then oxidatively capture an in situ-generated alkyl radical, forming a high energy (L)Ni^{III}(Ar)X(Alk) complex. Reductive elimination furnishes the desired Ar–Alk bond and an intermediate (L)Ni^{I}(X) complex. This nickel(I) intermediate can then undergo two- or single-electron steps to generate an alkyl radical or be directly reduced by a terminal reductant to regenerate the active (L)Ni^0 catalyst. While the exact elementary steps and catalyst speciation may change based on the reaction conditions, the overarching principles of differentiating electrophiles via their propensity to undergo two- and single-electron steps have enabled the coupling of a suite of electrophiles to form $C(sp^2)$–$C(sp^3)$ bonds.

Scheme 1.3 Cross-Electrophile Coupling Overview

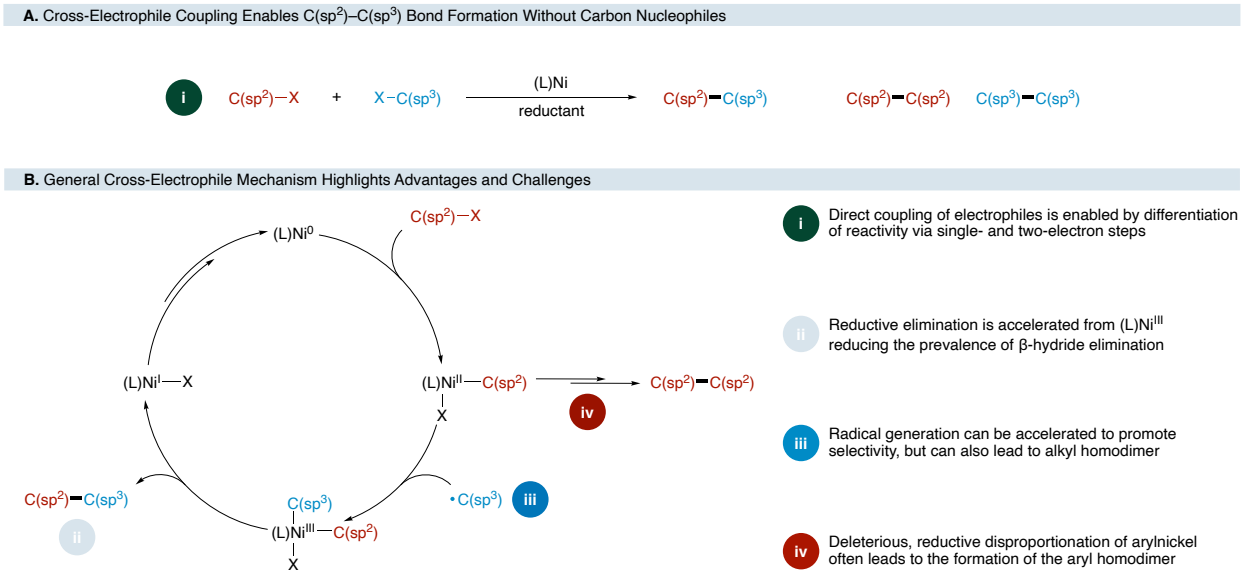

While catalytic differentiation between the two electrophiles is often not a major issue, one common obstacle to wider implementation of these methods is homodimerization of each coupling partner. One common deleterious byproduct is aryl

homodimer—which consumes two equivalents of the limiting reagent—presumably formed by disproportionation of the (L)Ni^{II}(Ar)X intermediate. Notably, the rate of aryl homodimerization is determined primarily by the ligand bound to the nickel catalyst. Early work in the Weix group identified 4,4′-dimethoxy- and 4,4′-di-tert-butyl-2,2′-bipyridine as suitable catalysts to promote selectivity in aryl-alkyl coupling, whereas other 2,2′-bipyridines derivatives led to decreased yield and selectivity.[24,28] As the scope and methods of cross-electrophile coupling expanded, methods to improve selectivity enabled the use of less electron-rich bipyridines, such as 2,2′-bipyridine—the canonical baseline of reactivity.[33]

Altogether, this propensity for the formation of dimeric side products hampers wider application of cross-electrophile coupling. While existing strategies to promote selectivity (Section 3.1.1) are often sufficient, they also introduce complexity compared to redox-neutral cross-couplings and require knowledge that is less developed compared to their redox-neutral counterparts. An ideal approach to overcome this gap in catalytic development would be the design of improved ligands that yields more robust, stable (L)Ni^{II}(Ar)X intermediates. These ligands would enable more general, robust, and selective cross-electrophile couplings.

Chapter 2: Reductive Arylation of Nitroarenes with Chloroarenes: Reducing Conditions Enable New Reactivity from Palladium Catalysts

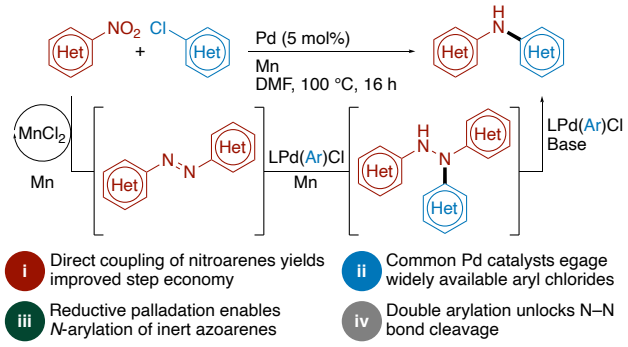

This chapter has been published and reprinted with permission from **Akana-Schneider, B. D.**; Weix, D. J. Reductive Arylation of Nitroarenes with Chloroarenes: Reducing Conditions Enable New Reactivity from Palladium Catalysts. *J. Am. Chem. Soc.* **2023**, *145* (29), 16150–16159. DOI: 10.1021/jacs.3c04647.

2.1 Introduction

While cross-electrophile strategies have been applied to the formation of C(sp^2)–C(sp^3)—and more recently C(sp^2)–C(sp^2)—bonds they have not been widely translated to other common redox-neutral cross-couplings, such as the formation of C(sp^2)–N, C(sp^2)–O, and C(sp^2)–S bonds. Unlike carbon nucleophiles—which require activation by metalation—amines, alcohols, and thiols possess native nucleophilicity in organic molecules. This Lewis basicity can be leveraged to promote association-deprotonation steps, enabling the formation of metal amide species that yield the desired bond via reductive elimination. Despite significant advances in catalyst design and substrate scope, obstacles related to substrate availability and synthesis still exist for these nucleophiles, mirroring the drawbacks of carbon nucleophiles described above (vide supra, Section 1.1).

Scheme 2.1 Synthetic Approaches to Diarylamines

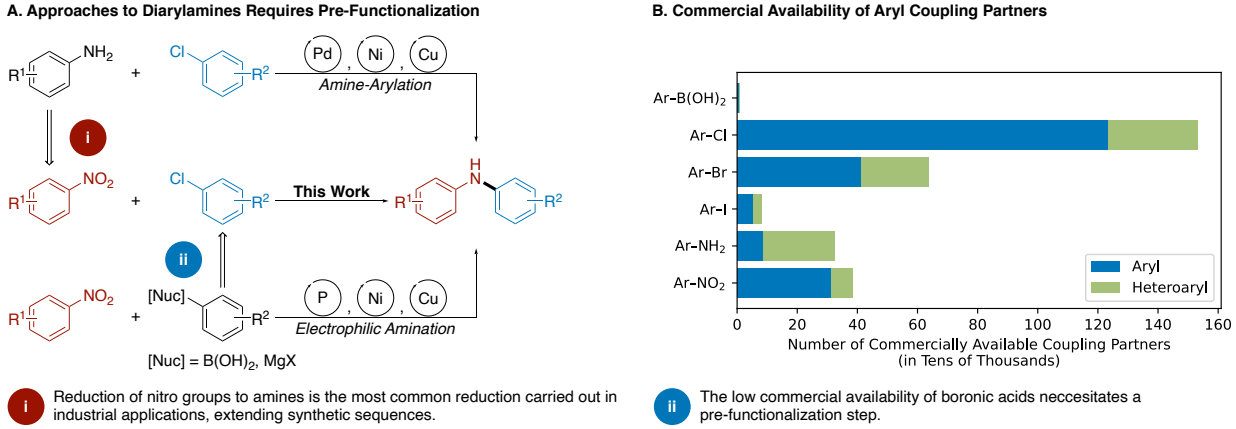

[a]Commercial availability of coupling partners was gathered via a search of the eMolecules database—via Reaxys—performed on 7/18/18. Aryl and heteroaryl coupling partners were specified as ARY–FG and HAR–FG (where FG represents the functional group in question, e.g., Cl, Br, NO_2) respectively. While the exact number of commercial coupling partners changes in magnitude depending on the database searched (e.g., PubChem Commercial Substances via Reaxys, Reaxys Commercially Available Filter, etc.), the trends observed are consistent.

For example, palladium-catalyzed amine arylation—the cross-coupling of aryl (pseudo)halide electrophiles with amine nucleophiles to form a new C–N bond (Scheme

2.1a)—is one of the most-used reactions in medicinal chemistry.[5,11,34] Buoyed by the importance of amines in pharmaceuticals, the abundance of starting materials, and wide functional group tolerance, the success of amine arylation has made secondary diarylamines a common feature in medicinal and materials chemistry, despite their rarity in natural products.[35] One key advantage of this chemistry is the ability to access a wide variety of aryl electrophiles; for example, advances in catalyst design have allowed for the use of more widely available chloroarenes instead of aryl bromides (Scheme 2.1b).[10,36–39] While there are many commercially available primary anilines, an analysis of industrial chemical reactions reveals that the synthesis of anilines by nitroarene reduction is common.[5,11,40] Indeed, a recent study on the most-used reactions in medicinal chemistry found that reduction of a nitroarene to a primary aniline was the most-used reduction. An obvious, but underdeveloped, alternative to this synthetic sequence is the direct, reductive arylation of nitroarenes with aryl chlorides (Scheme 2.1a). Despite its potential synthetic utility, this proposed reaction faces numerous challenges, such as managing a net six-electron reduction of the nitro group, resolving the disparate reactivity of the relatively inert chloroarene, and the high reactivity of the many possible nitrogen intermediates.

Strategies for the reductive arylation of nitroarenes have thus far relied on the in-situ conversion of the nitroarene to a transient, electrophilic nitrosoarene, which is trapped with a nucleophilic carbon source (Ar-[M]) or aryl radical.[41] In general, the propensity of nitrosoarenes to undergo deleterious over-reduction and dimerization necessitates the use of more reactive nucleophilic carbon sources such as aryl Grignard reagents.[42–46] Despite recent advances enabling the use of less reactive arylboronic acids,[47–54] arylboronic acids are less available than chloroarenes (~180× fewer commercially

available, Scheme 2.1b), adding synthetic complexity. Engagement of aryl chlorides would be simplest via oxidative addition to low-valent palladium or nickel catalysts, but the resulting arylpalladium and arylnickel intermediates are not known to form new C–N bonds with nitroarenes.

Scheme 2.2 Strategies for Nitroarene Arylation

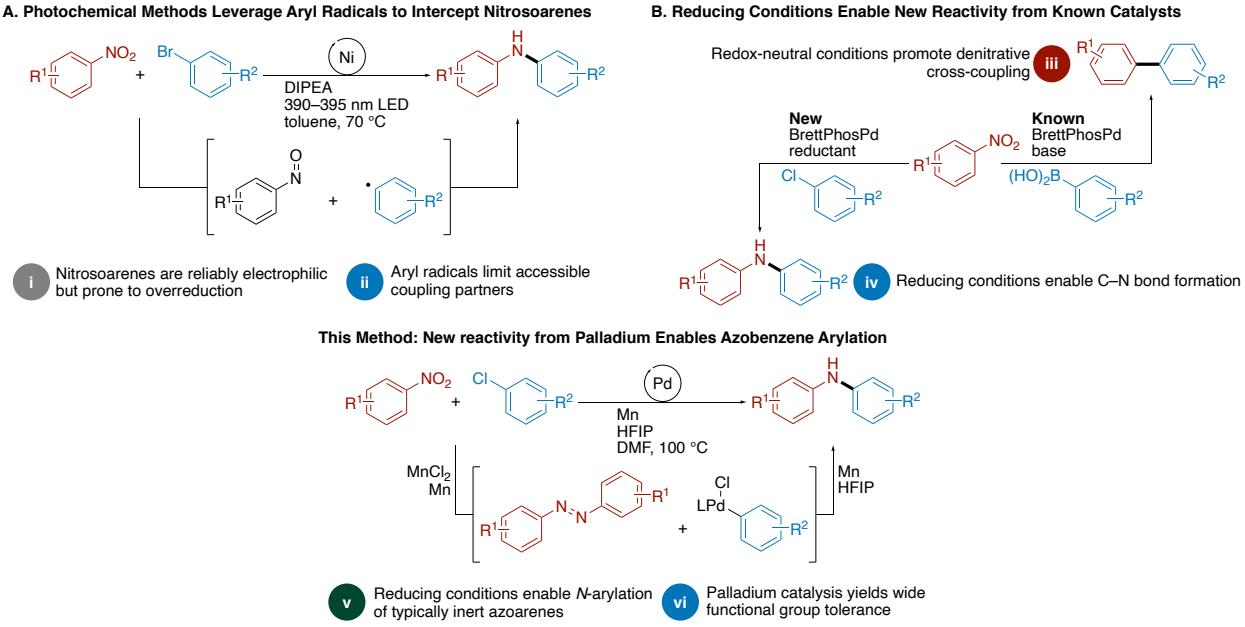

Recent work by Xue and coworkers has described the arylation of nitroarenes with bromoarenes via the photo-assisted generation of aryl radicals (Scheme 2.2a).[55] While an advance over the use of pre-formed aryl nucleophiles, the aryl radical intermediates limit compatibility with heterocycles and even more powerful reductants would be needed to extend this strategy to chloroarenes.[56–62] Harvey and Hu have reported on the reductive acylation of nitroarenes.[63,64] Unlike the known arylation reactions, this reaction proceeds via activation of an intermediate azoarene to form a reactive mixed nickel/zinc-imido complex. While the reactivity of these imido intermediates has been limited to acylation reactions, the intermediacy of an azoarene intermediate offers advantages over nitrosoarenes (vide infra). In contrast to nickel, palladium-catalyzed reductive arylation

or acylation of nitroarenes is unknown. Instead, palladium-catalyzed cross-couplings of nitroarenes feature C–NO_2 oxidative addition (Scheme 2.2b).[65–69]

Herein we demonstrate how the same palladium catalysts that favor C–NO_2 oxidative addition and promote C–N bond formation with amines[68,69] reveal new reactivity when subjected to reducing conditions: catalyzing the *N*-arylation of azoarenes via an association-reductive palladation sequence. The *N*-functionalization of azoarenes using arylpalladium(II) intermediates is notable because the N=N bond of azoarenes is generally considered inert towards arylpalladium(II) intermediates;[70] even functioning as a useful directing group for C–H bond activation.[71–79] Our studies show that C–N bond formation occurs via reductive dimerization of nitroarenes to azoarenes, followed by diarylation to form a tetra-arylhydrazine, and reductive cleavage of the hydrazine to form two molecules of product. This dimerization-functionalization-cleavage strategy avoids over-reduction that can plague nitrosoarenes, and changes the way that we view reactions of palladium(II) complexes with azo compounds.

2.2 Results and Discussion

Table 2.1 Standard Conditions and Effects of Select Deviations[a]

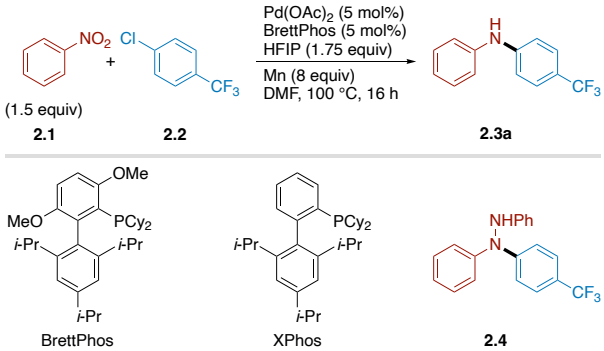

Entry	Deviation	**2.3a** (%)[b]
1	None	92
2	XPhos instead of BrettPhos	86
3	*rac*-BINAP instead of BrettPhos	1
4	No HFIP	0
5	TFE instead of HFIP	9
6	2-Butanol instead of HFIP	29
7	$PdCl_2$ instead of $Pd(OAc)_2$	81
8	$Pd_2(dba)_3$ instead of $Pd(OAc)_2$	87[c]
9	Zn instead of Mn	89
10	Benchtop setup with no exclusion of air or water (capped)	90[d]

[a]Reactions were assembled in a nitrogen filled glovebox at a 0.25 mmol scale in 0.5 mL of DMF. [b]Yields were determined by SFC-MS analysis. [c]2.5 mol% $Pd_2(dba)_3$ used instead of 5 mol% $Pd(OAc)_2$. [d]Reaction set up at 0.5 mmol scale in 1 mL of DMF.

We began by examining the reductive arylation of nitrobenzene (**2.1**) with 4-chlorobenzotrifluoride (**2.2**) (Table 2.1). Preliminary studies quickly established two key variables in the reaction: the identity of the ligand and the presence of an appropriate proton source. We found that BrettPhos, the same ligand known for promoting C–NO_2 oxidative addition in denitrative cross-couplings, was optimal. While other monodentate, dialkylbiarylphosphines such as XPhos also provided the desired product in good yield, common bidentate phosphines, such as *rac*-BINAP did not. Serendipitously, we found that alcohols modulate the extent of arylation, promoting conversion of intermediates to the desired product and preventing overarylation of the desired diarylamine. Tuning the pK_a of the alcohol is critical, as less acidic additives such as 2,2,2-trifluoroethanol (TFE)

provided the under-arylated 1,1,2-triarylhydrazine (**2.4**) as the major arylated product. As will be discussed in more detail below, the alcohol facilitates two proton transfers: mediating the arylation of **2.4** via association-deprotonation as the conjugate base and providing the desired product from the diarylamide (**2.7**), thereby preventing overarylation to triarylamine.[A] Besides these two variables, we found that many other components of the reaction conditions were flexible. A variety of palladium(II) and palladium(0) precatalysts provided similar results, although $Pd(OAc)_2$ was chosen due to its high solubility. Manganese powder was optimal, however zinc flake gave similar yields, despite it being a weaker reducing agent. The reactions were generally run under air-free conditions using dry, degassed solvents, but similar yields were obtained using wet DMF, under an air headspace when set up on the benchtop.

Given the impact of mechanistic understanding on reaction design, the importance of palladium catalysis, and the unique *N*-arylation observed in these conditions, we undertook a mechanistic investigation. We sought to: identify the catalytic species responsible for nitroarene reduction; confirm the identity of the active nitrogenous coupling partner; determine the mechanism by which *N*-arylation occurs; and establish the role of the alcohol in controlling the extent of arylation. Based on observations in catalytic reactions and specific mechanistic experiments described below, we propose the mechanism seen in Scheme 2.3.

[A] Triarylamine was observed in early optimization efforts utilizing electron-rich chloroarenes when a proton source was omitted.

Scheme 2.3 Key Aspects of the Proposed Mechanism of the Palladium-Catalyzed Reductive Arylation of Nitroarenes

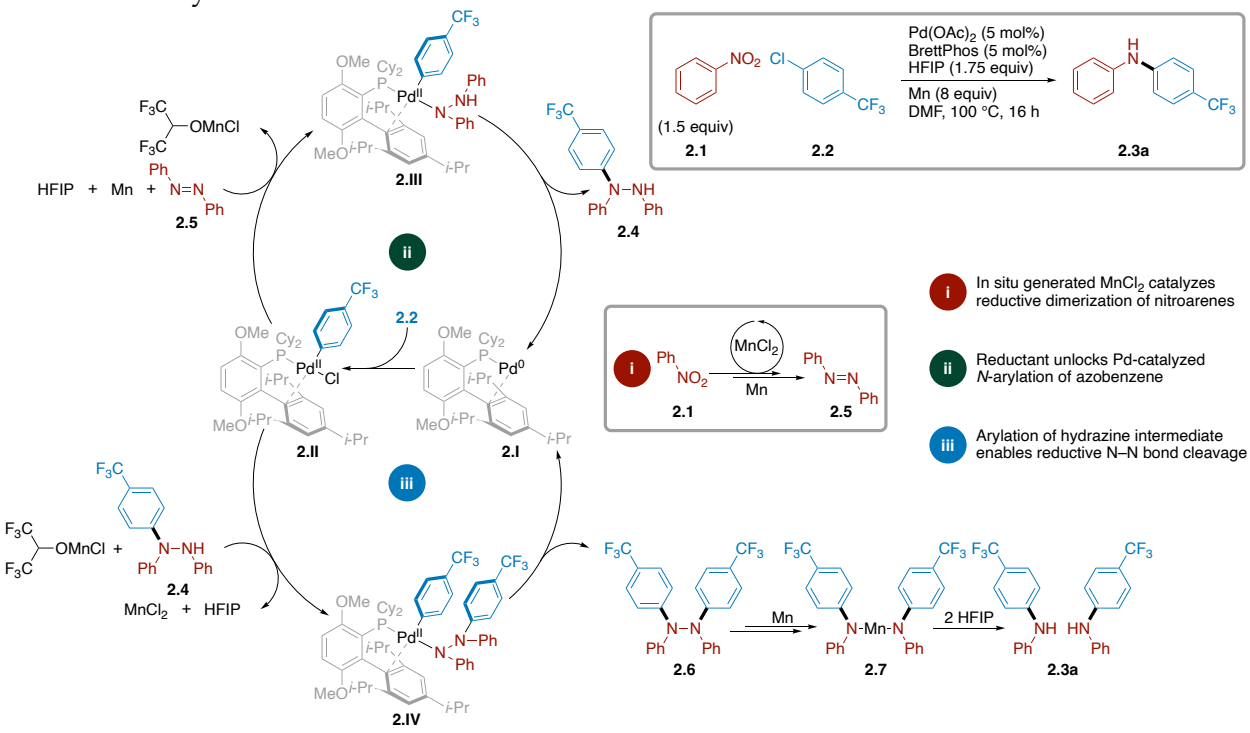

Initial reduction of nitrobenzene occurs via a $MnCl_2$-catalyzed, reductive dimerization to yield azobenzene (**2.5**).[80,81] While additional reduction to form hydrazobenzene is possible, experimental evidence suggests that this process is off-cycle and slow in comparison to productive *N*-arylation (Figure 2.9, Figure 2.16). Catalytic *N*-arylation of **2.5** begins with oxidative addition of **2.2** to in situ generated Pd^0 (**2.I**) to form the key oxidative addition intermediate (**2.II**). We posit that association of the Lewis basic nitrogen of **2.5** to the Lewis acidic Pd^{II} center forms [(BrettPhos)Pd(Ar^1)Cl(Ar^{2}N=NAr^2)].[82] This association then enables reduction of the N=N bond of **2.5** to form a transient mixed palladium(II)/manganese hydrazide which is protonated by HFIP to form palladium(II) aryl hydrazide (**2.III**) and an alkoxide base. This manganese dependent, reductive palladation could be imagined as analogous to reported reductions of bound ligands,

such as dinitrogen.[83] Reductive elimination forms the C–N bond of $Ar^1(Ar^2)N–NH(Ar^2)$ (**2.4**).

The second arylation of **2.4** occurs via an amine-arylation sequence involving oxidative addition of **2.2** to **2.I**, association-deprotonation of **2.4** to **2.II**, and C–N reductive elimination from intermediate **2.IV** to yield a transient 1,1,2,2-tetraarylhydrazine (**2.6**). The weak N–N bond of **2.6** then undergoes rapid homolysis,[84,85] followed by reductive capture by Mn, yielding manganese bisdiarylamide (**2.7**). Final protonation furnishes the desired product (**2.3a**) and prevents deleterious transmetalation onto **2.II**, stopping over-arylation to form $Ar^2N(Ar^1)_2$ (over-arylation not depicted in Scheme 2.3).

Table 2.2 Reduction of Nitrobenzene is Catalyzed by in situ-generated $MnCl_2$[a]

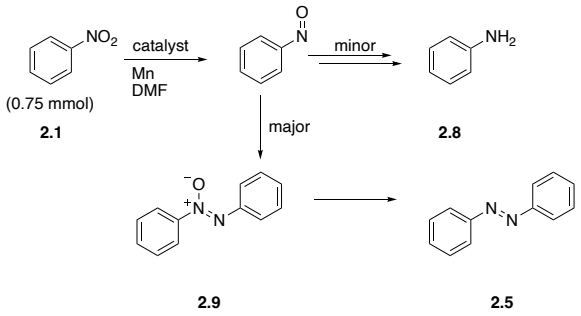

Catalyst	Conversion at 15 min (%)[b]	Conversion at 90 min (%)[b] (**2.9**:**2.5**:**2.8**)
(cod)Pd($CH_2TMS)_2$ and BrettPhos	0	5[c]
(BrettPhos)Pd(Ar)Cl (**2.II**)	<1	100 (4.7:1.2:1)
$MnCl_2$	18	72 (8.0:1.5:1)

[a]Reactions were assembled in a nitrogen filled glovebox. 0.75 mmol 1, 3.3 mol% catalyst, 5.33 equiv Mn, 1 ml DMF, 100 °C, 90 m. [b]Concentration was determined by SFC-MS. [c]No Reduction products were observed.

We began our mechanistic investigation by determining the conditions necessary for the reduction of nitrobenzene. In contrast to other reductive functionalizations of nitroarenes that employ manganese as the terminal reductant,[63,64,86–90] our conditions did not require the addition of a stoichiometric, oxophilic Lewis acid. We considered whether

Pd(0), Pd(II), or residual Mn salts catalyzed the Mn powder reduction step (Table 2.2). Neither inclusion of the optimal $Pd(OAc)_2$/BrettPhos precatalyst pair (not pictured), nor palladium(0) precursor $(cod)Pd(CH_2TMS)_2$, enabled reduction of nitrobenzene. While the addition of catalytic amounts of oxidative addition Pd(II) complex **2.II** did allow for reduction of nitrobenzene, the observed induction period led us to conclude that catalyst modification is necessary and **2.II** is not directly responsible for catalysis. Indeed, addition of catalytic $MnCl_2$—the byproduct of reductive decomposition of **2.II** by Mn—unlocked reduction of nitrobenzene. Based on these results, we concluded that the coupling reaction is autocatalytic, with initial, slow decomposition of small amounts of **2.II** turning on the productive pathway, which in turn produces more $MnCl_2$ (Figure 2.1).

Scheme 2.4 Evaluation of Possible Coupling Partners[a,b,c,d,e]

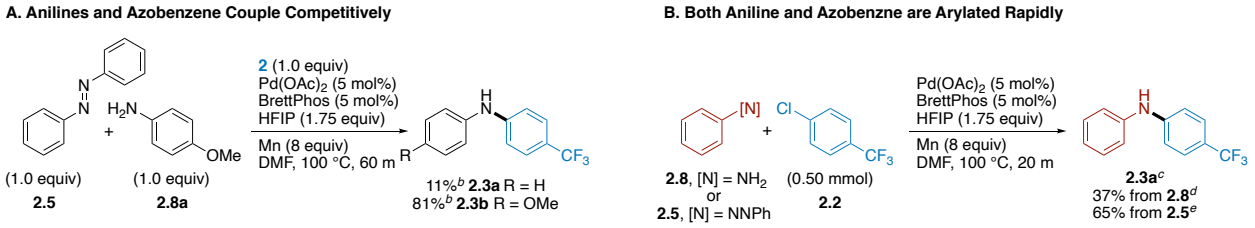

[a]Reactions were assembled in a nitrogen filled glovebox at a 0.50 mmol scale in 1.0 mL of DMF. [b]Yields were determined by ^{19}F NMR. [c]Yields were determined by SFC-MS analysis. [d]0.75 mmol of aniline. [e]0.375 mmol of azobenzene.

Over the course of catalytic reactions and discrete reduction studies, we observed two probable nitrogenous coupling partners: azobenzene (**2.5**) and aniline (**2.8**). While both coupling partners are rapidly arylated under reaction conditions at similar rates (Scheme 2.4), under these reducing conditions azoxybenzene (**2.9**) and azobenzene (**2.5**) form at higher concentration than aniline (Table 2.2 and Figure 2.9). Indeed, the reductive dimerization of nitrobenzene to form azobenzene is well known.[81,87,91] These observations, combined with the high rate of *N*-arylation of azobenzene (Scheme 2.4b, Figure 2.13), and differences in reaction outcomes between electron-poor anilines and electron-poor

nitroarenes (Figure 2.12) led us to conclude that while reductive amine arylation can occur under these conditions, it is a beneficial, convergent side reaction and that double *N*-arylation of azobenzene is the major pathway.

Scheme 2.5 Possible *N*-Arylation Pathways to Form Triarylhydrazine (**2.4**) from Azoarene and Arylpalladium(II)

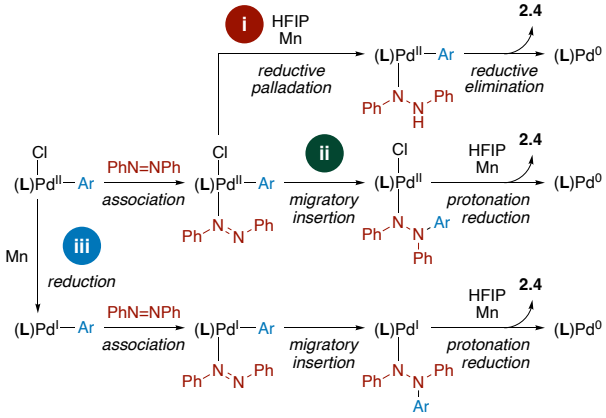

The N=N bond of azoarenes is typically inert to palladium catalysis, even serving as a directing group for C–H functionalization.[71–75] While limited examples of palladium(0)-mediated reductive functionalization of azo compounds have been reported;[92,93] catalytic, *N*-arylation from palladium oxidative addition complexes is unknown. As such, we sought to determine the elementary step by which arylation occurs, with the aim to better understand this coupling and expand the catalytic schema used to design new reactions. We envisioned three possible mechanisms by which palladation of azobenzene might occur: direct migratory insertion of the Pd–C bond across the N=N bond (Scheme 2.5ii); reduction of **2.II** to form a reactive palladium(I) intermediate that can capture azobenzene (Scheme 2.5iii); and association-reduction of azobenzene in a reductive transmetalation process (Scheme 2.5i).

To establish a baseline for reactivity, we reacted **2.II** with excess azobenzene **2.5** (Scheme 2.6a). In the absence of a reductant, no *N*-arylated products were observed

(Figure 2.14), indicating that direct migratory insertion (Scheme 2.5, pathway ii) is not probable. Only addition of manganese enabled arylation, as **2.3a** and **2.4** were observed in reactions containing stoichiometric or excess reductant. These results suggest that either reduction of **2.II**, azobenzene (**2.5**), or their association complex is necessary for arylation to occur.

Scheme 2.6 Additional Mechanistic Studies Support Double *N*-Arylation of Azobenzene[a,b]

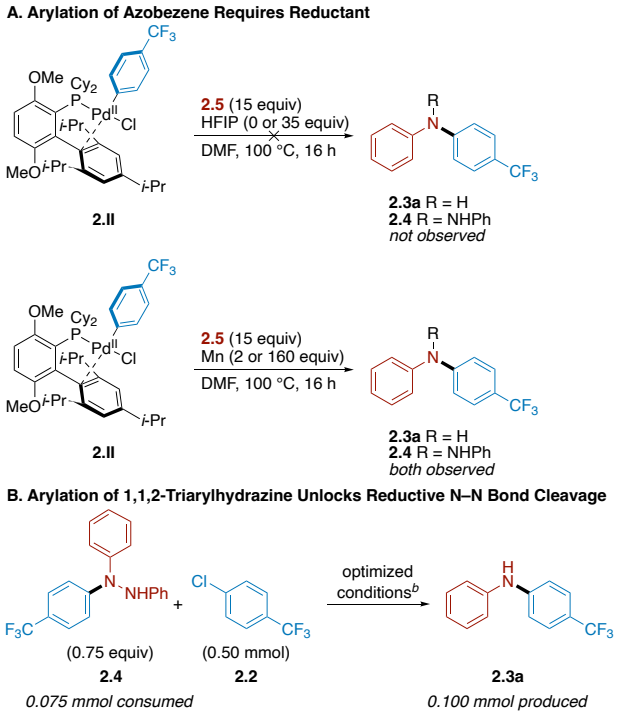

[a]Reactions were assembled in a nitrogen-filled glovebox. Yields were determined by SFC-MS analysis. [b]5 mol% $Pd(OAc)_2$, 5 mol% BrettPhos, 1.75 equiv HFIP, 8 equiv Mn, 1 ml DMF, 100 °C, 16 h.

We utilized cyclic voltammetry to distinguish between pathways involving the reduction of **2.II** and azobenzene **2.5**. While reductive decomposition of **2.II** does occur under reducing conditions (Scheme 2.4a), CV confirmed that irreversible reduction only occurs at very reducing potentials (-2.23 V vs. Fc/Fc^+). Contrastingly, direct, reversable, single-electron reduction of azobenzene is thermodynamically plausible under the

reaction conditions (-1.80 V vs. Fc/Fc^+). These data indicate that either direct reduction of azobenzene occurs – the resulting radical anion then exchanging for the chloride ligand on **2.II** – or that association of azobenzene to the Lewis acidic **2.II** enables reduction. We predict that association-reduction is the dominant pathway, as substituting manganese for the much less reducing zinc leads to little change in yield (89% vs 92%) and hydrazobenzene—the product of direct reduction of azobenzene—is not arylated under the optimized conditions (Figure 2.17).

The intermediacy of **2.4** was confirmed by replacing nitrobenzene with **2.4** in the optimized reaction conditions (Scheme 2.6b). Arylation yielded diarylamine **2.3a** in excess of the consumption of **2.4** (0.075 mmol of **2.4** consumed, 0.1 mmol of **2.3a** produced). While consumption of **2.4** was low, this result also confirms that direct reductive cleavage of the N–N bond of **2.4** (yielding an equivalent of **2.3a** and aniline **2.8**) is not operable. We hypothesize that the low conversion was due to the presence of an extra equivalent of protons compared to nitroarene or azoarene arylation reactions. This results in inefficient association-deprotonation of **2.4** and eventual reductive catalyst degradation.

Finally, we sought to rationalize the role of the alcohol in determining selectivity. As seen in Table 2.1, the exclusion of a proton source from reactions completely stops the formation of **2.3a**. However, its exclusion neither prevents reduction of nitrobenzene nor arylation of the resulting azoarene, as **2.4** is still observed. We propose that balancing the acidity and the steric profile of the alcohol is necessary to manage the protonation of intermediates and the binding of the alkoxide to **2.II**. Formation of palladium(II) alkoxide complexes is a known intermediate or off-cycle pathway in amine arylation reactions.[94–96] Indeed, we found that **2.II** is more stable under reducing conditions in the presence of

an alcohol (Figure 2.11). Employing the less acidic and sterically demanding trifluoroethanol in place of HFIP in arylations of nitrobenzene yielded **2.4** as the major product. We hypothesized that inefficient arylation of **2.4** is caused by exchange of 2,2,2-trifluoroethoxide for chloride on **2.II**, yielding an unreactive, stable, palladium(II) alkoxide that prevents association of **2.4**. Deprotonation of associated **2.4** is most likely not a limiting factor, as 2,2,2-trifluoroethoxide is more basic than 1,1,1,3,3,3-hexafluoroisopropoxide. Indeed, utilizing 2-butanol as the proton source in place of TFE yields increased conversion of **2.4** into **2.3a**. These results indicate that balancing the association of the alkoxide to **2.II**—via the use of an electron-poor, secondary alcohol—enables arylation of **2.4**, provides protons to quench the reactivity of the final product, while also stabilizing **2.II** under reducing conditions.

Having an effective understanding of the mechanism by which the reaction proceeds, we proceeded to investigate the scope accessible using these initial conditions (Scheme 2.7). Arylation of nitroarenes bearing synthetically valuable electron-donating groups such as a methyl ether (**2.3b**), methylenedioxy (**2.3c**), or an unprotected secondary amine (**2.3d**) all proceeded in high yield. In contrast to photochemical alternatives to this method,[55] easily oxidized tertiary alkylamines (**2.3e**) were also well-tolerated. Nitroarenes bearing a silyl protected aliphatic alcohol (**2.3f**) or substitution in the 2-position (**2.3g**) were also arylated effectively. Additionally, the optimized conditions enabled the arylation of a variety of nitroheteroarenes, which are not tolerated in photochemical methods due to the reactivity of aryl radicals.[55,57,97–99] We found that common heterocycles such as protected and unprotected indoles (**2.3h**, **2.3i**), pyridine (**2.3j**), and protected pyrazole (**2.3k**) were all tolerated.

Scheme 2.7 Substrate Scope for the Palladium-Catalyzed Reductive Arylation of Nitroarenes with Aryl Chlorides[a,b,c,d,e]

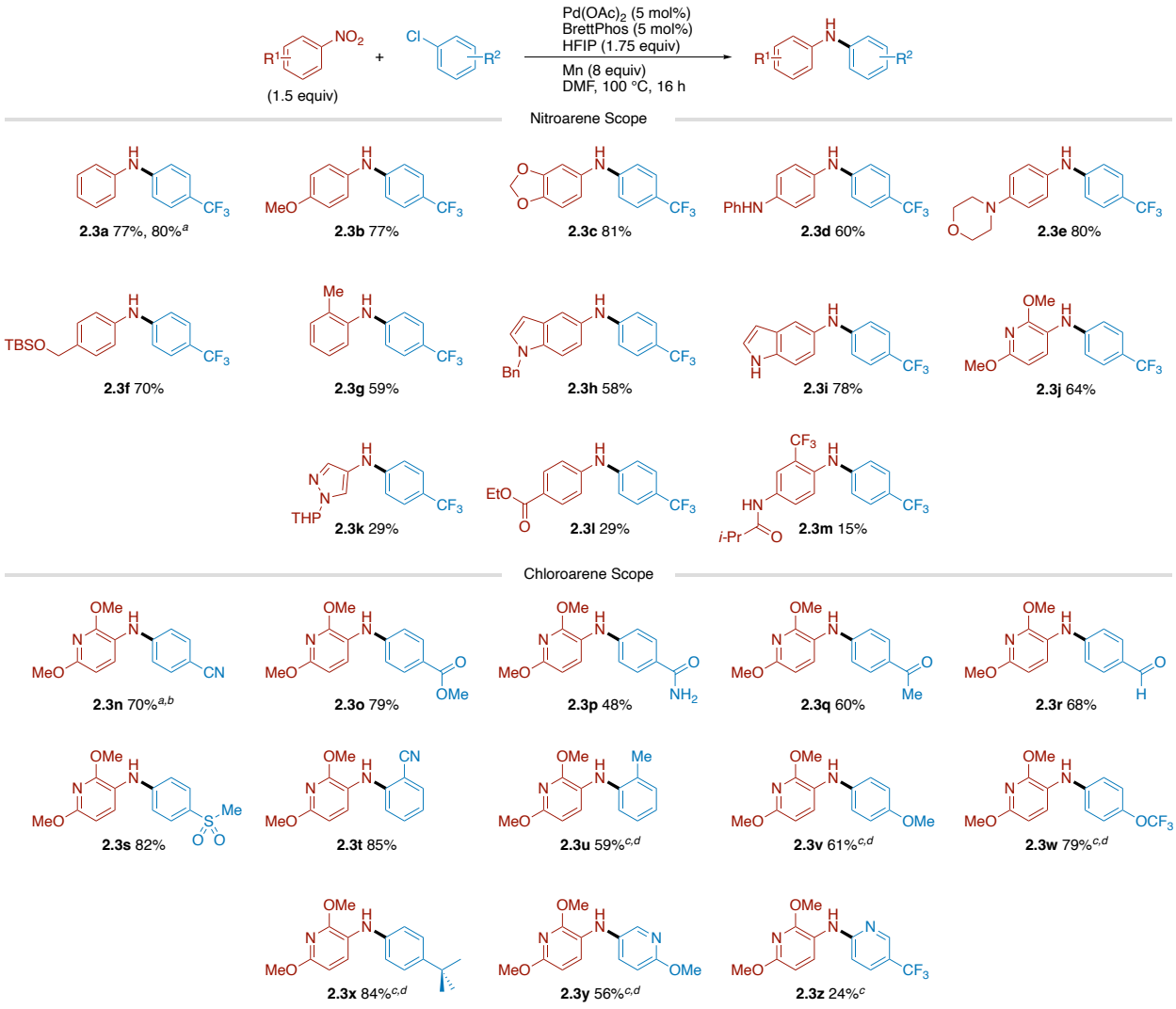

[a]Reactions were conducted at 0.5 mmol scale in DMF (1 mL). Isolated yields after purification are shown. [b]Reaction conducted at 2.0 mmol scale. [c]Reaction set up on the benchtop using standard air-free technique. [d]10 mol% each of $Pd(OAc)_2$ and BrettPhos. [e]TFE instead of HFIP.

We found that the introduction of an electron-withdrawing ethyl ester (**2.3l**) significantly decreased the yield of the desired diarylamine. As the major byproduct was the corresponding primary aniline, we hypothesize that direct reduction of an intermediate electron-poor nitrosoarene may occur faster than reductive dimerization. Despite this limitation, the diarylamine derived from arylation of electron-poor

chemotherapeutic flutamide (**2.3m**) was isolated in 15% yield. Again, the primary aniline derived from flutamide was isolated as the major byproduct. These results suggest that modification of the reaction conditions to avoid over-reduction or engage the aniline directly in amine-arylation may be successful in over-coming this limitation.

A variety of electron-poor chloroarenes were effectively engaged using the optimized conditions. We successfully coupled chloroarenes bearing carboxylic acid derivatives including nitriles (**2.3n**, **2.3t**), a methyl ester (**2.3o**), and a primary amide (**2.3p**). The reaction was amenable to increased scale and a benchtop setup while maintaining good yield (**2.3n** was synthesized at 2.0 mmol scale on the benchtop using standard air-free technique). Other oxidized functionalities that could be reduced were well tolerated, such as an acetophenone (**2.3q**), an unprotected benzaldehyde (**2.3r**), and a sulfone (**2.3s**). Further, activation of ortho-substituted chloroarenes yielded secondary diarylamines with either an electron-withdrawing nitrile (**2.3t**) or electron-donating methyl (**2.3u**) group in the two-position.

We found that two modifications were necessary to effectively couple electron-rich chloroarenes: increasing the catalyst loading from 5 to 10 mol% and replacing HFIP with the less acidic TFE. These conditions enabled the coupling of chloroarenes bearing electron-donating methyl and trifluoromethyl ethers (**2.3v**, **2.3w**), as well as simple alkyl substituents (**2.3u**, **2.3x**). We hypothesize that these two changes overcome sluggish arylation of the 1,1,2-triarylhydrazine intermediate afforded from the initial *N*-arylation of the azoarene and stabilize the critical oxidative addition intermediate (**2.II**). The decreased Lewis acidity of arylpalladium complexes bearing electron-rich aryl substituents most likely makes association and deprotonation of the hydrazine intermediate significantly less favorable. Utilizing TFE can have two beneficial effects.

First, the more associating 2,2,2-trifluoroethoxide anion may extend catalyst lifetime, forming a reservoir of stable palladium(II) alkoxide. Second, the more basic alkoxide may enable deprotonation of the hydrazine intermediate.

These modified conditions also allowed for the coupling of an electron-rich 3-chloropyridine, yielding diheteroarylamine (**2.3y**). The increased catalyst loading is also beneficial when coupling other heteroaryl chlorides, regardless of the electron density in the ring (**2.3z**). Together, these results demonstrate the synthetic utility, functional group tolerance, and electronic and steric limitations of this method.

2.3 Conclusions

In conclusion, we developed the first method for the reductive arylation of nitroarenes with chloroarenes. This method relies on a new dimerization-arylation-fragmentation mechanism that avoids deleterious overreduction of reduced nitrogenous intermediates. *N*-arylation of the typically inert azoarene intermediate is unlocked by the reducing conditions. Diarylation of the N=N bond of the azoarene activates it towards reductive cleavage. The resulting reaction tolerates a range of synthetically relevant functionalities, steric crowding, and heterocyclic cores. We expect that the mechanistic results in this study will provide a basis for rapid development of this new approach to diarylamines. For example, we are currently pursuing the expansion of this method to allow for arylation of nitroarenes with aryl tosylates. Based on mechanistic understanding, we have increased the yield by: (1) changing the pre-catalyst to $PdCl_2$, which increases the conversion of the nitroarene, and (2) employing the more associating 2-butanol in place of HFIP, which stabilizes the palladium catalyst (Table 2.3).

Table 2.3 Initial Optimization of Nitroarene Arylation with Tosylates

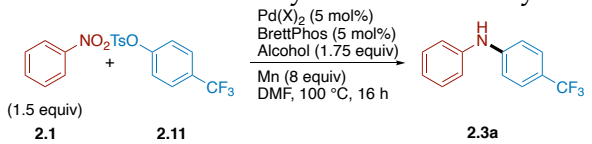

Entry	X	Alcohol	**2.3a** (%)[b]
1	OAc	HFIP	18
2	Cl	2-Butnaol	40

[a]Reactions were assembled in a nitrogen filled glovebox at a 0.25 mmol scale in 0.5 mL of DMF. [b]Yields were determined by SFC-MS analysis.

2.4 Experimental

2.4.1 General Information

2.4.1.1 Reagents

Metals and Catalysts

All metals and catalysts were stored in a nitrogen-filled glovebox and used without additional purification unless otherwise noted. Palladium(II) acetate was purchased from Chem-Impex International or Strem. Palladium(II) chloride was purchased from Alfa Aesar. Tris(dibenzylideneacetone)dipalladium(0) was purchased from Sigma Aldrich. [(2-Di-cyclohexylphosphino-3,6-dimethoxy-2′,4′,6′-triisopropyl-1,1′-biphenyl)-2-(2′-amino-1,1′-biphenyl)]palladium(II) methanesulfonate (BrettPhos Pd G3) was purchased from Sigma Aldrich. Dichloro(cycloocta-1,5-diene)palladium(II) was synthesized according to the literature procedure and analyzed by elemental analysis and NMR.[100] Characterization data matched those reported in the literature. Zinc flake (-325 mesh) was purchased from Alfa Aesar. Manganese powder (-325 mesh) was purchased from Alfa Aesar.

Ligands

Ligands were stored and handled in a nitrogen-filled glovebox and used without further purification. 2-Di-cyclohexylphosphino-3,6-dimethoxy-2′,4′,6′- triisopropyl-1,1′-biphenyl (BrettPhos) was purchased from Chem-Impex International or Sigma Aldrich. 2-Dicyclohexylphosphino-2′,4′,6′-triisopropylbiphenyl (XPhos) was purchased from Matrix Scientific. 1,1'-Bis(diphenylphosphino)ferrocene (dppf) was purchased from Strem. (±)-2,2'-Bis(diphenylphosphino)-1,1'-binaphthyl (*rac*-BINAP) was purchased from Alfa Aesar.

Solvents

All solvents were anhydrous and stored in a nitrogen-filled glovebox unless specified otherwise. *N*,*N*-Dimethylformamide (DMF) was purchased from Sigma Aldrich. *N*,*N*-Dimethylacetamide (DMA) was purchased from Sigma Aldrich.

Other Reagents

Nitroarenes, chloroarenes, alcohol additives, and other reagents were purchased from commercial sources, stored on the benchtop, and used without further purification unless otherwise specified.

2.4.1.2 Methods

NMR Spectroscopy

^{1}H, ^{13}C, ^{19}F, and ^{31}P NMR spectra were acquired on 400 and 500 MHz Bruker Avance III NMR instruments. NMR chemical shifts are reported in ppm. ^{1}H chemical shifts are referenced to tetramethylsilane (TMS) in $CDCl_3$ (δ = 0.00 ppm) or to the residual CH_2Cl_2 solvent peak (δ = 5.32 ppm). Signals for arising from 1,4-disbstituted arenes (e.g. **2.3b**) are most accurately characterized as AA'BB' patterns; however, minimal second order

coupling is observed in these spectra—little to no line broadening or shoulder peaks are observed. As such these signals are reported as doublets, with the apparent *J* value included. ^{13}C, ^{19}F, and ^{31}P chemical shifts are absolute referenced to ^{1}H NMR data. Coupling constants (*J*) are reported in Hertz.

High Resolution Mass Spectrometry

Mass spectrometry data was collected on a Thermo Scientific Q Exactive Plus Hybrid Quadrupole-Orbitrap via flow injection with electrospray ionization or via M&M Mass Spec Consulting ASAP-MS by the Paul Bender Chemical Instrumentation Center facility at the University of Wisconsin-Madison.

Supercritical Fluid Chromatography Mass Spectrometry (SFC-MS)

SFC-MS analyses were performed on a Waters ACQUITY UPC^2 equipped with an ACQUITY UPC^2 PDA and ACQUITY QDa detector. A Daicel DCpack SFC-A column (3mm ID × 150 mm L, 3 μm PS) was used for separations. The eluent was a mixture (97:3 CO_2/MeOH) with a flow rate of 2 mL/min at 40 °C with an automated back pressure of 1500 psi.

Gas Chromatography

GC analyses were performed on an Agilent 7890A GC equipped with dual DB-5 columns (20 m × 180 μm × 0.18 μm), dual FID detectors, and H_2 as the carrier gas. A sample volume of 1 μm was injected at a temperature of 300 °C and a 100:1 split ratio. The initial inlet pressure was 20.3 psi but varied as the column flow was held constant at 1.8 mL/min for the duration of the run. The initial oven temperature of 50 °C was held for 0.46 min followed by a temperature ramp of 65 °C/min up to 300 °C. The total run time was 5.0 min and the FID temperature was 325 °C.

Flash Chromatography

Flash chromatography was performed on a Teledyne ISCO Rf-200 (detection at 254 and 280 nm) equipped with an 80g Teledyne ISCO Redisep Rf Gold silica gel column (20–40 μm particle size). Products were visualized via UV or vanillin stain.

Elemental Analysis

Analysis was performed via a PerkinElmer 2400 Series II Analyzer by the CENTC Elemental Analysis Facility at the University of Rochester, funded by NSF CHE-0650456 to the CENTC.

Electrochemical Measurements

Cyclic voltammetry and differential pulse voltammetry were performed in a nitrogen filled glovebox utilizing a Pine Research WaveNow[XV] potentiostat. The working electrode was a 3.0 mm glassy carbon electrode that was polished with an alumina slurry prior to being rinsed, dried, and taken into the glovebox. The counter electrode was a 0.5 mm diameter platinum wire. Measurements were made in anhydrous DMF from Sigma Aldrich which was opened and stored in a glovebox. All measurements were acquired at 32 °C.

2.4.2 Preparation of Starting Materials and Organometallic Complexes

2.4.2.1 Synthesis of Nitroarene Starting Materials

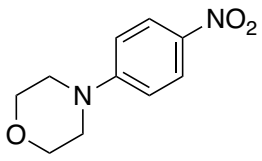

4-(4-nitrophenyl)morpholine (2.1e) was synthesized according to the literature procedure and characterization data matched those reported in the literature.[101]

^{1}H NMR (500 MHz, $CDCl_3$) δ 8.15 (d, *J* = 9.4 Hz, 2H), 6.84 (d, *J* = 9.4 Hz, 2H), 3.86 (dd, *J* = 5.9, 4.0 Hz, 4H), 3.37 (dd, *J* = 5.9, 4.0 Hz, 4H).

^{13}C{^{1}H} NMR (126 MHz, $CDCl_3$) δ 155.0, 139.1, 125.9, 112.7, 66.4, 47.2.

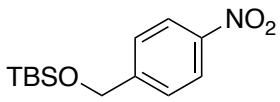

tert-butyldimethyl((4-nitrobenzyl)oxy)silane (2.1f) was synthesized according to the literature procedure and characterization data matched those reported in the literature.[102]

^{1}H NMR (500 MHz, $CDCl_3$) δ 8.15 (d, *J* = 9.0 Hz, 2H), 6.90 (d, *J* = 9.1 Hz, 2H), 1.00 (s, 9H), 0.26 (s, 6H).

^{13}C{^{1}H} NMR (126 MHz, $CDCl_3$) δ 161.6, 142.0, 125.8, 120.1, 25.5, -3.6, -4.4.

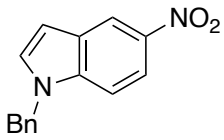

1-benzyl-5-nitro-1H-indole (2.1h)

To a 25 mL round-bottom flask was added 5-nitro-1*H*-indole (755.6 mg, 5.0 mmol), potassium carbonate (947.1 mg, 5.5 mmol), and DMF (6.7 mL). The flask was sealed with a rubber septum and the contents were heated to 100 °C. Benzyl bromide (891.4 mg, 5.5 mmol) was added dropwise through the septum. The reaction was stirred at 100 °C overnight, allowed to cool to rt, and was poured over 1 M HCl (25 mL). The mixture was extracted with ethyl acetate (3 × 20 mL). The combined organic layers were then washed

with water, saturated aq. $NaHCO_3$, and brine prior to being dried over Na_2SO_4. Following filtration and concentration, the resulting residue was purified by column chromatography (20 g of silica gel, 1 CV 5% EtOAc, then 5–25% EtOAc/hexanes across 15 CV) to yield **1h** (808.1 mg, 3.203 mmol, 64%, R_f = 0.275 in 10% EtOAc/hexanes) as a yellow solid. Characterization data matched those reported in the literature.[103]

^{1}H NMR (500 MHz, $CDCl_3$) δ 8.61 (d, *J* = 2.2 Hz, 1H), 8.08 (dd, *J* = 9.1, 2.3 Hz, 1H), 7.37 – 7.26 (m, 5H), 7.10 (dd, *J* = 8.0, 1.6 Hz, 2H), 6.73 (dd, *J* = 3.2, 0.8 Hz, 1H), 5.37 (s, 2H).

^{13}C{^{1}H} NMR (126 MHz, $CDCl_3$) δ 141.8, 139.1, 136.2, 131.4, 129.0, 128.1, 127.9, 126.7, 118.3, 117.5, 109.6, 104.4, 50.6.

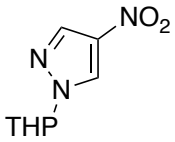

4-nitro-1-(tetrahydro-2H-pyran-2-yl)-1H-pyrazole (2.1k) was synthesized according to the literature procedure and characterization data matched those reported in the literature.[104]

^{1}H NMR (500 MHz, $CDCl_3$) δ 8.36 (s, 1H), 8.09 (s, 1H), 5.41 (dd, *J* = 9.1, 2.8 Hz, 1H), 4.15 – 4.01 (m, 1H), 3.73 (ddd, *J* = 11.6, 9.7, 3.7 Hz, 1H), 2.17 (ddd, *J* = 11.5, 5.8, 3.0 Hz, 1H), 2.06 – 1.93 (m, 2H), 1.86 – 1.61 (m, 3H).

^{13}C{^{1}H} NMR (126 MHz, $CDCl_3$) δ 135.5, 127.0, 88.4, 67.8, 30.7, 24.7, 21.6.

2.4.2.2 Synthesis of 1,1,2-Triarylhydrazine Byproduct

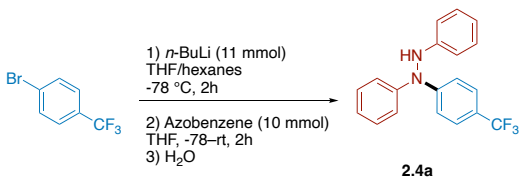

2.4a

1,2-diphenyl-1-(4-(trifluoromethyl)phenyl)hydrazine (2.4a) was prepared by the addition of 4-(trifluoromethyl)phenyl lithium to azobenzene.[105]

To an oven dried 50 mL round-bottom flask was added 4-bromobenzotrifluoride (2.48 g, 11.0 mmol). The flask was sealed with a rubber septum and purged with nitrogen. Anhydrous THF (10 mL) was added and the solution was cooled to -78° C. *n*-BuLi (1.6 M in hexanes, 7.5 mL) was added drop-wise at -78 °C over the course of 20 min. The reaction was stirred at -78° C for 2 h. Azobenzene (1.82 g, 10.0 mmol) was added to a separate oven-dried 100 mL round-bottom flask. The flask was sealed and purged with nitrogen for 5 min while stirring. Anhydrous THF (20 mL) was added to the flask and the solution was cooled to -78 °C. The solution of 4-(trifluoromethyl)phenyl lithium was then transferred to the solution of azobenzene drop-wise via cannula. After addition was complete, the reaction was stirred at -78 °C for 2 h, then was warmed slowly to rt, at which it was stirred for an additional 10 h. After stirring for 10 h, the mixture was poured over 100 mL of water, and extracted into ethyl acetate (3 × 75 mL). The combined organic layers were then washed with water, dried over anhydrous $MgSO_4$, filtered, and concentrated. The crude product was purified by column chromatography (80 g of silica, 1 CV hexanes, then 0-10% EtOAc/hexanes across 15 CV) to yield the product as a viscous orange liquid that crystallized upon standing in 20% yield (648.0 mg).

^{1}H NMR (500 MHz, $CDCl_3$) ^{1}H NMR (500 MHz, $CDCl_3$) δ 7.45 (d, *J* = 8.6 Hz, 2H), 7.32 (d, *J* = 4.2 Hz, 4H), 7.21 (dt, *J* = 8.4, 3.5 Hz, 4H), 7.12 (p, *J* = 4.4 Hz, 1H), 6.91 – 6.79 (m, 3H), 6.19 (s, 1H).

^{13}C{^{1}H} NMR (126 MHz, $CDCl_3$) δ 150.0, 146.8, 145.1, 129.6, 129.5, 126.4 (q, *J* = 3.8 Hz), 124.8, 124.5 (q, *J* = 271.0 Hz), 122.58 (q, *J* = 32.6 Hz), 121.9, 120.5, 115.9, 112.4.

$^{19}F\{^{1}H\}$ NMR (377 MHz, $CDCl_3$) δ -61.56.

HRMS-ESI (m/z): $[M-H]^-$ calcd for $C_{19}H_{14}F_3N_2^-$, 327.1115; found, 327.1116.

2.4.2.3 Synthesis of Palladium Complexes

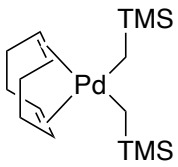

bis(trimethylsilylmethyl)-(cycloocta-1,5-diene) palladium(II) was synthesized according to the literature procedure and characterization data matched those reported in the literature.[106]

^{1}H NMR (500 MHz, C_6D_6) δ 5.15 (s, 4H), 2.02 – 1.74 (m, 8H), 0.78 (s, 4H), 0.35 (s, 16H).

$^{13}C\{^{1}H\}$ NMR (126 MHz, C_6D_6) δ 112.1, 29.2, 11.8, 3.9.

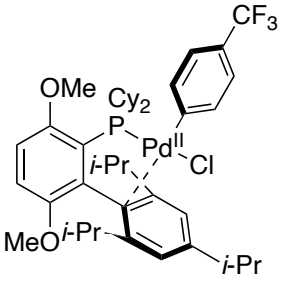

BrettPhos-(4-trifluoromethylphenyl)-chloro palladium(II) (2.II) was synthesized via modification of the literature procedure.[107]

In a nitrogen-filled glovebox, an oven-dried 20 mL vial equipped with a PTFE-coated stir bar was charged with bis(trimethylsilylmethyl)-(cycloocta-1,5-diene) palladium(II) (194.5 mg, 0.500 mmol, 1.00 equiv) and BrettPhos (268.4 mg, 0.500 mmol, 1.00 equiv). Anhydrous THF (5.00 mL) was added to the vial, followed by 4-chlorobenzotrifluoride

(90.3 mg, 0.500 mmol, 1.00 equiv). The vial was sealed with urea cap bearing a polyethylene conical seal. The reaction was stirred in the glovebox for 24 h. After stirring, the vial was removed from the glovebox and the solvent removed under reduced pressure. The resulting residue was resuspended in pentane, and the resulting suspension filtered. The resulting solid was triturated with pentane to yield the product (320.8 mg, 0.3894 mmol, 78% yield) as a light green solid.

^{1}H NMR (500 MHz, CD_2Cl_2, mixture of rotamers, 4.5:1 major/minor) δ 7.53 (d, *J* = 8.0 Hz, 2H, minor), 7.25 (d, *J* = 8.0 Hz, 2H, major), 7.13 (d, *J* = 7.95 Hz, major), 7.18 – 7.09 (m, 3H, minor), 7.09 – 7.06 (m, 2H), 6.95 – 6.85 (m, 2H, major), 4.33 (s, 3H, minor), 3.82 (s, 3H, major), 3.62 (s, 3H, minor), 3.37 (s, 3H, major), 3.02 (hept, *J* = 6.9 Hz, 1H, major), 2.94 (hept, *J* = 6.8 Hz, 1H, minor), 2.73 (qt, *J* = 11.9, 2.4 Hz, 2H, major), 2.52 (hept, *J* = 6.5 Hz, 2H, major), 2.36 (hept, *J* = 6.6 Hz, 2H, minor), 1.90 – 1.62 (m, 8H), 1.59 (d, *J* = 6.7 Hz, 6H, major), 1.51 – 1.42 (m, 1H), 1.36 (d, *J* = 6.9 Hz, 6H, major), 1.29 – 1.10 (m, 9H), 0.93 (d, *J* = 6.7 Hz, 6H, minor), 0.88 (dt, *J* = 12.8, 3.5 Hz, 2H, major), 0.83 (d, *J* = 6.7 Hz, 6H, major).

^{13}C{^{1}H} NMR (126 MHz, CD_2Cl_2) δ 157.2, 156.5, 154.8, 152.2, 152.0, 151.9, 149.1, 146.9, 138.1, 137.3, 133.1, 124.1, 122.2, 121.5, 113.6, 111.2, 111.0, 60.8, 54.8, 54.7, 54.3, 36.2, 36.0, 35.2, 35.0, 34.5, 34.3, 31.3, 30.8, 29.3, 27.8, 27.7, 27.5, 26.6, 26.5, 26.3, 26.2, 26.0, 25.2, 25.1, 24.4, 24.1, 23.7, 23.1.

^{19}F{^{1}H} NMR (377 MHz, CD_2Cl_2) δ -62.07, -62.27.

^{31}P{^{1}H} NMR (162 MHz, CD_2Cl_2) δ 47.24, 38.11.

HRMS-ESI (m/z): $[LPdAr]^+$ calcd for $C_{42}H_{57}F_3O_2PPd^+$, 787.3078; found, 787.3092.

Elemental Analysis: Anal. calcd for $C_{42}H_{57}F_3O_2PPd$: C, 61.24; H, 6.97. Found: C, 60.114; H, 6.601.

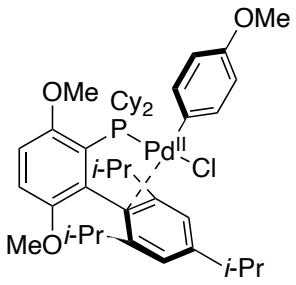

BrettPhos-(4-methoxyphenyl)-chloro palladium(II) (2.IIa) was synthesized via modification of the literature procedure.[107]

In a nitrogen-filled glovebox, an oven-dried 20 mL vial equipped with a PTFE-coated stir bar was charged with bis(trimethylsilylmethyl)-(cycloocta-1,5-diene) palladium(II) (389.0 mg, 1.000 mmol, 1.00 equiv) and BrettPhos (536.8 mg, 1.000 mmol, 1.00 equiv). Anhydrous THF (10.00 mL) was added to the vial, followed by 4-chloroanisole (178.2 mg, 1.250 mmol, 1.250 equiv). The vial was sealed with urea cap bearing a polyethylene conical seal. The reaction was stirred in the glovebox for 24 h. After stirring, the vial was removed from the glovebox and the solvent removed under reduced pressure. The resulting residue was resuspended in pentane, and the resulting suspension filtered. The resulting solid was triturated with pentane to yield the product (393.0 mg, 0.5000 mmol, 50% yield) as an ochre solid.

^{1}H NMR (500 MHz, $CDCl_3$, mixture of rotamers, 1.7:1 major/minor) δ 7.25 – 7.19 (d, 8.8 Hz, 2H, minor), 7.06 (s, 2H, major), 7.02 (d, *J* = 9.0 Hz, 1H, minor), 7.02 (s, 2H, minor), 6.97 (d, *J* = 9.1 Hz, 1H, minor), 6.92 (d, *J* = 7.0 Hz, 2H, major), 6.88 (d, *J* = 2.7 Hz, 1H, minor), 6.86 (d, *J* = 2.8 Hz, 1H, minor), 6.81 (d, *J* = 8.8 Hz, 1H, major), 6.61 (d, *J* = 8.5 Hz, 2H, minor), 6.56 (d, *J* = 8.6 Hz, 2H, major), 4.33 (s, 3H, minor), 3.82 (s, 3H, major), 3.69 (s, 3H, minor), 3.69 (s, 3H, major), 3.59 (s, 3H, minor), 3.37 (s, 3H, major), 3.02 (hept, *J* = 6.9 Hz, 1H, major), 2.92 (hept, *J* = 6.9 Hz, 1H, minor), 2.76 (q, *J* = 12.1 Hz, 2H, major), 2.49 (hept,

J = 6.7 Hz, 2H, major), 2.32 (hept, *J* = 6.7 Hz, 2H, minor), 1.93 – 1.82 (m, 3H), 1.81 – 1.62 (m, 6H), 1.59 (d, *J* = 6.7 Hz, 6H, major), 1.47 – 1.41 (m, 3H), 1.37 (d, *J* = 6.9 Hz, 6H, major), 1.26 (d, *J* = 7.0 Hz, 6H, minor), 1.24 (d, *J* = 7.0 Hz, 6H, minor), 1.21 – 1.09 (m, 2H), 0.99 (q, *J* = 12.6 Hz, 2H, major), 0.91 (d, *J* = 6.6 Hz, 6H, minor), 0.82 (d, *J* = 6.7 Hz, 6H, major), 0.61 (q, *J* = 13.0 Hz, 2H, minor).

^{13}C{^{1}H} NMR (126 MHz, $CDCl_3$, the spectrum is complicated due to the presence of rotamers and ^{31}P coupling) δ 156.8, 156.5, 156.4, 156.3, 154.6, 154.6, 153.9, 153.8, 152.1, 152.0, 151.2, 149.0, 146.7, 138.8, 138.7, 137.2, 137.2, 136.7, 136.6, 133.4, 130.3, 128.2, 125.7, 125.5, 124.1, 123.7, 121.3, 119.6, 118.8, 118.6, 117.1, 117.0, 113.1, 113.1, 113.0, 113.0, 113.0, 113.0, 110.8, 110.8, 110.6, 110.6, 68.0, 60.5, 55.2, 54.9, 54.6, 54.4, 36.1, 35.9, 35.2, 35.0, 34.5, 34.3, 31.3, 30.8, 30.7, 29.4, 27.9, 27.8, 27.7, 26.7, 26.6, 26.4, 26.3, 26.1, 26.1, 25.4, 25.3, 25.3, 25.3, 24.7, 24.5, 24.0, 23.3.

^{31}P{^{1}H} NMR (162 MHz, $CDCl_3$) δ 47.05, 38.18.

HRMS-ESI (m/z): $[LPdAr]^+$ calcd for $C_{42}H_{60}O_3PPd^+$, 748.3325; found, 748.3327.

2.4.3 Additional Control and Deviation from Standard Conditions Experiments

Figure 2.1 Timecourse of Optimized Reaction

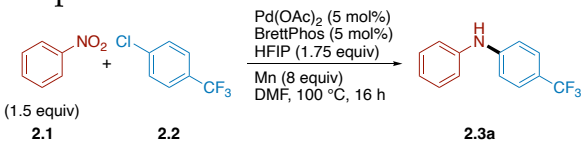

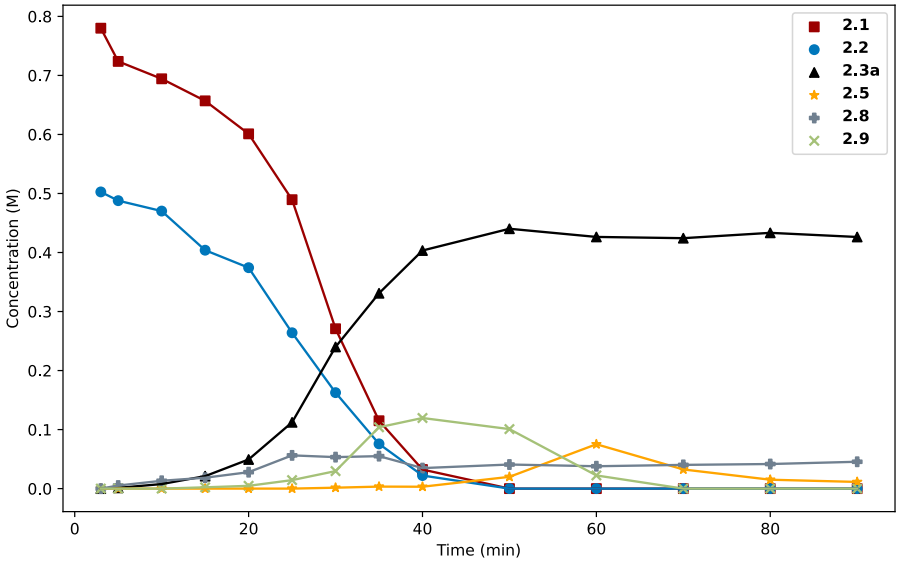

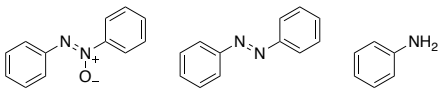

In a nitrogen-filled glovebox, an oven-dried 1 dram vial equipped with a PTFE-coated stir bar was charged with palladium(II) acetate (5.6 mg, 0.025 mmol, 0.050 equiv), BrettPhos (13.4 mg, 0.0250 mmol, 0.0500 equiv), 1,3,5-trimethoxybenzene (30.0 mg, 0.178 mmol, as an internal standard), and manganese (219.8 mg, 4.000 mmol, 8.000 equiv). DMF (1.000 mL) was added to the vial, followed by nitrobenzene (66.7 μL, 92.3 mg, 0.750 mmol, 1.50 equiv), and 4-chlorobenzotrifluoride (76.9 μL, 90.3 mg, 0.500 mmol, 1.00 equiv). The vial was sealed with a Thermo Scientific Mininert valve with an auxiliary rubber septum. The reaction was removed from the glovebox and HFIP (91.9 μL, 147.0 mg, 0.8750 mmol, 1.750 equiv) was added through the valve via gas-tight syringe. The reaction was then placed on a pre-heated stir plate where it was stirred (100 °C, 1250 rpm).

Aliquots were taken from the ongoing reaction, while stirring, by opening the valve and withdrawing 10 μL of the reaction mixture via gas-tight syringe. The aliquots were

immediately quenched in 1.0 mL of 0.1 M citric acid and extracted into 1.5 mL of diethyl ether. The organic layer was then passed through a short (1.5 cm in a pipette) silica plug. Samples were analyzed by SFC-MS and GC-FID to determine the concentration of each reagent using 1,3,5-trimethoxybenzene as an internal standard.

While omitted from the graph for clarity, we also observe slow—7.5×10^{-4} M/min—formation of 4% of 4,4′-bis(trifluoromethyl)biphenyl over the first 30 min of the reaction. We hypothesize that this and $MnCl_2$ are byproducts of necessary decomposition of **2.II** that enables the initiation of nitroarene reduction.

Figure 2.2. Omission Control Experiments

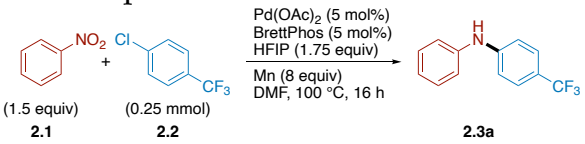

Entry	Omission	Yield (%)
1	None	92
2	$Pd(OAc)_2$	0
3	BrettPhos	0
4	HFIP	0
5	Mn	0

Procedure for the standard conditions: In a nitrogen-filled glovebox, an oven-dried 1 dram vial equipped with a PTFE-coated stir bar was charged with palladium(II) acetate (2.8 mg, 0.015 mmol, 0.050 equiv), BrettPhos (6.7 mg, 0.0125 mmol, 0.050 equiv), 1,3,5-trimethoxybenzene (15.0 mg, 0.0892 mmol, as an internal standard), and manganese (109.9 mg, 2.000 mmol, 8.000 equiv). DMF (500 μL) was added to the vial, followed by nitrobenzene (38.5 μL, 46.1 mg, 0.375 mmol, 1.50 equiv), and 4-chlorobenzotrifluoride (33.4 μL, 45.1 mg, 0.250 mmol, 1.00 equiv). The vial was sealed with a phenolic screw cap bearing a PTFE-backed silicone septum and removed from the glovebox. HFIP (45.9 μL, 73.5 mg, 0.4375 mmol, 1.75 equiv) was added to the vial through the septum via gas-tight

syringe. The reaction was placed on a pre-heated stir plate where it was stirred (100 °C, 1250 rpm) for 16 h.

After stirring, a 30 μL aliquot was taken from the reaction via gas-tight syringe. The aliquot was immediately quenched in 1.0 mL of 0.1 M citric acid and extracted into 1.5 mL of diethyl ether. The organic layer was then passed through a short (1.5 cm in a pipette) silica plug. Samples were analyzed by SFC-MS to determine the concentration of **2.3a** using 1,3,5-trimethoxybenzene as an internal standard.

Figure 2.3. Effects of Deviation from Standard Conditions

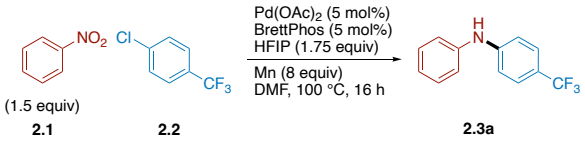

Entry	Deviation	Yield (%)
1	none	92
2	$PdCl_2$ instead of $Pd(OAc)_2$	81
3	$Pd_2(dba)_3$ instead of $Pd(OAc)_2$	87
4	XPhos instead of BrettPhos	86
5	*rac*-BINAP instead of BrettPhos	1
6	TFE instead of HFIP	9
7	2-butanol instead of HFIP	29
8	6.0 equiv of Mn	91
9	Zn instead of Mn	89
10	DMA instead of DMF	85
11	80 °C	79

Procedure for the standard conditions: In a nitrogen-filled glovebox, an oven-dried 1 dram vial equipped with a PTFE-coated stir bar was charged with palladium(II) acetate (2.8 mg, 0.0125 mmol, 0.05 equiv), BrettPhos (6.7 mg, 0.0125 mmol, 0.05 equiv), 1,3,5-trimethoxybenzene (15.0 mg, 0.0892 mmol, as an internal standard), and manganese (109.9 mg, 2.000 mmol, 8.00 equiv). DMF (500 μL) was added to the vial, followed by nitrobenzene (38.5 μL, 46.1 mg, 0.375 mmol, 1.50 equiv), and 4-chlorobenzotrifluoride (33.4 μL, 45.1 mg, 0.250 mmol, 1.00 equiv). The vial was sealed with a phenolic screw cap bearing a PTFE-backed silicone septum and removed from the glovebox. HFIP (45.9 μL,

73.5 mg, 0.4375 mmol, 1.75 equiv) was added to the vial through the septum via gas-tight syringe. The reaction was placed on a pre-heated stir plate where it was stirred (100 °C, 1250 rpm) for 16 h.

After stirring, a 30 μL aliquot was taken from the reaction via gas-tight syringe. The aliquot was immediately quenched in 1.0 mL of 0.1 M citric acid and extracted into 1.5 mL of diethyl ether. The organic layer was then passed through a short (1.5 cm in a pipette) silica plug. Samples were analyzed by SFC-MS to determine the concentration of **2.3a** using 1,3,5-trimethoxybenzene as an internal standard.

Deviations were made by employing: palladium(II) chloride (2.2 mg, 0.0125 mmol, 0.05 equiv, Figure 2.3 Entry 2) in place of palladium(II) acetate; tris(dibenzylideneacetone)dipalladium(0) (5.7 mg, 0.0063 mmol, 0.025 equiv, Figure 2.3 Entry 3) in place of palladium(II) acetate; XPhos (6.0 mg, 0.0125 mmol, 0.05 equiv, Figure 2.3 Entry 4) in place of BrettPhos; *rac*-BINAP (7.8 mg, 0.0125 mmol, 0.05 equiv, Figure 2.3 Entry 5) in place of BrettPhos; 2,2,2-trifluoroethanol (31.5 μL, 43.8 mg, 0.4375 mmol, 1.75 equiv, Figure 2.3 Entry 6) in place of HFIP; 2-butanol (40.2 μL, 32.4 mg, 0.4375 mmol, 1.75 equiv, Figure 2.3 Entry 7) in place of HFIP; 6 equiv of manganese (82.4 mg, 1.500 mmol, Figure 2.3 Entry 8) instead of 8 equiv; zinc flake (130.8 mg, 2.000 mmol, 8.00 equiv, Figure 2.3 Entry 9) in place of manganese; DMA (500 μL, Figure 2.3 Entry 10) in place of DMF; or heating the reaction to 80 °C (Figure 2.3 Entry 11) instead of 100 °C.

Figure 2.4. Effects of Decreased Catalyst Loading

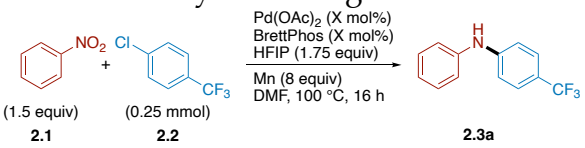

Entry	X mol%	Yield (%)
1	1	31
2	1[a]	36
3	2	90
4	5	92

[a]The palladium precatalyst and ligand were pre-stirred to ensure ligation.

Procedure for catalyst screening: In a nitrogen-filled glovebox, oven-dried 1 dram vials equipped with PTFE-coated stir bars were charged with palladium(II) acetate (0.6 mg, 0.0025 mmol, 0.01 equiv, Figure 2.4 Entry 1; 1.1 mg, 0.0050 mmol, 0.02 equiv, Figure 2.4 Entry 3; 2.8 mg, 0.0125 mmol, 0.05 equiv, Figure 2.4 Entry 4), BrettPhos (1.3 mg, 0.0025 mmol, 0.01 equiv, Figure 2.4 Entry 1; 2.7 mg, 0.005 mmol, 0.02 equiv, Figure 2.4 Entry 3; 6.7 mg, 0.0125 mmol, 0.05 equiv, Figure 2.4 Entry 4), 1,3,5-trimethoxybenzene (15.0 mg, 0.0892 mmol, as an internal standard), and manganese (109.9 mg, 2.000 mmol, 8.00 equiv). DMF (500 μL) was added to the vials, followed by nitrobenzene (38.5 μL, 46.1 mg, 0.375 mmol, 1.50 equiv), and 4-chlorobenzotrifluoride (33.4 μL, 45.1 mg, 0.250 mmol, 1.00 equiv). The vials were sealed with phenolic screw caps bearing PTFE-backed silicone septa and were removed from the glovebox. HFIP (45.9 μL, 73.5 mg, 0.4375 mmol, 1.75 equiv) was added to the vials through the septa via gas-tight syringe. The reactions were placed on a pre-heated stir plate where they were stirred (100 °C, 1250 rpm) for 16 h.

For Figure 2.4 Entry 2, an oven-dried 1 dram vial equipped with a PTFE-coated stir bar was charged with palladium(II) acetate (0.6 mg, 0.0025 mmol, 0.01 equiv, Figure 2.4 Entry 2), BrettPhos (1.3 mg, 0.0025 mmol, 0.01 equiv, Figure 2.4 Entry 2), and 1,3,5-trimethoxybenzene (15.0 mg, 0.0892 mmol, as an internal standard). DMF was added to the vial and the contents were stirred for 15 min at rt. Nitrobenzene (38.5 μL, 46.1 mg,

0.375 mmol, 1.50 equiv), 4-chlorobenzotrifluoride (33.4 µL, 45.1 mg, 0.250 mmol, 1.00 equiv), and manganese (109.9 mg, 2.000 mmol, 8.00 equiv) were added to the vial prior to it being sealed with a phenolic screwcap bearing a PTFE-backed silicone septum. The vial was then removed from the glovebox and HFIP(45.9 µL, 73.5 mg, 0.4375 mmol, 1.75 equiv) was added to the vial through the septum via gas-tight syringe. The reaction was placed on a pre-heated stir plate where it was stirred (100 °C, 1250 rpm) for 16 h.

After stirring, a 30 µL aliquot was taken from each reaction via gas-tight syringe. The aliquots were immediately quenched in 1.0 mL of 0.1 M citric acid and extracted into 1.5 mL of diethyl ether. The organic layers were then passed through a short (1.5 cm in a pipette) silica plug. Samples were analyzed by SFC-MS to determine the concentration of **2.3a** using 1,3,5-trimethoxybenzene as an internal standard.

Figure 2.5. Effects of Using a Palladacycle Precatalyst

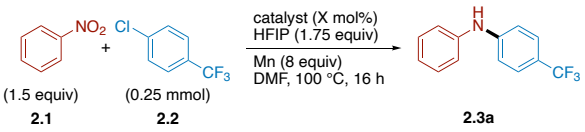

Entry	Catalyst	X mol%	Yield (%)
1	$Pd(OAc)_2$/BrettPhos	5	92
2	BrettPhos Pd G3	1	76
3	BrettPhos Pd G3	5	92

Procedure for catalyst screening: In a nitrogen-filled glovebox, oven-dried 1 dram vials equipped with PTFE-coated stir bars were charged with either palladium(II) acetate (2.8 mg, 0.0125 mmol, 0.05 equiv, Entry 1) and BrettPhos (6.7 mg, 0.0125 mmol, 0.05 equiv, Figure 2.5 Entry 1), or BrettPhos Pd G3 (2.3 mg, 0.0025 mmol, 0.01 equiv, Figure 2.5 Entry 2; 11.3 mg, 0.0125 mmol, 0.05 equiv, Figure 2.5 Entry 3). The vials were then charged with 1,3,5-trimethoxybenzene (15.0 mg, 0.0892 mmol, as an internal standard) and manganese (109.9 mg, 2.000 mmol, 8.00 equiv). DMF (500 µL) was added to the vials, followed by nitrobenzene (38.5 µL, 46.1 mg, 0.375 mmol, 1.50 equiv) and 4-chlorobenzotrifluoride

(33.4 μL, 45.1 mg, 0.250 mmol, 1.00 equiv). The vials were sealed with phenolic screw caps bearing PTFE-backed silicone septa and were removed from the glovebox. HFIP (45.9 μL, 73.5 mg, 0.4375 mmol, 1.75 equiv) was added to the vials through the septa via gas-tight syringe. The reactions were placed on a pre-heated stir plate where they were stirred (100 °C, 1250 rpm) for 16 h.

After stirring, a 30 μL aliquot was taken from each reaction via gas-tight syringe. The aliquots were immediately quenched in 1.0 mL of 0.1 M citric acid and extracted into 1.5 mL of diethyl ether. The organic layers were then passed through a short (1.5 cm in a pipette) silica plug. Samples were analyzed by SFC-MS to determine the concentration of **2.3a** using 1,3,5-trimethoxybenzene as an internal standard.

These results demonstrate that Buchwald palladacycle precatalysts can be utilized under these conditions despite the lack of a strong base. As shown in Figure 2.5 Entry 2, the reliable ligation and speciation afforded by these catalysts may be useful when lower catalyst loadings are necessary, such as during large scale reactions.

Figure 2.6. Water and Air Tolerance on the Benchtop

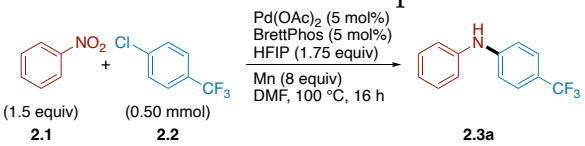

Entry	Setup	Yield (%)
1	Rigorously anhydrous and air free	99[a]
2	Sparged, wet solvent and nitrogen headspace	87[b]
3	Wet solvent and air headspace	90[c]

Manganese was stored in a vial on the benchtop for over 2 years. [a]Anhydrous DMF was sourced from Sigma Aldrich in a Sure/Seal™ bottle. [b]DMF from a 4-liter bottle was sparged for 30 min while sonicating. [c]DMF was sourced from a 4-liter bottle stored on the bench.

Setup for Figure 2.6 Entry 1: An oven-dried 1 dram vial equipped with a PTFE-coated stir bar was charged with palladium(II) acetate (5.6 mg, 0.025 mmol, 0.05 equiv), BrettPhos (13.4 mg, 0.025 mmol, 0.05 equiv), 1,3,5-trimethoxybenzene (30.0 mg, 0.178

mmol, as an internal standard), and manganese (219.8 mg, 4.000 mmol, 8.00 equiv). The vial was sealed with a phenolic screw cap bearing a PTFE-backed silicone septum and connected to a nitrogen manifold and a bubbler. The flask was purged with nitrogen for 5 min. The bubbler was disconnected prior to anhydrous DMF (1.000 mL) being added to the vial using air-free technique. Nitrobenzene (66.7 μL, 92.3 mg, 0.750 mmol, 1.50 equiv), 4-chlorobenzotrifluoride (76.9 μL, 90.3 mg, 0.500 mmol, 1.00 equiv), and HFIP (91.9 μL, 147.0 mg, 0.8750 mmol, 1.75 equiv) were added through the septum under positive pressure of nitrogen via gas-tight syringe. The vial was disconnected from the manifold and placed on a pre-heated stir plate where it was stirred (100 °C, 1250 rpm) for 16 h.

Setup for Figure 2.6 Entry 2: A 1 dram vial equipped with a PTFE-coated stir bar was charged with palladium(II) acetate (5.6 mg, 0.025 mmol, 0.05 equiv), BrettPhos (13.4 mg, 0.025 mmol, 0.05 equiv), 1,3,5-trimethoxybenzene (30.0 mg, 0.178 mmol, as an internal standard), and manganese (219.8 mg, 4.000 mmol, 8.00 equiv). The vial was sealed with a phenolic screw cap bearing a PTFE-backed silicone septum and connected to a nitrogen manifold and a bubbler. The flask was purged with nitrogen for 5 min. The bubbler was disconnected prior to sparged, wet DMF (1.000 mL) being added to the vial. Nitrobenzene (66.7 μL, 92.3 mg, 0.750 mmol, 1.50 equiv), 4-chlorobenzotrifluoride (76.9 μL, 90.3 mg, 0.500 mmol, 1.00 equiv), and HFIP (91.9 μL, 147.0 mg, 0.8750 mmol, 1.75 equiv) were added through the septum under positive pressure of nitrogen via gas-tight syringe. The vial was disconnected from the manifold and placed on a pre-heated stir plate where it was stirred (100 °C, 1250 rpm) for 16 h.

Setup for Figure 2.6 Entry 3: A 1 dram vial equipped with a PTFE-coated stir bar was charged with palladium(II) acetate (5.6 mg, 0.025 mmol, 0.05 equiv), BrettPhos (13.4 mg,

0.025 mmol, 0.05 equiv), 1,3,5-trimethoxybenzene (30.0 mg, 0.178 mmol, as an internal standard), and manganese (219.8 mg, 4.000 mmol, 8.00 equiv). DMF (1.000 mL) was added to the vial, followed by nitrobenzene (66.7 μL, 92.3 mg, 0.750 mmol, 1.50 equiv), 4-chlorobenzotrifluoride (76.9 μL, 90.3 mg, 0.500 mmol, 1.00 equiv). The vial was sealed with a phenolic screw cap bearing a PTFE-backed silicone septum. HFIP (91.9 μL, 147.0 mg, 0.8750 mmol, 1.75 equiv) was added through the septum via syringe. The vial was then placed on a pre-heated stir plate where it was stirred (100 °C, 1250 rpm) for 16 h.

After stirring, a 30 μL aliquot was taken from each reaction via gas-tight syringe. The aliquots were immediately quenched in 1.0 mL of 0.1 M citric acid and extracted into 1.5 mL of diethyl ether. The organic layers were then passed through a short (1.5 cm in a pipette) silica plug. Samples were analyzed by SFC-MS to determine the concentration of **2.3a** using 1,3,5-trimethoxybenzene as an internal standard.

These results demonstrate that the optimized reaction conditions are tolerant of both wet solvent and an ambient air headspace (2.5:1 ratio of headspace to reaction volume). We hypothesize that the excess reductant in the system ensures that the catalyst remains on cycle, even in the presence of oxygen. While we chose to proceed using rigorous anhydrous and air-free techniques to avoid any inconsistency in reactivity, we expect that they are not necessary in most cases.

2.4.4 Nitroarene Reduction Studies

Figure 2.7. Effects of Different Catalyst Types on Nitroarene Reduction

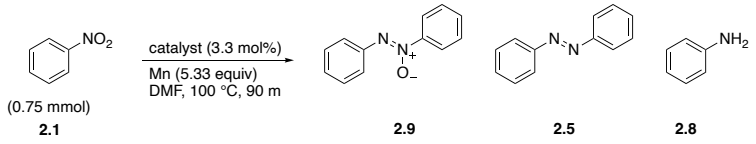

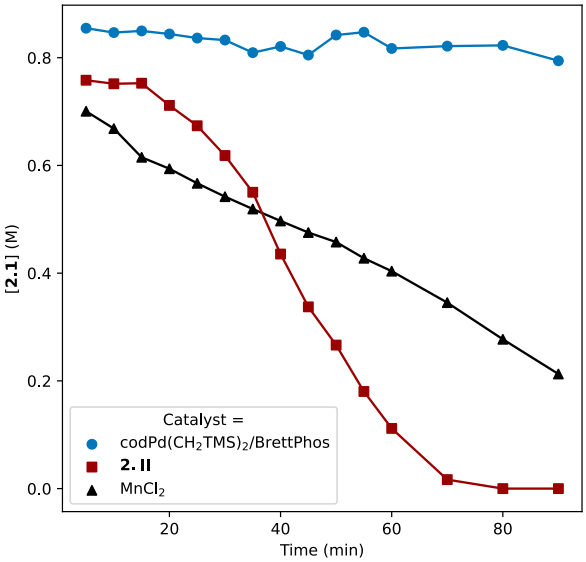

In a nitrogen-filled glovebox, three oven-dried 1 dram vials, each equipped with a PTFE-coated stir bar, were charged with the appropriate catalyst or mixture—bis(trimethylsilylmethyl)-(cycloocta-1,5-diene) palladium(II) (9.7 mg, 0.025 mmol, 0.033 equiv) and BrettPhos (13.4 mg, 0.025 mmol, 0.033 equiv), **2.II** (20.6 mg, 0.025 mmol, 0.033 equiv) or manganese(II) chloride (3.1 mg, 0.025 mmol, 0.033 equiv)—1,3,5-trimethoxybenzene (30.0 mg, 0.178 mmol, as an internal standard), and manganese (219.8 mg, 4.000 mmol, 5.33 equiv). DMF (1.000 mL) was added to each vial, followed by nitrobenzene (66.7 µL, 92.3 mg, 0.750 mmol, 1.00 equiv). The vials were sealed with Thermo Scientific Mininert valve screw caps with auxiliary rubber septa. The reactions were removed from the glovebox and placed on a pre-heated stir plate where they were stirred (100 °C, 1250 rpm) for 90 min.

Aliquots were taken from the ongoing reactions, while stirring, by opening the valve and withdrawing 10 µL of the reaction mixture via gas-tight syringe. The aliquots were immediately quenched in 1.0 mL of 0.1 M citric acid and extracted into 1.5 mL of diethyl ether. The organic layer was then passed through a short (1.5 cm in a pipette) silica plug.

Samples were analyzed by SFC-MS to determine the concentration of nitrobenzene using 1,3,5-trimethoxybenzene as an internal standard.

Figure 2.8 Effects of Catalyst Loading on Nitroarene Reduction

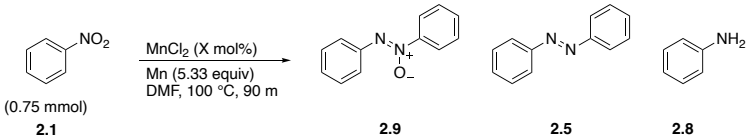

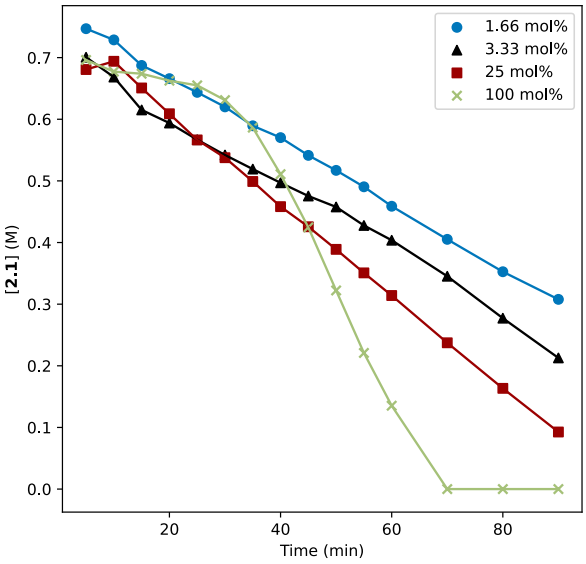

In a nitrogen-filled glovebox, four oven-dried 1 dram vials, each equipped with a PTFE-coated stir bar, were charged with the appropriate amount of manganese(II) chloride (1.6 mg, 0.0125 mmol, 0.0167 equiv; 3.1 mg, 0.025 mmol, 0.033 equiv; 23.6 mg, 0.1875 mmol, 0.25 equiv; 94.4 mg, 0.750 mmol, 1.00 equiv), 1,3,5-trimethoxybenzene (30.0 mg, 0.178 mmol, as an internal standard), and manganese (219.8 mg, 4.000 mmol, 5.33 equiv). DMF (1.000 mL) was added to each vial, followed by nitrobenzene (66.7 μL, 92.3 mg, 0.750 mmol, 1.00 equiv). The vials were sealed with Thermo Scientific Mininert screw caps with auxiliary rubber septa. The reactions were removed from the glovebox and placed on a pre-heated stir plate where they were stirred (100 °C, 1250 rpm) for 90 min.

Aliquots were taken from the ongoing reactions, while stirring, by opening the valve and withdrawing 10 μL of the reaction mixture via gas-tight syringe. The aliquots were immediately quenched in 1.0 mL of 0.1 M citric acid and extracted into 1.5 mL of diethyl ether. The organic layer was then passed through a short (1.5 cm in a pipette) silica plug. Samples were analyzed by SFC-MS to determine the concentration of nitrobenzene using 1,3,5-trimethoxybenzene as an internal standard.

These results demonstrate a positive kinetic order in manganese(II) chloride, which explains the autocatalysis observed in Figure 2.1. We do not fully understand the induction period observed when using stoichiometric manganese(II) chloride. However inhibition of reduction at zinc surfaces has been observed in the presence of stoichiometric zinc(II) chloride.[108]

Figure 2.9. Products of Nitroarene Reduction

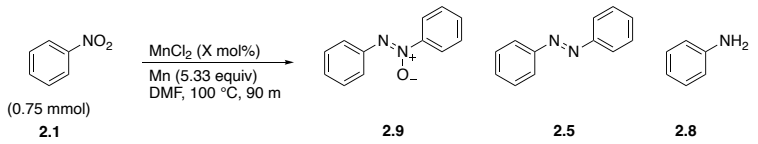

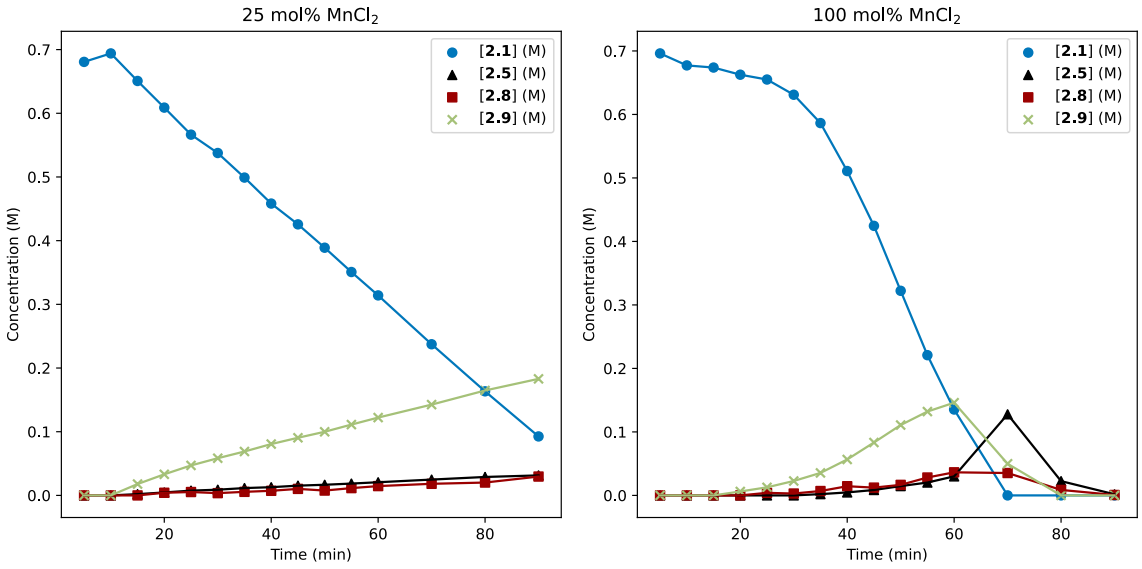

In a nitrogen-filled glovebox, two oven-dried 1 dram vials, each equipped with a PTFE-coated stir bar, were charged with an appropriate amount of manganese(II) chloride (23.6 mg, 0.1875 mmol, 0.250 equiv, left graph; 94.4 mg, 0.750 mmol, 1.00 equiv, right graph), 1,3,5-trimethoxybenzene (30.0 mg, 0.178 mmol, as an internal standard), and manganese (219.8 mg, 4.000 mmol, 5.33 equiv). DMF (1.000 mL) was added to each vial, followed by nitrobenzene (66.7 μL, 92.3 mg, 0.750 mmol, 1.00 equiv). The vials were sealed with Thermo Scientific Mininert screw caps with auxiliary rubber septa. The reactions were removed from the glovebox and placed on a pre-heated stir plate where they were stirred (100 °C, 1250 rpm) for 90 min.

Aliquots were taken from the ongoing reactions, while stirring, by opening the valve and withdrawing 10 μL of the reaction mixture via gas-tight syringe. The aliquots were immediately quenched in 1.0 mL of 0.1 M citric acid and extracted into 1.5 mL of diethyl ether. The organic layer was then passed through a short (1.5 cm in a pipette) silica plug. Samples were analyzed by SFC-MS to determine the concentration of each reagent using 1,3,5-trimethoxybenzene as an internal standard.

The mass balance of reductions is typically high (80%) until only azobenzene (**2.5**) remains, at which point reduction to hydrazobenzene (**2.10**) occurs. **2.10** is not observed in catalytic arylation reactions and is most likely not a productive intermediate (Figure 2.17). We found the concentration of **2.10** difficult to track in the presence of other reduced intermediates; as such it is not pictured here.

Figure 2.10. Effects of Various Chloride Salts on Nitroarene Reduction

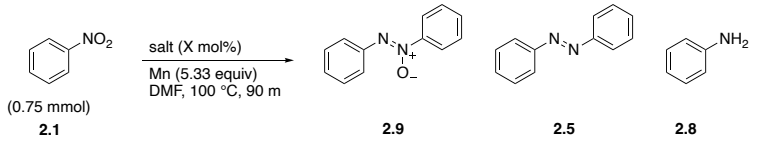

Entry	Catalyst	X mol%	Recovered **2.1** (mmol)
1	$MnCl_2$	3.3	0.22
2	LiCl	6.7	0.17
3	NaCl	6.7	0.40
4	n-Bu_4NCl	6.7	0.66
5	none	none	0.74[a]

[a]No products of reduction were observed.

In a nitrogen-filled glovebox, four oven-dried 1 dram vials, each equipped with a PTFE-coated stir bar, were charged with one of: manganese(II) chloride (3.1 mg, 0.025 mmol, 0.033 equiv, Figure 2.10 Entry 1), lithium chloride (2.1 mg, 0.050 mmol, 0.067 equiv, Figure 2.10 Entry 2), sodium chloride (2.9 mg, 0.050 mmol, 0.067 equiv, Figure 2.10 Entry 3), or tetrabutylammonium chloride (14.0 mg, 0.050 mmol, 0.067 equiv, Figure 2.10 Entry 4). 1,3,5-trimethoxybenzene (30.0 mg, 0.178 mmol, as an internal standard) and manganese (219.8 mg, 4.000 mmol, 5.33 equiv) were added to each vial. DMF (1.000 mL) was then added, followed by nitrobenzene (66.7 μL, 92.3 mg, 0.750 mmol, 1.00 equiv). The vials were sealed with phenolic screw caps bearing PTFE-backed silicone septa. The reactions were removed from the glovebox and placed on a pre-heated stir plate where they were stirred (100 °C, 1250 rpm) for 90 min.

After stirring, a 30 μL aliquot was taken from each reaction via gas-tight syringe. The aliquots were immediately quenched in 1.0 mL of 0.1 M citric acid and extracted into 1.5 mL of diethyl ether. The organic layers were then passed through a short (1.5 cm in a pipette) silica plug. Samples were analyzed by SFC-MS to determine the concentration of each reagent using 1,3,5-trimethoxybenzene as an internal standard.

Figure 2.11. Effects of Alcohol Additive and Arene Electronics on the Induction Period of Nitrobenzene Reduction

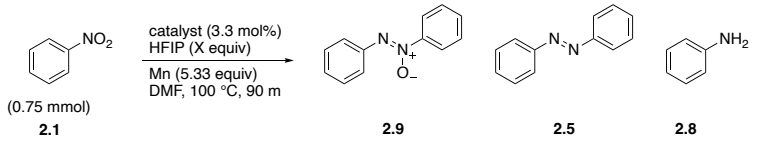

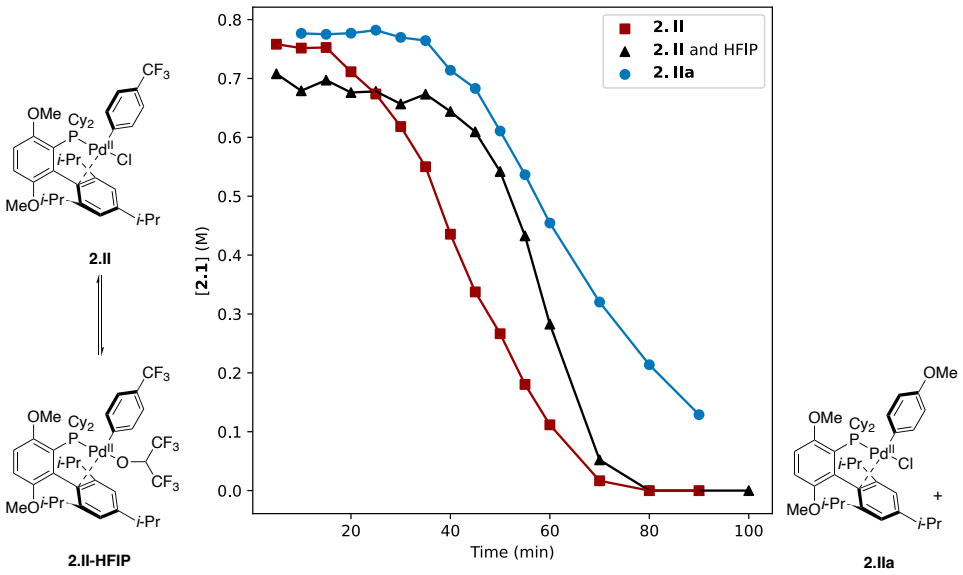

In a nitrogen-filled glovebox, three oven-dried 1 dram vials, each equipped with a PTFE-coated stir bar, were charged with the appropriate catalyst—**2.II** (20.6 mg, 0.025 mmol, 0.033 equiv) or **2.IIa** (19.6 mg, 0.025 mmol, 0.033 equiv)—1,3,5-trimethoxybenzene (30.0 mg, 0.178 mmol, as an internal standard), and manganese (219.8 mg, 4.000 mmol, 5.33 equiv). DMF (1.000 mL) was added to each vial, followed by nitrobenzene (66.7 μL, 92.3 mg, 0.750 mmol, 1.00 equiv). The vials were sealed with Thermo Scientific Mininert screw caps with auxiliary rubber septa. The reactions were removed from the glovebox and HFIP (91.9 μL, 147.0 mg, 0.8750 mmol, 1.17 equiv) was added to one reaction containing **2.II** through the valve via gas-tight syringe. The vials were then placed on a pre-heated stir plate where they were stirred at 100 ° C and 1250 rpm.

Aliquots were taken from the ongoing reactions, while stirring, by opening the valve and withdrawing 10 μL of the reaction mixture via gas-tight syringe. The aliquots were immediately quenched in 1.0 mL of 0.1 M citric acid and extracted into 1.5 mL of diethyl ether. The organic layer was then passed through a short (1.5 cm in a pipette) silica plug.

Samples were analyzed by SFC-MS to determine the concentration of nitrobenzene using 1,3,5-trimethoxybenzene as an internal standard.

The extended induction period observed when nitrobenzene (**2.1**) is reduced in the presence of **2.II** and HFIP may suggests that the addition of an alcohol extends the lifetime of **2.II** under reducing conditions, delaying the formation of $MnCl_2$, the presumed active reduction catalyst. It is unclear if this extension is due to association of neutral HFIP to **2.II** or if anionic hexafluoroisopropoxide is formed via reaction of HFIP with either Mn^0 or trace MnO on the surface of the reductant. We hypothesize that formation of larger amounts of alkoxides throughout the course of catalytic arylation reactions leads to accessible palladium(II) alkoxide (**2.II-HFIP**). Similarly, an extended induction period is observed with an electron-rich oxidative addition complex **2.IIa** is used. This may explain the lower overall reactivity of electron-rich chloroarenes, as initiation to the catalytic cycle may be delayed, and the lower Lewis acidity of the intermediate **2.IIa** may make association of the intermediate 1,1,2-triarylhydrazine sluggish.

2.4.5 Studies on the Mechanism of *N*-Arylation

Figure 2.12. Competition Experiments between Anilines and Azobenzene

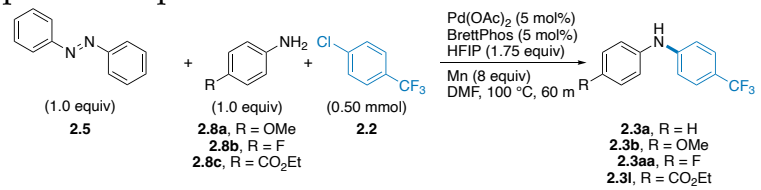

Entry	Aniline Derivative	**2.3a** (%)	**2.3b**, **2.3aa**, or **2.3l** (%)
1	8a	11	81
2	8b	7	91
3	8c	13	89

In a nitrogen-filled glovebox, three oven-dried 1 dram vials, equipped with PTFE-coated stir bars, were charged with palladium(II) acetate (5.6 mg, 0.0250 mmol, 0.05 equiv), BrettPhos (13.4 mg, 0.0250 mmol, 0.05 equiv), the appropriate aniline—*p*-anisidine (61.6 mg, 0.500 mmol, 1.00 equiv, Figure 2.12 Entry 1), 4-fluoroaniline (47.5 μL, 55.6 mg, 0.500 mmol, 1.00 equiv, Figure 2.12 Entry 2), or benzocaine (82.6 mg, 0.500 mmol, 1.00 equiv, Figure 2.12 Entry 3)—azobenzene (91.1 mg, 0.500 mmol, 1.00 equiv), and manganese (219.8 mg, 4.000 mmol, 8.00 equiv). DMF (1.000 mL) was added to the vials, followed by 4-chlorobenzotrifluoride (76.9 μL, 90.3 mg, 0.500 mmol, 1.00 equiv) and 1,3-bis(trifluoromethyl)benzene (38.8 μL, 53.5 mg, 0.250 mmol, 0.50 equiv, as an internal standard). The vials were then sealed with Thermo Scientific Mininert screw caps with auxiliary rubber septa. The reactions were removed from the glovebox and HFIP (91.9 μL, 147.0 mg, 0.8750 mmol, 1.75 equiv) was added to each through the valve via gas-tight syringe. The reactions were then placed on a pre-heated stir plate (100 °C, 1250 rpm).

Aliquots were taken from the ongoing reaction, while stirring, by opening the valve and withdrawing 50 μL of the reaction mixture via gas-tight syringe. The aliquots were immediately quenched in 1.0 mL of 0.1 M citric acid and extracted into 1.0 mL of diethyl ether. The organic layer was then passed through a short (1.5 cm in a pipette) silica plug. Samples were analyzed by ^{19}F NMR (10 second relaxation delay) to determine the concentration of the possible arylation products using 1,3-bis(trifluoromethyl)benzene as an internal standard.

These experiments show that when present in high concentrations, aniline derivatives are selectively arylated in the presence of azobenzene. Notably, this selectivity is not affected by the electron-density of the aniline derivative. As a result, the arylation of the electron-poor aniline derivative **2.8c** occurs in high yield, contrasting the low yield

observed for the arylation of the corresponding nitroarene (29% vide infra). This suggests that aniline arylation occurs via a different mechanism than nitroarene arylation. We hypothesize that the observed selectivity is mainly due to the preferential association of the aniline nitrogen compared to the azobenzene nitrogen to the oxidative addition complex **2.II**.

Figure 2.13. Investigation of the Feasibility of Nitrogenous Coupling Partners

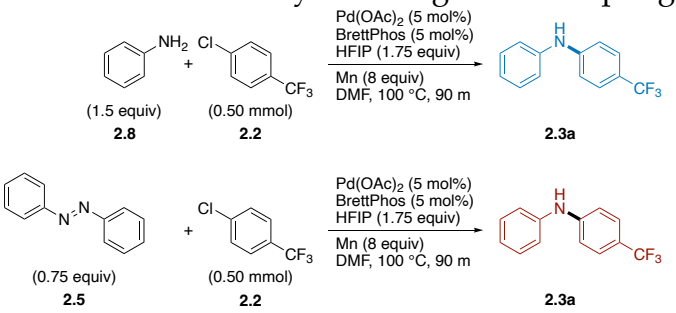

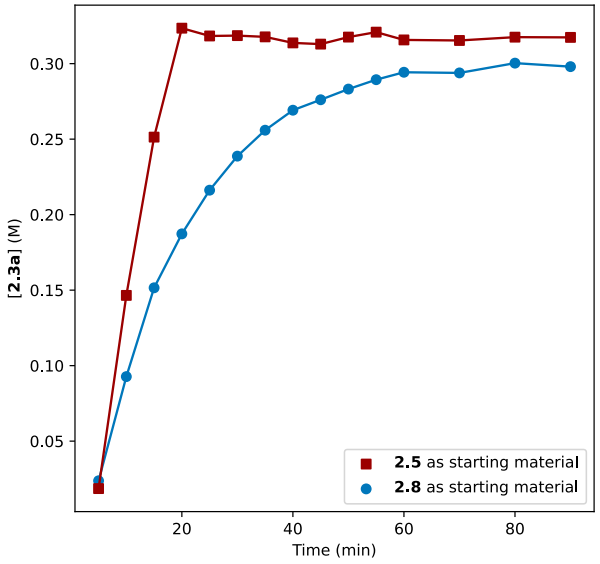

In a nitrogen-filled glovebox, two oven-dried 1 dram vials, equipped with PTFE-coated stir bars, were charged with palladium(II) acetate (5.6 mg, 0.0250 mmol, 0.05 equiv), BrettPhos (13.4 mg, 0.0250 mmol, 0.05 equiv), 1,3,5-trimethoxybenzene (30.0 mg, 0.178 mmol, as an internal standard), and manganese (219.8 mg, 4.000 mmol, 8.00 equiv). Azobenzene (68.3 mg, 0.375 mmol, 0.75 equiv) was then added to one vial. DMF (1.000

mL) was added to the vials, followed by 4-chlorobenzotrifluoride (76.9 μL, 90.3 mg, 0.500 mmol, 1.00 equiv). Aniline (68.5 μL, 69.8 mg, 0.750 mmol, 1.50 equiv) was added to the vial not containing azobenzene. The vials were then sealed with Thermo Scientific Mininert screw caps with auxiliary rubber septa. The reactions were removed from the glovebox and HFIP (91.9 μL, 147.0 mg, 0.8750 mmol, 1.75 equiv) was added to each through the valve via gas-tight syringe. The reactions were then placed on a pre-heated stir plate (100 °C, 1250 rpm).

Aliquots were taken from the ongoing reaction, while stirring, by opening the valve and withdrawing 10 μL of the reaction mixture via gas-tight syringe. The aliquots were immediately quenched in 1.0 mL of 0.1 M citric acid and extracted into 1.5 mL of diethyl ether. The organic layer was then passed through a short (1.5 cm in a pipette) silica plug. Samples were analyzed by SFC-MS and GC-FID to determine the concentration of **2.3a** using 1,3,5-trimethoxybenzene as an internal standard.

Figure 2.14. Necessity of Reductant in *N*-Arylation

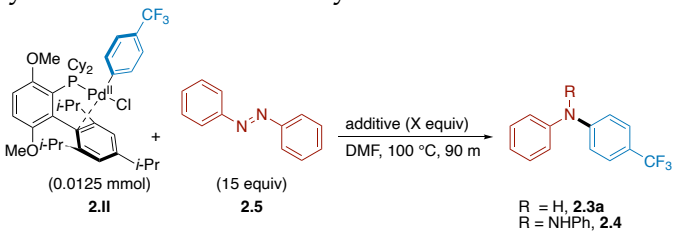

Entry	Additive	X equiv	**2.3a**	**2.4**
1	none	N/A	Not observed	Not observed
2	$MnCl_2$	2	Not observed	Not observed
3	HFIP	35	Not observed	Not observed
4	Mn	2	20%	4%
5	Mn	160	Not observed	120%

In a nitrogen-filled glovebox, five oven-dried 1 dram vials, equipped with PTFE-coated stir bars, were charged with **2.II** (10.3 mg, 0.0125 mmol, 1.00 equiv), 1,3,5-trimethoxybenzene (7.5 mg, 0.045 mmol, as an internal standard), and azobenzene (34.2

mg, 0.1875 mmol, 15.00 equiv). The appropriate solid additive was then added to each vial—manganese(II) chloride (3.1 mg, 0.025 mmol, 2.00 equiv, Figure 2.14 Entry 1) or manganese (1.4 mg, 0.025 mmol, 2.00 equiv, Figure 2.14 Entry 4; 111.9 mg, 2.00 mmol, 160 equiv, Figure 2.14 Entry 5). The vials were sealed with phenolic screw caps bearing PTFE-backed, silicone septa and removed from the glovebox. HFIP (45.9 μL, 73.5 mg, 0.4375 mmol, 35 equiv, Figure 2.14 Entry 3) was added to one vial through the septum via gas-tight syringe. The reactions were then placed on a pre-heated stir plate (100 °C, 1250 rpm) where they remained for 90 min.

After stirring, a 30 μL aliquot was taken from each reaction via gas-tight syringe. The aliquots were immediately quenched in 1.0 mL of 0.1 M citric acid and extracted into 1.5 mL of diethyl ether. The organic layers were then passed through a short (1.5 cm in a pipette) silica plug. Samples were analyzed by SFC-MS to identify any arylation products present. The yields of products were not quantified due to the low concentration.

We hypothesize that conversion of **2.4** to **2.3a** occurs in Figure 2.14 Entry 5 due to the low excess of manganese. As there is no proton source, the resulting manganese hydrazide can transmetallate onto **2.II**, enabling further arylation. In the case of Figure 2.14 Entry **5**. The association-reduction of azobenzene most likely outcompetes transmetalation when an excess of manganese is present, leading to the exclusive formation of **2.4**. The high mass balance observed in Figure 2.14 Entry 5 is most likely due to instrument variance as the quantitative yield of **2.4** is only 4.9 mg. The absence of **2.3a** and **2.4** in Figure 2.14 Entries 1–3 was confirmed via searching directly for the m/z of each product.

Figure 2.15. Electrochemical Studies

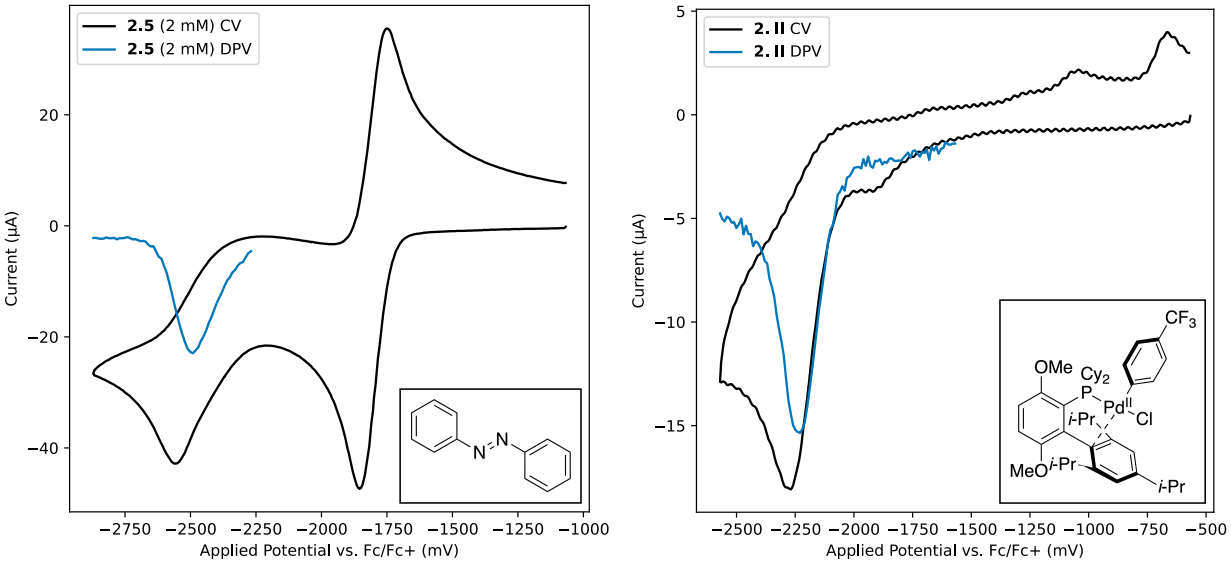

Electrochemical measurements were performed in a nitrogen-filled glovebox at 32 °C. Electrodes used were: a $Ag/AgNO_3$ reference electrode, a glassy carbon working electrode, and a platinum wire counter electrode. The reference electrode was filled with 10 mM $AgNO_3$, 100 mM $TBAPF_6$ in MeCN. The working and counter electrodes were immersed in the analyte solution without a frit. A ferrocene standard (10 mM ferrocene, 100 mM $TBAPF_6$, in DMF) was analyzed prior to other measurements. The CVs of **2.5** and **2.II** were gathered with a sweep rate of 100 mV/s and are referenced to the $E_{1/2}$ of the ferrocene standard. The applied voltages were not corrected for IR compensation. Plots were constructed utilizing IUPAC conventions.

The reduction potentials for **2.5** were measured as -1.802 and -2.491 V vs. Fc/Fc^+. DPV was utilized to confirm the observed irreversible reduction ($E_{DP,\,H}$ 50 mV, $T_{DP,\,W}$ 10 ms, $T_{DP,\,P}$ 500 ms, $E_{DP,\,I}$ 10 mV, $T_{DP,\,PRE}$ (τ′) 3 ms, $T_{DP,\,POST}$ (τ) 3 ms).

A single irreversible reduction of **2.II** was measured at -2.229 V vs. Fc/Fc^+ and confirmed by DPV ($E_{DP,H}$ 50 mV, $T_{DP,W}$ 10 ms, $T_{DP,P}$ 50 ms, $E_{DP,I}$ 10 mV, $T_{DP,PRE}$ (τ') 3 ms, $T_{DP,POST}$ (τ) 3 ms).

Figure 2.16. 1,1,2-Triarylhydrazine Arylation

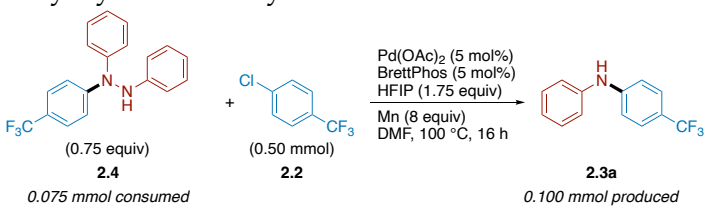

In a nitrogen-filled glovebox, an oven-dried 1 dram vial equipped with a PTFE-coated stir bar was charged with palladium(II) acetate (5.6 mg, 0.0250 mmol, 0.05 equiv), BrettPhos (13.4 mg, 0.0250 mmol, 0.05 equiv), 1,3,5-trimethoxybenzene (30.0 mg, 0.178 mmol, as an internal standard), 1,2-diphenyl-1-(4-(trifluoromethyl)phenyl)hydrazine (74.3 mg, 0.375 mmol, 0.75 equiv), and manganese (219.8 mg, 4.000 mmol, 8.00 equiv). DMF (1.000 mL) was added to the vial, followed by nitrobenzene (66.7 μL, 92.3 mg, 0.750 mmol, 1.50 equiv). The vial was sealed with a phenolic screw cap bearing a PTFE-backed silicone septum. The reaction was removed from the glovebox and HFIP (91.9 μL, 147.0 mg, 0.8750 mmol, 1.75 equiv) was added through the valve via gas-tight syringe. The reaction was then placed on a pre-heated stir plate where it was stirred (100 °C, 1250 rpm) for 16 h.

After stirring, a 30 μL aliquot was taken from the reaction via gas-tight syringe. The aliquot was immediately quenched in 1.0 mL of 0.1 M citric acid and extracted into 1.5 mL of diethyl ether. The organic layer was then passed through a short (1.5 cm in a pipette) silica plug. The sample was analyzed by SFC-MS to determine the concentration of reagents using 1,3,5-trimethoxybenzene as an internal standard.

From this result we made two conclusions. First, the production of **2.3a** exceeding the consumption of **2.4** supports the hypothesis that **2.4** is an intermediate in the production of **2.3a**. Second, the low total consumption of **2.4** suggests that liberating **2.3a** occurs only via arylation of **2.4** and N–N cleavage of the resulting 1,1,2,2-tetraarylhydrazine product and not via N–N cleavage and arylation of the resulting aniline. We hypothesize that the low total consumption of **2.4** is due to the low nucleophilicity of **2.4** leading to slow arylation. In the absence of a productive pathway—either in the form of arylation of **2.4** in this case or **2.5** in the optimized coupling—reductive decomposition of **2.II** leads to catalyst deactivation. It is also probable that the excess 1.5 equiv of protons compared to the optimized nitroarene arylation also contributes to this outcome.

Figure 2.17. Hydrazobenzene Arylation

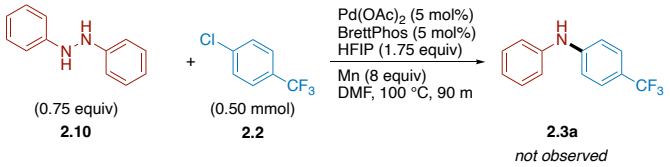

In a nitrogen-filled glovebox, an oven-dried 1 dram vial equipped with a PTFE-coated stir bar was charged with palladium(II) acetate (5.6 mg, 0.0250 mmol, 0.05 equiv), BrettPhos (13.4 mg, 0.0250 mmol, 0.05 equiv), 1,3,5-trimethoxybenzene (30.0 mg, 0.178 mmol, as an internal standard), hydrazobenzene (69.1 mg, 0.375 mmol, 0.75 equiv), and manganese (219.8 mg, 4.000 mmol, 8.00 equiv). DMF (1.000 mL) was added to the vial, followed by nitrobenzene (66.7 μL, 92.3 mg, 0.750 mmol, 1.50 equiv). The vial was sealed with a phenolic screw cap bearing a PTFE-backed silicone septum. The reaction was removed from the glovebox and HFIP (91.9 μL, 147.0 mg, 0.8750 mmol, 1.75 equiv) was added through the valve via gas-tight syringe. The reaction was then placed on a pre-heated stir plate where it was stirred (100 °C, 1250 rpm) for 90 min.

After stirring, a 30 μL aliquot was taken from the reaction via gas-tight syringe. The aliquot was immediately quenched in 1.0 mL of 0.1 M citric acid and extracted into 1.5 mL of diethyl ether. The organic layer was then passed through a short (1.5 cm in a pipette) silica plug. The sample was analyzed by SFC-MS to determine the concentration of reagents using 1,3,5-trimethoxybenzene as an internal standard.

This result demonstrates that **2.10** is not a likely intermediate in the reductive coupling of nitroarenes with chloroarenes. While **2.10** is observed in reduction studies, it is often only observed after azobenzene (**2.5**) is the only remaining species that can be easily reduced.

2.4.6 General Procedures

2.4.6.1 General Procedure A: Isolation Scale in a Glovebox (Electron-poor Chloroarenes)

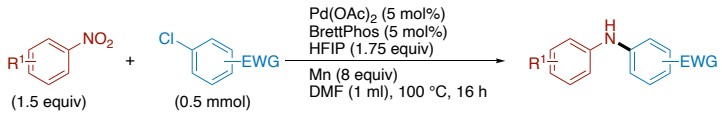

In a nitrogen-filled glovebox, an oven-dried 1 dram vial equipped with a PTFE-coated stir bar was charged with palladium(II) acetate (5.6 mg, 0.025 mmol, 0.05 equiv), BrettPhos (13.4 mg, 0.025 mmol, 0.05 mmol), chloroarene (if solid, 0.500 mmol), and nitroarene (if solid, 0.750 mmol). Manganese powder (219.8 mg, 4.000 mmol, 8.00 equiv) and DMF (1 mL) were then added, followed by chloroarene (if liquid, 0.5 mmol) and nitroarene (if liquid, 0.75 mmol). The vial was then sealed with a phenolic screw cap bearing a PTFE-backed silicone septum and removed from the glovebox. 1,1,1,3,3,3-hexafluoro-2-propanol (HFIP) (91.9 μL, 147.0 mg, 0.875 mmol, 1.75 equiv) was added to

the vial through the septum via gas-tight syringe. The reaction was then placed on a pre-heated stir plate, where it was stirred (1250 rpm) at 100 °C for 16 h.

After stirring, the reaction mixture was allowed to cool to rt and was poured over 45 mL of 0.1 M citric acid solution in a separatory funnel. The vial was then rinsed with 5 mL each of diethyl ether and 0.1 M citric acid, and the washings were added to the separatory funnel. The mixture was extracted with diethyl ether (3 × 30 mL). The combined organic layers were then dried over anhydrous Na_2SO_4 and filtered directly into a flask containing Celite, and concentrated. The immobilized residue was purified by column chromatography to yield the desired product.

2.4.6.2 General Procedure B: Isolation Scale in a Glovebox (Electron-rich Chloroarenes)

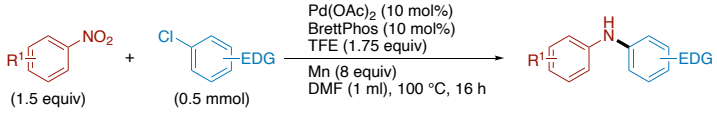

In a nitrogen-filled glovebox, an oven-dried 1 dram vial equipped with a PTFE-coated stir bar was charged with palladium(II) acetate (11.2 mg, 0.05 mmol, 0.1 equiv), BrettPhos (26.8 mg, 0.05 mmol, 0.1 mmol), chloroarene (if solid, 0.500 mmol), and nitroarene (if solid, 0.750 mmol). Manganese powder (219.8 mg, 4.000 mmol, 8.00 equiv) and DMF (1 mL) were then added, followed by chloroarene (if liquid, 0.5 mmol) and nitroarene (if liquid, 0.75 mmol). The vial was then sealed with a phenolic screw cap bearing a PTFE-backed silicone septum and removed from the glovebox. 2,2,2-Trifluoroehtanol (TFE) (63.0 μL, 87.5 mg, 0.875 mmol, 1.75 equiv) was added to the vial through the septum via gas-tight syringe. The reaction was then placed on a pre-heated stir plate, where it was stirred (1250 rpm) at 100 °C for 16 h.

After stirring, the reaction mixture was allowed to cool to rt and was poured over 45 mL of 0.1 M citric acid solution in a separatory funnel. The vial was then rinsed with 5 mL each of diethyl ether and 0.1 M citric acid, and the washings were added to the separatory funnel. The mixture was extracted with diethyl ether (3 × 30 mL). The combined organic layers were then dried over anhydrous Na_2SO_4 and filtered directly into a flask containing Celite, and concentrated. The immobilized residue was purified by column chromatography to yield the desired product.

2.4.6.3 General Procedure C: Preparative Scale Glovebox Procedure

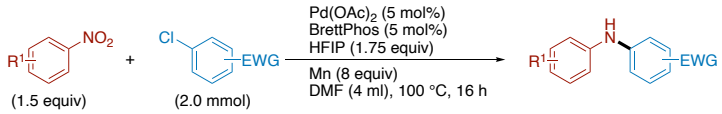

In a nitrogen-filled glovebox, an oven-dried 1 dram vial equipped with a PTFE-coated stir bar was charged with palladium(II) acetate (22.5 mg, 0.10 mmol, 0.05 equiv), BrettPhos (53.7 mg, 0.10 mmol, 0.05 mmol), chloroarene (if solid, 2.0 mmol), and nitroarene (if solid, 3.0 mmol). Manganese powder (879.0 mg, 16.0 mmol, 8.00 equiv) and DMF (4 mL) were then added, followed by chloroarene (if liquid, 2.0 mmol) and nitroarene (if liquid, 3.0 mmol). The vial was then sealed with a phenolic screw cap bearing a PTFE-backed silicone septum and removed from the glovebox. HFIP (367.6 μL, 588.1 mg, 3.5 mmol, 1.75 equiv) was added to the vial through the septum via gas-tight syringe. The reaction was then placed on a pre-heated stir plate, where it was stirred (1250 rpm) at 100 °C for 16 h.

After stirring, the reaction mixture was allowed to cool to rt and was poured over 90 mL of 0.1 M citric acid solution in a separatory funnel. The vial was then rinsed with 10 mL each of diethyl ether and 0.1 M citric acid, and the washings were added to the separatory

funnel. The mixture was extracted with diethyl ether (3 × 50 mL). The combined organic layers were then dried over anhydrous Na_2SO_4, filtered directly into a flask containing Celite, and concentrated. The immobilized residue was purified by column chromatography to yield the desired product.

2.4.6.4 General Procedure D: Preparative Scale Benchtop Procedure

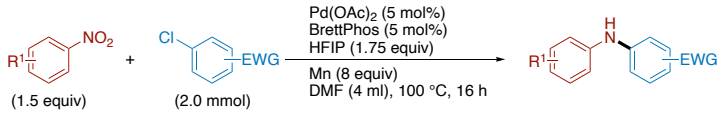

A 50 mL round bottom flask equipped with a PTFE-coated stir bar was charged with palladium(II) acetate (22.5 mg, 0.10 mmol, 0.05 equiv), BrettPhos (53.7 mg, 0.10 mmol, 0.05 equiv), chloroarene (if solid, 2.0 mmol), nitroarene (if solid, 3.0 mmol), and manganese (879.0 mg, 16.0 mmol, 8.00 equiv). The flask was then sealed with a septum and connected to both a nitrogen manifold and a bubbler via two needles inserted through the septum. The flask was purged with nitrogen for 5 min. The needle connecting the bubbler was then removed and anhydrous DMF, chloroarene (if liquid, 2.0 mmol), nitroarene (if liquid, 3.0 mmol), and HFIP (367.6 μL, 588.1 mg, 3.5 mmol, 1.75 equiv) were added to the flask under positive pressure of nitrogen. The reaction was then disconnected from the nitrogen manifold and immersed in a pre-heated oil bath, where it was stirred at 1000 rpm and 100 °C overnight.

After stirring overnight, a 40 μL aliquot was taken via gas-tight syringe, quenched in 1 mL 0.1 M citric acid, and extracted into 1.5 mL of diethyl ether. The organic layer was then passed through a short (1.5 cm in a pipette) silica plug and analyzed via SFC-MS to check for complete consumption of chloroarene.

After the reaction had reached completion, the reaction was allowed to cool to rt, and the contents were poured into a 500 mL separator funnel containing 150 mL of 0.1 M citric acid solution. The flask was then washed with 0.1 M aq. citric acid (2 × 10 mL) and diethyl ether (2 × 10 mL) and the washings were added to the separatory funnel. The mixture was then extracted with diethyl ether (3 × 120 mL), the combined organic layers were dried over anhydrous Na_2SO_4, and filtered directly through 20 grams of celite. The solvent was then removed under reduced pressure, and the immobilized residue was purified via column chromatography

2.4.7 Specific Procedures and Product Characterization

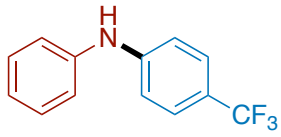

_N_-phenyl-4-(trifluoromethyl)aniline (2.3a)

General Procedure A was followed using nitrobenzene (92.3 mg, 0.75 mmol, 1.5 equiv) and 4-chlorobenzotrifluoride (90.3 mg, 0.50 mmol, 1.0 equiv). The crude product was purified via column chromatography (80 g of silica gel, 1 CV hexanes, then 0–10% EtOAc/hexanes across 15 CV) to afford the product (92.1 mg, 0.388 mmol, 78% yield, R_f = 0.37 in 10% EtOAc/hexanes) as a white solid.

General Procedure C was followed using nitrobenzene (369.2 mg, 3.0 mmol, 1.5 equiv) and 4-chlorobenzotrifluoride (361.1 mg, 2.0 mmol, 1.0 equiv). The crude product was purified via column chromatography (80 g of silica gel, 1 CV hexanes, then 0–10% EtOAc/hexanes across 15 CV) to afford the product (378.4 mg, 1.595 mmol, 80% yield, R_f = 0.50 in 20% EtOAc/hexanes) as a white solid. Characterization data match those reported in the literature.[109]

^{1}H NMR (500 MHz, $CDCl_3$) δ 7.47 (d, *J* = 8.2 Hz, 2H), 7.37 – 7.29 (m, 2H), 7.15 (d, *J* = 8.6 Hz, 2H), 7.08 – 7.02 (m, 3H), 5.91 (s, 1H).

^{13}C{^{1}H} NMR (126 MHz, $CDCl_3$) δ 146.8, 141.2, 129.6, 126.7 (q, *J* = 3.8 Hz), 124.6 (q, *J* = 270.8 Hz), 123.0, 121.7 (q, *J* = 32.6 Hz), 120.1, 115.3.

^{19}F{^{1}H} NMR (377 MHz, $CDCl_3$) δ -61.45.

HRMS-ESI (m/z): $[M+H]^+$ calcd for $C_{13}H_{11}F_3N^+$, 238.08381; found, 238.0836.

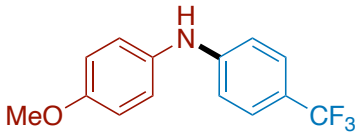

4-methoxy-*N*-(4-(trifluoromethyl)phenyl)aniline (2.3b)

General Procedure A was followed using 4-nitroanisole (114.9 mg, 0.75 mmol, 1.5 equiv) 4-chlorobenzotrifluoride (90.3 mg, 0.50 mmol, 1.0 equiv). The crude product was purified via column chromatography (80 g of silica gel, 1 CV hexanes, then 0–10% EtOAc/hexanes across 15 CV) to afford the product (102.5 mg, 0.384 mmol, 77% yield, R_f = 0.24 in 10% EtOAc/hexanes) as a white solid. Characterization data match those reported in the literature.[109]

^{1}H NMR (500 MHz, $CDCl_3$) δ 7.41 (d, *J* = 8.4 Hz, 2H), 7.11 (d, *J* = 8.8 Hz, 2H), 6.90 (d, *J* = 8.8 Hz, 2H), 6.85 (d, *J* = 8.4 Hz, 2H), 5.71 (s, 1H), 3.82 (s, 3H).

^{13}C{^{1}H} NMR (126 MHz, $CDCl_3$) δ 156.5, 148.6, 133.7, 126.7 (q, *J* = 3.8 Hz), 124.8 (q, *J* = 270.5 Hz), 124.3, 120.5 (q, *J* = 32.6 Hz), 114.8, 113.8, 55.6.

^{19}F{^{1}H} NMR (377 MHz, $CDCl_3$) δ -61.25.

HRMS-ESI (m/z): $[M-H]^-$ calcd for $C_{14}H_{11}F_3NO^-$, 266.0798; found, 266.0798.

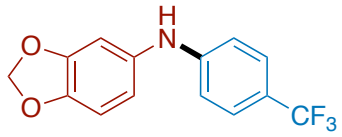

***N*-(4-(trifluoromethyl)phenyl)benzo[*d*][1,3]dioxol-5-amine (2.3c)**

General Procedure A was followed using 1,2-(methylenedioxy)-4-nitrobenzene (125.3 mg, 0.75 mmol, 1.5 equiv) and 4-chlorobenzotrifluoride (90.3 mg, 0.50 mmol, 1.0 equiv). The crude product was purified via column chromatography (80 g of silica gel, 1 CV hexanes, then 0–10% EtOAc/hexanes across 15 CV) to afford the product (113.7 mg, 0.404 mmol, 81% yield, R_f = 0.28 in 10% EtOAc/hexanes) as a pale-yellow oil.

^{1}H NMR (500 MHz, $CDCl_3$) δ 7.42 (d, *J* = 8.3 Hz, 2H), 6.87 (d, *J* = 8.4 Hz, 2H), 6.78 (d, *J* = 8.2 Hz, 1H), 6.71 (d, *J* = 2.2 Hz, 1H), 6.62 (dd, *J* = 8.2, 2.2 Hz, 1H), 5.97 (s, 2H), 5.70 (s, 1H).

^{13}C{^{1}H} NMR (126 MHz, $CDCl_3$) δ 148.4, 148.2, 144.3, 135.0, 126.7 (q, *J* = 3.8 Hz), 124.7 (q, *J* = 270.4 Hz), 120.8 (q, *J* = 32.6 Hz), 115.5, 114.1, 108.7, 104.5, 101.3.

^{19}F{^{1}H} NMR (377 MHz, $CDCl_3$) δ -61.34.

HRMS-ESI (m/z): $[M-H]^-$ calcd for $C_{14}H_9F_3NO_2^-$, 280.0591; found, 280.0590.

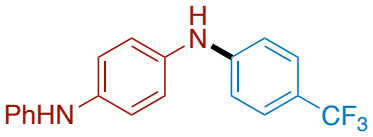

***N*^{1}-phenyl-*N*^{4}-(4-(trifluoromethyl)phenyl)benzene-1,4-diamine (2.3d)**

General Procedure A was followed using 4-nitrodiphenylamine (160.7 mg, 0.75 mmol, 1.5 equiv) and 4-chlorobenzotrifluoride (90.3 mg, 0.50 mmol, 1.0 equiv). The crude product was purified via column chromatography (80 g of silica gel, 1 CV hexanes, then

0–10% EtOAc/hexanes across 15 CV) to afford the product (98.1 mg, 0.299 mmol, 60% yield, R_f = 0.18 in 10% EtOAc/hexanes) as an off-white solid.

^{1}H NMR (500 MHz, $CDCl_3$) δ 7.43 (d, *J* = 8.4 Hz, 2H), 7.27 (t, *J* = 7.9 Hz, 2H), 7.12 – 7.06 (m, 4H), 7.03 (d, *J* = 7.9 Hz, 2H), 6.95 – 6.88 (m, 3H), 5.76 (s, 1H), 5.64 (s, 1H).

^{13}C{^{1}H} NMR (126 MHz, $CDCl_3$) δ 148.2, 143.6, 139.3, 134.5, 129.4, 126.7 (q, *J* = 3.8 Hz), 124.7 (q, *J* = 270.5 Hz), 123.4, 120.7 (q, *J* = 32.5 Hz), 119.7, 117.2, 114.1.

^{19}F{^{1}H} NMR (377 MHz, $CDCl_3$) δ -61.30.

HRMS-ESI (m/z): $[M-H]^-$ calcd for $C_{19}H_{14}F_3N_2^-$, 327.1115; found, 327.1114.

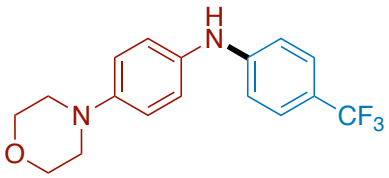

4-morpholino-*N*-(4-(trifluoromethyl)phenyl)aniline (2.3e)

General Procedure A was followed using 1-morpholino-4-nitrobenzene (156.1 mg, 0.75 mmol, 1.5 equiv) and 4-chlorobenzotrifluoride (90.3 mg, 0.50 mmol, 1.0 equiv). The crude product was purified via column chromatography (80 g of silica gel, 1 CV 10% EtOAc/hexanes, then 10–30% EtOAc/hexanes across 15 CV) to afford the product (128.4 mg, 0398 mmol, 80% yield, R_f = 0.50 in 25% EtOAc/hexanes) as a white solid.

^{1}H NMR (500 MHz, $CDCl_3$) δ 7.41 (d, *J* = 8.4 Hz, 2H), 7.11 (d, *J* = 8.8 Hz, 2H), 6.91 (d, *J* = 8.9 Hz, 2H), 6.87 (d, *J* = 8.4 Hz, 2H), 5.72 (s, 1H), 3.94 – 3.84 (m, 4H), 3.17 – 3.11 (m, 4H).

^{13}C{^{1}H} NMR (126 MHz, $CDCl_3$) δ 148.4, 148.1, 133.3, 126.6 (q, *J* = 3.8 Hz), 124.7 (q, *J* = 270.5 Hz), 123.7, 120.5 (q, *J* = 32.6 Hz), 116.9, 113.8, 66.9, 49.8.

$^{19}F\{^{1}H\}$ NMR (377 MHz, $CDCl_3$) δ -61.25.

HRMS-ESI (m/z): $[M-H]^-$ calcd for $C_{17}H_{16}F_3N_2O^-$, 321.1220; found, 321.1218.

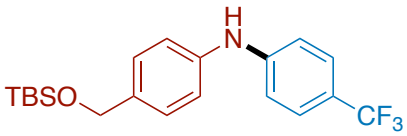

4-(((*tert*-butyldimethylsilyl)oxy)methyl)-*N*-(4-(trifluoromethyl)phenyl)aniline (2.3f)

General Procedure A was followed using *tert*-butyl-dimethyl((4-nitrobenzyl)oxy)silane (200.6 mg, 0.75 mmol, 1.5 equiv) and 4-chlorobenzotrifluoride (90.3 mg, 0.50 mmol, 1.0 equiv). The crude product was purified via column chromatography (80 g of silica gel, 1 CV hexanes, then 0–10% EtOAc/hexanes across 15 CV) to afford the product (132.8 mg, 0.348 mmol, 70% yield, R_f = 0.35 in 10% EtOAc/hexanes) as a yellow oil.

^{1}H NMR (500 MHz, $CDCl_3$) δ 7.45 (d, *J* = 8.4 Hz, 2H), 7.29 (d, *J* = 8.4 Hz, 2H), 7.11 (d, *J* = 8.4 Hz, 2H), 7.00 (d, *J* = 8.4 Hz, 2H), 5.88 (s, 1H), 4.71 (s, 2H), 0.95 (s, 9H), 0.11 (s, 6H).

$^{13}C\{^{1}H\}$ NMR (126 MHz, $CDCl_3$) δ 147.1, 139.9, 136.3, 127.5, 126.7 (q, *J* = 3.8 Hz), 124.6 (q, *J* = 270.8 Hz), 121.4 (q, *J* = 32.7 Hz), 120.3, 1[26,28,59–61]15.0, 64.7, 26.0, -5.2.

$^{19}F\{^{1}H\}$ NMR (377 MHz, $CDCl_3$) δ -61.44.

HRMS-ESI (m/z): $[M-H]^-$ calcd for $C_{20}H_{25}F_3NOSi^-$, 380.1663; found, 380.1663.

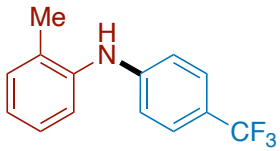

2-methyl-*N*-(4-(trifluoromethyl)phenyl)aniline (2.3g)

General Procedure A was followed using 2-nitrotoluene (102.9 mg, 0.75 mmol, 1.5 equiv) and 4-chlorobenzotrifluoride (90.3 mg, 0.50 mmol, 1.0 equiv). The crude product was purified via column chromatography (80 g of silica gel, 1 CV hexanes, then 0–10% EtOAc/hexanes across 15 CV) to afford the product (74.0 mg, 0.295 mmol, 59% yield, R_f = 0.43 in 10% EtOAc/hexanes) as a yellow oil. Characterization data match those reported in the literature.[110]

^{1}H NMR (500 MHz, $CDCl_3$) δ 7.43 (d, *J* = 8.3 Hz, 2H), 7.25 (d, *J* = 6.8 Hz, 1H), 7.19 (t, *J* = 7.7 Hz, 1H), 7.07 (t, *J* = 7.5 Hz, 1H), 6.84 (d, *J* = 8.3 Hz, 2H), 5.58 (s, 1H), 2.24 (s, 3H).

^{13}C{^{1}H} NMR (126 MHz, $CDCl_3$) δ 147.9, 139.2, 131.4, 131.3, 127.0, 126.7 (q, *J* = 3.8 Hz), 124.7 (q, *J* = 270.6 Hz), 124.4, 122.5, 121.0 (q, *J* = 32.7 Hz), 114.7, 17.9.

^{19}F{^{1}H} NMR (377 MHz, $CDCl_3$) δ -61.34.

HRMS-ESI (m/z): $[M+H]^+$ calcd for $C_{14}H_{13}F_3N^+$, 252.0995; found, 252.0989.

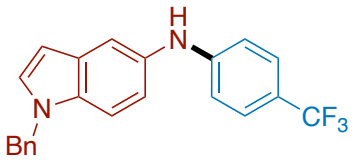

1-benzyl-*N*-(4-(trifluoromethyl)phenyl)-1*H*-indol-5-amine (2.3h)

General Procedure A was followed using 1-benzyl-5-nitro-1*H*-indole (189.2 mg, 0.75 mmol, 1.5 equiv) and 4-chlorobenzotrifluoride (90.3 mg, 0.50 mmol, 1.0 equiv). The crude product was purified via column chromatography (80 g of silica gel, 1 CV hexanes, then 0–20% EtOAc/hexanes across 13 CV) to afford the product (106.7 mg, 0.291 mmol, 58% yield, R_f = 0.15 in 10% EtOAc/hexanes) as a yellow solid.

^{1}H NMR (500 MHz, $CDCl_3$) δ 7.45 (d, *J* = 2.0 Hz, 1H), 7.38 (d, *J* = 8.4 Hz, 2H), 7.34 – 7.21 (m, 5H), 7.15 (d, *J* = 3.2 Hz, 1H), 7.13 (d, *J* = 6.9 Hz, 1H), 6.99 (dd, *J* = 8.7, 2.1 Hz, 1H), 6.85 (d, *J* = 8.5 Hz, 2H), 6.49 (d, *J* = 3.1 Hz, 1H), 5.81 (s, 1H), 5.30 (s, 2H).

^{13}C{^{1}H} NMR (126 MHz, $CDCl_3$) δ 149.4, 137.3, 134.0, 133.0, 129.4, 129.3, 128.8, 127.7, 126.8, 126.5 (q, *J* = 3.8 Hz), 124.9 (q, *J* = 270.4 Hz), 119.9 (q, *J* = 32.6 Hz), 118.9, 115.4, 113.5, 110.5, 101.5, 50.3.

^{19}F{^{1}H} NMR (377 MHz, $CDCl_3$) δ -61.17.

HRMS-ESI (m/z): $[M+H]^+$ calcd for $C_{22}H_{18}F_3N_2^+$, 367.1417; found, 367.1410.

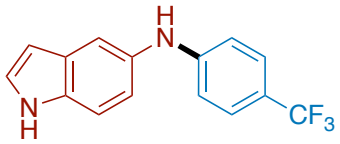

***N*-(4-(trifluoromethyl)phenyl)-1*H*-indol-5-amine (2.3i)**

General Procedure A was followed using 5-nitroindole (121.6 mg, 0.75 mmol, 1.5 equiv) and 4-chlorobenzotrifluoride (90.3 mg, 0.50 mmol, 1.0 equiv). The crude product was purified via column chromatography (80 g of silica gel, 1 CV hexanes, then 0–30% EtOAc/hexanes across 15 CV) to afford the product (107.9 mg, 0.391 mmol, 78% yield, R_f = 0.10 in 10% EtOAc/hexanes) as a white solid. Characterization data match those reported in the literature.[111]

^{1}H NMR (500 MHz, $CDCl_3$) δ 8.15 (br, 1H), 7.47 (d, *J* = 2.3 Hz, 1H), 7.44 – 7.34 (m, 3H), 7.24 (t, *J* = 2.8 Hz, 1H), 7.04 (dd, *J* = 8.6, 2.1 Hz, 1H), 6.87 (d, *J* = 8.4 Hz, 2H), 6.52 (t, *J* = 2.5 Hz, 1H), 5.85 (s, 1H).

^{13}C{^{1}H} NMR (126 MHz, $CDCl_3$) δ 149.5, 133.4, 133.2, 128.6, 126.6 (q, *J* = 3.8 Hz), 125.2, 124.9 (q, *J* = 270.5 Hz), 119.9 (q, *J* = 32.5 Hz), 119.3, 115.3, 113.5, 111.8, 102.6.

$^{19}F\{^{1}H\}$ NMR (377 MHz, $CDCl_3$) δ -61.15.

HRMS-ESI (m/z): $[M+H]^+$ calcd for $C_{15}H_{12}F_3N_2^+$ 277.0947, found 277.0943.

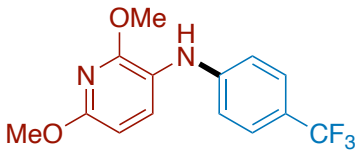

2,6-dimethoxy-*N*-(4-(trifluoromethyl)phenyl)pyridin-3-amine (2.3j)

General Procedure A was followed using 2,6-dimethoxy-3-nitropyridine (138.1 mg, 0.75 mmol, 1.5 equiv) and 4-chlorobenzotrifluoride (90.3 mg, 0.50 mmol, 1.0 equiv). The crude product was purified via column chromatography (80 g of silica gel, 1 CV hexanes, then 0–20% EtOAc/hexanes across 15 CV) to afford the product (95.5 mg, 0.320 mmol, 64% yield, R_f = 0.47 in 20% EtOAc/hexanes) as a yellow oil.

^{1}H NMR (500 MHz, $CDCl_3$) δ 7.52 (d, *J* = 8.2 Hz, 1H), 7.43 (d, *J* = 8.5 Hz, 2H), 6.87 (d, *J* = 8.4 Hz, 2H), 6.32 (d, *J* = 8.2 Hz, 1H), 5.68 (s, 1H), 3.97 (s, 3H), 3.92 (s, 3H).

$^{13}C\{^{1}H\}$ NMR (126 MHz, $CDCl_3$) δ 158.6, 155.0, 147.8, 133.0, 126.6 (q, *J* = 3.8 Hz), 124.7 (q, *J* = 270.6 Hz), 120.9 (q, *J* = 32.6 Hz), 116.9, 114.0, 100.2, 53.8, 53.6.

$^{19}F\{^{1}H\}$ NMR (377 MHz, $CDCl_3$) δ -61.35.

HRMS-ESI (m/z): $[M+H]^+$ calcd for $C_{14}H_{14}F_3N_2O_2^+$, 299.1002; found, 299.0997.

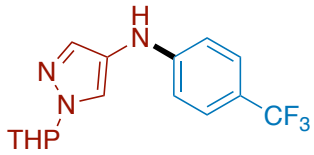

1-(tetrahydro-2*H*-pyran-2-yl)-*N*-(4-(trifluoromethyl)phenyl)-1*H*-pyrazol-4-amine (2.3k)

General Procedure A was followed using 4-nitro-1-(tetrahydro-2*H*-pyran-2-yl)-1*H*-pyrrazole (147.9 mg, 0.75 mmol, 1.5 equiv) and 4-chlorobenzotrifluoride (90.3 mg, 0.50 mmol, 1.0 equiv). The crude product was purified via column chromatography (80 g of silica gel, 1 CV 3% EtOAc/hexanes, then 30–50% EtOAc/hexanes across 15 CV) to afford the product (44.5 mg, 0.143 mmol, 29% yield, R_f = 0.09 in 30% EtOAc/hexanes) as a yellow solid.

^{1}H NMR (500 MHz, $CDCl_3$) δ 7.59 (s, 1H), 7.50 (s, 1H), 7.40 (d, *J* = 8.6 Hz, 2H), 6.76 (d, *J* = 8.1 Hz, 2H), 5.39 – 5.30 (m, 2H), 4.08 (ddt, *J* = 11.1, 3.6, 1.9 Hz, 1H), 3.71 (ddd, *J* = 13.7, 8.8, 3.0 Hz, 1H), 2.18 – 2.01 (m, 3H), 1.78 – 1.56 (m, 4H).

^{13}C{^{1}H} NMR (126 MHz, $CDCl_3$) δ 149.4, 136.2, 126.7 (q, *J* = 3.8 Hz), 124.7 (q, *J* = 270.6 Hz), 123.6, 123.0, 120.25 (q, *J* = 32.6 Hz), 112.8, 88.1, 67.8, 30.4, 24.9, 22.4.

^{19}F{^{1}H} NMR (377 MHz, $CDCl_3$) δ -61.23.

HRMS-ESI (m/z): $[M+H]^+$ calcd for $C_{15}H_{17}F_3N_3O^+$, 312.1318; found, 312.1312.

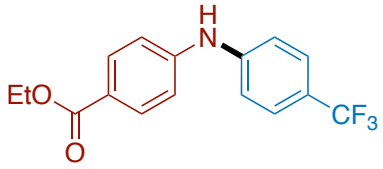

ethyl 4-((4-(trifluoromethyl)phenyl)amino)benzoate (2.3l)

General Procedure A was followed using ethyl 4-nitrobenzoate (146.4 mg, 0.75 mmol, 1.5 equiv) and 4-chlorobenzotrifluoride (90.3 mg, 0.50 mmol, 1.0 equiv). The crude product was purified via column chromatography (80 g of silica gel, 1 CV 10% EtOAc/hexanes, then 10–30% EtOAc/hexanes across 15 CV) to afford the product (44.7 mg, 0.145 mmol, 29% yield, R_f = 0.56 in 25% EtOAc/hexanes) as a white solid.

^{1}H NMR (500 MHz, $CDCl_3$) δ 7.98 (d, *J* = 8.6 Hz, 2H), 7.55 (d, *J* = 8.3 Hz, 2H), 7.19 (d, *J* = 8.3 Hz, 2H), 7.10 (d, *J* = 8.5 Hz, 2H), 6.18 (s, 1H), 4.36 (q, *J* = 7.1 Hz, 2H), 1.39 (t, *J* = 7.1 Hz, 3H).

^{13}C{^{1}H} NMR (126 MHz, $CDCl_3$) δ 166.2, 145.9, 144.6, 131.4, 126.8 (q, *J* = 3.8 Hz), 124.3 (q, *J* = 271.1 Hz), 123.6 (q, *J* = 32.8 Hz), 123.4, 117.8, 116.5, 60.7, 14.4.

^{19}F{^{1}H} NMR (377 MHz, $CDCl_3$) δ -61.80.

HRMS-ESI (m/z): $[M+H]^+$ calcd for $C_{16}H_{15}F_3NO_2^+$, 310.1049; found, 310.1046.

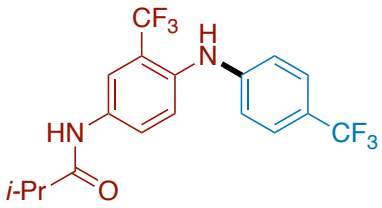

***N*-(3-(trifluoromethyl)-4-((4-(trifluoromethyl)phenyl)amino)phenyl)isobutyramide (2.3m)**

General Procedure A was followed using flutamide (207.2 mg, 0.75 mmol, 1.5 equiv) and 4-chlorobenzotrifluoride (90.3 mg, 0.50 mmol, 1.0 equiv). The crude product was purified via column chromatography (80 g of silica gel, 1 CV 10% EtOAc/hexanes, then 10–30% EtOAc/hexanes across 15 CV) to afford the product (29.1 mg, 0.075 mmol, 15% yield) as a pale-yellow oil.

^{1}H NMR (500 MHz, $CDCl_3$) δ 7.84 (d, *J* = 2.5 Hz, 1H), 7.68 (dd, *J* = 8.9, 2.6 Hz, 1H), 7.48 (d, *J* = 8.3 Hz, 2H), 7.41 (d, *J* = 8.8 Hz, 1H), 6.98 (d, *J* = 8.3 Hz, 2H), 5.99 (s, 1H), 2.53 (p, *J* = 6.9 Hz, 1H), 1.27 (d, *J* = 6.9 Hz, 6H).

^{13}C{^{1}H} NMR (126 MHz, $CDCl_3$) δ 175.4, 146.3, 135.6, 133.3, 126.8 (q, *J* = 3.8 Hz), 124.4 (q, *J* = 270.9 Hz), 124.4, 123.8 (q, *J* = 273.0 Hz), 123.2, 122.6 (q, *J* = 32.9 Hz), 122.0 (q, *J* = 29.7

Hz), 118.7 (q, J = 5.5 Hz), 116.2, 36.6, 19.5. The resonance corresponding to the amino-substituted carbon of the flutamide-derived ring is not observed. The resonance is expected to be a quartet with J = 30 Hz.

$^{19}F\{^{1}H\}$ NMR (377 MHz, $CDCl_3$) -61.64, -61.69.

HRMS-ESI (m/z): $[M+H]^+$ calcd for $C_{18}H_{17}F_6N_2O^+$, 391.1240; found, 391.1235.

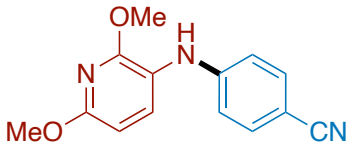

4-((2,6-dimethoxypyridin-3-yl)amino)benzonitrile (2.3n)

General Procedure A was followed using 2,6-dimethoxy-3-nitropyridine (138.1 mg, 0.75 mmol, 1.5 equiv) and 4-chlorobenzonitrile (68.8 mg, 0.50 mmol, 1.0 equiv). The crude product was purified via column chromatography (80 g of silica gel, 1 CV hexanes, then 0–25% EtOAc/hexanes across 15 CV) to afford the product (103.8 mg, 0.407 mmol, 81% yield, R_f = 0.50 in 20% EtOAc/hexanes) as a yellow solid.

General Procedure D was followed using 2,6-dimethoxy-3-nitropyridine (552.5 mg, 3.0 mmol, 1.5 equiv) and 4-chlorobenzonitrile (361.1 mg, 2.0 mmol, 1.0 equiv). The crude product was purified via column chromatography (160 g of silica gel, 2 CV hexanes, then 0–25% EtOAc/hexanes across 30 CV) to afford the product (359.8 mg, 1.409 mmol, 70% yield, R_f = 0.50 in 20% EtOAc/hexanes) as a yellow solid.

^{1}H NMR (500 MHz, $CDCl_3$) δ 7.50 (d, J = 8.1 Hz, 1H), 7.45 (d, J = 8.7 Hz, 2H), 6.80 (d, J = 8.8 Hz, 2H), 6.33 (d, J = 8.2 Hz, 1H), 5.77 (s, 1H), 3.97 (s, 3H), 3.93 (s, 3H).

$^{13}C\{^{1}H\}$ NMR (126 MHz, $CDCl_3$) δ 159.4, 155.6, 148.9, 134.3, 133.7, 120.0, 115.6, 114.0, 101.0, 100.5, 53.8, 53.6.

HRMS-ESI (m/z): $[M+H]^+$ calcd for $C_{14}H_{14}N_3O_2^+$, 256.1081; found, 256.1079.

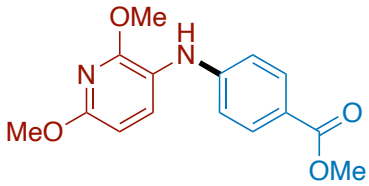

methyl 4-((2,6-dimethoxypyridin-3-yl)amino)benzoate (2.3o)

General Procedure A was followed using 2,6-dimethoxy-3-nitropyridine (138.1 mg, 0.75 mmol, 1.5 equiv) and methyl 4-chlorobenzoate (85.3 mg, 0.50 mmol, 1.0 equiv). The crude product was purified via column chromatography (80 g of silica gel, 1 CV hexanes, then 0–25% EtOAc/hexanes across 20 CV) to afford the product (114.1 mg, 0.396 mmol, 79% yield, R_f = 0.22 in 20% EtOAc/hexanes) as a white solid.

^{1}H NMR (500 MHz, $CDCl_3$) δ 7.88 (d, *J* = 8.8 Hz, 2H), 7.55 (d, *J* = 8.3 Hz, 1H), 6.82 (d, *J* = 8.8 Hz, 2H), 6.33 (d, *J* = 8.2 Hz, 1H), 5.79 (s, 1H), 3.97 (s, 3H), 3.92 (s, 3H), 3.86 (s, 3H).

$^{13}C\{^{1}H\}$ NMR (126 MHz, $CDCl_3$) δ 167.0, 158.7, 155.0, 149.0, 133.1, 131.5, 120.5, 116.7, 113.5, 100.2, 53.8, 53.6, 51.6.

HRMS-ESI (m/z): $[M+H]^+$ calcd for $C_{15}H_{17}N_2O_4^+$, 289.11828; found, 289.1180.

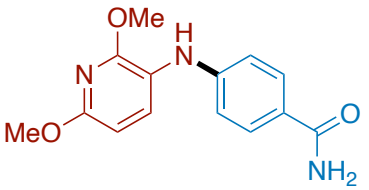

4-((2,6-dimethoxypyridin-3-yl)amino)benzamide (2.3p)

General Procedure A was followed using 2,6-dimethoxy-3-nitropyridine (138.1 mg, 0.75 mmol, 1.5 equiv) and 4-chlorobenzamide (77.8 mg, 0.50 mmol, 1.0 equiv). The crude product was purified via column chromatography (80g of silica gel, 1 CV 70% EtOAc/hexanes, then 70–100% EtOAc/hexanes across 15 CV) to afford the product (65.2 mg, 0.239 mmol, 48% yield, R_f = 0.21 in 80% EtOAc/hexanes) as a light brown solid.

^{1}H NMR (500 MHz, $CDCl_3$) δ 7.68 (d, *J* = 8.6 Hz, 2H), 7.54 (d, *J* = 8.3 Hz, 1H), 6.85 (d, *J* = 8.7 Hz, 2H), 6.33 (d, *J* = 8.2 Hz, 1H), 5.76 (s, 1H), 5.71 (br, 2H), 3.97 (s, 2H), 3.92 (s, 2H).

^{13}C{^{1}H} NMR (126 MHz, $CDCl_3$) δ 168.9, 158.6, 154.9, 148.3, 132.9, 129.2, 123.4, 116.9, 113.9, 100.2, 53.8, 53.6.

HRMS-ESI (m/z): $[M+H]^+$ calcd for $C_{14}H_{16}N_3O_3^+$, 274.11862; found, 274.1181.

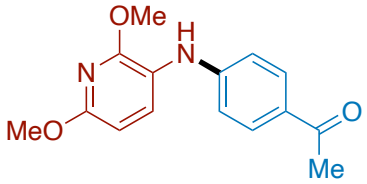

1-(4-((2,6-dimethoxypyridin-3-yl)amino)phenyl)ethan-1-one (2.3q)

General Procedure A was followed using 2,6-dimethoxy-3-nitropyridine (138.1 mg, 0.75 mmol, 1.5 equiv) and 4'-chloroacetophenone (77.3 mg, 0.50 mmol, 1.0 equiv). The crude product was purified via column chromatography (80g of silica gel, 1 CV hexanes, then 0–20% EtOAc/hexanes across 15 CV) to afford the product (81.9 mg, 0.301 mmol, 60% yield) as a yellow solid.

^{1}H NMR (500 MHz, $CDCl_3$) δ 7.84 (d, *J* = 8.7 Hz, 2H), 7.55 (d, *J* = 8.3 Hz, 1H), 6.83 (d, *J* = 8.8 Hz, 2H), 6.33 (d, *J* = 8.3 Hz, 1H), 5.84 (s, 1H), 3.97 (s, 3H), 3.93 (s, 3H), 2.52 (s, 3H).

$^{13}C\{^1H\}$ NMR (126 MHz, $CDCl_3$) δ 196.3, 158.8, 155.1, 149.3, 133.4, 130.6, 128.5, 116.4, 113.4, 100.2, 53.8, 53.6, 26.1.

HRMS-ESI (m/z): $[M+H]^+$ calcd for $C_{15}H_{17}N_2O_3^+$, 273.1234; found, 273.1229.

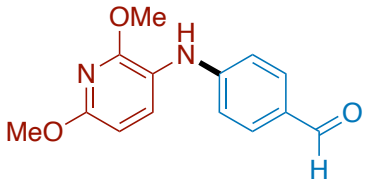

4-((2,6-dimethoxypyridin-3-yl)amino)benzaldehyde (2.3r)

General Procedure A was followed using 2,6-dimethoxy-3-nitropyridine (138.1 mg, 0.75 mmol, 1.5 equiv) and 4-chlorobenzaldehyde (70.3 mg, 0.50 mmol, 1.0 equiv). The crude product was purified via column chromatography (80g of silica gel, 1 CV hexanes, then 0–40% EtOAc/hexanes across 15 CV) to afford the product (88.0 mg, 0.341 mmol, 68% yield, R_f = 0.19 in 20% EtOAc/hexanes) as a yellow solid.

^1H NMR (500 MHz, $CDCl_3$) δ 9.77 (s, 1H), 7.72 (d, *J* = 8.6 Hz, 2H), 7.56 (d, *J* = 8.2 Hz, 1H), 6.86 (d, *J* = 8.6 Hz, 2H), 6.35 (d, *J* = 8.2 Hz, 1H), 5.91 (s, 1H), 3.97 (s, 3H), 3.93 (s, 3H).

$^{13}C\{^1H\}$ NMR (126 MHz, $CDCl_3$) δ 190.3, 159.2, 155.4, 150.7, 134.1, 132.1, 128.2, 115.8, 113.7, 100.4 53.8, 53.6.

HRMS-ESI (m/z): $[M+H]^+$ calcd for $C_{14}H_{15}N_2O_3^+$, 259.1077; found, 259.1076.

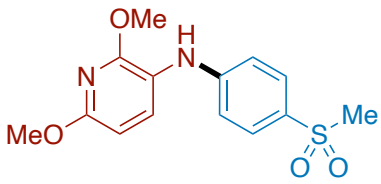

2,6-dimethoxy-*N*-(4-(methylsulfonyl)phenyl)pyridin-3-amine (2.3s)

General Procedure A was followed using 2,6-dimethoxy-3-nitropyridine (138.1 mg, 0.75 mmol, 1.5 equiv) and 4-chlorophenyl methyl sulfone (95.3 mg, 0.50 mmol, 1.0 equiv). The crude product was purified via column chromatography (80g of silica gel, 1 CV hexanes, then 0–20% EtOAc/hexanes across 15 CV) to afford the product (126.9 mg, 0.412 mmol, 82% yield, R_f = 0.37 in 20% EtOAc/hexanes) as a brown solid.

^{1}H NMR (500 MHz, $CDCl_3$) δ 7.72 (d, *J* = 8.8 Hz, 2H), 7.52 (d, *J* = 8.3 Hz, 1H), 6.86 (d, *J* = 8.7 Hz, 2H), 6.35 (d, *J* = 8.2 Hz, 1H), 5.84 (s, 1H), 3.97 (s, 3H), 3.93 (s, 3H), 3.01 (s, 3H).

^{13}C{^{1}H} NMR (126 MHz, $CDCl_3$) δ 159.5, 155.7, 149.9, 134.5, 129.5, 129.3, 115.6, 113.7, 100.5, 53.8, 53.6, 45.0.

HRMS-ESI (m/z): $[M+H]^+$ calcd for $C_{14}H_{17}N_2O_4S^+$, 309.09035; found, 309.0900.

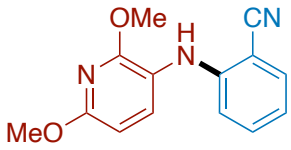

2-((2,6-dimethoxypyridin-3-yl)amino)benzonitrile (2.3t)

General Procedure A was followed using 2,6-dimethoxy-3-nitropyridine (138.1 mg, 0.75 mmol, 1.5 equiv) and 2-chlorobenzonitrile (68.8 mg, 0.50 mmol, 1.0 equiv). The crude product was purified via column chromatography (80g of silica gel, 1 CV hexanes, then 0–20% EtOAc/hexanes across 15 CV) to afford the product (109.0 mg, 0.427 mmol, 85% yield, R_f = 0.55 in 20% EtOAc/hexanes) as a white solid.

^{1}H NMR (500 MHz, $CDCl_3$) δ 7.49 (d, *J* = 8.2 Hz, 1H), 7.47 (dd, *J* = 7.6, 1.5 Hz, 1H), 7.32 (ddd, *J* = 8.7, 7.2, 1.6 Hz, 1H), 6.82 (d, *J* = 8.6 Hz, 1H), 6.78 (td, *J* = 7.5, 1.0 Hz, 1H), 6.33 (d, *J* = 8.2 Hz, 1H), 6.04 (s, 1H), 3.96 (s, 3H), 3.93 (s, 3H).

$^{13}C\{^{1}H\}$ NMR (126 MHz, $CDCl_3$) δ 159.7, 156.1, 148.3, 135.2, 133.9, 133.0, 118.5, 117.6, 115.3, 112.9, 100.5, 97.8, 53.8, 53.6.

HRMS-ESI [(m/z): $M+H]^+$ calcd for $C_{14}H_{14}N_3O_2^+$, 256.1081; found, 256.1077.

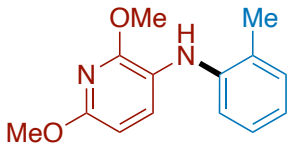

2,6-dimethoxy-*N*-(*o*-tolyl)pyridin-3-amine (2.3u)

General Procedure B was followed using 2,6-dimethoxy-3-nitropyridine (138.1 mg, 0.75 mmol, 1.5 equiv) and 2-chlorotoluene (63.3 mg, 0.50 mmol, 1.0 equiv). The crude product was purified via column chromatography (80g of silica gel, 1 CV hexanes, then 0–15% EtOAc/hexanes across 15 CV) to afford the product (71.8 mg, 0.294 mmol, 59% yield, R_f = 0.76 in 20% EtOAc/hexanes) as a clear, colorless oil.

^{1}H NMR (500 MHz, $CDCl_3$) δ 7.34 (d, J = 8.2 Hz, 1H), 7.16 (d, J = 7.4 Hz, 1H), 7.09 (t, J = 7.7 Hz, 1H), 7.00 (d, J = 8.0 Hz, 1H), 6.84 (t, J = 7.3 Hz, 1H), 6.26 (d, J = 8.2 Hz, 1H), 5.31 (s, 1H), 3.99 (s, 3H), 3.90 (s, 3H), 2.27 (s, 3H).

$^{13}C\{^{1}H\}$ NMR (126 MHz, $CDCl_3$) δ 156.9, 153.4, 142.3, 130.8, 129.5, 126.7, 126.4, 120.6, 120.1, 115.5, 99.6, 53.7, 53.5, 17.7.

HRMS-ESI (m/z): $[M+H]^+$ calcd for $C_{14}H_{17}N_2O_2^+$, 245.12845; found, 245.1282.

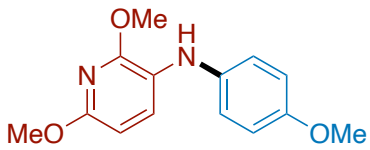

2,6-dimethoxy-*N*-(4-methoxyphenyl)pyridin-3-amine (2.3v)

General Procedure B was followed using 2,6-dimethoxy-3-nitropyridine (138.1 mg, 0.75 mmol, 1.5 equiv) and 4-chloroanisole (71.3 mg, 0.50 mmol, 1.0 equiv). The crude product was purified via column chromatography (80g of silica gel, 1 CV hexanes, then 0–15% EtOAc/hexanes across 15 CV) to afford the product (79.0 mg, 0.304 mmol, 61% yield, R_f = 0.43 in 20% EtOAc/hexanes) as a clear, colorless oil.

^{1}H NMR (500 MHz, $CDCl_3$) δ 7.31 (d, *J* = 8.2 Hz, 1H), 6.95 (d, *J* = 8.3 Hz, 2H), 6.83 (d, *J* = 8.9 Hz, 2H), 6.22 (d, *J* = 8.2 Hz, 1H), 5.42 (s, 1H), 3.99 (s, 3H), 3.88 (s, 3H), 3.78 (s, 3H).

^{13}C{^{1}H} NMR (126 MHz, $CDCl_3$) δ 156.1, 154.5, 152.4, 137.0, 126.5, 121.8, 120.0, 114.7, 99.3, 55.6, 53.8, 53.4.

HRMS-ESI (m/z): $[M+H]^+$ calcd for $C_{14}H_{17}N_2O_3^+$, 261.12337; found, 261.1231.

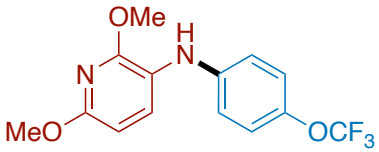

2,6-dimethoxy-*N*-(4-(trifluoromethoxy)phenyl)pyridin-3-amine (2.3w)

General Procedure B was followed using 2,6-dimethoxy-3-nitropyridine (138.1 mg, 0.75 mmol, 1.5 equiv) and 1-chloro-4-(trifluoromethoxy)benzene (98.3 mg, 0.50 mmol, 1.0 equiv). The crude product was purified via column chromatography (80g of silica gel, 1 CV hexanes, then 0–20% EtOAc/hexanes across 15 CV) to afford the product (124.0 mg, 0.395 mmol, 79% yield, R_f = 0.42 in 20% EtOAc/hexanes) as a white solid.

^{1}H NMR (500 MHz, $CDCl_3$) δ 7.46 (d, *J* = 8.2 Hz, 1H), 7.06 (d, *J* = 8.7 Hz, 1H), 6.86 (d, *J* = 9.0 Hz, 2H), 6.29 (d, *J* = 8.2 Hz, 1H), 5.54 (s, 1H), 3.97 (s, 3H), 3.91 (s, 3H).

$^{13}C\{^{1}H\}$ NMR (126 MHz, $CDCl_3$) δ 157.8, 154.2, 143.4, 142.1, 131.0, 122.3, 120.6 (q, J = 255.7 Hz), 118.5,116.2, 99.9, 53.7, 53.5.

$^{19}F\{^{1}H\}$ NMR (377 MHz, $CDCl_3$) δ -58.41.

HRMS-ESI (m/z): $[M+H]^+$ calcd for $C_{14}H_{14}F_3N_2O_3^+$, 315.0951; found, 315.0944.

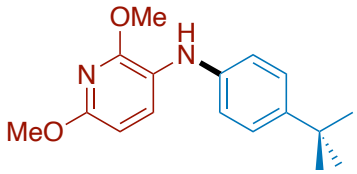

***N*-(4-(*tert*-butyl)phenyl)-2,6-dimethoxypyridin-3-amine (2.3x)**

General Procedure B was followed using 2,6-dimethoxy-3-nitropyridine (138.1 mg, 0.75 mmol, 1.5 equiv) and 4-*tert*-butyl-1-chlorobenzene (84.3 mg, 0.50 mmol, 1.0 equiv). The crude product was purified via column chromatography (80g of silica gel, 1 CV hexanes, then 0–10% EtOAc/hexanes across 15 CV) to afford product (119.7 mg, 0.4180 mmol, 84% yield, R_f = 0.65 in 20% EtOAc/hexanes) as a pale yellow oil. The product was 95% pure; the impurity was 3,3'-(1-(4-(*tert*-butyl)phenyl)hydrazine-1,2-diyl)bis(2,6-dimethoxypyridine).

^{1}H NMR (500 MHz, $CDCl_3$) δ 7.48 (d, J = 8.2 Hz, 1H), 7.26 (d, J = 8.6 Hz, 2H), 6.91 (d, J = 8.6 Hz, 2H), 6.25 (d, J = 8.2 Hz, 1H), 5.53 (s, 1H), 3.98 (s, 3H), 3.89 (s, 3H), 1.30 (s, 9H).

$^{13}C\{^{1}H\}$ NMR (126 MHz, $CDCl_3$) δ 156.7, 153.1, 143.2, 141.5, 128.6, 126.1, 120.2, 116.4, 99.4, 53.7, 53.4, 34.1, 31.5.

HRMS-ESI (m/z): $[M+H]^+$ calcd for $C_{17}H_{23}N_2O_2^+$, 287.1754; found, 287.1749.

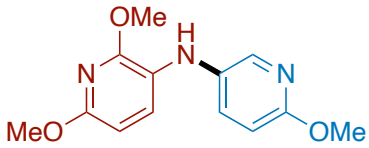

2,6-dimethoxy-*N*-(6-methoxypyridin-3-yl)pyridin-3-amine (2.3y)

General Procedure B was followed using 2,6-dimethoxy-3-nitropyridine (138.1 mg, 0.75 mmol, 1.5 equiv) and 5-chloro-2-methoxypyridine (71.8 mg, 0.50 mmol, 1.0 equiv). The crude product was purified via column chromatography (80g of silica gel, 1 CV hexanes, then 0–20% EtOAc/hexanes across 15 CV) to afford the product (72.9 mg, 0.279 mmol, 56% yield, R_f = 0.31 in 20% EtOAc/hexanes) as a yellow oil.

^{1}H NMR (500 MHz, $CDCl_3$) δ 7.31 (d, *J* = 8.2 Hz, 1H), 6.95 (d, *J* = 8.9 Hz, 2H), 6.82 (d, *J* = 8.9 Hz, 2H), 6.21 (d, *J* = 8.2 Hz, 1H), 5.43 (s, 1H), 3.99 (s, 3H), 3.88 (s, 3H), 3.77 (s, 3H).

^{13}C{^{1}H} NMR (126 MHz, $CDCl_3$) δ 156.1, 154.5, 152.4, 137.0, 126.5, 121.8, 120.0, 114.7, 99.3, 55.6, 53.7, 53.4.

HRMS-ESI (m/z): $[M+H]^+$ calcd for $C_{13}H_{16}N_3O_3^+$, 262.1186; found, 262.1183.

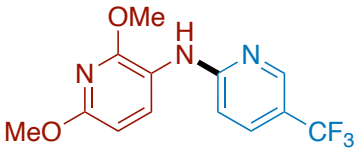

***N*-(2,6-dimethoxypyridin-3-yl)-5-(trifluoromethyl)pyridin-2-amine (2.3z)**

General Procedure A was followed using palladium(II) acetate (11.2 mg, 0.05 mmol, 0.1 equiv), BrettPhos (26.8 mg, 0.05 mmol, 0.1 equiv), 2,6-dimethoxy-3-nitropyridine (138.1 mg, 0.75 mmol, 1.5 equiv) and 2-chloro-5-(trifluoromethyl)pyridine (90.8 mg, 0.50 mmol, 1.0 equiv). The increased catalyst loading was necessary to ensure complete conversion of the heteroaryl chloride. The crude product was purified via column chromatography

(80g of silica gel, 1 CV hexanes, then 0–20% EtOAc/hexanes across 15 CV) to afford the product (36.0 mg, 0.120 mmol, 24% yield, R_f = 0.34 in 20% EtOAc/hexanes) as a white solid.

^{1}H NMR (500 MHz, $CDCl_3$) δ 8.42 (m, 1H), 8.15 (d, *J* = 8.3 Hz, 1H), 7.62 (dd, *J* = 8.8, 2.4 Hz, 1H), 6.69 (s, 1H), 6.61 (d, *J* = 8.8 Hz, 1H), 6.35 (d, *J* = 8.3 Hz, 1H), 3.99 (s, 3H), 3.92 (s, 3H).

^{13}C{^{1}H} NMR (126 MHz, $CDCl_3$) δ 158.6, 158.3, 153.9, 145.9 (q, *J* = 4.4 Hz), 134.4 (q, *J* = 3.3 Hz), 133.2, 124.4 (q, *J* = 270.4 Hz), 117.0 (q, *J* = 33.0 Hz), 115.7, 108.0, 100.2, 77.2, 77.0, 76.7, 53.8, 53.6.

^{19}F{^{1}H} NMR (377 MHz, $CDCl_3$) δ -61.37.

HRMS-ESI (m/z): $[M+H]^+$ calcd for $C_{13}H_{13}F_3N_3O_2^+$, 300.0954; found, 300.0949.

2.4.8 Comments and FAQ

Which conditions should I use?

If using an electron-poor chloroarene, use 5 mol% catalyst loading and HFIP as the proton source. If using an electron-rich chloroarene, use 10 mol% catalyst loading and TFE as the proton source. If using a heteroaryl chloride, use 10 mol% catalyst loading regardless of electronics and choose the proton source as above. The presence of *N*-heterocycles on the nitroarene does not appear to necessitate any changes in conditions.

Can I use a different palladium precatalyst instead of $Pd(OAc)_2$?

To the best of our knowledge, this reaction appears to work with almost any common palladium precatalyst, including $PdCl_2$, $Pd_2(dba)_3$, $Pd(OAc)_2$, and Buchwald

palladacycles. The use of an exogenous reductant enables facile initiation, mitigating many of the issues that necessitate specific precatalysts in other cross-couplings.

Comments on Isolation and Purification

We found that aqueous workup in 0.1 M citric acid was particularly effective at breaking the emulsion caused by the presence of manganese salts and particles following catalytic reactions. Even when using 0.1 M citric acid, a slight emulsion still forms at the boundary of the organic and aqueous layer; we found it best to carry this emulsion with the aqueous layer.

We found it best to dry-load the crude product on Celite prior to column chromatography. Attempts to dry load on silica gel led to apparent rapid oxidation of the product and any aniline formed during the reaction. While we did not quantify the extent or rate of this oxidation, we decided that it was prudent to avoid it altogether by using Celite. We did not observe any significant decomposition of the products during column chromatography. Wet loading was also effective.

Typically, the product and the 1,1,2-triarylhydrazine byproduct have identical R_f in TLC analysis. We were able to resolve the two via SFC-MS to determine the makeup of the reaction mixture, but caution against GC-FID analysis when the carrier gas is H_2; as any trace metals on the column can enable hydrogenation of the N–N bond, leading to erroneously high apparent yields. We did not observe any decomposition of the 1,1,2-triarylhydrazine on a GC-MS utilizing He as the carrier gas. When using auto-columns with inline detection for purification, any 1,1,2-triarylhydrazine typically elutes directly after the desired product and can often be distinguished by the ratio of absorbances at

254 and 280 nm; the desired product absorbs more strongly at 280 nm, the 1,1,2-triarylhydrazine absorbs more strongly at 254 nm.

In cases where the amount of 1,1,2-triarylhydrazine is significantly complicating the isolation of the desired product or is reducing the yield to unacceptable levels, we had success employing a reductive quench adapted from work by Sapountzis and Knochel (cleaving the N–N bond liberates additional diarylaniline and aniline).[112] We expect that this quench would be most useful when coupling electron-rich chloroarenes, which tend to yield more 1,1,2-triarylhydrazine. A general procedure is provided below. The catalyst loading and proton source should still be adjusted based on the starting materials as in Section 2.4.8.

General Procedure for Reactions with a Reductive Quench

In a nitrogen-filled glovebox, an oven-dried test tube (15 × 85 mm) was charged with a PTFE-coated stir bar, palladium(II) acetate (11.2 mg, 0.05 mmol, 0.1 equiv), BrettPhos (26.8 mg, 0.05 mmol, 0.1 equiv), chloroarene (if solid, 0.500 mmol), and nitroarene (if solid, 0.750 mmol). Manganese powder (219.8 mg, 4.000 mmol, 8.00 equiv) and DMF (1 mL) were then added, followed by chloroarene (if liquid, 0.5 mmol) and nitroarene (if liquid, 0.75 mmol). The tube was then sealed with a rubber septum (14/20) and removed from the glovebox. 2,2,2-Trifluoroehtanol (TFE) (63.0 μL, 87.5 mg, 0.875 mmol, 1.75 equiv) was added to the tube through the septum via gas-tight syringe. The reaction was then immersed in a pre-heated oil bath, where it was stirred (1250 rpm) at 100 °C for 16 h.

Reductive quench. After stirring, the reaction mixture was cooled to 60 °C, uncapped, and manganese (274.7 mg, 5.00 mmol, 10.00 equiv) was added. The tube was then recapped and connected to a bubbler via a needle inserted through the septum. While

stirring, a mixture of trifluoroacetic acid (1 mL) and acetic acid (5 mL) was added slowly through the septum, taking care to not allow the gas formation to force the reaction mixture out of the needle into the bubbler. After addition, the reaction was left to stir at 60 °C for 1 h.

Workup. After stirring, the reaction mixture was allowed to cool to rt and poured onto a mixture of crushed ice (15 g) and 10 mL of 2 M NaOH solution. The mixture was extracted with diethyl ether (3 × 30 mL). The combined organic layers were washed with saturated $NaHCO_3$ solution and brine. The organic layer was then dried over anhydrous Na_2SO_4, filtered directly into a flask containing Celite, and concentrated. The immobilized residue was purified by column chromatography to yield the desired product.

Figure 2.18. Limitations in Scope for First-Generation Conditions

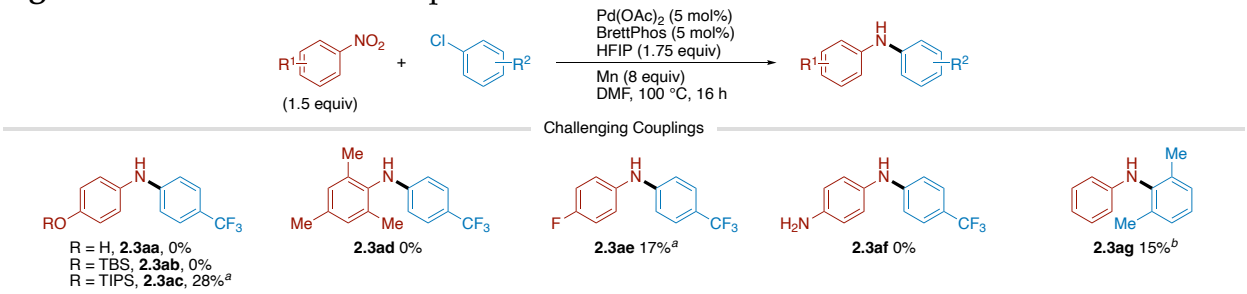

All reactions were set up according to General Procedure A unless otherwise specified. For reactions stating 0% yield, no product was observed by SFC-MS analysis. [a]Isolated yield. [b]General Procedure B was followed. The yield vs. 1,3,5-trimethoxybenzene as an internal standard is provided. This is an assay yield and is not intended to be quantitative. It is included to demonstrate that while the product is produced, it is not made in high yield.

As seen in the low yield of **2.3l** (not pictured in this figure), electron-poor nitroarenes perform poorly in this reaction. The major observed side product is the corresponding aniline derivative.

Unprotected aliphatic and aromatic alcohols shut down the desired reaction completely as seen in **2.3aa**. While the desired product can be obtained by protecting aliphatic alcohols as the TBS ether as seen in **2.3f** (not pictured in this figure), a larger TIPS group

(**2.3ac**) is required to protect phenols. Even then, the TIPS group is relatively unstable under the reaction conditions leading to a low isolated yield. Methyl ethers were well-tolerated.

2,6-disubstitution of either the nitroarene (**2.3ad**) or the chloroarene (**2.3ag**) leads to significantly decreased yield.

Primary amines and anilines are not tolerated under these conditions (**2.3af**) as they couple competitively. Despite azobenzene arylation occurring faster than aniline arylation (Figure 2.13), competition experiments demonstrated that primary aniline derivatives outcompete nitroarenes when both are present in the same reaction (Figure 2.12). This is most likely due to a low effective concentration of the active azoarene during the reaction and strong binding of primary anilines to BrettPhosPd^{II}(Ar)Cl complexes. We suggest utilizing a benzyl protecting group if possible.

Substrates bearing electron-poor aryl fluorides provide low yields of the desired product, **2.3ae**. We hypothesize that competitive S_NAr may occur, where aniline or even the desired product acts as a nucleophile.

Chapter 3: Catalyst Design in Ni-Catalyzed Cross-Electrophile Couplings: Computational Methods Enable Improvements in Selectivity

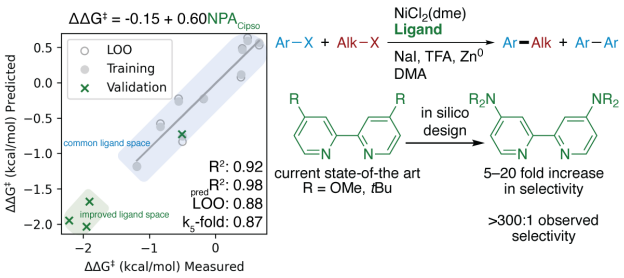

The work described in this chapter has been published and is reprinted in its adapted form with permission from Akana, M. E.; Tcyrulnikov, S.; **Akana-Schneider, B. D**.; Reyes, G. P.; Monfette, S.; Sigman, M. S.; Hansen, E. C.; Weix, D. J. Computational Methods Enable the Prediction of Improved Catalysts for Nickel-Catalyzed Cross-Electrophile Coupling" *J. Am. Chem. Soc*. **2023**. DOI: 10.1021/jacs.3c09554.

3.1 Introduction

3.1.1 Selectivity in Nickel-Catalyzed Cross-Electrophile Coupling

Scheme 3.1 Bipyridines Enable Diverse Reactivity

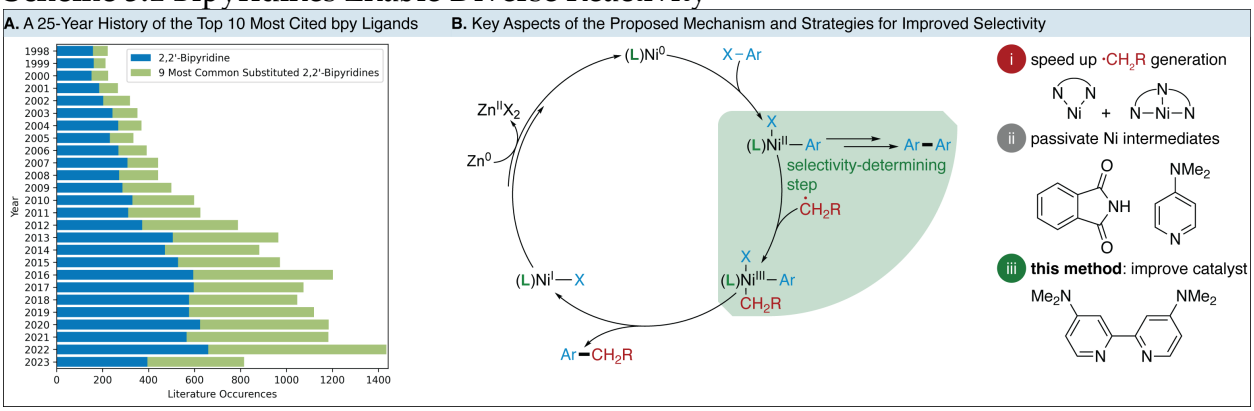

[a]Occurrences and prevalence of 2,2'-bipyridine ligands were gathered from a Reaxys structure search performed on 6/28/23 for 2,2'-bipyridine with attached GH groups in each available position. The results were filtered to exclude higher order polypyridines and compounds most utilized in organic light emitting diodes (MW > 500).

Despite distinct advantages compared to redox-neutral alternatives, widespread adoption of C(sp^2)–C(sp^3) cross-electrophile coupling is hampered by the prevalence of off-cycle pathways, particularly the formation of aryl homodimer. Slow oxidative radical capture and reductive elimination can allow for degradative reduction and disproportionation of the (L)Ni^{II}(Ar)X intermediate to form the aryl homodimer.[32,113] Two major approaches are commonly employed to mitigate this side reaction: (1) accelerating the desired reaction by increasing the concentration of alkyl radical in solution, and (2) extending the lifetime of the (L)Ni^{II}(Ar)X intermediate (Scheme 3.1b).

Increasing the rate of alkyl radical generation is an attractive approach to improve selectivity as it often is accompanied by an increase reaction rate. One common approach to achieve this is to employ a cocatalyst that is responsible for activating the C(sp^3) coupling partner. For example, methods from Weix,[114–116] Sevov,[117] and others[118] have employed separate L3-ligated nickel catalysts that selectively activate the alkyl coupling

partner, leading to improved selectivity. Other methods employ stoichiometric additives either alone or in combination with a separate catalyst to activate the radical precursor. One attractive advantage of this method is that it can enable the activation of less-reactive coupling partners, thereby broadening the scope of compatible substrate pools. While this method can be effective, it introduces complexity into the catalytic system, as tuning the catalyst ratio is necessary to avoid a flip in selectivity—radical recombination to form the alkyl homodimer can occur when the concentration of alkyl radical is too high in solution.

Stabilization of the (L)Ni^{ii}(Ar)X intermediate is typically achieved via the addition of additional catalytic ligands or stoichiometric additives.[118,119] These can saturate open coordination sites on the square planar (L)Ni^{ii}(Ar)X—preventing unwanted side reactions—or participate in ligand exchange yielding a more stable intermediate. For example, the MacMillan group showed that addition of stoichiometric phthalimide can expand the robustness of decarboxylative metallophotoredox couplings by forming a stable (L)Ni^{II}(Ar)phth complex.[120] These complexes were found to be significantly more stable than their halide analogues, expanding the lifetime of the nickel intermediate. While this approach may be widely applicable, it is still unclear whether the resulting passivated nickel species will effectively participate in the diverse set of one-electron steps as their halide analogues. Further the use of stoichiometric additives decreases the mass efficiency of these reactions and complicates purification.

Instead of the above strategies, an ideal approach would be the systematic development of a suite of improved ligands that form catalysts resistant to the most common off-cycle pathways. These ligands would provide inherent selectivity, expanding the applicability, robustness, and generality of C(sp^2)–C(sp^3) cross-

electrophile couplings. Additionally, since they would undergo the same set of single- and two-electron steps as existing catalysts, these improved ligands should be employable in concert with existing strategies to further improve selectivity.

3.1.2 Bipyridine Ligands and Methods for Improved Ligand Design

Selection of an appropriate ligand is often the critical enabling point in the development and implementation of a cross-electrophile coupling reaction.[1,118,121] Most often a derivative of 2,2'-bipyridine (bpy; Scheme 3.1a), these ligands are critical for enabling the diverse suite of single- and two-electron processes[122–125] that have helped cement first-row transition metal-catalyzed processes as a unique class of reactions rather than simple, economically attractive alternatives to precious-metal catalysis. The increased demand for more diverse and robust cross-coupling reactions has driven the implementation of an increasingly diverse suite of substituted bpy ligands. Despite this diversification, in-depth, systematic studies of the effects of molecular structure on the reactivity of bipyridines remain limited.

Bpy ligands are significantly less developed than phosphines. As such, the diversity of known bpy ligands is significantly lower than that of common phosphines. In fact, there are only one quarter as many commercially available nitrogen donors of any type compared to phosphorous donors. This inaccessibility of ligands hampers methodology development, as the breadth of accessible reactivity is limited to commonly available ligands. While new ligands can be accessed, they must be synthesized prior to testing, lengthening the experimental process.

Several approaches have been employed to overcome this developmental gap. First, high-throughput experimentation (HTE) searching of pharmaceutical compound

libraries has yielded new classes of ligands that allow access to previously inaccessible coupling partners. For example, the Weix group discovered that pyridyl carboxamidines (PyCam, and the related PyBCam and bpyCam ligands) allow for the cross-electrophile coupling of unactivated chloroarenes, as well as difficult halo-*N*-heterocycles.[126] Other approaches have centered on the skeletal modification of bipyridines to promote reliable mono-ligation,[127] or general surveys of reactivity.[123,128] More often, HTE approaches are used to identify the best ligand amongst a suite of ligands with validated reactivity.[129,130] These methods have offered understanding of the differences between *N*-donors and *P*-donors, and the general reactivity of individual catalysts, but have yet to offer a detailed model of selectivity and reactivity.

One attractive approach to the development of improved models of selectivity and reactivity is statistical modelling using DFT-derived molecular descriptors. This approach has revolutionized the design, selection, and commercialization of optimal phosphine ligands.[131–133] Despite this success, translation of these methods to dinitrogen ligands remains limited. For example, the Sigman group has published extensive work on the use of multivariate linear regression to rationalize and design improved 2-(2-pyridyl)oxazoline ligands in enantioselective Heck arylations.[134,135] Additionally, the Doyle group have utilized a similar workflow to explain the improved enantioselectivity provided by 2,2′-biimidazoline ligands compared to related bioxazolines.[136] While these studies provide significant insight into their respective systems, they focus only on enantioinduction, rather than overall yield or selectivity for off-cycle products. Based on the success of these studies, we hypothesized that a similar statistical approach could be applied to more general obstacles of selectivity and robustness in cross-electrophile couplings.

This chapter describes the application of modern computational and statistical methods to the development of a model of selectivity in bipyridine-nickel-catalyzed C(sp^2)–C(sp^3) cross-electrophile coupling. The resulting models provide key mechanistic insight into the source of selectivity in cross-electrophile coupling based on the geometric and electronic properties of the critical (L)Ni^{II}(Ar)X intermediate: (1) 6- and 6,6′-(di)substituted bpy ligands promote a tetrahedral (L)Ni^{II}(Ar)Br intermediate in the ground state, which rapidly dimerizes the haloarene, and (2) the selectivity of bipyridine-ligated catalyst is determined by the least donating of the two pyridine units, with strongly donating, symmetric ligands providing higher selectivity. This model is robust and predictive, allowing for the interpolative and extrapolative prediction of the selectivity of bipyridine ligands. Using this model to inform and validate our hypotheses, we designed a suite of improved 4,4′-bis(dialkylamino)-2,2′-bipyridine ligands in silico, which demonstrate significant improvements in selectivity, robustness, and generality.

3.2 Results and Discussion

3.2.1 Model Development and Mechanistic Insight

Scheme 3.2 Model Reaction and Initial Data Processing Efforts

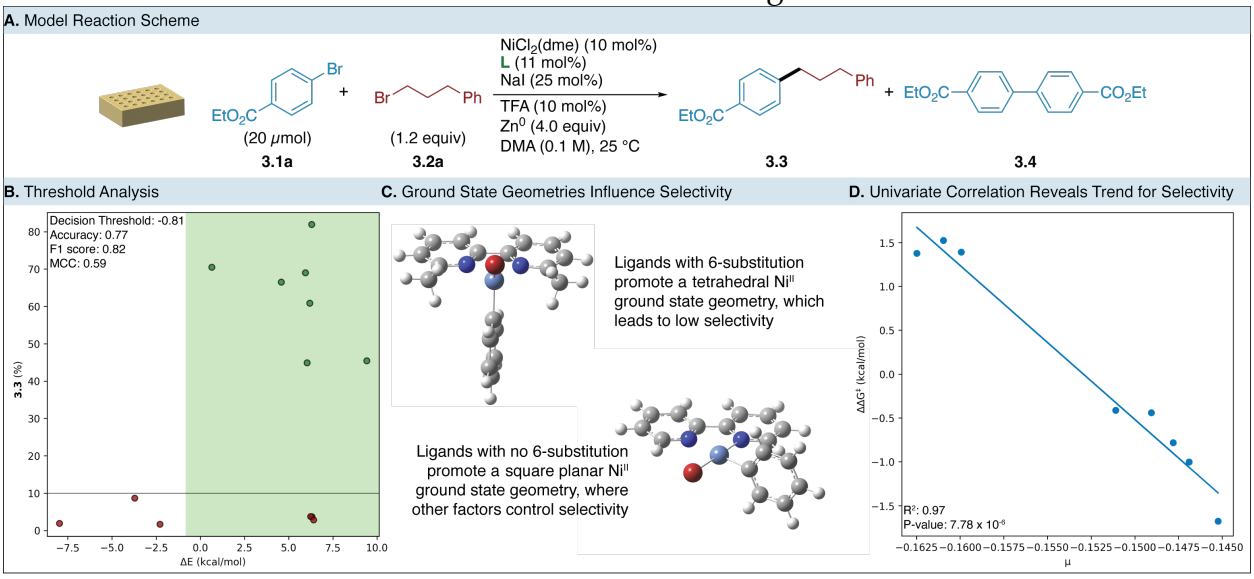

We constructed an initial training set by employing common 4,4′-, 5,5′- and 6,6′-bipyridines in a model cross-electrophile coupling reaction (Scheme 3.2a). This model coupling—the cross-electrophile coupling of aryl and primary alkyl bromides—has been used for ligand development and searching in previous efforts and in the translation of cross-electrophile coupling to other reductive systems.[126,136] Notably, this reaction is known to provide a consistent set of byproducts, mainly the aryl homodimer; with the selectivity being determined mainly by the identity of the bipyridine ligand. When screened in 96-well plates (20 μmol scale), the training set yielded a wide range of yield and selectivity (2–82% yield[B]). Further, these results confirmed that the yield of the model reaction is almost entirely a function of selectivity for the cross-product over the aryl homodimer.

Due to the diversity in substitution pattern and the conjugated π-backbone of bpy ligands, we hypothesized that common tabulated molecular descriptors would be insufficient to model selectivity. Instead, we generated a library of DFT-optimized (L)Ni^{II}(Ph)Br catalysts from which we could derive molecular parameters.[137–144] These molecular descriptors provide insight into the intrinsic characteristics of each catalyst.[136] We chose to derive molecular descriptors directly from the (L)Ni^{II}(Ph)Br intermediate—which participates in the selectivity determining step—for two reasons: (1) previous studies have shown that using an on-cycle intermediate—rather than an unbound ligand—provides unique insight into the structure of the catalyst–leading to more robust models, and (2) the resulting dataset could be translated to a variety of bipyridine-nickel catalyzed processes, as the model intermediate is common to many different cross-couplings. From these DFT-optimized structures, we calculated a variety of electronic

[B] This corresponds to an energetic range of 3.51 kcal/mol in $\Delta\Delta G^{\ddagger}$.

and steric parameters. Further, we also calculated the structure of the tetrahedral (L)Ni^{II}(Ph)Br complex, as access to this triplet geometry has been hypothesized as necessary for reductive elimination in some cases.[145]

Initial statistical analysis centered around binary classification of results based on the molecular descriptors. This decision was informed by the observation that initial correlations consistently failed to account for several experimental observations where the observed yield and selectivity were low. This led us to hypothesize that there may be two different classes of catalyst within the experimental set, where different structural features were determining selectivity. Threshold analysis showed a shift in selectivity based on the ground state geometry of the (L)Ni^{II}(Ph)Br complex. 6, and 6,6'-(di)substituted ligands were found to promote a tetrahedral ground state, and to rapidly dimerize the haloarene, leading to low selectivity (Scheme 3.2b, Scheme 3.2c).[146] Contrastingly, ligands with 4,4'- and 5,5'-disubstitution yielded a ground state square planar (L)Ni^{II}(Ph)Br complex, and provided a range of selectivity.

6'- and 6,6'-(di)substituted bpys—and related phenanthrolines—are well known to display reactivity distinct from their unhindered analogues.[147] This difference is most likely due to their ability to support stable, well-defined nickel(I) complexes. One notable observation This difference in reactivity has led to the widespread use of these ligands in classes of reactions where otherwise undesirable reaction pathways are preferred, such as insertion-elimination pathways in "chain-walking" functionalizations.[147] We hypothesize that under reducing conditions, these ligands promote the reduction of the tetrahedral (L)Ni^{II}(Ar)Br to (L)Ni^{I}(Ar), which then undergoes rapid decomposition to form the aryl homodimer. about these ligands is that while their electrochemical properties are similar to that of L3 ligands—such as terpyridines—the selective

dimerization of the aryl halide in the presence of a C(sp^3)–X electrophile differentiates their reactivity.[128]

Scheme 3.3 Collinear Variables Decrease Specificity

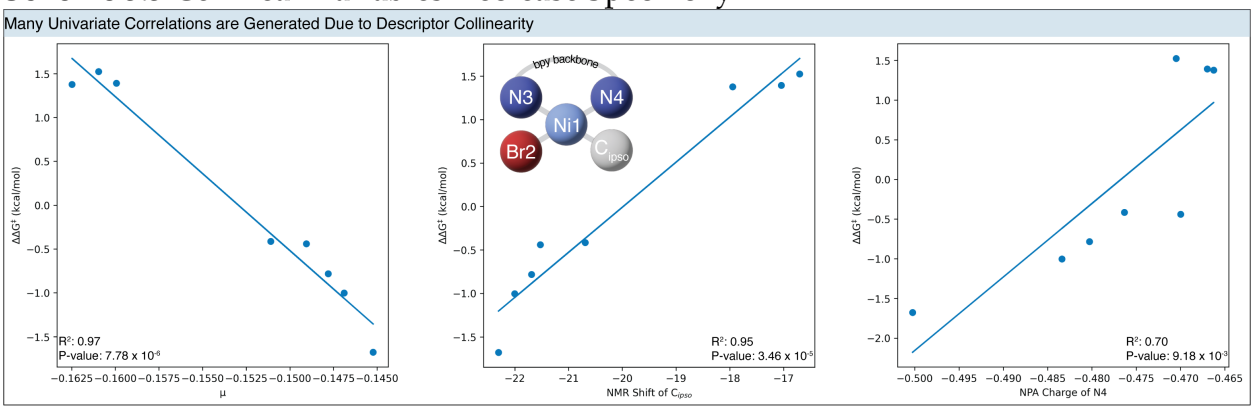

Following the identification of separate classes of ligands via threshold analysis, we limited the training set to 4,4′- and 5,5′-disubsittuted bipyridines. Utilizing this dataset, we found several strong correlations between molecular descriptors and observed selectivity (Scheme 3.2d). While we were able to find a robust single parameter model based on μ, the average of the HOMO and LUMO energies, the high collinearity between many descriptors (Scheme 3.3) led to uncertainty about the specificity and translatability of our model. This model did support the qualitative observation that more donating ligands yielded higher selectivity. However, the many similarly strong descriptor correlations made it difficult to determine if the critical feature determining selectivity was associated with the nickel center, a particular nitrogen donor, or the electronic character of one of the other ligands.

The high collinearity in molecular descriptors was attributed to the symmetric nature of the ligands in the training set. To deconvolute the computational dataset, we designed a suite of non-symmetrically substituted 4- and 4,4′-(di)substituted bipyridines, making and effort to cover a suite of electronic properties on each pyridine unit. We

hypothesized that in the square planar (L)Ni^{II}(Ar)Br intermediate, directional parameters—such as the NPA charge of an individual nitrogen, carbon, or bromine atom—would be determined by only one of the pyridine units in the low energy isomer. Contrastingly, μ, which is centered on the nickel, should be determined by the average donation of the two rings. Further, we imagined several possible benefits of non-symmetrically substituted bipyridines, such as accelerated reduction of donating-withdrawing-bpy ligated, tetrahedral (L)Ni^{II}(X)$_2$, and improved stability of (L)Ni^0 due to the lower total electron density.

Scheme 3.4 A Tailored Dataset Enables a More Robust Model

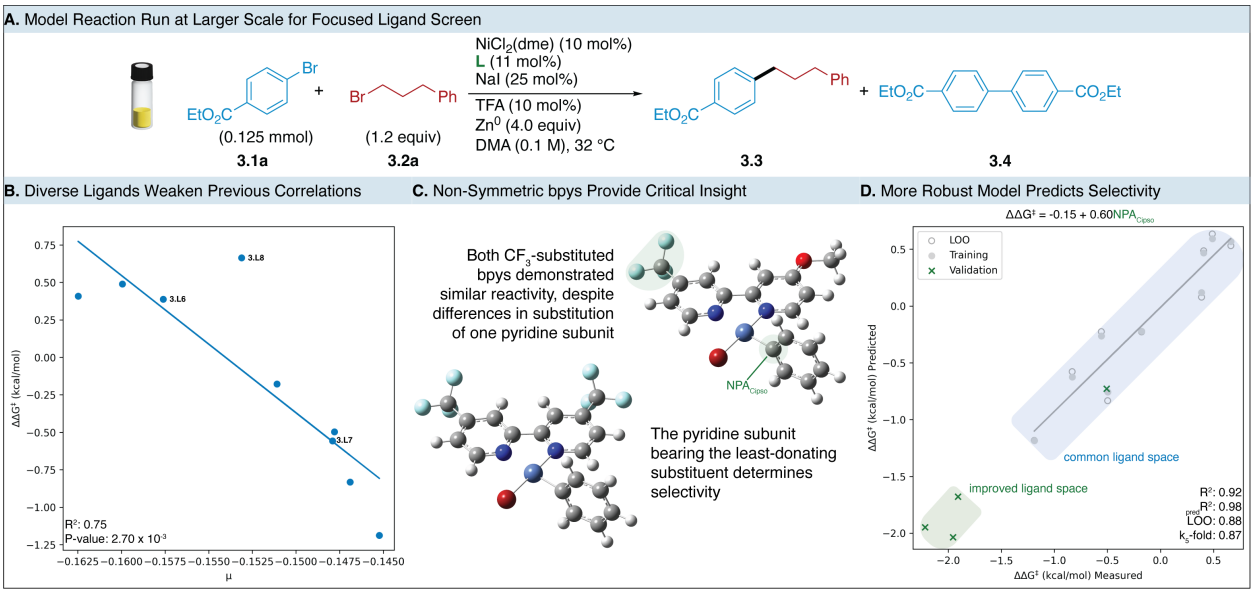

In combination with select symmetric 4,4'-disubstituted bipyridines, we utilized the suite of non-symmetric bipyridines to construct a tailored ligand suite that we screened on a larger scale (0.125 mmol, Scheme 3.4a). Univariate correlations between the new dataset and molecular descriptors showed that the previous strongest correlations, utilizing μ, was significantly weakened (R^2 decreased from 0.97 to 0.75) by the introduction of non-symmetric bipyridines (Scheme 3.4b). This suggested that nickel-centered parameters were inferior to atom-specific or directional descriptors. This

supported our qualitative observation that selectivity is purely determined by the least donating pyridine unit (Scheme 3.4c). For example, 4-methoxy-4′-(trifluoromethyl)-2,2′-bipyridine yields selectivity similar to 4,4′-bis(trifluoromethyl)-2,2′-bipyridine, not 4,4′-dimethoxy-2,2′-bipyridine. This observation is explained by the consistent arrangement of ligands in the low energy isomer of the $(L)Ni^{II}(Ph)Br$ complex. For non-symmetric bipyridines, the least donating pyridine is consistently trans to the phenyl structure in the low energy isomer. While the energy difference between the two isomers is often low (as little as 0.5 kcal/mol), the consistent arrangement of atoms allows for delineation of the molecular descriptors and provides a handle to build more robust models.

Based on these results, we found a strong (R^2 = 0.92), robust (k_5-fold = 0.87) univariate model for selectivity in nickel-catalyzed cross-electrophile coupling (Scheme 3.4d). This model relies on the NPA charge of the ipso carbon (C_{ipso}) of the phenyl ligand. We found that this model allows for the prediction of symmetric and non-symmetric bipyridine ligands. Leave-one-out validation—an internal validation method—yielded a high Q^2 (0.88), indicating that the model can accurately predict the selectivity of individual points when they are withheld from the regression. Further, external validation showed that the model is predictive via extrapolation and interpolation ($_{pred}R^2$ = 0.98).

Notably, the use of molecular descriptors derived directly from the critical $(L)Ni^{II}(Ar)Br$ intermediate offers several distinct benefits over tabulated electronic features such as Hammett (σ) constants. First, the model correctly predicts the selectivity of non-symmetrically substituted bipyridines without direct intervention. Second, the model allows for accurate prediction of the selectivity promoted by 5,5′-disubstituted bipyridines, despite none being included in the training set. While the positive σ^m value

for the methoxy group (0.12) would suggest that 5,5′-dimethoxy-2,2′-bipyridine would perform more poorly than bpy, the model appropriately gauged the mitigation of the σ-withdrawing effect by π-donation across the bipyridine backbone.[148] Indeed, 5,5′-dimethoxy-2,2′-bipyridine was accurately predicted to yield higher selectivity than bpy.

This model also offers mechanistic insight. The commonly proposed mechanism for aryl homodimerization from $(L)Ni^{II}(Ar)X$ is direct disproportionation to form $(L)Ni^{II}(Ar)_2$. Osakada found that the rate of disproportionation was higher for electron-rich haloarenes than electron-neutral or -poor haloarenes.[149] This would suggest that a more negative charge on C_{ipso} would lead to a higher rate of disproportionation.[150] Our model suggests the opposite is true under reducing conditions. We hypothesize that under reducing conditions, aryl homodimerization occurs not via direct disproportionation of $(L)Ni^{II}(Ar)X$, but rather by reduction of $(L)Ni^{II}(Ar)X$ to from $(L)Ni^{I}(Ar)$ followed by decomposition. This is supported by the observation that 6,6′-disubstituted bipyridines—which are known to form stable nickel(I) complexes—and electron-poor bipyridines—which also have recently been shown to form (L)NiI(Ar) complexes—both lead to rapid dimerization of the aryl halide.[128,151] We imagine that formation of the aryl homodimer may occur via two possible pathways: (1) disproportionation of two $(L)Ni^{I}(Ar)$ complexes to form $(L)Ni^{0}$ and $(L)Ni^{II}(Ar)_2$; or transmetalation between $(L)Ni^{II}(Ar)Br$ and $(L)Ni^{I}(Ar)$, forming $(L)Ni^{II}(Ar)_2$ and $(L)Ni^{I}(Br)$. While oxidative addition of Ar–X to $(L)Ni^{I}(Ar)$ to form $(L)Ni^{III}(Ar)_2X$ is also possible, we observed that selectivity increases as catalyst concentration decreases (Figure 3.7), indicating that two nickel centers are involved in the rate-determining step. Further computational and experimental investigation is needed to support these hypotheses.

Table 3.1 Ligands Designed In Silico Outperform State-of-the-art Bipyridines[a]

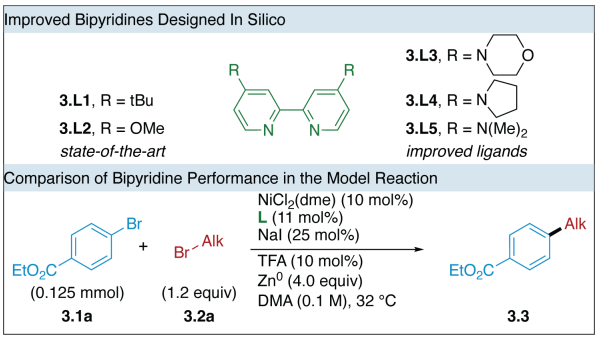

Entry	L	**3.3** (%)	Selectivity (**3.3**:**3.4**)	ΔΔG‡ (kcal/mol)
1	**3.L1**	49	2:1	-0.5
2	**3.L2**	61	7:1	-1.19
3	**3.L3**	82	23:1	-1.91
4	**3.L4**	88	25:1	-1.95
5	**3.L5**	79	39:1	-2.22

[a]Alk = 3-Phenylpropyl. Reactions were assembled in a nitrogen filled glovebox at a 0.125 mmol scale in 1.25 mL of DMA. Yields and selectivity were determined by GC-FID.

Using this model, we designed and validated a series of 4,4′-bis(dialkylamino)-2,2′-bipyridines in silico that were predicted to have improved selectivity. After synthesizing these ligands, we found that they displayed an over five-fold increase in selectivity (from 7:1 to 39:1 for **3.L2** and **3.L5** respectively), demonstrating the impact of the model (Table 3.1). Further, the ability to test hypothesized ligands in silico can save synthetic effort. We had hypothesized that 4,4′,5,5′-tetramethoxy-2,2′-bpyridine (**3.L24**) would provide an increase in selectivity; however, the model predicted that this ligand—which is made in six steps via the published synthesis—would provide little benefit over the common **3.L2** (Figure 3.16). In fact, we had already initiated the synthesis of this ligand—and failed alternative syntheses—when we developed the model and determined that it was not worth significant investment.

3.2.2 Applications of Improved Bipyridines

Table 3.2 Benchmarking of Improved Bipyridines in the XEC of Aryl Halides

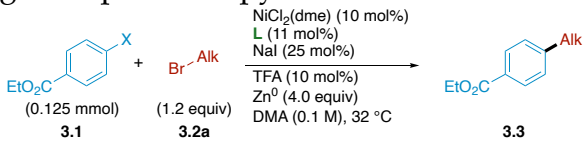

Entry	X	Result with **3.L5** (**3.3**%, **3.3**: **3.4**)	Result with **3.L2** (**3.3**%, **3.3**: **3.4**)
1	Cl	93, 311:1	85, 17:1
2	Br	79, 39:1	61, 7:1
3	I	72, 25:1	90, 130:1

[a]Alk = 3-Phenylpropyl. Reactions were assembled in a nitrogen filled glovebox at a 0.125 mmol scale in 1.25 mL of DMA. Yields and selectivity were determined by GC-FID.

To investigate the generality of the improved suite of ligands, we began by investigating the coupling of common aryl and alkyl halides (Table 3.2). We found that both the overall and relative selectivity—an almost 20-fold increase from 17:1 to 311:1 compared to **3.L2**—significantly improved when coupling less reactive and more abundant chloroarenes. Further increases in selectivity (364:1) were achieved by decreasing the catalyst loading (Figure 3.7). Despite this success, we saw an inversion in selectivity when coupling the equivalent iodoarene, where **3.L2** outperformed **3.L5**. These results demonstrate that in many validated couplings, our improved ligands, can be employed to enable more selective, higher yielding reactions.

Table 3.3 NMe_2bpy Enables the Coupling of Alkyl Chlorides

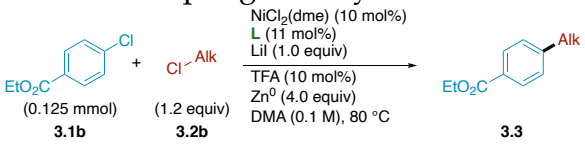

Entry	L	**3.3** (%)	Selectivity (**3.3**: **3.4**)
1	**3.L1**	4	1:114
2	**3.L2**	11	1:9
3	**3.L5**	62	25:1

[a]Alk = 3-Phenylpropyl. Reactions were assembled in a nitrogen filled glovebox at a 0.125 mmol scale in 1.25 mL of DMA. Yields and selectivity were determined by GC-FID.

We also hypothesized that the increased stability of (**3.L5**)Ni^{II}(Ar)X may enable the improved coupling of previously difficult substrate pools (Table 3.3). The coupling of chloroalkanes is an attractive method for late-stage cross-electrophile coupling, as primary alkyl chlorides are tolerated in a variety of other cross-couplings–including other cross-electrophile couplings.[33] The coupling of chloroalkanes is complicated by the difficulty in their activation; the slow alkyl radical generation leads to significant amounts of aryl dimerization. While the Weix and MacMillan groups have both been successful in coupling chloroalkanes—either by the use of improved PyBCam ligands or stoichiometric silane reagents—the selective coupling of these substrates is unknown with a traditional bipyridine-nickel system.[152,153] We found that by modifying the model system, we were able to couple an activated chloroarene and a primary chloroalkane in yields similar to other published methods (62%). This was accomplished by increasing the reaction temperature to 80 °C and using 1 equivalent of lithium iodide in place of catalytic sodium iodide. These two modifications enabled more facile radical generation via in situ conversion of the chloroalkane to the iodoalkane. Notably neither **3.L1**, nor **3.L2** yielded significant amounts of products. Even when 2.0 equiv of LiI were employed, the maximum yield obtained was 30%. These data clearly show the benefits afforded by the increased stability of (L)Ni^{II}(Ar)X when 4,4′-bis(dimethylamino)-2,2′-bipyridne is used.

Table 3.4 NMe_2bpy Increases the Efficiency of Existing Coupling and Unlocks New Substrate Pairings

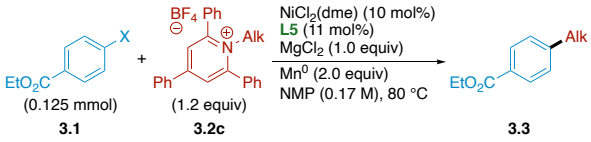

Entry	X	**3.3** (%)[b]	Selectivity (**3.3: 3.4**)[b]
1	Br	98	84:1
2	Cl	55	7:1
3	Cl	86[c]	8:1

[a]Alk = 3-Phenylpropyl. Reactions were assembled in a nitrogen filled glovebox at a 0.125 mmol scale in 735 μL of NMP. Yields and selectivity were determined by GC-FID. [c]20 mol% of $NiCl_2$(dme) and 22 mol% of **3.L5** were used.

We also were able to substitute 4,4′-bis(dimethylamino)-2,2′-bipyridne for the optimal 4,4′-dimethoxy-bipyridine in the cross-electrophile coupling of *N*-alkyl-2,4,6-pyridinium salts with bromoarenes (Table 3.4).[154] We found that use of this ligand yielded the desired product in 98% yield. This result continues the electronic trend observed in the Watson group's original optimization: **3.L1** < **3.L2** < **3.L5**. While arylation of *N*-alkylpyridiniums with bromoarenes is well known, coupling of chloroarenes remains elusive.[117] This is most likely due to differential rates in the formation of (L)Ni^{II}(Ar)Cl and alkyl radical, as oxidative addition into the chloroarene is slower than a bromoarene, but radical generation occurs at the same rate, since reduction and fragmentation of the *N*-alkylpyridnium is proposed to be driven by manganese, not the nickel catalyst. As such, we hypothesized that the highly donating 4,4′-bis(dialkylamino)-2,2′-bipyridine might accelerate oxidative addition. We found that substituting the equivalent chloroarene in the published conditions yielded the cross-product in 55% yield. We found that by doubling the catalyst loading, the yield increased to 86% yield. We hypothesize that the increase in the concentration of (L)Ni^{II}(Ar)Cl increases the rate of radical capture, improving selectivity. The inherent stability afforded by **3.L5** mitigates aryl dimerization, which is exacerbated at higher catalyst loadings—**3.L1** and **3.L5** provide lower yields

(Figure 3.9). Together, these yields show that these improved ligands can be applied to other cross-electrophile couplings and allow combinations of substrates that were previously inaccessible.

Overall, this suite of 4,4′-bis(dialkylamino)-2,2′bipyridines offers a significant increase in selectivity over the common state-of-the-art bipyridine ligands. Despite their utility and presence in the development of novel photocatalysts, application of any of these ligands to nickel catalysis is relegated to ineffective entries in optimization tables and a single use of **3.L5** on a particularly challenging substrate.[155] We expect that the relatively low increase in yield from **3.L1** to **3.L2** combined with the difficulty in synthesizing novel, electron-rich bipyridines made these ligands an unattractive target for synthetic efforts. We hope that these results will accelerate the adoption of these ligands into the canon of bpy ligands in nickel catalysis. Currently, only our highest performing ligand, **3.L5** is commercially available for a reasonable price. While we found them to be slightly less selective, **3.L3** and **3.L5** may offer benefits in solubility or selectivity in specific applications. Additionally, we identified one additional ligand that is predicted to provide even higher selectivity than those screened in this work—4,4′-bis(diethylamino)-2,2′-bipyridine (**3.L26**) (Figure 3.16). While we chose not to synthesize **3.L26**, it may be beneficial in certain applications. While additional improvements in bpy ligand donicity and selectivity may be possible via further innovation and structural modifications, we expect that these will be minimal compared to the large increases observed in this study. Instead, the next frontier in ligand design likely lies in the discovery and refinement of new ligand classes such as PyCams.

3.3 Conclusions

In conclusion, we have applied modern computational and statistical methods to develop a model for selectivity for cross-product and aryl homodimer in nickel-catalyzed cross-electrophile coupling. The two resulting models—a binary classification of a ligands' applicability based on the ground state of their (L)Ni^{II}(Ph)Br complex and a linear relationship between the NPA charge of the ipso carbon of the low energy (L)Ni^{II}(Ph)Br complex—enable the prediction of the performance of a variety of substituted bipyridines with diverse functionalities. This study also highlighted the importance of designing a diverse, informative training set to minimize collinearity in computational parameters, and maximize interpretability. The use of parameters derived from a representative on-cycle intermediate enable strong models and mechanistic insight. These results suggest that, in contrast to previous stoichiometric studies under redox-neutral conditions, the primary dimerization pathway in cross-electrophile coupling may proceed via degradative reduction of (L)Ni^{II}(Ar)X.

Using our model, designed a suite of improved 4,4'-bis(dialkylamino)-2,2'-bipyridines. These ligands display significant improvements in selectivity and yield compared to the current common bipyridines. Further, they can be easily substituted into other cross electrophile couplings to increase yield and selectivity, as well as allow access to more diverse coupling partners. We expect that adoption of these ligands—in combination with existing strategies—will enable more robust, selective, and widely applicable cross electrophile couplings, driving adoption of cross-electrophile coupling in industrial and academic settings.

3.4 Experimental

3.4.1 General Information

3.4.1.1 Reagents

Metals and Catalysts

Nickel(II) chloride dimethoxyethane, $NiCl_2$(dme), was purchased from Sigma-Aldrich. Zinc flake (-325 mesh) and manganese powder (-325 mesh) were purchased from Alfa Aesar. Palladium(II) acetate was purchased from Chem-Impex International. All metals and catalysts were stored in a nitrogen-filled glovebox and used without additional purification.

Ligands

4,4′-Bis(trifluoromethyl)-2,2′-bipyridine and 4,4′-bis(dimethylamino)-2,2′-bipyridine were purchased from Ambeed. 2,2′-bipyridine was purchased from Sigma-Aldrich. 4,4′-dimethoxy-2,2′-bipyridine was purchased from Ambeed or Sigma-Aldrich. Dimethyl ([2,2′-bipyridine]-4,4′-dicarboxylate) was purchased from AstaTech. 4,4′-di-*tert*-butyl-2,2′-bipyridine was purchased from Sigma-Aldrich; reactions utilizing this ligand sourced from Ambeed and TCI America provided consistently lower selectivity. Ligands were stored and handled in a nitrogen-filled glovebox and used without further purification.

Substrates

Ethyl 4-bromobenzoate was purchased from Oakwood. Ethyl 4-chlorobenzoate was purchased from Alfa Aesar. Ethyl 4-iodobenzoate was purchased from Matrix Scientific. 1-Bromo-3-phenylpropane was purchased from TCI America. 1-Chloro-3-phenylpropane

was purchased from Sigma-Aldrich. Unless otherwise specified, all substrates were purchased from commercial sources, stored on the benchtop and used without further purification.

Solvents

N,*N*-Dimethylacetamide (DMA), *N*-Methylpyrrolidone (NMP), Toluene, and DMSO were purchased from Sigma-Aldrich. All solvents were anhydrous and stored in a nitrogen-filled glovebox unless otherwise specified.

Other Reagents

Sodium iodide and trifluoroacetic acid (TFA) were purchased from Sigma-Aldrich. 4,4''-Dimethyl-1,1'-biphenyl was purchased from Thermo Fisher Scientific. Other reagents, substrates, and solvents were purchased from commercial sources, stored on the benchtop, and used without further purification unless otherwise specified.

3.4.1.2 Methods

NMR Spectroscopy

^{1}H, ^{13}C, and ^{19}F NMR spectra were acquired on 400 and 500 MHz Bruker Avance III NMR instruments. NMR chemical shifts are reported in ppm. ^{1}H chemical shifts are referenced to tetramethylsilane (TMS) in $CDCl_3$ (δ = 0.00 ppm). ^{13}C and ^{19}F chemical shifts were absolute referenced to the accompanying ^{1}H spectrum. Coupling constants (*J*) are reported in Hertz.

High Resolution Mass Spectrometry

Mass spectrometry data was collected on a Thermo Scientific Q Exactive Plus Hybrid Quadrupole-Orbitrap via flow injection with electrospray ionization by the Paul Bender Chemical Instrumentation Center facility at the University of Wisconsin-Madison.

Gas Chromatography

GC analyses were performed on an Agilent 7890A GC equipped with dual DB-5 columns (20 m × 180 μm × 0.18 μm), dual FID detectors, and H_2 as the carrier gas. A sample volume of 1 μL was injected at a temperature of 300 °C and a 100:1 split ratio. The initial inlet pressure was 20.3 psi but varied as the column flow was held constant at 1.8 mL/min for the duration of the run. The initial oven temperature of 50 °C was held for 0.46 min followed by a temperature ramp of 65 °C/min up to 300 °C. The total run time was 5.0 min and the FID temperature was 325 °C.

Flash Chromatography

Flash chromatography was performed on a Teledyne ISCO Rf-200 (detection at 254 and 280 nm) equipped with an 80 g Teledyne ISCO Redisep Rf Gold silica gel column (20–40 μm particle size) or on a Biotage Isolera One (detection at 210 nm and 400 nm) equipped with a 25 g KPsil column (40-63 μm particle size). Products were visualized by UV.

3.4.2 Ligand Key and Preparation

3.4.2.1 Ligand Key

Figure 3.1 Bipyridine Ligand Key

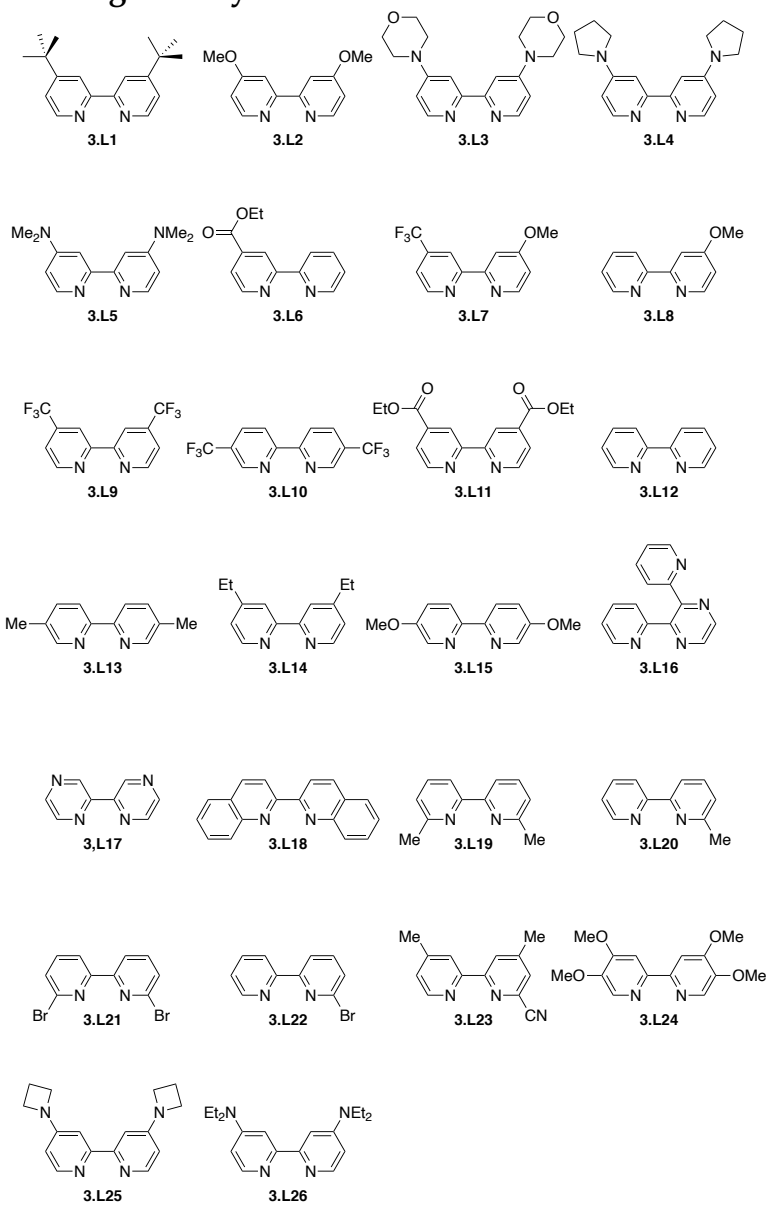

3.4.2.2 Preparation of Ligands

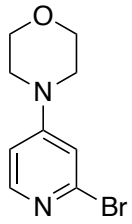

4-(2-bromopyridin-4-yl)morpholine (3.L3a)

An oven-dried 1 dram vial equipped with a PTFE-coated stir bar was sealed with a phenolic screw cap bearing a PTFE-backed silicone septum. Using anhydrous technique, the vial was charged with 2-bromo-4-fluoropyridine (414.3 μL, 704.0 mg, 4.000 mmol, 1.000 equiv), DMSO (1.5 mL), DIPEA (1034.0 mg, 8.0000 mmol, 2.0000 equiv), and morpholine (415.3 μL, 418.2 mg, 4.800 mmol, 1.200 equiv). The reaction was stirred at 100 °C for 1 h, allowed to cool to rt, and poured over DI water (50 mL). The mixture was extracted with EtOAc (3 × 30 mL). The combined organic layers were then washed with water (2 × 100 mL) and brine (2 × 100 mL) prior to being dried over Na_2SO_4, filtered, and concentrated to yield **3.L3a** (819.6 mg, 3.371 mmol, 84%) as an off-white solid.

^{1}H NMR (500 MHz, $CDCl_3$) δ 8.03 (d, *J* = 6.0 Hz, 1H), 6.82 (d, *J* = 2.4 Hz, 1H), 6.60 (dd, *J* = 6.0, 2.5 Hz, 1H), 3.86 – 3.80 (m, 4H), 3.32 – 3.26 (m, 4H).

^{13}C{^{1}H} NMR (126 MHz, $CDCl_3$) δ 156.7, 150.0, 143.6, 111.2, 107.6, 77.2, 77.0, 76.7, 66.2, 46.1.

HRMS-ESI (m/z): $[M+H]^+$ calcd for $C_9H_{12}BrN_2O^+$, 243.0128; found, 243.0126.

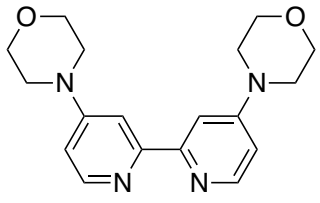

4,4′-dimorpholino-2,2′-bipyridine (3.L3) was prepared by modification of the literature procedure.[156]

In a nitrogen-filled glovebox, an oven-dried 1 dram vial equipped with a PTFE-coated stir bar was charged with nickel(II) bromide dimethoxyethane (30.9 mg, 0.100 mmol, 0.100 equiv), 4,4′-bis(trifluoromethyl)-2,2′-bipyridine (29.2 mg, 0.100 mmol, 0.100 equiv), and DMF (1.000 mL). The vial was sealed with a phenolic screw cap bearing a PTFE-backed silicone septum and placed on a stir plate (1000 rpm, rt) for 20 min. After stirring the vial was unsealed, and 4-(2-bromopyridin-4-yl)morpholine (243.1 mg, 1.000 mmol, 1.000 equiv) was added, followed by manganese (164.8 mg, 3.000 mmol, 3.000 equiv). The vial was resealed, removed from the glovebox, and placed on a pre-heated stir plate where the contents were stirred (100 °C, 1000 rpm) for 24 h. After stirring, the reaction mixture was allowed to cool to rt and was poured over 100 mL of saturated Na_4EDTA solution. The mixture was stirred for 20 min. After stirring, the mixture was diluted with 50 mL of water and extracted with DCM (3 × 30 mL). The combined organic layers were dried over Na_2SO_4, filtered, and concentrated. The resulting residue was purified by column chromatography (80 g of silica gel, 1 CV of DCM, then 0–30% iPrOH/DCM across 25 CV) to yield **3.L3** (79.7 mg, 0.244 mmol, 49%) as a light brown solid.

^{1}H NMR (500 MHz, $CDCl_3$) δ 8.36 (d, *J* = 5.9 Hz, 1H), 7.89 (d, *J* = 2.6 Hz, 1H), 6.68 (dd, *J* = 5.9, 2.7 Hz, 1H), 3.91 – 3.79 (m, 4H), 3.41 (dd, *J* = 5.9, 4.0 Hz, 4H).

^{13}C{^{1}H} NMR (126 MHz, $CDCl_3$) δ 157.1, 156.1, 149.6, 108.1, 105.6, 66.5, 46.4.

HRMS-ESI (m/z): $[M+H]^+$ calcd for $C_{18}H_{23}N_4O_2^+$, 327.1816; found, 327.1811.

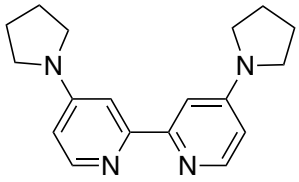

4,4′-di(pyrrolidin-1-yl)-2,2′-bipyridine (3.L4) was synthesized according to the literature procedure and characterization data matched those reported in the literature.[157]

^{1}H NMR (500 MHz, CDCl3) δ 8.27 (d, J = 5.8 Hz, 2H), 7.54 (d, J = 2.5 Hz, 2H), 6.38 (dd, J = 5.8, 2.5 Hz, 2H), 3.49 – 3.30 (AA'XX', 8H), 2.07 – 1.97 (AA'XX', 8H).

^{13}C{^{1}H} NMR (126 MHz, $CDCl_3$) δ 156.9, 152.6, 148.9, 106.7, 104.3, 47.1, 25.4.

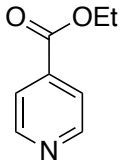

ethyl isonicotinate (3.L6a) was synthesized according to the literature procedure and characterization data matched those reported in the literature.[158]

^{1}H NMR (500 MHz, $CDCl_3$) δ 8.78 (d, *J* = 4.5 Hz, 2H), 7.85 (d, *J* = 4.6 Hz, 2H), 4.42 (q, *J* = 7.2 Hz, 2H), 1.42 (t, *J* = 7.2 Hz, 2H).

^{13}C{^{1}H} NMR (126 MHz, $CDCl_3$) δ 165.1, 150.6, 137.6, 122.8, 61.8, 14.2.

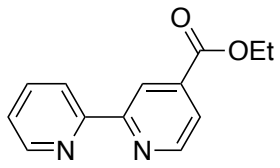

ethyl [2,2′-bipyridine]-4-carboxylate (3.L6) was synthesized according to the literature procedure and characterization data matched those reported in the literature.[11][159]

^{1}H NMR (500 MHz, $CDCl_3$) δ 8.93 (dd, *J* = 1.6, 0.9 Hz, 1H), 8.82 (dd, *J* = 4.9, 0.9 Hz, 1H), 8.73 (ddd, *J* = 4.7, 1.8, 0.9 Hz, 1H), 8.42 (dt, *J* = 8.0, 1.1 Hz, 1H), 7.88 (dd, *J* = 5.0, 1.6 Hz, 1H), 7.84 (td, *J* = 7.7, 1.8 Hz, 1H), 7.35 (ddd, *J* = 7.5, 4.8, 1.2 Hz, 1H), 4.46 (q, *J* = 7.1 Hz, 2H), 1.44 (t, *J* = 7.1 Hz, 3H).

^{13}C{^{1}H} NMR (126 MHz, $CDCl_3$) δ 165.3, 157.3, 155.4, 149.9, 149.3, 138.9, 137.0, 124.1, 122.8, 121.3, 120.4, 61.8, 14.3.

HRMS-ESI (m/z): $[M+H]^+$ calcd for $C_{13}H_{13}N_2O_2^+$, 229.0972; found, 229.0969.

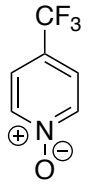

4-(trifluoromethyl)pyridine 1-oxide (3.L7a) was synthesized according to the literature procedure and characterization data matched those reported in the literature.[159]

^{1}H NMR (500 MHz, $CDCl_3$) δ 8.28 (d, *J* = 6.5 Hz, 2H), 7.51 (d, *J* = 6.6 Hz, 2H).

^{13}C{^{1}H} NMR (126 MHz, $CDCl_3$) δ 139.8, 126.6 (q, *J* = 35.7 Hz), 123.0 (q, *J* = 3.7 Hz), 122.4 (q, *J* = 271.8 Hz).

^{19}F{^{1}H} NMR (377 MHz, $CDCl_3$) δ -63.61.

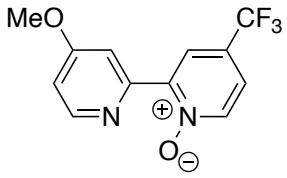

4′-methoxy-4-(trifluoromethyl)-[2,2′-bipyridine] 1-oxide (3.L7b) was prepared by modification of the literature procedure.[159]

In a nitrogen-filled glovebox, 2 oven-dried 1 dram vials equipped with PTFE-coated stir bars were each charged with palladium(II) acetate (11.2 mg, 0.0500 mmol, 0.0500 equiv), 4-(trifluoromethyl)pyridine *N*-oxide (326.2 mg, 2.000 mmol, 2.000 equiv), potassium carbonate (276.4 mg, 2.000 mmol, 2.000 equiv), tri-*tert*-butylphosphine (12.1 mg, 0.0598 mmol, 0.0600 equiv, in 2 mL of toluene), and 2-bromo-4-methoxypyridine (188.0 mg, 1.000 mmol, 1.000 equiv). The vials were sealed with phenolic screw caps bearing PTFE-backed silicone septa and removed from the glovebox. The reactions were stirred at rt for 15 min, then at 100 °C overnight. The reactions were allowed to cool to rt, poured over a single plug of Celite (pre-wetted with DCM), and further rinsed with DCM (50 mL). The combined filtrate was concentrated, and the resulting residue was purified by column chromatography (80 g of silica gel, 10% acetone/hexanes for 1 CV, then 10–40% acetone/hexanes across 20 CV) to yield **3.L7b** (262.5 mg, 0.9715 mmol, 50%) as a light tan solid.

^{1}H NMR (500 MHz, $CDCl_3$) δ 8.62 (d, *J* = 2.6 Hz, 1H), 8.60 (d, *J* = 2.8 Hz, 1H), 8.55 (d, *J* = 5.6 Hz, 1H), 8.36 (d, *J* = 6.9 Hz, 1H), 7.46 (dd, *J* = 6.9, 2.8 Hz, 1H), 6.92 (dd, *J* = 5.6, 2.5 Hz, 1H), 3.93 (s, 3H).

^{13}C{^{1}H} NMR (126 MHz, $CDCl_3$) δ 166.0, 150.4, 149.6, 147.7, 141.5, 126.8 (q, *J* = 35.5 Hz), 125.1 (q, *J* = 3.9 Hz), 122.6 (q, *J* = 272.2 Hz), 121.3 (q, *J* = 3.5 Hz), 111.4, 111.3, 55.4.

^{19}F{^{1}H} NMR (377 MHz, $CDCl_3$) δ -63.56.

HRMS-ESI (m/z): $[M+Na]^+$ calcd for $C_{12}H_9F_3N_2NaO_2^+$, 293.0508; found, 293.0502.

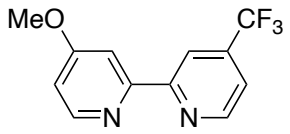

4-methoxy-4′-(trifluoromethyl)-2,2′-bipyridine (3.L7) was prepared by modification of the literature procedure.[159]

A 100 mL three-neck flask equipped with a PTFE-coated stir bar was connected to a nitrogen manifold via a three-way adapter, the side necks were sealed with rubber septa. The flask was evacuated and backfilled with nitrogen 3 times. Under positive pressure of nitrogen, Pd/C (5 wt%) was added through the side neck (50.0 mg, 0.0235 mmol, 0.0470 equiv, in 15 mL of MeOH), and the vessel containing the Pd/C solution was washed with MeOH (5 mL) and the washings were added to the reaction flask. 4′-methoxy-4-(trifluoromethyl)-[2,2′-bipyridine] 1-oxide (135.1 mg, 0.5000 mmol, 1.000 equiv, in 15 mL of MeOH) was added to the flask, and a hydrogen balloon was connected to the top of the three-way adapter. The flask was evacuated and backfilled with nitrogen three times before it was evacuated once more and refilled with hydrogen from the balloon. The reaction was stirred at rt for 2 h. After the reaction was confirmed complete by TLC, the flask was evacuated and backfilled with nitrogen three times. The reaction mixture was poured over Celite—pre-wetted with MeOH—in a sintered funnel. The flask was rinsed with MeOH (2 × 50 mL), the rinse was added to the funnel, and the filter cake was rinsed with MeOH (50 mL, whilst avoiding drying the cake). The filtrate was concentrated under reduced pressure to yield **3.L7** (116.5 mg, 0.4583 mmol, 92%) as a brown solid.

^{1}H NMR (500 MHz, $CDCl_3$) δ 8.83 (d, *J* = 5.0 Hz, 1H), 8.69 (d, *J* = 2.0 Hz, 1H), 8.52 (d, *J* = 5.6 Hz, 1H), 8.02 (d, *J* = 2.6 Hz, 1H), 7.52 (dd, *J* = 5.0, 1.6 Hz, 1H), 6.89 (dd, *J* = 5.6, 2.6 Hz, 1H), 3.96 (s, 3H).

^{13}C{^{1}H} NMR (126 MHz, $CDCl_3$) δ 166.8, 157.4, 156.5, 150.5, 149.9, 139.3 (q, *J* = 34.1 Hz), 123.0 (q, *J* = 273.3 Hz), 119.2 (q, *J* = 3.5 Hz), 117.1 (q, *J* = 3.7 Hz), 111.4, 106.5, 55.4.

$^{19}F\{^{1}H\}$ NMR (377 MHz, $CDCl_3$) δ -64.74.

HRMS-ESI (m/z): $[M+H]^+$ calcd for $C_{12}H_{10}F_3N_2O^+$, 255.0740; found, 255.0737.

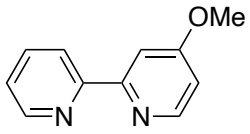

4-methoxy-2,2′-bipyridine (3.L8)

In a nitrogen-filled glovebox, an oven-dried 1 dram vial equipped with a PTFE-coated stir bar was charged with tris(dibenzylideneacetone)dipalladium(0) (27.5 mg, 0.0300 mmol, 0.030 equiv), tri-*tert*-butylphosphine (20.2 mg, 0.100 mmol, 0.100 equiv), Tributyl(2-pyridyl)tin (405.0 mg, 1.100 mmol, 1.100 equiv), and 1,4-dioxane (3.000 mL). 2-Bromo-4-methoxypyridine (188.0 mg, 1.000 mmol, 1.000 equiv) was added to the vial prior to it being sealed with a phenolic screw cap bearing a PTFE-backed silicone septum. The vial was removed from the glovebox and placed on a pre-heated stir plate (90 °C, 1000 rpm), for 16 h. The reaction mixture was allowed to cool to rt and was poured over Celite—pre-wetted with DCM—in a sintered funnel, and the filter cake was rinsed with DCM (50 mL). The filtrate was then concentrated and purified by column chromatography (25 g of silica gel, 1 CV of 40% EtOAc/hexanes, then 40–80% EtOAc/hexanes across 20 CV) to yield **3.L8** (126.8 mg, 0.6809 mmol, 68%) as a white solid.

^{1}H NMR (500 MHz, $CDCl_3$) δ 8.68 (ddd, J = 4.9, 1.8, 1.0 Hz, 1H), 8.49 (d, J = 5.7 Hz, 1H), 8.40 (dt, J = 8.0, 1.1 Hz, 1H), 7.98 (d, J = 2.6 Hz, 1H), 7.81 (td, J = 7.7, 1.8 Hz, 1H), 7.31 (ddd, J = 7.5, 4.8, 1.2 Hz, 1H), 6.85 (dd, J = 5.6, 2.6 Hz, 1H), 3.96 (s, 3H).

$^{13}C\{^{1}H\}$ NMR (126 MHz, $CDCl_3$) δ 166.7, 158.1, 156.0, 150.3, 149.0, 136.9, 123.8, 121.3, 110.9, 106.0, 55.3.

HRMS-ESI (m/z): $[M+H]^+$ calcd for $C_{11}H_{11}N_2O^+$, 187.0866; found, 187.066.

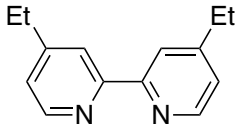

4,4′-diethyl-2,2′-bipyridine (3.L14) was obtained as a byproduct of the oxidative coupling of 4-ethylpyridine to form 4,4′,4′′-triethyl-2,2′:6′,2′′-terpyridine. We recommend synthesis of **L14** via dimerization of 2-bromo-4-ethylpyridine.[156]

In a nitrogen-filled glovebox, an oven-dried, 1 L, three-neck flask was charged with freshly distilled 4-ethylpyridine (40.00 g, 373.3 mmol, 1.000 equiv) and anhydrous DMA (200 mL). 10% Pd/C was added to the flask (5.36 g, 5.04 mmol, 0.0135 equiv), followed by manganese(IV) oxide (41.00 g, 471.6 mmol, 1.260 equiv). The flask was sealed and removed from the glovebox. On the bench, the flask was equipped with a reflux condenser, an internal thermometer, and an overhead stirrer via the three necks. The contents were placed under an argon atmosphere via an inlet at the top of the condenser. The contents were heated to reflux (162 °C) for 8 days. After the reaction was determined complete by TLC, the contents were allowed to cool to rt, diluted in DCM, and passed twice through a sintered glass funnel. The residue was washed with additional DCM until the washings were colorless. The filtrate and washings were combined, washed with DI water (2 × 400 mL), dried over $MgSO_4$, filtered, and concentrated. The resulting mixture was separated by vacuum distillation to yield 4-ethylpyridine (19 g, 177 mmol, bp 56 °C at 15 mmHg) and 4,4′-diethyl-2,2′-bipyridine (4.6 g, 22 mmol, obtained as a low-melting, light yellow solid, bp 130 °C at 0.5 mmHg). The pot residue was purified by sublimation (170–180 °C at 2.5 mmHg) to yield 4,4′,4′′-triethyl-2,2′:6′,2′′-terpyridine.

^{1}H NMR (500 MHz, CDCl3) δ 8.56 (dd, J = 4.9, 0.8 Hz, 2H), 8.25 (dd, J = 1.7, 0.8 Hz, 2H), 7.14 (dd, J = 5.0, 1.7 Hz, 2H), 2.73 (q, J = 7.6 Hz, 4H), 1.30 (t, J = 7.7 Hz, 6H).

^{13}C{^{1}H} NMR (126 MHz, CDCl3) δ 156.2, 154.0, 149.0, 123.3, 120.8, 28.4, 14.4.

HRMS-ESI (m/z): $[M+H]^+$ calcd for $C_{14}H_{17}N_2^+$, 213.1386; found, 213.1383.

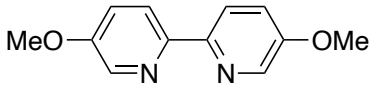

5,5′-dimethoxy-2,2′-bipyridine (3.L15) was prepared by modification of the literature procedure.[156]

In a nitrogen-filled glovebox, an oven-dried 1 dram vial equipped with a PTFE-coated stir bar was charged with nickel(II) chloride dimethoxyethane (30.0 mg, 0.137 mmol, 0.050 equiv), 4,4′-bis(trifluoromethyl)-2,2′-bipyridine (47.9 mg, 0.164 mmol, 0.060 equiv) and DMF (1.0 mL). The vial was sealed with a phenolic screw cap bearing a PTFE-backed silicone septum and placed on a stir plate, where it was stirred at rt for 20 min. After this time, the cap was removed and 2-bromo-5-methoxypyridine (510.4 mg, 0.2730 mmol, 1.00 equiv, in 800 μL of DMF) was added, followed by manganese powder (300.0 mg, 5.460 mmol, 2.00 equiv). The vial was resealed with the screw cap and placed on a pre-heated stir plate (60 °C, 1000 rpm), where it was stirred overnight.

After stirring, the reaction mixture was transferred to an Erlenmeyer flask and diluted with a saturated solution of tetrasodium EDTA (100 mL). The mixture was stirred for 20 min before being transferred to a separatory funnel containing water (50 mL). The mixture was extracted with DCM (3 × 50 mL). The combined organic layers were dried over Na_2SO_4, filtered, concentrated, and the resulting residue was purified by column chromatography (25 g of silica gel, 1 CV of 40% EtOAc/hexanes, then 40–80%

EtOAc/hexanes across 15 CV) to yield **3.L15** (196.8 mg, 0.9101 mmol, 67%) as a white solid.

^{1}H NMR (500 MHz, $CDCl_3$) δ 8.33 (d, *J* = 2.9 Hz, 1H), 8.25 (d, *J* = 8.7 Hz, 1H), 7.30 (dd, *J* = 8.8, 3.0 Hz, 1H), 3.91 (s, 3H).

^{13}C{^{1}H} NMR (126 MHz, $CDCl_3$) δ 155.5, 149.0, 136.6, 121.1, 120.9, 55.7.

3.4.3 General Procedures

3.4.3.1 General Procedure A: Ligand Screening in High-Throughput Format

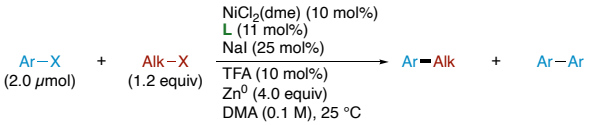

Stock solutions were prepared and stored in a nitrogen-filled glovebox. Separate stock solutions of nickel(II) chloride dimethoxyethane (48.3 mg, 0.220 mmol) and NaI (82.4 mg, 0.550 mmol) were each prepared in 5.5 mL of EtOH. A stock solution of aryl halide (0.200 M, 1.00 equiv), alkyl halide (0.240 M, 1.20 equiv), and 2,2'-dimethylbiphenyl (as an internal standard; 0.050 M, 0.25 equiv) were prepared in DMA. A 20.0 mM stock solution of TFA was prepared in DMA.

Stock ligand screening plates were prepared in a nitrogen-filled glovebox. A slurry of each ligand (110 μmol) was prepared in 2.5 mL of MeOH. While stirring, 50 μL (2.2 μmol) aliquots of each ligand slurry were taken and dispensed into the 1 mL wells of 96-well plates. The contents were heated uncovered overnight at 40 °C to evaporate the solvent. After this time, the plates were sealed and stored in a desiccator under inert atmosphere until needed for screening.

For screening, in a nitrogen-filled glovebox, each well of a pre-prepared 96-well plate—containing 2.2 μmol of the desired ligand—was charged with nickel(II) chloride dimethoxyethane (2.0 μmol, 0.10 equiv, in 50 μL of EtOH) and NaI (5.0 μmol, 0.25 equiv, in 50 μL of EtOH), evaporating the solvent after each addition. Zinc flake (5.2 mg, 80 μmol, 4.0 equiv) was dispensed into each well via a Mettler-Toledo QX96 solid handling robot, followed by a magnetic stir bar. Aryl halide (20.0 μmol, 1.00 equiv), alkyl halide (24.0 μmol, 1.20 equiv), and 2,2'-dimethylbiphenyl (5.0 μmol, 0.25 equiv) were added as a solution in DMA (100 μL). Finally, TFA (2.0 μmol, 0.10 equiv, in 100 μL of DMA) was added to each vial. The plate was left uncovered and placed into a tumble stirrer, where it was stirred (250 rpm) at 25 °C.

Aliquots were taken at 15, 30, 45, 60, 75, and 195 min to determine the concentrations of the product and side products, and at 24 h to establish the final yield. Each aliquot (15 μL) was obtained by sampling the stirring reactions of the 96-well plate with a 12-channel autopipette. Each aliquot was diluted into 750 μL of MeCN /DMSO (3:1), removed from the glovebox, and analyzed by UPLC. The concentrations of the starting materials, desired product, and aryl homodimer were determined as calibrated ratios of absorbances against the internal standard.

3.4.3.2 General Procedure B: Ligand Screening in 1-Dram Vials

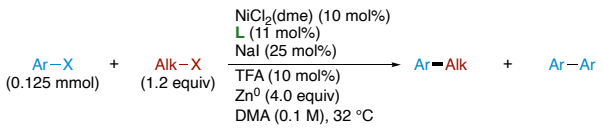

Stock solutions were prepared in a nitrogen-filled glovebox. A stock solution of nickel(II) chloride dimethoxyethane (274.6 mg, 1.250 mmol) in DMA was prepared in an oven-dried 25 mL volumetric flask. This solution was stored in a sealed 20 mL vial in the

glovebox and stirred immediately prior to use. A stock solution of 4,4'-dimethylbiphenyl (1500.0 mg, 8.2300 mmol), aryl halide (12.500 mmol), and alkyl halide (15.000 mmol) in DMA was prepared in an oven-dried 25 mL volumetric flask. This solution was stored in a sealed 20 mL vial in the glovebox and stirred immediately prior to use. Additionally, separate stock solutions of sodium iodide (183.6 mg, 1.225 mmol) and TFA (57.0 mg, 0.500 mmol) in DMA were prepared in oven-dried 5 mL volumetric flasks. These solutions were prepared fresh each time screening was performed.

In a nitrogen-filled glovebox, an oven-dried 1 dram vial equipped with a PTFE-coated stir bar was charged with the ligand (0.014 mmol, 0.11 equiv), nickel(II) chloride dimethoxyethane (2.70 mg, 0.0125 mmol, 0.100 equiv, in 250 μL DMA), and DMA (500 μL). The vial was then sealed with a phenolic screw cap bearing a PTFE-backed silicone septum and placed on a stir plate, where it was stirred (1000 rpm) at 30 °C for 30 min. After this time, the cap was removed and sodium iodide (4.70 mg, 0.0313 mmol, 0.250 equiv, in 125 μL of DMA) was added, followed by a mixture of: aryl halide (0.125 mmol, 1.00 equiv); alkyl halide (0.150 mmol, 1.20 equiv); and 4,4'-dimethylbiphenyl (as an internal standard; 15.0 mg, 0.0823 mmol, 0.658 equiv, in 250 μL of DMA). Zinc flake (32.7 mg, 0.500 mmol, 4.00 equiv) was added to the vial. The contents of the vial were briefly swirled to incorporate the zinc and TFA (1.40 mg, 0.0125 mmol, 0.100 equiv, in 125 μL of DMA) was added. The vial was resealed with the screw cap and placed on a pre-heated stir plate, where it was stirred (1000 rpm) at 32 °C.

Aliquots were taken at 0, 15, 30, 45, 60, 75, 90, 120, and 180 min to determine the concentrations of the product and side products, and at 24 h to establish the final yield. The aliquot (20 μL) was obtained by removing the screw cap and sampling the stirring reaction with an autopipette. The aliquot was diluted into 1000 μL of ethyl acetate,

removed from the glovebox, and quenched with 1 mL of deionized water. The organic layer was then passed through a short (1.5 cm in a pipette) silica plug and analyzed by GC-FID. Concentrations of the reactants, desired product, and side products were determined as calibrated ratios of the area of the analyte peak compared to the area of the internal standard peak.

3.4.4 Results of Ligand Screens

3.4.4.1 High-Throughput Ligand Screens

Figure 3.2 Results of High Throughput Ligand Screening

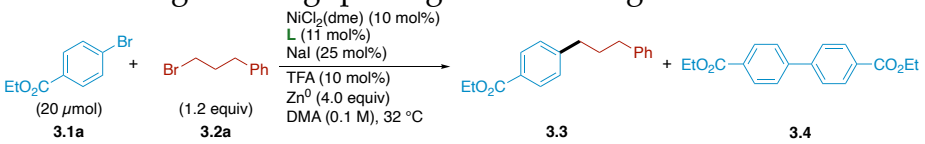

Ligand	**3.3** (%)	**3.4** (%)	ΔΔG‡
3.L1	61	16	-0.78
3.L2	82	5	-1.68
3.L9	4	38	1.39
3.L10	3	37	1.52
3.L11	4	38	1.38
3.L12	45	22	-0.41
3.L13	45	22	-0.44
3.L14	69	13	-1.00
3.L16	73	9	-1.22
3.L17	52	6	-1.32
3.L18	21	18	-0.09
3.L19	2	19	1.38
3.L20	2	36	1.84
3.L22	9	34	0.82
3.L23	70	11	-1.12

General Procedure A was followed using ethyl 4-bromobenzoate and 1-bromo-3-phenylpropane.

Figure 3.3 Correlation Between Concentrations of **3.3** and **3.4**

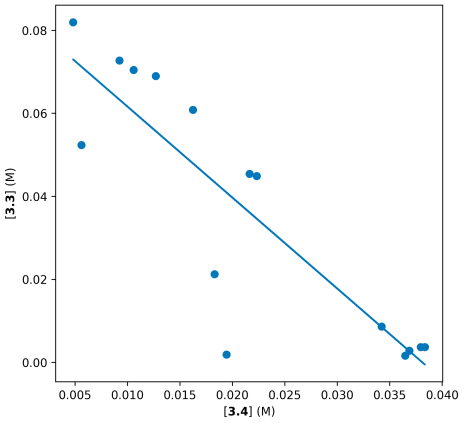

The yield of the desired product, **3.3**, is determined primarily by the selectivity for **3.3** over the aryl homodimer **3.4**. Notable exceptions include **3.L19**, which experienced catalyst deactivation—we observed remaining **3.1a**—and ligands based on *N*-heterocycles other than pyridine (**3.L18**, Figure 3.2).

Together, these results demonstrate that modelling for selectivity of **3.3** over **3.4** is a valid way to improve the efficiency and utility of $C(sp^2)$–$C(sp^3)$ cross-electrophile coupling.

3.4.4.2 Focused Ligand Screens

Figure 3.4 Performance of the Training and Validation Set in the Model Reaction

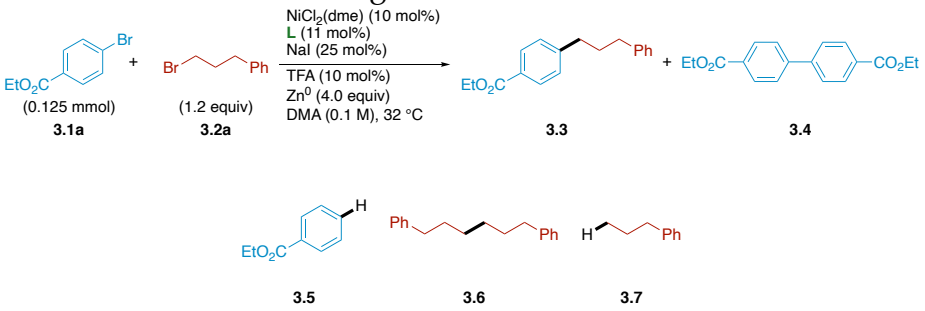

Ligand	**3.3** (%)	**3.4** (%)	ΔΔG‡
3.L1	49	21	-0.50
3.L2	61	9	-1.19
3.L3	82	4	-1.91
3.L4	88	4	-1.95
3.L5	79	2	-2.22
3.L6	13	25	0.39
3.L7	13	38	0.66
3.L8	40	16	-0.56
3.L9	11	25	0.49
3.L11	14	27	0.41
3.L12	34	25	-0.18
3.L14	53	14	-0.83
3.L15	47	20	-0.51

Reactions were set up according to General Procedure B using ethyl 4-bromobenzoate (28.6 mg, 0.125 mmol, 1.00 equiv) and 1-bromo-3-phenylpropane (30.0 mg, 0.150 mmol, 1.20 equiv).

Figure 3.5 Effects of Stirring and TFA Addition

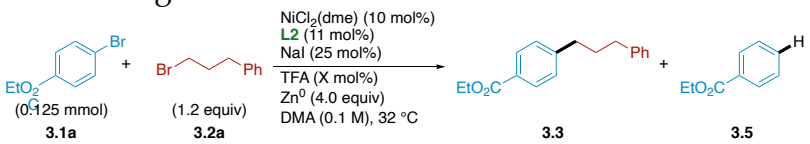

Entry	X	Stir Rate (rpm)	**3.3** (%)	**3.5** (%)
1	10	1000	68	7
2	5	1000	63	10
3	0	1000	69	7
4	10	300	65	15
5	5	300	66	13
6	0	300	36	12

Reactions were set up according by modification of General Procedure B using ethyl 4-bromobenzoate (28.6 mg, 0.125 mmol, 1.00 equiv), 1-bromo-3-phenylpropane (30.0 mg, 0.150 mmol, 1.20 equiv), and 4,4'-dimethoxybipyridine (**3.L2**) (3.0 mg, 0.014 mmol, 0.11 equiv). For reactions using 5 or 0 mol% of TFA, additional DMA was added to maintain a consistent reaction volume.

The differences in selectivity and yield between the high-throughput and focused ligand screens are due to formation of the dibrominated product (**3.5**) in the focused ligand screens. We considered that the change in stirring method—from tumble stirring to traditional magnetic stir bars—may mechanically activate the zinc, encouraging the formation of an organozinc. While less likely, we also considered direct protodemetalation of (L)Ni^{II}(Ar)Br by residual TFA. We found that slower stir rates had little effect on either the rate or yield of the model reaction with **3.L2** in the presence of TFA. Only when TFA was omitted did the stir rate impact the rate and yield of the reaction.

These results suggest that another mechanism is responsible for the formation of **3.5**. Notably, we found that the majority of **3.5** forms between the 3 and 24 h timepoints, when the majority of the productive coupling has already taken place.

Figure 3.6 Benchmarking of Improved Bipyridines in the Coupling of Aryl Halides with Alkyl Bromides

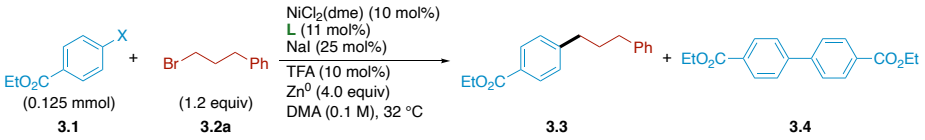

Entry	X	L	**3.3** (%)	Selectivity (**3.3**:**3.4**)
1	Cl	**3.L2**	85	17:1
2	Cl	**3.L5**	93	311:1
3	Br	**3.L2**	61	7:1
4	Br	**3.L5**	79	39:1
5	I	**3.L2**	90	130:1
6	I	**3.L5**	72	25:1

General Procedure B was followed using: ethyl 4-chlorobenzoate (23.1 mg, 0.125 mmol, 1.00 equiv, Entries 1 and 2), ethyl 4-bromobenzoate (28.6 mg, 0.125 mmol, 1.00 equiv, Entries 3 and 4), or ethyl 4-iodobenzoate (34.5 mg, 0.125 mmol, 1.00 equiv, Entries 5 and 6); 1-bromo-3-phenylpropane (30.0 mg, 0.150 mmol, 1.20 equiv); and 4,4′-dimethoxybipyridine (**3.L2**) (3.0 mg, 0.014 mmol, 0.11 equiv, Entries 1, 3, and 5) or 4,4′-bis(dimethylamino)-2,2′-bipyridine (**3.L5**), (3.3 mg, 0.014 mmol, 0.11 equiv, Entries 2, 4, and 6). Reactions were stirred for 24 h prior to sampling.

These results demonstrate a general increase in selectivity when employing **3.L5** in place of **3.L2**. The shift in selectivity trends when **3.L2** is used to couple ethyl 4-iodobenzoate may be due to a shift in mechanism or due to significant acceleration of alkyl radical formation is the presence of stoichiometric iodide salt byproducts.

Figure 3.7 Decreasing Catalyst Loading Increases Selectivity

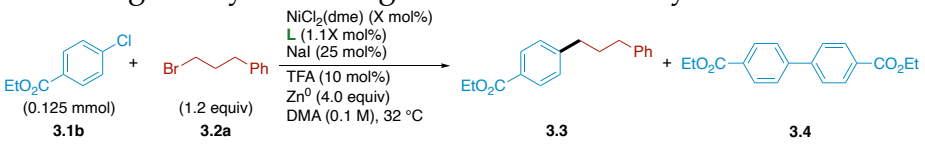

Entry	X mol%	L	**3.3** (%)	Selectivity (**3.3**: **3.4**)
1	10	3.L2	85	17:1
2	10	3.L5	93	311:1
3	5	3.L2	89	25:1
4	5	3.L5	96	364:1

Reactions were performed by modification of General Procedure B, using ethyl 4-chlorobenzoate (23.1 mg, 0.125 mmol, 1.00 equiv), 1-bromo-3-phenylpropane (30.0 mg, 0.150 mmol, 1.20 equiv), and either 4,4′-dimethoxybipyridine (**3.L2**)—(3.0 mg, 0.014 mmol, 0.11 equiv, Entry 1) or (1.5 mg, 6.9 μmol, 0.055 equiv, Entry 3)—or 4,4′-bis(dimethylamino)-2,2′-bipyridine (**3.L5**)—(3.3 mg, 0.014 mmol, 0.11 equiv, Entry 2) or (1.8 mg, 6.9 μmol, 0.055 equiv, Entry 4). For reactions with 5 mol% loading of $NiCl_2$(dme) (Entries 3 and 4), 125 μL of $NiCl_2$(dme) stock solution was used and an additional 125 μL of DMA was added to maintain a consistent reaction volume. Reactions were stirred for 24 h prior to sampling.

These results demonstrate that further improvements in selectivity and efficiency may be achieved by decreasing the concentration of the catalyst. This improvement is consistent with similar observations in the coupling of (*Z*)-vinyl bromides and supports a mechanism of biaryl formation involving either disproportionation or ligand transfer between two nickel centers.[33] Based on other observed electronic and steric trends, we hypothesize that aryl homodimerization occurs via disproportionation of $(L)Ni^{I}(Ar)$ or ligand transfer between $(L)Ni^{I}(Ar)$ and $(L)Ni^{II}(Ar)Br$.

Reactions set up with significantly lower catalyst loadings (<1 mol%) gave low conversion of the aryl halide. We hypothesize that issues with catalyst speciation and

initiation, or competitive zinc insertion may be the cause. Previous reports employing pre-ligated (L)$Ni^{II}I_2$ and manganese did not appear to encounter these issues.[33] We hypothesize that these solutions could be combined with application of **3.L5** to yield further increases in selectivity.

Figure 3.8 Coupling of Aryl and Alkyl Chlorides

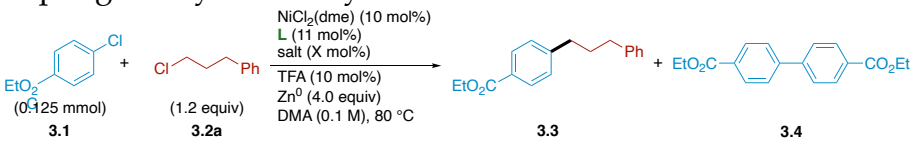

Entry	L	Salt	X mol%	**3.3** (%)	Selectivity (**3.3**:**3.4**)
1	**3.L2**	NaI	25	11	0.5:1
2	**3.L5**	NaI	25	25	2:1
3	**3.L5**	NaI	50	40	7:1
4	**3.L1**	NaI	100	2	0.003:1
5	**3.L2**	NaI	100	16	0.2:1
6	**3.L5**	NaI	100	52	14:1
7	**3.L1**	NaI	200	3	0.007:1
8	**3.L2**	NaI	200	21	0.5:1
9	**3.L5**	NaI	200	55	19:1
10	**3.L5**	LiI	50	52	12:1
11	**3.L1**	LiI	100	4	0.009:1
12	**3.L2**	LiI	100	11	0.1:1
13	**3.L5**	LiI	100	62	25:1
14	**3.L1**	LiI	200	3	0.006:1
15	**3.L2**	LiI	200	30	1:1
16	**3.L5**	LiI	200	51	15:1

Reactions were set up by modification of General Procedure B using ethyl 4-chlorobenzoate (23.1 mg, 0.125 mmol, 1.00 equiv), 1-Chloro-3-phenylpropane (23.2 mg, 0.150 mmol, 1.20 equiv), and either, 4,4′-di-*tert*-butyl-2,2′-bipyridine (**3.L1**) (3.7 mg, 0.014 mmol, 0.11 equiv, Entries 4, 7, 11, and 14), 4,4′-dimethoxybipyridine (**3.L2**) (3.0 mg, 0.014 mmol, 0.11 equiv, Entries 1, 5, 8, 12, and 15) or 4,4′-bis(dimethylamino)-2,2′-bipyridine (**3.L5**) (3.3 mg, 0.014 mmol, 0.11 equiv, Entries 2, 3, 6, 9, 10, 13, and 16). All reactions were set up by adding solid LiI or NaI directly to the precatalyst solution along with an

additional 125 μL of DMA. The mixture was then stirred at rt until the salt was dissolved prior to starting materials being added. Reactions were stirred for 24 h prior to sampling.

These results demonstrate that when alkyl radical formation is slow, **3.L5** offers improvements in selectivity over the previous state-of-the-art ligand **3.L3**. The increased stability of **(L5)**Ni^{II}(Ar)Cl provides sufficient intermediate lifetime to enable generally selective reactions without the formation of significant amounts of **3.4**. While the use of increased amounts of LiI (>2.00 equiv) may enable the use of **3.L3** with similar yields and selectivity, this would decrease the overall mass efficiency of the reaction.

Figure 3.9 Coupling of *N*-Alkyl 2,4,6-Triphenylpyridinium Salts with Aryl Halides

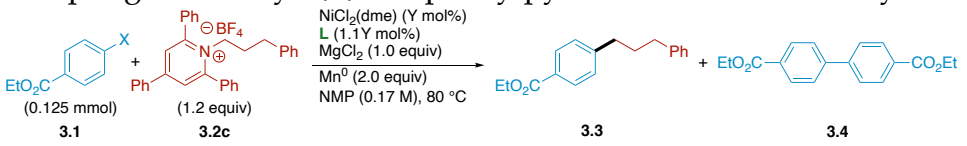

Entry	L	X	Y mol%	**3.3** (%)	Selectivity (**3.3**:**3.4**)
1	**3.L5**	Br	10	98	84:1
2	**3.L5**	Cl	10	55	7:1
3	**3.L5**	Cl	20	86	8:1
4	**3.L1**	Cl	20	65	5:1
5	**3.L2**	Cl	20	49	3:1

Reactions were set up by modification of the literature procedure.[154] In a nitrogen-filled glovebox, 3 oven-dried 1 dram vials equipped with PTFE-coated stir bars were charged with 4,4′-bis(dimethylamino)-2,2′-bipyridine (**3.L5**)—(3.3 mg, 0.014 mmol, 0.11 equiv, Entries 1 and 2) or (6.7 mg, 0.028 mmol, 0.22 equiv, Entry 3)—4,4′-di-*tert*-butyl-2,2′-bipyridine (**3.L1**) (7.4 mg, 0.028 mmol, 0.22 equiv, Entry 4), or 4,4′-dimethoxybipyridine (**3.L2**) (6.0 mg, 0.028 mmol, 0.22 equiv, Entry 5); nickel(II) chloride dimethoxyethane—(2.7 mg, 0.0125 mmol, 0.10 equiv, Entries 1 and 2) or (5.5 mg, 0.025 mmol, 0.20 equiv, Entries 3–5)—4,4′-dimethylbiphenyl (as an internal standard; 15.0 mg, 0.0823 mmol, 0.658 equiv), magnesium(II) chloride (11.9 mg, .125 mmol, 1.00 equiv), manganese powder (13.7 mg, 0.250 mmol, 2.00 equiv), and 2,4,6-triphenyl-1-(3-phenylpropyl)-pyridin-1-ium

tetrafluoroborate (77.0 mg, .150 mmol, 1.20 equiv). NMP (735 μL) was added to each vial, followed by the appropriate aryl halide—either ethyl 4-bromobenzoate (28.6 mg, 0.125 mmol, 1.00 equiv, Entry 1) or ethyl 4-chlorobenzoate (23.1 mg, 0.125 mmol, 1.00 equiv, Entries 2 and 3). The vials were sealed with phenolic screw caps bearing PTFE-backed silicone septa, removed from the glovebox, and placed on a pre-heated stir plate (80 °C, 1000 rpm) for 24 h.

An aliquot (20 μL) was taken from each reaction via gas-tight syringe The aliquots were diluted into 1000 μL of ethyl acetate and quenched with 1 mL of deionized water. The organic layers were then passed through short (1.5 cm in a pipette) silica plugs and analyzed by GC-FID. Concentrations of the reactants, desired product, and side products were determined as calibrated ratios of the area of the analyte peak compared to the area of the internal standard peak.

These results demonstrate that **3.L5** also offers benefits in existing reactions (Entry 1) and new combinations of substrates (Entries 2 and 3). The observed improvements when increasing the catalyst loading from 10 to 20 mol% suggest that selectivity and yield are governed by the rate of oxidative addition to the chloroarene. Radical formation from **3.2c** most likely proceeds via direct reduction by manganese and fragmentation of the resulting radical anion.[160] As such, the stability of $(L)Ni^{II}(Ar)X$ most likely plays a small role in the overall selectivity of the reaction compared to the rate of formation of $(L)Ni^{II}(Ar)X$. Compared to the other reactions in our work, the alkyl radical precursor is the more reactive of the two substrates and generating sufficient $(L)Ni^{II}(Ar)X$ to capture the resulting alkyl radical is critical to providing high yield and selectivity. We hypothesize that the formation of **3.4** occurs after the complete consumption of **3.1**.

3.4.5 Computational Details and Selection of Model Target

All computations were performed using the Gaussian 16, Rev. C.01 suite—using defaults unless noted otherwise—at the UM06/cc-pVTZ,SDD(Ni)//UM06/cc-pVDZ,LANL2DZ(Ni) level of theory with the SMD continuum solvation model for DMA (*N*,*N*-dimethylacetamide).[137–143,161] The Gaussian keywords "ultrafine" and "noraman" were used to ensure accuracy whilst improving computational efficiency. Conformers of higher energy were accounted for in all cases and are not included in the discussion. Stationary points were characterized as ground states by the absence of negative eigenvalues (zero imaginary frequencies) in frequency analysis at the same level of theory as the geometry optimization. To account for common nickel(II) coordination geometries, square planar singlet and tetrahedral triplet geometries were considered, as well as the unbound ligand in the absence of a metal. Bromobenzene was utilized as a simplified aryl halide in computed nickel complexes.

Figure 3.10 Atom Numbering Scheme for Free Ligand, (L)Ni(Ph)Br Square Planar, and (L)Ni(Ph)Br Tetrahedral DFT-Optimized Structures

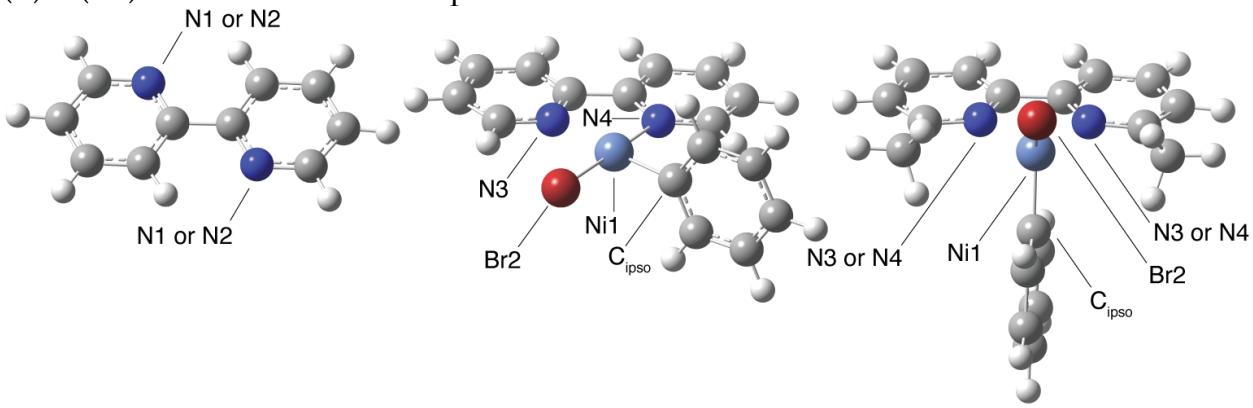

Atom numbering (Figure 3.10) was conserved for atoms common and relevant to all square planar structures, namely Ni1, Br2, N3 (binding nitrogen always trans to the phenyl ligand), N4 (binding nitrogen always trans to the bromine ligand), and C5 (C_{ipso}

of the phenyl ligand). For tetrahedral geometries, Ni1, Br2, and C5 were conserved across all structures, and an attempt was made to maintain consistency in the numbering scheme (relative to the analogous square planar geometries) for N3 and N4, especially for the non-symmetric bipyridine ligands. For the unbound ligand, the donor nitrogens are numbered N1 and N2; no attempt was made to standardize atom numbering beyond the donor atoms, as we did not have a numbering schema in place at the time these geometries were computed.

Descriptors were collected from DFT output files using Python scripts created by the Sigman Group (University of Utah) and the Paton Group (Colorado State University), as well as NBO 7.0.[144,162]

Selectivity was defined as the ratio of the averaged concentrations of cross-coupled product, [**3.3**], to aryl homodimer, [**3.4**], at 24 h, where each reaction was performed in quadruplicate (high-throughput dataset) or duplicate (focused ligand screen dataset). The observed selectivity of each catalyst (Figure 3.2, Figure 3.4) was converted to relative free energies with the equation

$$\Delta\Delta G^{\ddagger} = -RTln\left(\frac{[\mathbf{3}]}{[\mathbf{4}]}\right)$$

and used as the target in the subsequent modeling.

3.4.6 Data Science Workflow

3.4.6.1 Threshold Analysis

Threshold analysis was performed using the workflow and scripts and developed by the Sigman and Doyle groups.[137–143,146,161] The algorithm was performed using a plot step size of 0.02, a y_cut of 10 (corresponding to ~10% yield), and a "balanced" class weight.

Figure 3.11 Threshold Analysis with Full HTE Dataset

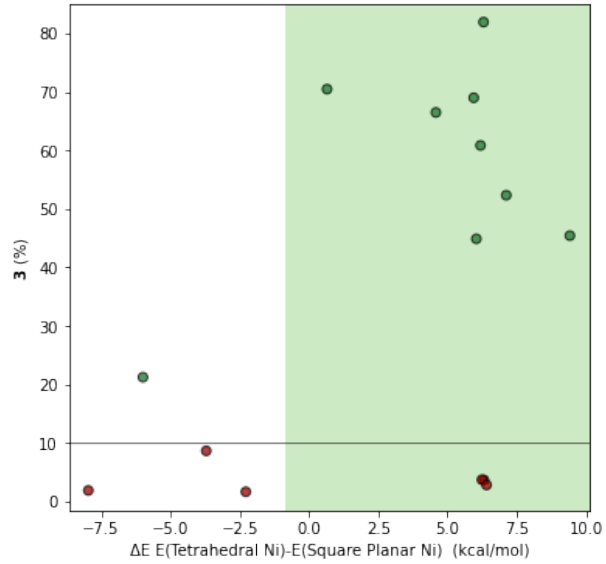

Threshold = -0.81 with ΔE (E(Tetrahedral Ni)-E(Square Planar Ni)) in kcal/mol. Accuracy = 0.73, F1 = 0.80, and MCC = 0.43.

The yield analysis revealed that substitution in the 6-position enforces a tetrahedral ground state, which promotes rapid downstream dimerization of the aryl halide. As a result, these ligands were excluded from further analysis.

3.4.6.2 Modeling Workflow

Regressive studies correlating molecular descriptors to reaction outcomes were performed using Python scripts developed by the Sigman group. Univariate correlations were limited to those with $R^2 > 0.70$ and p-value <0.01; 1-parameter models were internally validated with leave-one-out (LOO) and *k*-fold ($k = 5$) cross-validation and externally validated with **3.L3**, **3.L4**, **3.L5**, **3.L15** (for which we did not have any prior experimental observations). Training sets were comprised of 4-, 4,4'-, and 5,5'-(di)substituted-2,2'-bipyridines (5 HTE and 9 focused screening observations). HTE and focused screening observations were not combined for the generation of univariate correlations nor models.

3.4.7 Univariate Correlations and Models

We observed a variety of strong univariate correlations from the HTE dataset; however, many of the descriptors that were examined were collinear. We hypothesized that the use of symmetrically substituted ligands in the training set resulted in spurious collinearity in seemingly unrelated parameters.

Figure 3.12 Best 1-Parameter Model (μ) from High-Throughput Screening Results

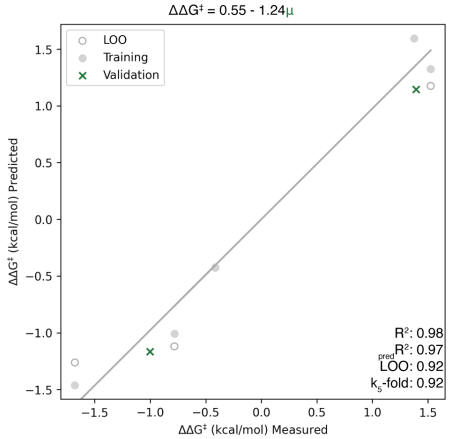

Our strongest model with this dataset was a 1-parameter model with μ (chemical potential), which is approximately the average of the HOMO and LUMO orbital energies.[163] However, we were dissatisfied with the specificity it provided. We felt that designing a more tailored dataset would enable more insight into the catalytic system and lead to more effective predictions of reaction outcomes. When designing non-symmetric ligands, an effort was made to cover a range and combination of electron-donating and -withdrawing characteristics.

Figure 3.13 Univariate Correlations from Focused Screening Results

Descriptor	R^2	p-value
$NMR_{\delta xx})_{N3}$	0.93	2.61E-05
NPA_{Cipso}	0.92	5.19E-05
$NMR(\delta_{iso})_{N3}$	0.91	5.43E-05
NPA_{N3}	0.88	1.96E-04
$NMR(\delta_{yy})_{N3}$	0.85	4.08E-04
$NMR(\delta_{zz})_{Cipso}$	0.81	9.65E-04
E(HOMO)	0.76	2.29E-03
$NMR(\delta_{xx})_{Cipso}$	0.76	2.25E-03
μ	0.75	2.70E-03
E(LUMO)	0.73	3.25E-03
$E(d_{z2})$	0.73	3.52E-03
$NMR(\delta_{iso})_{Cipso}$	0.73	3.44E-03
$E(d_{yz})$	0.72	3.82E-03
$NMR(\delta_{yy})_{Cipso}$	0.72	3.85E-03
E(LUMO) - E(HOMO)	0.71	4.43E-03
η	0.71	4.43E-03
$E(d_{xz})$	0.71	4.16E-03

Figure 3.14 Best 1-Parameter Models from Focused Screening Results

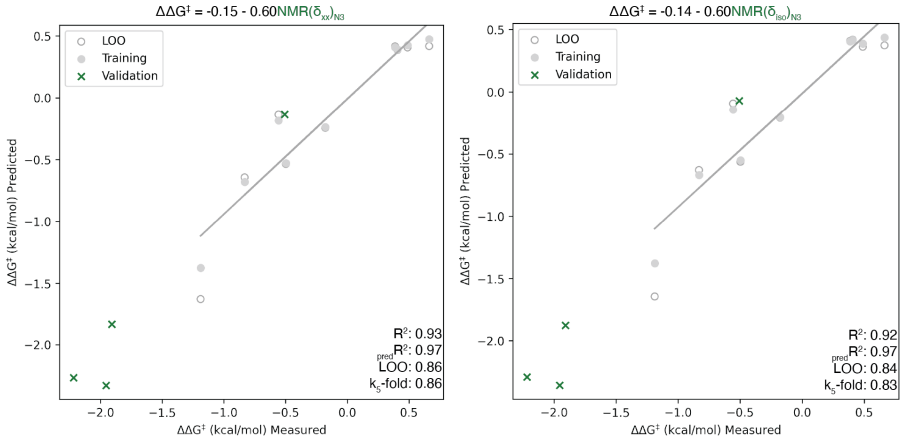

The external validation set for the focused screening models consists of three extrapolated points (**3.L3–3.L5**) and a single interpolated point (**3.L15**). We selected our best model (Scheme 3.4d) from that which had the highest predicted R^2 (and the lowest associated mean absolute error: MAE = 0.200 for the NPA_{Cipso} model, 0.219 for the $NMR(\delta_{xx})_{N3}$ model, and 0.237 for the $NMR(\delta_{iso})_{N3}$ model; Figure 3.14). This finding demonstrates the transferability of this model to other substitution patterns present in the bpy class of

ligands (exclusive of 6- or 6,6′-substitution), as the focused screen training set did not contain any 5,5′-disubstituted ligands.

Figure 3.15 1-Parameter Model (μ) Using Focused Screening Results

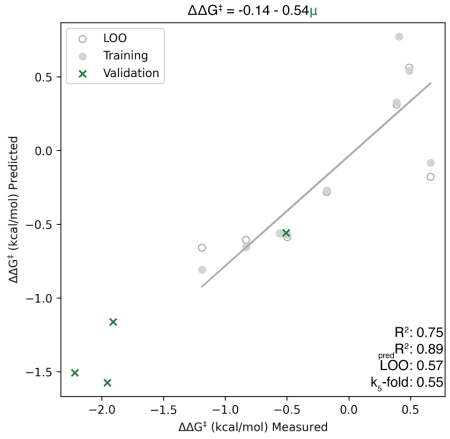

When we revisited the descriptor used to generate the best 1-parameter model for the high-throughput screening results (Figure 3.12), we noticed that this descriptor failed to appropriately account for non-symmetric ligands (Figure 3.15). This supports our hypothesis that the collinearity of descriptors within the initial dataset was limiting specificity and translatability of the model.

Figure 3.16 Predicted Selectivity of In Silico Ligands Utilizing Optimal Model with NPA_{Cipso}

Ligand	NPA_{Cipso}	Predicted $\Delta\Delta G^{‡}$ (kcal/mol)
3.L24	-0.15321	-1.27
3.L25	-0.15456	-1.79
3.L26	-0.15503	-1.96

Selectivity was predicted from the equation for the univariate correlation with C_{ipso} (Figure 3.16) without normalization of the descriptor. It is evident that this model of selectivity does not appropriately handle this type of ligand. As such, for predicting the selectivity of new ligands, we first recommend removal of 6- or 6,6′-(di)substituted ligands, then applying this model.

Chapter 4: Identification of Novel 2,2′-Bipyridine-6-Carbonitrile Ligands

4.1 Introduction

Identification of new classes of ligands is an active area of research in nickel-catalyzed cross-couplings. New ligands can enable improvements in the coupling of existing substrate pools, accessibility to previously inaccessible substrate classes, and generally more robust couplings.[126,153,164,165] Often, these new ligand classes exist and are contextualized as structural (backbone) modifications of previously known L2 and L3 ligands, where electronic modulation of substituents follows existing trends (vide supra, Section 3.1.2). An illustration of this concept can be seen in the case of PyCams—which were introduced as an alternative to and thus far appear to provide reactivity similar to bpys.[126] However, the identification of new ligand classes that exhibit contrasting reactivity is less common. To enable the development of increasingly diverse cross-coupling reactions, new ligands that expand upon the suite of accessible elementary steps are needed; ideally, these ligands will not detrimentally impact existing elementary steps that have driven the adoption of nickel-catalyzed processes whilst they enable new avenues of reactivity.

Activation of $C(sp)^3$ electrophiles is an area of interest in nickel-catalyzed cross-couplings. L3-ligated nickel catalysts are frequently employed due to their capacity to participate in the SET process of alkyl radical generation. An alternative strategy is the use of electron-deficient olefins to promote an S_N2-style oxidative addition to alkyl electrophiles.[166–168] While this approach has seen implementation in redox-neutral cross couplings, application of similar ligands in cross-electrophile couplings has thus far been limited. We propose that the resulting nickel complexes struggle to participate in the

diverse single- and two-electron elementary steps necessitated by cross-electrophile coupling, leading to low selectivity. An attractive approach would be the identification of a catalyst that incorporates the benefits of the most common heterocycle-based L2 dinitrogen catalysts whilst also allowing for the distinct reactivity of π-bound nickel. This chapter discusses our identification and initial survey of the reactivity of 2,2′-bipyridine-6-carbonitrile ligands in contrast to their non-cyanated bpy analogues. We hypothesize that the introduction of the nitrile group to these ligands allows for dynamic changes in ligand binding based on the oxidation state of the nickel throughout the mechanistic cycle. While we have not yet had an opportunity to conduct an in-depth investigation of these ligands, we expect that our strategies outlined in this chapter may enable further diversification of these modified 2,2′-bipyridine ligands and their application to new transformations.[33,169]

4.2 Results

Table 4.1 6-Cyanation Changes Ligand Reactivity

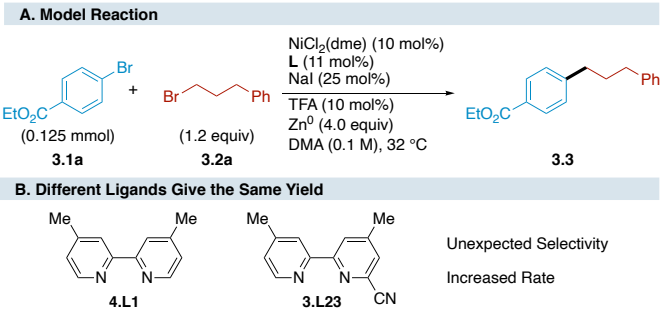

Entry	L	**3.3** (%)	Rate (M/min)[b]
1	**4.L1**	70	1.1×10^{-4}
2	**3.L23**	70	3.4×10^{-4}

[a]Reactions were assembled in a nitrogen filled glovebox at a 20 μmol scale in 200 μL of DMA. Data is taken from Figure 3.2. Yields and selectivity were determined by UPLC-MS. [b]Rate was determined from 15–75 min to account for any induction period.

During the studies described in Chapter 3, we identified a single bipyridine—4,4'-dimethyl-2,2'-bipyridine-6-carbonitrile (**3.L23**)—that produced the same yield as its non-

6-substituted analogue, 4,4′-dimethyl-2,2′-bipyridine (**4.L1**), with a concomitant increase in rate despite substitution by a nitrile in the 6-position (Table 4.1). This finding directly contradicted both nodes of the two node-decision tree (Scheme 3.2b) utilized to predict the selectivity provided by bipyridines. Our initial expectations of this ligand were: (1) the low ΔE between the tetrahedral and square planar geometries should enable more rapid reduction of the (L)Ni^{II}(Ar)Br via the accessible tetrahedral geometry, and (2) the introduction of the nitrile—a strong electron-withdrawing group—to one of the pyridine rings should decrease the NPA charge of C_{ipso}, leading to decreased selectivity. This discrepancy led us to hypothesize that these ligands may promote a different mechanism than canonical bipyridines (Scheme 3.2b, Section 3.2.1). However, it remained unclear if the increase in rate and conserved yield of the cross-product was a generalizable trend or merely a coincidental outcome.

To investigate the behavior of cyanation in the 6-position of 2,2′-bipyridines, we synthesized a suite of 4,4'-di(substituted)-2,2'-bipyridine-6-carbonitrile ligands (**4.L2**–**4.L5**). These bpy^{CN} ligands are accessed via a two-step oxidation, deoxygenative-cyanation sequence (Section 4.4.2.2) from the parent 4,4′-disubstituted-2,2′-bipyridine. We surveyed the reactivity of these ligands by evaluating their performance relative to their non-cyanated analogues in a modified version of the cross-electrophile coupling utilized in Chapter 3 (Table 4.2).

Table 4.2 bpy^{CN} Ligands Display Inverted Selectivity and Reactivity

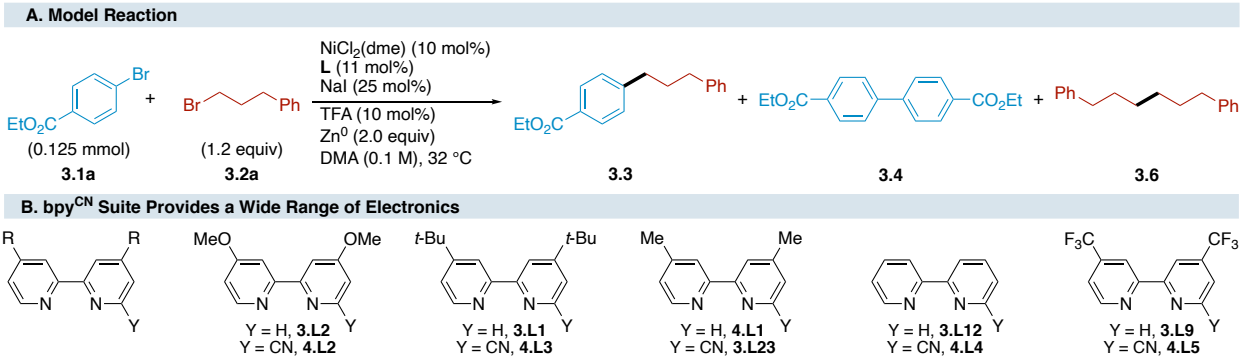

Entry	Ligand		**3.3** (%)	**3.4** (%)	**3.6** (%)
	R	Y			
1	OMe	H	67	6	20[b]
2	OMe	CN	43	5	35
3	*t*-Bu	H	44	21	26[b]
4	*t*-Bu	CN	49	6	30
5	Me	H	41	22	26[b]
6	Me	CN	45	5	32
7	H	H	38	25	16[b]
8	H	CN	53	3	26
9	CF_3	H	13	31	6[b]
10	CF_3	CN	65	4	12

[a]Reactions were assembled in a nitrogen filled glovebox at a 0.125 mmol scale in 1.25 mL of DMA. Yields and selectivity were determined by GC-FID. [b]**3.6** was not observed until after complete consumption of **3.1a**.

We found that the bpy^{CN} ligands display distinct reactivity from canonical bipyridines. First, we observed a shift in the resulting byproduct distribution, as the bpy^{CN} ligands provided the alkyl homodimer (**3.6**) as the major byproduct rather than the aryl homodimer (vide supra, Section 3.1.1). Further, we observed an inversion in the electronic trends of the ligand: while electron-rich bpy ligands (**3.L2**) provided the highest yield of the cross-product (**3.3**), electron-poor bpy^{CN} ligands (**4.L5**) provided the highest yields of cross-product. These observations conferred support to our hypothesis that these ligands promote a different mechanism or altered the selectivity determining step.

Scheme 4.1 Electronic-trends Reveal that bpy^{CN} Ligands Activate C(sp^3)–X

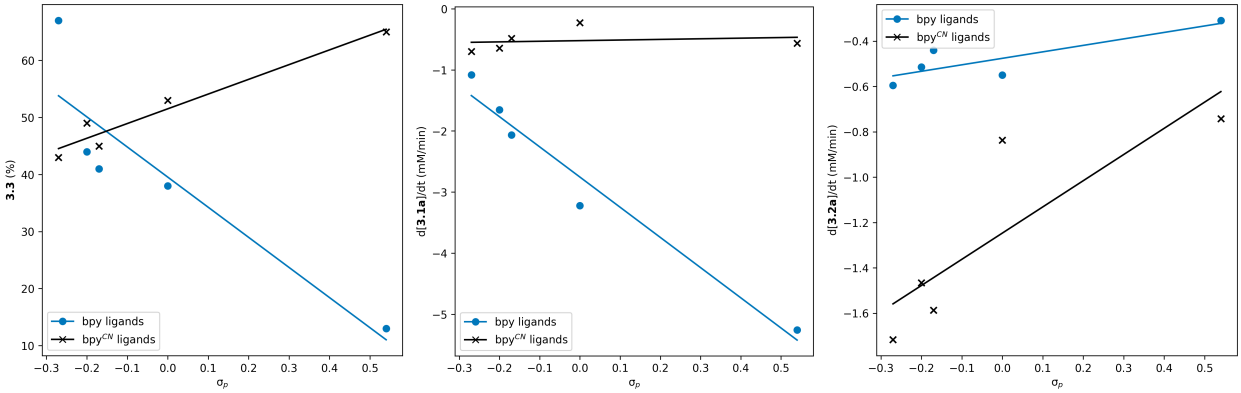

[a]Reactions were assembled in a nitrogen filled glovebox at a 0.125 mmol scale in 1.25 mL of DMA. Concentrations of all reagents were determined by GC-FID. Rates were determined from 0–30 min when the reaction rate was linear. For reactions that were complete in under 30 min, the rate was estimated from 0–15 min.

Further insight was obtained from the construction of Hammett plots (Scheme 4.1), wherein the rate of consumption of each coupling partner was related to the electronic character of the bipyridine core These plots revealed that—in contrast to traditional bipyridines—the electronics of the bipyridine backbone in bpy^{CN} ligands has no effect on the rate of consumption of the bromoarene. As the increase in turnover of bpy-nickel catalysts is attributed to regeneration of (L)Ni^0 upon deleterious homodimerization to form aryl dimer; this result suggests that either: (1) bpy^{CN} ligands form (L)Ni^{II}(Ar)Br complexes that do not undergo deleterious reduction and disproportionation, or (2) activation of the bromoarene does not occur in the rate limiting span. We hypothesize that the latter scenario best fits our present observations, informed by the observation that a Hammett plot of the rate of bromoalkane consumption reveals that electron-rich bpy^{CN} ligands rapidly activate—and subsequently dimerize—the bromoalkene.

The observed preferential reactivity of bpy^{CN}-nickel catalysts with the bromoalkane in the presence of bromoarene led us to hypothesize that the pendent nitrile

group may act as a third donor, forming an L3-ligated nickel center. Indeed, when we compared bpy^{CN} (**4.L4**) to 2,2′;6′,2′′-terpyridine (**4.L6**) in the model reaction, we observed rapid formation of the alkyl homodimer in both cases. While this supported our initial hypothesis, we remained unsure if the geometry of the bpy^{CN} enabled efficient overlap of the π system with the nickel center. To further test our hypothesis, we synthesized and evaluated 2,2′-bipyridine-4-carbonitrile, which delivered similar yield and selectivity to the 6-carbonitrile analogue. This result clearly demonstrated that bpy^{CN} ligands are distinct from both bipyridine and L3 donors and that the placement of the cyano group has little effect on the selectivity of the cross-coupling.

Table 4.3 bpy^{CN} Ligands Provide Unique Reactivity

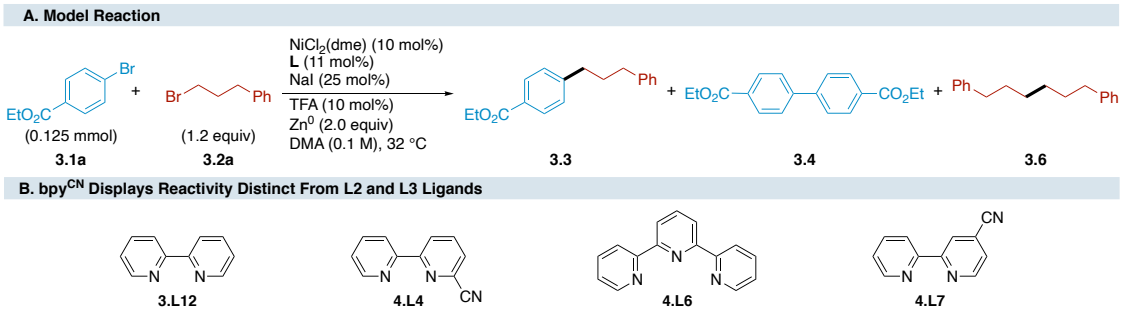

Entry	Ligand	**3.3** (%)	**3.4** (%)	**3.6** (%)
1	**3.L12**	38	25	16[b]
2	**4.L4**	55	3[c]	26
3	**4.L6**	32	5[d]	23
4	**4.L7**	55	12[d]	20

[a]Reactions were assembled in a nitrogen filled glovebox at a 0.125 mmol scale in 1.25 mL of DMA. Yields and selectivity were determined by GC-FID. [b]**3.6** was not observed until after complete consumption of **3.1a**. [c]**3.4** was not observed until after complete consumption of **3.2a**. [d]**3.4** was formed concurrently with **3.3** and **3.6**.

Scheme 4.2 Computational Studies Indicate Dynamic Binding Changes

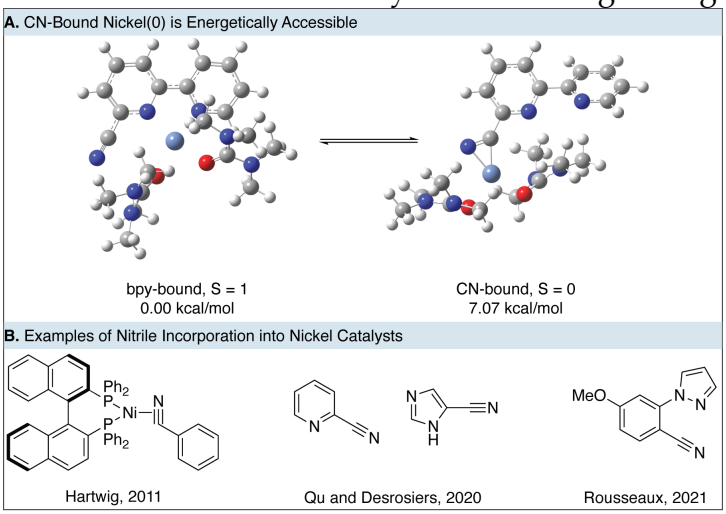

We are currently undertaking computational and mechanistic experiments to survey the reactivity of bpy^{CN} ligands and investigate the source of selectivity. We currently hypothesize that the pendant nitrile enables dynamic interchange in binding modes depending on the oxidation state of the nickel center. Initial computational experiments indicate that de-ligation of the bipyridine backbone is thermodynamically accessible in the nickel(0) oxidation state, leading to a π-bound nickel-nitrile complex (Scheme 4.2). This initial result informs our current hypothesis that in low oxidation states, bpy^{CN} ligands promote oxidative addition of the alkyl coupling partner via a π-bound, sterically unhindered nickel(0) complex. Further studies are needed to firmly establish the binding characteristics and reactivity of bpy^{CN}.

4.3 Discussion and Future Work

The addition of nitrile groups to existing ligand classes has been an effective method for the development of new redox-neutral and cross-electrophile couplings. For example, a recent publication by researchers at Boehringer Ingelheim identified 2-pyridine-carbonitrile as an efficient ligand for the cross-electrophile coupling of primary

alkyl and aryl bromides.[170] Further, they found that the related 1-*H*-imidazole-5-carbonitile enabled the efficient cross-electrophile coupling of neopentyl bromides. While they did not characterize the binding of these ligands, we hypothesize that the decreased steric requirements of the ligand, in combination with the increased reactivity of cyano-(bi)pyridine-ligated nickel complexes with C(sp^3)–X electrophiles may enable more facile activation of the sterically demanding neopentyl coupling partner. Similarly, the Rousseaux group recently developed a class of benzonitrile-containing pyrazole-based ligands that promote the cross-coupling of tertiary organomagnesium reagents with iodoarenes.[171] Mechanistic investigations demonstrated that the pendent nitrile promoted reductive elimination by withdrawing electron-density from the (L)Ni^n(Ar)Alk intermediate, accelerating reductive elimination. The nitrile group most likely also stabilizes low-valent nickel intermediates. This stabilization of low-valent nickel is well known and has driven the incorporation of benzonitrile as an additional ligand in a variety nickel-catalyzed processes.[172–174] Further, related electron-poor π systems, such as stilbenes have been used to synthesize air stable nickel(0) precatalysts[175] and promote oxidative addition into challenging C(sp^3) electrophiles.[166,176–178] These studies suggest that the nitrile group in bpy^{CN} ligands may play a number of roles, from enabling more facile reductive elimination to stabilizing the low-valent nickel(0) intermediate. Given these precedents, our continuing investigations will center on: (1) establishing whether the bipyridine backbone is necessary to promote the observed reactivity via nitrogen knockouts, (2) determining the ligation mode of bpy^{CN} ligands in nickel(0) and nickel(II) complexes, (3) determining the mechanism by which the nickel catalyst activates and dimerizes the haloalkane, and (4) surveying the reactivity of bpy^{CN}-ligated nickel complexes in the cross electrophile coupling of diverse alkyl coupling partners. We

expect that application of these and other mixed L2-π ligands may enable the marriage of single-electron dependent cross-electrophile couplings with substrates most often confined to redox-neutral nickel-olefin catalysis.

4.4 Experimental

4.4.1 General Information

4.4.1.1 Reagents

Metals and Catalysts

Nickel(II) chloride dimethoxyethane, $NiCl_2$(dme), was purchased from Sigma-Aldrich. Zinc flake (-325 mesh) was purchased from Alfa Aesar. Tetrakis(triphenylphosphine)palladium(0) was purchased from Oakwood Products. All metals and catalysts were stored in a nitrogen-filled glovebox and used without additional purification.

Ligands

2,2′-Bipyridine was purchased from Sigma-Aldrich. 4,4′-dimethoxy-2,2′-bipyridine was purchased from Ambeed or Sigma-Aldrich. 4,4′-Bis(trifluoromethyl)-2,2′-bipyridine was purchased from Ambeed. 4,4′-Di-*tert*-butyl-2,2′-bipyridine was purchased from TCI.[C] 2,2′:6′,2′′-Terpyridine was purchased from Strem. Ligands were stored and handled in a nitrogen-filled glovebox and used without further purification.

Substrates

[C] These experiments were performed prior to the observation that **3.L1** purchased from different suppliers yielded different selectivity. It is unclear if the impurity was carried through the generation of **4.L3**.

Ethyl 4-bromobenzoate was purchased from Oakwood. 1-Bromo-3-phenylpropane was purchased from TCI America. Unless otherwise specified, all substrates were purchased from commercial sources, stored on the benchtop, and used without further purification.

Solvents

Anhydrous *N*,*N*-Dimethylacetamide (DMA) was purchased from Sigma-Aldrich and stored in a nitrogen-filled glovebox.

Other Reagents

Sodium iodide and trifluoroacetic acid (TFA) were purchased from Sigma-Aldrich. 4,4''-Dimethyl-1,1'-biphenyl was purchased from Thermo Fisher Scientific. Other reagents, substrates, and solvents were purchased from commercial sources, stored on the benchtop, and used without further purification unless otherwise specified.

4.4.1.2 Methods

NMR Spectroscopy

^{1}H, ^{13}C, and ^{19}F NMR spectra were acquired on 400 and 500 MHz Bruker Avance III NMR instruments. NMR chemical shifts are reported in ppm. ^{1}H chemical shifts are referenced to tetramethylsilane (TMS) in $CDCl_3$ (δ = 0.00 ppm). ^{13}C and ^{19}F chemical shifts were absolute referenced to the accompanying ^{1}H spectrum. Coupling constants (*J*) are reported in Hertz.

High Resolution Mass Spectrometry

Mass spectrometry data was collected on a Thermo Scientific Q Exactive Plus Hybrid Quadrupole-Orbitrap via flow injection with electrospray ionization by the Paul Bender Chemical Instrumentation Center facility at the University of Wisconsin-Madison.

Gas Chromatography

GC analyses were performed on an Agilent 7890A GC equipped with dual DB-5 columns (20 m × 180 μm × 0.18 μm), dual FID detectors, and H_2 as the carrier gas. A sample volume of 1 μL was injected at a temperature of 300 °C and a 100:1 split ratio. The initial inlet pressure was 20.3 psi but varied as the column flow was held constant at 1.8 mL/min for the duration of the run. The initial oven temperature of 50 °C was held for 0.46 min followed by a temperature ramp of 65 °C/min up to 300 °C. The total run time was 5.0 min and the FID temperature was 325 °C.

Flash Chromatography

Flash chromatography was performed on a Teledyne ISCO Rf-200 (detection at 254 and 280 nm) equipped with an 80 g Teledyne ISCO Redisep Rf Gold silica gel column (20–40 μm particle size) or on a Biotage Isolera One (detection at 210 nm and 400 nm) equipped with a 25 g KPsil column (40-63 μm particle size). Products were visualized by UV.

4.4.2 Ligand Key and Preparation

4.4.2.1 Ligand Key

Figure 4.1 Ligand Key

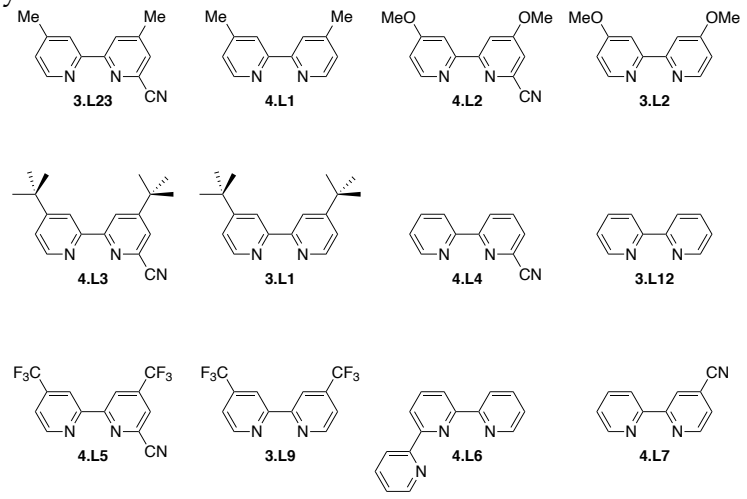

4.4.2.2 Preparation of Ligands

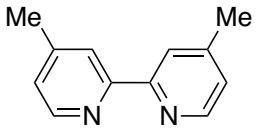

4,4′-dimethyl-2,2′-bipyridine (4.L1) was obtained as a byproduct of the oxidative coupling of 4-methylpyridine to form 4,4′,4′′-trimethyl-2,2′:6′,2′′-terpyridine. For an analogous procedure, see the preparation of **3.L14**. Characterization data match those of commercial samples.

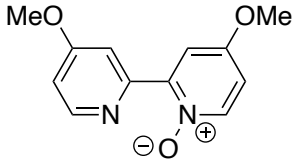

4,4'-dimethoxy-[2,2'-bipyridine] 1-oxide (4.L2a) was prepared by modification of the literature procedure.[115]

A 100 mL round-bottom flask equipped with a PTFE-coated stir bar was charged with 4,4′-dimethoxy-2,2′-bipyridine (2162.4 mg, 10.000 mmol, 1.00 equiv). The flask was placed in a water bath and TFA (6.5 mL) was added. Hydrogen peroxide (30 wt%, 15.000 mmol, 1.50 equiv, 1610 μL) was added in a steady stream. The resulting solution was left to stir at rt overnight. Additional aliquots of hydrogen peroxide (30 wt%, 5.000 mmol, 0.50 equiv, 537 μL) were added daily until the starting material was completely consumed as determined by SFC–MS. The reaction was then diluted with chloroform (20 mL) and neutralized via the addition of 6 M NaOH. The biphasic mixture was transferred to a separatory funnel, and the organic layer isolated. The organic layer was washed with 6 M NaOH (2 × 10 mL), dried over $MgSO_4$, filtered, and concentrated to yield a mixture

of the starting material and desired product. The product was used without further characterization or purification.

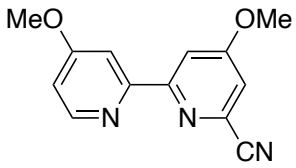

4,4'-di-methoxy-[2,2'-bipyridine]-6-carbonitrile (4.L2) was prepared by modification of the literature procedure.[115]

A flame-dried 50 mL round-bottom flask equipped with a PTFE-coated stir bar was charged with 4,4'-di-methoxy-[2,2'-bipyridine]-1-oxide (464.5 mg, 2.000 mmol, 1.000 equiv). The flask was sealed with a rubber septum and purged with nitrogen for 5 min. Under positive pressure of nitrogen, anhydrous DCM (5 mL) was added to the flask. The reaction was then cooled to 0 °C and trimethylsilyl cyanide (992.1 mg, 10.00 mmol, 5.000 equiv, 1251 μL) was slowly added over the course of 5 min via syringe. Afterwards, benzoyl chloride (562.3 mg, 4.000 mmol, 2.000 equiv, 465.0 μL) was added dropwise over the course of 5 min. The reaction mixture was allowed to warm to rt while stirring for 24 h. After stirring, a 10% solution of $NaHCO_3$ in H_2O was slowly added until gas evolution ceased, and the resulting biphasic mixture was stirred at rt for 24 h. The mixture was poured into a separatory funnel and the organic layer was set aside. The aqueous layer was extracted with DCM (2 × 10 mL), and the combined organic layers were dried over $MgSO_4$, filtered, and concentrated. The resulting residue was purified by column chromatography (40 g of silica gel, 35% EtOAc/hexanes for 1 CV, then 35–60% EtOAc/hexanes across 25 CV) to yield the product (192.2 mg, 0.7972 mmol, 40%) as a light pink solid.

^{1}H NMR (500 MHz, $CDCl_3$) δ 8.47 (d, *J* = 5.6 Hz, 1H), 8.20 (d, *J* = 2.4 Hz, 1H), 8.02 (d, *J* = 2.6 Hz, 1H), 7.23 (d, *J* = 2.4 Hz, 1H), 6.89 (dd, *J* = 5.7, 2.6 Hz, 1H), 4.00 (s, 3H), 3.97 (s, 3H).

^{13}C{^{1}H} NMR (126 MHz, $CDCl_3$) δ 166.9, 166.8, 159.3, 155.9, 150.2, 133.9, 117.4, 116.4, 111.9, 108.7, 106.7, 56.0, 55.5.

HRMS-ESI (m/z): $[M+H]^+$ calcd for $C_{13}H_{12}N_3O_2^+$, 242.0924; found, 242.0924.

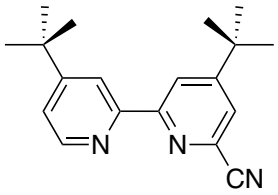

4,4'-di-tert-butyl-[2,2'-bipyridine]-6-carbonitrile (4.L3) was synthesized according to the literature procedure and characterization data matched those reported in the literature.[115]

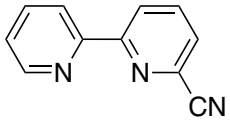

2,2′-bipyridine-6-carbonitrile (4.L4) was synthesized by a former lab member via modification of the literature procedure and characterization data matched those reported in the literature.

^{1}H NMR (500 MHz, $CDCl_3$) δ 8.70 (dd, *J* = 1.8, 0.9 Hz, 1H), 8.68 (dd, *J* = 8.2, 1.1 Hz, 1H), 8.47 (dt, *J* = 8.1, 1.1 Hz, 1H), 7.95 (t, *J* = 7.9 Hz, 1H), 7.86 (td, *J* = 7.8, 1.8 Hz, 1H), 7.70 (dd, *J* = 7.6, 1.1 Hz, 1H), 7.38 (ddd, *J* = 7.6, 4.8, 1.2 Hz, 1H).

^{13}C{^{1}H} NMR (126 MHz, $CDCl_3$) δ 157.7, 154.0, 149.3, 137.9, 137.2, 133.2, 128.1, 124.8, 124.2, 121.6, 117.4.

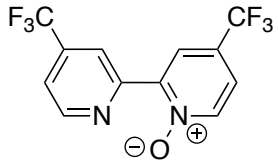

4,4'-bis(trifluoromethyl)-[2,2'-bipyridine] 1-oxide (4.L5a)

To a 50 mL round-bottom flask equipped with a PTFE-coated stir bar was charged with 4,4'-bis-(trifluoromethyl)-2,2'-bipyridine (1460.9 mg, 5.0000 mmol, 1.0000 equiv). The flask was submerged in a water bath and TFA (3.25 mL) was added. While stirring, hydrogen peroxide was added in a steady stream (30 wt%, 7.500 mmol, 1.500 equiv, 850.3 μL). The resulting solution was left to stir at rt overnight. The reaction was then diluted with chloroform (10 mL) and neutralized via the slow addition of 6 M NaOH. The mixture was then transferred to a separatory funnel and the organic layer isolated. The organic layer was then washed with 6 M NaOH (2 × 5 ml), dried over $MgSO_4$, filtered, and concentrated. The resulting residue was purified by column chromatography (ISCO, 40 g silica, 1 CV hexanes, then 0–40% acetone/hexanes across 25 CV) to yield the desired product (271.9 mg, 0.8823 mmol, 18% yield) as a white solid. The remaining mass balance was recovered as the equivalent 1,1'-dioxide.

^{1}H NMR (500 MHz, $CDCl_3$) δ 9.36 – 9.31 (m, 1H), 8.94 (d, *J* = 5.0 Hz, 1H), 8.63 (d, *J* = 2.2 Hz, 1H), 8.40 (d, *J* = 6.8 Hz, 0H), 7.63 (dd, *J* = 5.0, 0.9 Hz, 1H), 7.52 (dd, *J* = 6.8, 2.8 Hz, 1H).

^{13}C{^{1}H} NMR (126 MHz, $CDCl_3$) δ 150.2, 149.5, 146.4, 141.6, 139.1 (q, *J* = 34.4 Hz), 126.9 (q, *J* = 35.6 Hz), 125.0 (q, *J* = 4.0 Hz), 122.6 (q, *J* = 273.6 Hz), 122.5 (q, *J* = 272.1 Hz), 122.0 (q, *J* = 3.5 Hz), 121.1 (q, *J* = 3.8 Hz), 120.6 (q, *J* = 3.5 Hz).

^{19}F{^{1}H} NMR (377 MHz, $CDCl_3$) δ -63.61, -64.69.

HRMS-ESI (m/z): $[M+H]^+$ calcd for $C_{12}H_7F_6N_2O^+$, 309.0457; found, 309.0451.

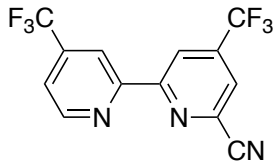

4,4'-bis-(trifluoromethyl)-[2,2'bipyridine]-6-carbonitrile (4.L5) was prepared by modification of the literature procedure.[115]

A flame-dried 50 mL round-bottom flask equipped with a PTFE-coated stir bar was charged with 4,4'-bis-(trifluoromethyl)-[2,2'-bipyridine]-1-oxide (154.1 mg, 0.5000 mmol, 1.000 equiv). The flask was sealed with a rubber septum and purged with nitrogen for 5 min. Under positive pressure of nitrogen, anhydrous DCM (3 mL) was added to the flask. The reaction was then cooled to 0 °C and trimethylsilyl cyanide (248.0 mg, 2.500 mmol, 5.000 equiv, 312.8 μL) was slowly added over the course of 5 min. Following this, benzoyl chloride (140.6 mg, 1.000 mmol, 2.000 equiv, 116.2 μL) was added dropwise over the course of 5 min. The reaction mixture was allowed to warm to rt while stirring for 24 h. After this time, a 10% solution of $NaHCO_3$ in H_2O was slowly added until gas evolution stopped, and the resulting biphasic mixture was stirred at rt for 24 h. The mixture was then poured into a separatory funnel and the organic layer set aside. The aqueous layer was extracted with DCM (2 × 10 mL), and the combined organic layers were dried over $MgSO_4$, filtered, and concentrated. The resulting residue was purified by column chromatography (40 g of silica gel, hexanes for 1 CV, then 0–20% EtOAc/hexanes across 15 CV) to yield the product (147.4 mg, 0.4670 mmol, 93%) as a white solid.

^{1}H NMR (500 MHz, $CDCl_3$) δ 8.98 (d, J = 0.8 Hz, 1H), 8.92 (d, J = 5.0 Hz, 2H), 8.74 (d, J = 0.9 Hz, 1H), 7.96 (d, J = 1.4 Hz, 1H), 7.67 (dd, J = 4.6, 1.4 Hz, 2H).

$^{13}C\{^{1}H\}$ NMR (126 MHz, $CDCl_3$) δ 157.9, 154.0, 150.6, 141.2 (q, *J* = 35.4 Hz), 140.1 (q, *J* = 34.7 Hz), 134.5, 124.3 (q, *J* = 3.5 Hz), 122.6 (q, *J* = 273.6 Hz), 121.8 (q, *J* = 274.1 Hz), 121.1 (q, *J* = 3.5 Hz), 120.5 (q, *J* = 3.6 Hz), 117.7 (q, *J* = 3.7 Hz), 116.0.

$^{19}F\{^{1}H\}$ NMR (377 MHz, $CDCl_3$) δ -64.79, -64.85.

HRMS-ESI (m/z): $[M+H]^+$ calcd for $C_{13}H_6F_6N_3^+$, 318.0460; found, 318.0455.

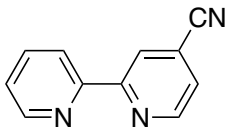

2,2′-bipyridine-4-carbonitrile (4.L7)

In a nitrogen-filled glovebox, an oven-dried 50 mL two-neck flask equipped with a PTFE-coated stir bar was charged with tetrakis(triphenylphosphine)palladium(0) (138.7 mg, 0.1200 mmol, 0.06000 equiv) and 2-bromoisonicotinonitrile (366.0 mg, 2.0000 mmol, 1.000 equiv). The flask was sealed with a rubber septum and removed from the glovebox. The flask was equipped with a condenser via the top neck and purged with nitrogen. Anhydrous toluene (20 mL) and 2-(tributylstannyl)pyridine (809.9 mg, 2.200 mmol, 1.100 equiv, 712.3 μL) were added, then the contents were heated to reflux and stirred for 4 days. After stirring, the reaction mixture was allowed to cool to rt and was filtered through a plug of Celite pre-wetted with DCM, and the filter cake was washed with DCM (3 × 25 mL). The resulting filtrate was concentrated, and the residue purified by column chromatography to yield the product (200.7 mg, 1.108 mmol, 55%) as a white solid.

^{1}H NMR (500 MHz, $CDCl_3$) δ 8.84 (dd, *J* = 4.9, 0.9 Hz, 1H), 8.73 – 8.69 (overlapping signals, 2H), 8.43 (dt, *J* = 8.0, 1.1 Hz, 1H), 7.86 (td, *J* = 7.8, 1.8 Hz, 1H), 7.52 (dd, *J* = 5.0, 1.6 Hz, 1H), 7.38 (ddd, *J* = 7.5, 4.8, 1.2 Hz, 1H).

^{13}C{^{1}H} NMR (126 MHz, $CDCl_3$) δ 157.6, 154.1, 150.0, 149.5, 137.2, 124.8, 124.7, 123.0, 121.4, 121.3, 116.7.

4.4.3 Results of Ligand Screens

Figure 4.2 Results of Screening bpy, bpy^{CN}, and tpy Ligands

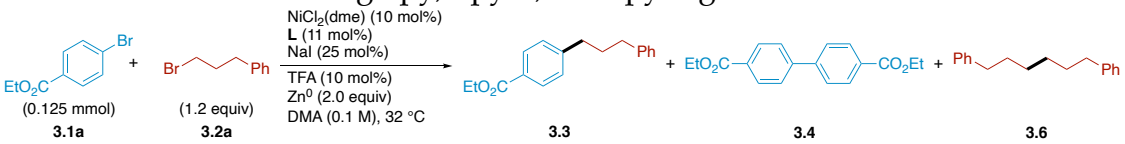

Entry	Ligand	**3.3** (%)	**3.4** (%)	**3.6** (%)
1	**3.L2**	67	6	20[b]
2	**3.L1**	44	21	26[b]
3	**4.L1**	41	22	26[b]
4	**3.L12**	38	25	16[b]
5	**3.L9**	13	31	6[b]
6	**4.L2**	43	5	35
7	**4.L3**	49	6	30
8	**3.L23**	45	5	32
9	**4.L4**	53	3	26
10	**4.L5**	65	4	12
11	**4.L6**	32	5	23
12	**4.L7**	55	12	20

[a]Reactions were assembled in a nitrogen filled glovebox at a 0.125 mmol scale in 1.25 mL of DMA. Yields and selectivity were determined by GC-FID. [b]**3.6** was not observed until after complete consumption of **3.1a**.

Stock solutions were prepared in a nitrogen-filled glovebox. A stock solution of nickel(II) chloride dimethoxyethane (274.6 mg, 1.250 mmol) in DMA was prepared in an oven-dried 25 mL volumetric flask. This solution was stored in a sealed 20 mL vial in the glovebox and stirred immediately prior to use. A stock solution of 4,4'-dimethylbiphenyl (1500.0 mg, 8.2300 mmol), ethyl 4-bromobenzoate (2,863.4 mg, 12.500 mmol), and alkyl halide (2,986.4 mg, 15.000 mmol) in DMA was prepared in an oven-dried 25 mL volumetric flask. This solution was stored in a sealed 20 mL vial in the glovebox and stirred immediately prior to use. Additionally, separate stock solutions of sodium iodide (183.6 mg, 1.225 mmol) and TFA (57.0 mg, 0.500 mmol) in DMA were prepared in oven-

dried 5 mL volumetric flasks. These solutions were prepared fresh each time reactions were set up.

In a nitrogen-filled glovebox, an oven-dried 1 dram vial equipped with a PTFE-coated stir bar was charged with the ligand (0.014 mmol, 0.11 equiv), nickel(II) chloride dimethoxyethane (2.70 mg, 0.0125 mmol, 0.100 equiv, in 250 μL DMA), and DMA (500 μL). The vial was then sealed with a phenolic screw cap bearing a PTFE-backed silicone septum and placed on a stir plate, where it was stirred (1000 rpm) at 30 °C for 30 min. After this time, the cap was removed and sodium iodide (4.70 mg, 0.0313 mmol, 0.250 equiv, in 125 μL of DMA) was added, followed by a mixture of: ethyl 4-bromobenzoate (28.6 mg, 0.125 mmol, 1.00 equiv); 1-bromo-3-phenylpropane (30.0 mg, 0.150 mmol, 1.20 equiv); and 4,4′-dimethylbiphenyl (as an internal standard; 15.0 mg, 0.0823 mmol, 0.658 equiv, in 250 μL of DMA). Zinc flake (16.3 mg, 0.250 mmol, 2.00 equiv) was added to the vial. The contents of the vial were briefly swirled to incorporate the zinc and TFA (1.40 mg, 0.0125 mmol, 0.100 equiv, in 125 μL of DMA) was added. The vial was resealed with the screw cap and placed on a pre-heated stir plate, where it was stirred (1000 rpm) at 32 °C.

Aliquots were taken at 0, 15, 30, 45, 60, 75, 90, 120, and 180 min to determine the concentrations of the product and side products, and at 24 h to establish the final yield. The aliquot (20 μL) was obtained by removing the screw cap and sampling the stirring reaction with an autopipette. The aliquot was diluted into 1000 μL of ethyl acetate, removed from the glovebox, and quenched with 1 mL of deionized water. The organic layer was then passed through a short (1.5 cm in a pipette) silica plug and analyzed by GC-FID. Concentrations of the reactants, desired product, and side products were

determined as calibrated ratios of the area of the analyte peak compared to the area of the internal standard peak.

4.4.3.1 Electronic Trends and Calculation of ρ

Figure 4.3 Observed Electronic Trends

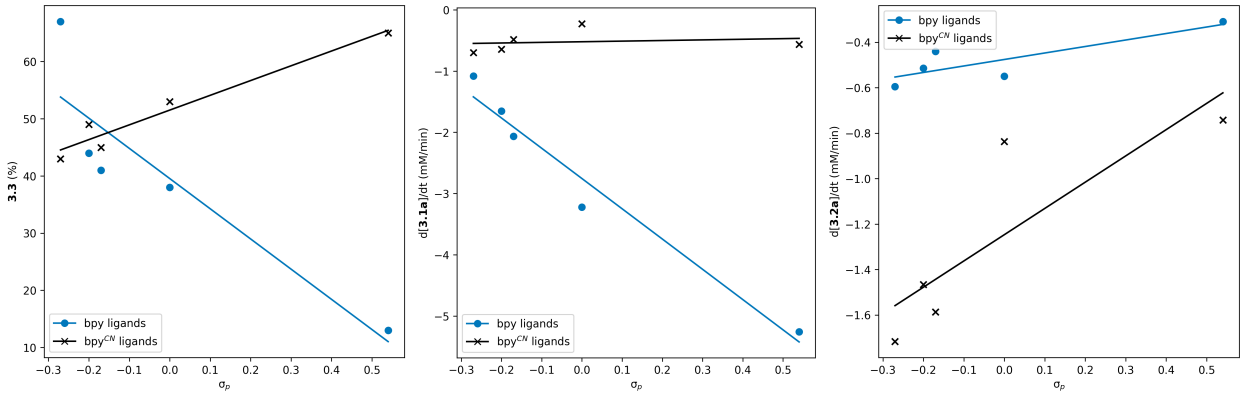

[a]Reactions were assembled in a nitrogen filled glovebox at a 0.125 mmol scale in 1.25 mL of DMA. Concentrations of all reagents were determined by GC-FID. Rates were determined from 0–30 min when the reaction rate was linear. For reactions that were complete in under 30 min, the rate was estimated from 0–15 min.

Entry	Ligand Class	Substrate	ρ	R^2
1	bpy	**3.1a**	0.74	0.84
2	bpy^{CN}	**3.1a**	-0.075	0.02
3	bpy	**3.2a**	-0.30	0.76
4	bpy^{CN}	**3.2a**	-0.45	0.75

Hammett plots are not shown. However, the results of rate transformation and regression are listed below. Note that the low value of R^2 for entry 2 indicates a weak regression and that the value of ρ is 0.

4.4.4 Computational Details

All computations were performed using the Gaussian 16, Rev. C.01 suite—using defaults unless noted otherwise—at the UM06/cc-pVTZ,SDD(Ni)//UM06/cc-pVDZ,LANL2DZ(Ni) level of theory with the SMD continuum solvation model for DMA (*N*,*N*-dimethylacetamide).[137–143,161] The Gaussian keywords "ultrafine" and "noraman" were used to ensure accuracy whilst improving computational efficiency. Conformers of

higher energy were accounted for in all cases and are not included in the discussion. Stationary points were characterized as ground states by the absence of negative eigenvalues (zero imaginary frequencies) in frequency analysis at the same level of theory as the geometry optimization.

References

(1) Lovering, F.; Bikker, J.; Humblet, C. Escape from Flatland: Increasing Saturation as an Approach to Improving Clinical Success. *J. Med. Chem.* **2009**, *52* (21), 6752–6756. https://doi.org/10.1021/jm901241e.

(2) Boström, J.; Brown, D. G.; Young, R. J.; Keserü, G. M. Expanding the Medicinal Chemistry Synthetic Toolbox. *Nat. Rev. Drug Discov.* **2018**, *17* (10), 709–727. https://doi.org/10.1038/nrd.2018.116.

(3) Campeau, L.-C.; Hazari, N. Cross-Coupling and Related Reactions: Connecting Past Success to the Development of New Reactions for the Future. *Organometallics* **2019**, *38* (1), 3–35. https://doi.org/10.1021/acs.organomet.8b00720.

(4) Firsan, S. J.; Sivakumar, V.; Colacot, T. J. Emerging Trends in Cross-Coupling: Twelve-Electron-Based L $_1$ Pd(0) Catalysts, Their Mechanism of Action, and Selected Applications. *Chem. Rev.* **2022**, *122* (23), 16983–17027. https://doi.org/10.1021/acs.chemrev.2c00204.

(5) Brown, D. G.; Boström, J. Analysis of Past and Present Synthetic Methodologies on Medicinal Chemistry: Where Have All the New Reactions Gone?: Miniperspective. *J. Med. Chem.* **2016**, *59* (10), 4443–4458. https://doi.org/10.1021/acs.jmedchem.5b01409.

(6) Miyaura, Norio.; Suzuki, Akira. Palladium-Catalyzed Cross-Coupling Reactions of Organoboron Compounds. *Chem. Rev.* **1995**, *95* (7), 2457–2483. https://doi.org/10.1021/cr00039a007.

(7) Johansson Seechurn, C. C. C.; Kitching, M. O.; Colacot, T. J.; Snieckus, V. Palladium-Catalyzed Cross-Coupling: A Historical Contextual Perspective to the 2010 Nobel Prize. *Angew. Chem. Int. Ed.* **2012**, *51* (21), 5062–5085. https://doi.org/10.1002/anie.201107017.

(8) Guram, A. S.; Rennels, R. A.; Buchwald, S. L. A Simple Catalytic Method for the Conversion of Aryl Bromides to Arylamines. *Angew. Chem. Int. Ed.* **1995**, *34* (12), 1348–1350. https://doi.org/10.1002/anie.199513481.

(9) Louie, J.; Hartwig, J. F. Palladium-Catalyzed Synthesis of Arylamines from Aryl Halides. Mechanistic Studies Lead to Coupling in the Absence of Tin Reagents. *Tetrahedron Lett.* **1995**, *36* (21), 3609–3612. https://doi.org/10.1016/0040-4039(95)00605-C.

(10) Dorel, R.; Grugel, C. P.; Haydl, A. M. The Buchwald–Hartwig Amination After 25 Years. *Angew. Chem. Int. Ed.* **2019**, *58* (48), 17118–17129. https://doi.org/10.1002/anie.201904795.

(11) Roughley, S. D.; Jordan, A. M. The Medicinal Chemist's Toolbox: An Analysis of Reactions Used in the Pursuit of Drug Candidates. *J. Med. Chem.* **2011**, *54* (10), 3451–3479. https://doi.org/10.1021/jm200187y.

(12) Schneider, N.; Lowe, D. M.; Sayle, R. A.; Tarselli, M. A.; Landrum, G. A. Big Data from Pharmaceutical Patents: A Computational Analysis of Medicinal Chemists' Bread and Butter. *J. Med. Chem.* **2016**, *59* (9), 4385–4402. https://doi.org/10.1021/acs.jmedchem.6b00153.

(13) Chemler, S. R.; Trauner, D.; Danishefsky, S. J. The B-Alkyl Suzuki-Miyaura Cross-Coupling Reaction: Development, Mechanistic Study, and Applications in Natural Product Synthesis. *Angew. Chem. Int. Ed.* **2001**, *40* (24), 4544–4568. https://doi.org/10.1002/1521-3773(20011217)40:24<4544::AID-ANIE4544>3.0.CO;2-N.

(14) Doucet, H. Suzuki–Miyaura Cross-Coupling Reactions of Alkylboronic Acid Derivatives or Alkyltrifluoroborates with Aryl, Alkenyl or Alkyl Halides and Triflates. *Eur. J. Org. Chem.* **2008**, *2008* (12), 2013–2030. https://doi.org/10.1002/ejoc.200700984.
(15) Beletskaya, I. P.; Alonso, F.; Tyurin, V. The Suzuki-Miyaura Reaction after the Nobel Prize. *Coord. Chem. Rev.* **2019**, *385*, 137–173. https://doi.org/10.1016/j.ccr.2019.01.012.
(16) Pearson, R. G.; Figdore, P. E. Relative Reactivities of Methyl Iodide and Methyl Tosylate with Transition-Metal Nucleophiles. *J. Am. Chem. Soc.* **1980**, *102* (5), 1541–1547. https://doi.org/10.1021/ja00525a013.
(17) Ariafard, A.; Lin, Z. Understanding the Relative Easiness of Oxidative Addition of Aryl and Alkyl Halides to Palladium(0). *Organometallics* **2006**, *25* (16), 4030–4033. https://doi.org/10.1021/om060236x.
(18) Frisch, A. C.; Beller, M. Catalysts for Cross-Coupling Reactions with Non-Activated Alkyl Halides. *Angew. Chem. Int. Ed.* **2005**, *44* (5), 674–688. https://doi.org/10.1002/anie.200461432.
(19) Culkin, D. A.; Hartwig, J. F. Carbon−Carbon Bond-Forming Reductive Elimination from Arylpalladium Complexes Containing Functionalized Alkyl Groups. Influence of Ligand Steric and Electronic Properties on Structure, Stability, and Reactivity. *Organometallics* **2004**, *23* (14), 3398–3416. https://doi.org/10.1021/om049726k.
(20) Knapp, D. M.; Gillis, E. P.; Burke, M. D. A General Solution for Unstable Boronic Acids: Slow-Release Cross-Coupling from Air-Stable MIDA Boronates. *J. Am. Chem. Soc.* **2009**, *131* (20), 6961–6963. https://doi.org/10.1021/ja901416p.
(21) St. Denis, J. D.; Scully, C. C. G.; Lee, C. F.; Yudin, A. K. Development of the Direct Suzuki–Miyaura Cross-Coupling of Primary *B* -Alkyl MIDA-Boronates and Aryl Bromides. *Org. Lett.* **2014**, *16* (5), 1338–1341. https://doi.org/10.1021/ol500057a.
(22) Jana, R.; Pathak, T. P.; Sigman, M. S. Advances in Transition Metal (Pd,Ni,Fe)-Catalyzed Cross-Coupling Reactions Using Alkyl-Organometallics as Reaction Partners. *Chem. Rev.* **2011**, *111* (3), 1417–1492. https://doi.org/10.1021/cr100327p.
(23) Ackerman-Biegasiewicz, L. K. G.; Kariofillis, S. K.; Weix, D. J. Multimetallic-Catalyzed C–C Bond-Forming Reactions: From Serendipity to Strategy. *J. Am. Chem. Soc.* **2023**, *145* (12), 6596–6614. https://doi.org/10.1021/jacs.2c08615.
(24) Everson, D. A.; Jones, B. A.; Weix, D. J. Replacing Conventional Carbon Nucleophiles with Electrophiles: Nickel-Catalyzed Reductive Alkylation of Aryl Bromides and Chlorides. *J. Am. Chem. Soc.* **2012**, *134* (14), 6146–6159. https://doi.org/10.1021/ja301769r.
(25) Anka-Lufford, L. L.; Huihui, K. M. M.; Gower, N. J.; Ackerman, L. K. G.; Weix, D. J. Nickel-Catalyzed Cross-Electrophile Coupling with Organic Reductants in Non-Amide Solvents. *Chem. Eur. J.* **2016**, *22* (33), 11564–11567. https://doi.org/10.1002/chem.201602668.
(26) Suzuki, N.; Hofstra, J. L.; Poremba, K. E.; Reisman, S. E. Nickel-Catalyzed Enantioselective Cross-Coupling of *N* -Hydroxyphthalimide Esters with Vinyl Bromides. *Org. Lett.* **2017**, *19* (8), 2150–2153. https://doi.org/10.1021/acs.orglett.7b00793.
(27) Chan, A. Y.; Perry, I. B.; Bissonnette, N. B.; Buksh, B. F.; Edwards, G. A.; Frye, L. I.; Garry, O. L.; Lavagnino, M. N.; Li, B. X.; Liang, Y.; Mao, E.; Millet, A.; Oakley, J. V.; Reed, N. L.; Sakai, H. A.; Seath, C. P.; MacMillan, D. W. C. Metallaphotoredox: The

Merger of Photoredox and Transition Metal Catalysis. *Chem. Rev.* **2022**, *122* (2), 1485–1542. https://doi.org/10.1021/acs.chemrev.1c00383.
(28) Everson, D. A.; Shrestha, R.; Weix, D. J. Nickel-Catalyzed Reductive Cross-Coupling of Aryl Halides with Alkyl Halides. *J. Am. Chem. Soc.* **2010**, *132* (3), 920–921. https://doi.org/10.1021/ja9093956.
(29) Yu, X.; Yang, T.; Wang, S.; Xu, H.; Gong, H. Nickel-Catalyzed Reductive Cross-Coupling of Unactivated Alkyl Halides. *Org. Lett.* **2011**, *13* (8), 2138–2141. https://doi.org/10.1021/ol200617f.
(30) Amatore, M.; Gosmini, C. Direct Method for Carbon-Carbon Bond Formation: The Functional Group Tolerant Cobalt-Catalyzed Alkylation of Aryl Halides. *Chem. Eur. J.* **2010**, *16* (20), 5848–5852. https://doi.org/10.1002/chem.201000178.
(31) Kambe, N.; Iwasaki, T.; Terao, J. Pd-Catalyzed Cross-Coupling Reactions of Alkyl Halides. *Chem. Soc. Rev.* **2011**, *40* (10), 4937. https://doi.org/10.1039/c1cs15129k.
(32) Biswas, S.; Weix, D. J. Mechanism and Selectivity in Nickel-Catalyzed Cross-Electrophile Coupling of Aryl Halides with Alkyl Halides. *J. Am. Chem. Soc.* **2013**, *135* (43), 16192–16197. https://doi.org/10.1021/ja407589e.
(33) Johnson, K. A.; Biswas, S.; Weix, D. J. Cross-Electrophile Coupling of Vinyl Halides with Alkyl Halides. *Chem. Eur. J.* **2016**, *22* (22), 7399–7402. https://doi.org/10.1002/chem.201601320.
(34) Ruiz-Castillo, P.; Buchwald, S. L. Applications of Palladium-Catalyzed C–N Cross-Coupling Reactions. *Chem. Rev.* **2016**, *116* (19), 12564–12649. https://doi.org/10.1021/acs.chemrev.6b00512.
(35) Ertl, P.; Altmann, E.; McKenna, J. M. The Most Common Functional Groups in Bioactive Molecules and How Their Popularity Has Evolved over Time. *J. Med. Chem* **2020**, *63* (15), 8408–8418. https://doi.org/10.1021/acs.jmedchem.0c00754.
(36) Hamann, B. C.; Hartwig, J. F. Sterically Hindered Chelating Alkyl Phosphines Provide Large Rate Accelerations in Palladium-Catalyzed Amination of Aryl Iodides, Bromides, and Chlorides, and the First Amination of Aryl Tosylates. *J. Am. Chem. Soc.* **1998**, *120* (29), 7369–7370. https://doi.org/10.1021/ja981318i.
(37) Old, D. W.; Wolfe, J. P.; Buchwald, S. L. A Highly Active Catalyst for Palladium-Catalyzed Cross-Coupling Reactions: Room-Temperature Suzuki Couplings and Amination of Unactivated Aryl Chlorides. *J. Am. Chem. Soc.* **1998**, *120* (37), 9722–9723. https://doi.org/10.1021/ja982250+.
(38) Ehrentraut, A.; Zapf, A.; Beller, M. A New Improved Catalyst for the Palladium-Catalyzed Amination of Aryl Chlorides. *Journal of Molecular Catalysis A: Chemical* **2002**, *182–183*, 515–523. https://doi.org/10.1016/S1381-1169(01)00503-9.
(39) Mao, J.; Zhang, J.; Zhang, S.; Walsh, P. J. NIXANTPHOS: A Highly Active Ligand for Palladium Catalyzed Buchwald–Hartwig Amination of Unactivated Aryl Chlorides. *Dalton Trans.* **2018**, *47* (26), 8690–8696. https://doi.org/10.1039/C8DT01852A.
(40) Carey, J. S.; Laffan, D.; Thomson, C.; Williams, M. T. Analysis of the Reactions Used for the Preparation of Drug Candidate Molecules. *Org. Biomol. Chem* **2006**, *4* (12), 2337. https://doi.org/10.1039/b602413k.
(41) Gilman, H.; McCracken, R. The Reaction Between Nitrosobenzene and Phenylmagnesium Bromide. *J. Am. Chem. Soc.* **1927**, *49* (4), 1052–1061. https://doi.org/10.1021/ja01403a026.
(42) Sapountzis, I.; Knochel, P. A New General Preparation of Polyfunctional Diarylamines by the Addition of Functionalized Arylmagnesium Compounds to

Nitroarenes. *J. Am. Chem. Soc.* **2002**, *124* (32), 9390–9391. https://doi.org/10.1021/ja026718r.
(43) Dhayalan, V.; Sämann, C.; Knochel, P. Synthesis of Polyfunctional Secondary Amines by the Addition of Functionalized Zinc Reagents to Nitrosoarenes. *Chem. Commun.* **2015**, *51* (15), 3239–3242. https://doi.org/10.1039/C4CC08846H.
(44) Rauser, M.; Ascheberg, C.; Niggemann, M. Electrophilic Amination with Nitroarenes. *Angew. Chem. Int. Ed.* **2017**, *56* (38), 11570–11574. https://doi.org/10.1002/anie.201705356.
(45) Roscales, S.; Csákÿ, A. G. Synthesis of Di(Hetero)Arylamines from Nitrosoarenes and Boronic Acids: A General, Mild, and Transition-Metal-Free Coupling. *Org. Lett.* **2018**, *20* (6), 1667–1671. https://doi.org/10.1021/acs.orglett.8b00473.
(46) Yu, Y.; Srogl, J.; Liebeskind, L. S. Cu(I)-Mediated Reductive Amination of Boronic Acids with Nitroso Aromatics. *Org. Lett.* **2004**, *6* (15), 2631–2634. https://doi.org/10.1021/ol048982q.
(47) Nykaza, T. V.; Cooper, J. C.; Li, G.; Mahieu, N.; Ramirez, A.; Luzung, M. R.; Radosevich, A. T. Intermolecular Reductive C–N Cross Coupling of Nitroarenes and Boronic Acids by PIII/PV═O Catalysis. *J. Am. Chem. Soc.* **2018**, *140* (45), 15200–15205. https://doi.org/10.1021/jacs.8b10769.
(48) Suárez-Pantiga, S.; Hernández-Ruiz, R.; Virumbrales, C.; Pedrosa, M. R.; Sanz, R. Reductive Molybdenum-Catalyzed Direct Amination of Boronic Acids with Nitro Compounds. *Angew. Chem. Int. Ed.* **2019**, *58* (7), 2129–2133. https://doi.org/10.1002/anie.201812806.
(49) Li, G.; Nykaza, T. V.; Cooper, J. C.; Ramirez, A.; Luzung, M. R.; Radosevich, A. T. An Improved P^{III}/P^{V}═O-Catalyzed Reductive C–N Coupling of Nitroaromatics and Boronic Acids by Mechanistic Differentiation of Rate- and Product-Determining Steps. *J. Am. Chem. Soc.* **2020**, *142* (14), 6786–6799. https://doi.org/10.1021/jacs.0c01666.
(50) Manna, K.; Ganguly, T.; Baitalik, S.; Jana, R. Visible-Light- and PPh_3 -Mediated Direct C–N Coupling of Nitroarenes and Boronic Acids at Ambient Temperature. *Org. Lett.* **2021**, *23* (21), 8634–8639. https://doi.org/10.1021/acs.orglett.1c03343.
(51) Guan, X.; Zhu, H.; Driver, T. G. Cu-Catalyzed Cross-Coupling of Nitroarenes with Aryl Boronic Acids to Construct Diarylamines. *ACS Catal.* **2021**, *11* (20), 12417–12422. https://doi.org/10.1021/acscatal.1c03113.
(52) Wang, D.; Wan, Z.; Zhang, H.; Alhumade, H.; Yi, H.; Lei, A. Electrochemical Reductive Arylation of Nitroarenes with Arylboronic Acids. *ChemSusChem* **2021**, *14* (24), 5399–5404. https://doi.org/10.1002/cssc.202101924.
(53) Song, H.; Shen, Y.; Zhou, H.; Ding, D.; Yang, F.; Wang, Y.; Xu, C.; Cai, X. Light-Promoted Low-Valent-Tungsten-Catalyzed Ambient Temperature Amination of Boronic Acids with Nitroaromatics. *J. Org. Chem.* **2022**, *87* (8), 5303–5314. https://doi.org/10.1021/acs.joc.2c00138.
(54) Talukdar, H.; Gogoi, D.; Phukan, P. Chemoselective Chan-Lam and Reductive Nitroarene Coupling of Boronic Acid Using an Octahedral Ni-DMAP Complex as Catalyst. *Tetrahedron* **2023**, *132*, 133251. https://doi.org/10.1016/j.tet.2023.133251.
(55) Li, G.; Yang, L.; Liu, J.; Zhang, W.; Cao, R.; Wang, C.; Zhang, Z.; Xiao, J.; Xue, D. Light-Promoted C–N Coupling of Aryl Halides with Nitroarenes. *Angew. Chem. Int. Ed.* **2021**, *60* (10), 5230–5234. https://doi.org/10.1002/anie.202012877.

(56) Ghosh, I.; Ghosh, T.; Bardagi, J. I.; König, B. Reduction of Aryl Halides by Consecutive Visible Light-Induced Electron Transfer Processes. *Science* **2014**, *346* (6210), 725–728. https://doi.org/10.1126/science.1258232.
(57) Kim, H.; Kim, H.; Lambert, T. H.; Lin, S. Reductive Electrophotocatalysis: Merging Electricity and Light To Achieve Extreme Reduction Potentials. *J. Am. Chem. Soc.* **2020**, *142* (5), 2087–2092. https://doi.org/10.1021/jacs.9b10678.
(58) MacKenzie, I. A.; Wang, L.; Onuska, N. P. R.; Williams, O. F.; Begam, K.; Moran, A. M.; Dunietz, B. D.; Nicewicz, D. A. Discovery and Characterization of an Acridine Radical Photoreductant. *Nature* **2020**, *580* (7801), 76–80. https://doi.org/10.1038/s41586-020-2131-1.
(59) Chmiel, A. F.; Williams, O. P.; Chernowsky, C. P.; Yeung, C. S.; Wickens, Z. K. Non-Innocent Radical Ion Intermediates in Photoredox Catalysis: Parallel Reduction Modes Enable Coupling of Diverse Aryl Chlorides. *J. Am. Chem. Soc.* **2021**, *143* (29), 10882–10889. https://doi.org/10.1021/jacs.1c05988.
(60) Shen, N.; Li, R.; Liu, C.; Shen, X.; Guan, W.; Shang, R. Photocatalytic Cross-Couplings of Aryl Halides Enabled by *o* -Phosphinophenolate and *o* -Phosphinothiophenolate. *ACS Catal.* **2022**, *12* (5), 2788–2795. https://doi.org/10.1021/acscatal.1c05941.
(61) Widness, J. K.; Enny, D. G.; McFarlane-Connelly, K. S.; Miedenbauer, M. T.; Krauss, T. D.; Weix, D. J. CdS Quantum Dots as Potent Photoreductants for Organic Chemistry Enabled by Auger Processes. *J. Am. Chem. Soc.* **2022**, *144* (27), 12229–12246. https://doi.org/10.1021/jacs.2c03235.
(62) Wang, S.-D.; Yang, B.; Zhang, H.; Qu, J.-P.; Kang, Y.-B. Reductive Cleavage of C–X or N–S Bonds Catalyzed by Super Organoreductant CBZ6. *Org. Lett.* **2023**, *25* (5), 816–820. https://doi.org/10.1021/acs.orglett.2c04346.
(63) Cheung, C. W.; Ploeger, M. L.; Hu, X. Direct Amidation of Esters with Nitroarenes. *Nat. Commun.* **2017**, *8*, 14878. https://doi.org/10.1038/ncomms14878.
(64) Ploeger, M. L.; Darù, A.; Harvey, J. N.; Hu, X. Reductive Cleavage of Azoarene as a Key Step in Nickel-Catalyzed Amidation of Esters with Nitroarenes. *ACS Catal.* **2020**, *10* (4), 2845–2854. https://doi.org/10.1021/acscatal.9b05049.
(65) Yadav, M. R.; Nagaoka, M.; Kashihara, M.; Zhong, R.-L.; Miyazaki, T.; Sakaki, S.; Nakao, Y. The Suzuki–Miyaura Coupling of Nitroarenes. *J. Am. Chem. Soc.* **2017**, *139* (28), 9423–9426. https://doi.org/10.1021/jacs.7b03159.
(66) Muto, K.; Okita, T.; Yamaguchi, J. Transition-Metal-Catalyzed Denitrative Coupling of Nitroarenes. *ACS Catal.* **2020**, *10* (17), 9856–9871. https://doi.org/10.1021/acscatal.0c02990.
(67) Kashihara, M.; Nakao, Y. Cross-Coupling Reactions of Nitroarenes. *Acc. Chem. Res.* **2021**, *54* (14), 2928–2935. https://doi.org/10.1021/acs.accounts.1c00220.
(68) Inoue, F.; Kashihara, M.; Yadav, M. R.; Nakao, Y. Buchwald–Hartwig Amination of Nitroarenes. *Angew. Chem. Int. Ed.* **2017**, *56* (43), 13307–13309. https://doi.org/10.1002/anie.201706982.
(69) Feng, L.; Yao, J.; Yu, L.; Duan, W. Palladium-Catalyzed Denitrative *N* -Arylation of Nitroarenes with Pyrroles, Indoles, and Carbazoles. *Org. Chem. Front.* **2022**, *9* (9), 2351–2356. https://doi.org/10.1039/D2QO00010E.
(70) Walther, M.; Kipke, W.; Schultzke, S.; Ghosh, S.; Staubitz, A. Modification of Azobenzenes by Cross-Coupling Reactions. *Synthesis* **2021**, *53* (07), 1213–1228. https://doi.org/10.1055/s-0040-1705999.

(71) Cope, A. C.; Siekman, R. W. Formation of Covalent Bonds from Platinum or Palladium to Carbon by Direct Substitution. *J. Am. Chem. Soc.* **1965**, *87* (14), 3272–3273. https://doi.org/10.1021/ja01092a063.
(72) Fahey, D. R. The Homogeneous Palladium-Catalysed Ortho-Chlorination of Azobenzene. *J. Chem. Soc. D* **1970**, No. 7, 417a. https://doi.org/10.1039/c2970000417a.
(73) R. Fahey, D. The Coordination-Catalyzed Ortho-Halogenation of Azobenzene. *J. Organomet. Chem.* **1971**, *27* (2), 283–292. https://doi.org/10.1016/S0022-328X(00)80577-X.
(74) Murahashi, S.; Tamba, Y.; Yamamura, M.; Yoshimura, N. Reactions of Cyclometalated Palladium Complexes with Organolithium Compounds or Grignard Reagents. Selective Ortho Alkylation and Arylation of Benzaldehydes, Azobenzenes, and Tertiary Benzylic Amines. *J. Org. Chem.* **1978**, *43* (21), 4099–4106. https://doi.org/10.1021/jo00415a024.
(75) Wu, Guangzhong.; Rheingold, A. L.; Heck, R. F. Cinnolinium Salt Synthesis from Cyclopalladated Azobenzene Complexes and Alkynes. *Organometallics* **1987**, *6* (11), 2386–2391. https://doi.org/10.1021/om00154a019.
(76) Bartolomé, C.; Espinet, P.; Vicente, L.; Villafañe, F.; Charmant, J. P. H.; Orpen, A. G. Neutral Organometallic Palladium(II) Aquo Complexes. *Organometallics* **2002**, *21* (17), 3536–3543. https://doi.org/10.1021/om020198r.
(77) Dick, A. R.; Hull, K. L.; Sanford, M. S. A Highly Selective Catalytic Method for the Oxidative Functionalization of C−H Bonds. *J. Am. Chem. Soc.* **2004**, *126* (8), 2300–2301. https://doi.org/10.1021/ja031543m.
(78) Ma, X.-T.; Tian, S.-K. Palladium-Catalyzed Regioselective Halogenation of Aromatic Azo Compounds. *Adv. Synth. Catal.* **2013**, *335* (2–3), 337–340. https://doi.org/10.1002/adsc.201200902.
(79) Li, H.; Li, P.; Wang, L. Direct Access to Acylated Azobenzenes via Pd-Catalyzed C–H Functionalization and Further Transformation into an Indazole Backbone. *Org. Lett.* **2013**, *15* (3), 620–623. https://doi.org/10.1021/ol303434n.
(80) Ghosh, A.; Limaye, A. S.; K. N., M.; Patil, S. A.; Dateer, R. B. Zn-Mediated Selective Reduction of Nitroarenes: A Sustainable Approach for Azoxybenzenes Synthesis. *Organic Preparations and Procedures International* **2022**, *54* (3), 284–293. https://doi.org/10.1080/00304948.2021.2022441.
(81) Bigelow, H. E.; Robinson, D. B. Azobenzene. *Org. Synth.* **1942**, *22*, 28. https://doi.org/10.15227/orgsyn.022.0028.
(82) Hicks, J. D.; Hyde, A. M.; Cuezva, A. M.; Buchwald, S. L. Pd-Catalyzed N-Arylation of Secondary Acyclic Amides: Catalyst Development, Scope, and Computational Study. *J. Am. Chem. Soc.* **2009**, *131* (46), 16720–16734. https://doi.org/10.1021/ja9044357.
(83) Chalkley, M. J.; Drover, M. W.; Peters, J. C. Catalytic N_2-to-NH_3 (or -N_2H_4) Conversion by Well-Defined Molecular Coordination Complexes. *Chem. Rev.* **2020**, *120* (12), 5582–5636. https://doi.org/10.1021/acs.chemrev.9b00638.
(84) Franzen, V. Zur Dissoziation von Tetraphenylhydrazin. *Justus Liebigs Ann. Chem.* **1957**, *604* (1), 251–256. https://doi.org/10.1002/jlac.19576040127.
(85) Cain, C. K.; Wiselogle, F. Y. D. N. I. The Rate of Dissociation of Tetraphenylhydrazine. *J. Am. Chem. Soc.* **1940**, *62* (5), 1163–1169. https://doi.org/10.1021/ja01862a050.

(86) Cheung, C. W.; Hu, X. Amine Synthesis via Iron-Catalysed Reductive Coupling of Nitroarenes with Alkyl Halides. *Nat. Commun.* **2016**, *7*, 12494. https://doi.org/10.1038/ncomms12494.
(87) Cheung, C. W.; Ma, J.-A.; Hu, X. Manganese-Mediated Reductive Transamidation of Tertiary Amides with Nitroarenes. *J. Am. Chem. Soc.* **2018**, *140* (22), 6789–6792. https://doi.org/10.1021/jacs.8b03739.
(88) Cheung, C. W.; Shen, N.; Wang, S.-P.; Ullah, A.; Hu, X.; Ma, J.-A. Manganese-Mediated Reductive Amidation of Esters with Nitroarenes. *Org. Chem. Front.* **2019**, *6* (6), 756–761. https://doi.org/10.1039/C8QO01405A.
(89) Cheung, C. W.; Ploeger, M. L.; Hu, X. Amide Synthesis via Nickel-Catalysed Reductive Aminocarbonylation of Aryl Halides with Nitroarenes. *Chem. Sci.* **2018**, *9* (3), 655–659. https://doi.org/10.1039/C7SC03950F.
(90) He, H.-D.; Zhang, Z.-K.; Tang, H.-B.; Xu, Y.-Q.; Xu, X.-B.; Cao, Z.-Y.; Xu, H.; Li, Y. Manganese-Mediated Reductive *N*, *N* -Dialkylation of Nitroarenes: A Dramatic NiI_2 Effect. *Org. Chem. Front.* **2022**, *9* (18), 4875–4881. https://doi.org/10.1039/D2QO00928E.
(91) Merino, E. Synthesis of Azobenzenes: The Coloured Pieces of Molecular Materials. *Chem. Soc. Rev.* **2011**, *40* (7), 3835–3853. https://doi.org/10.1039/c0cs00183j.
(92) Muñiz, K.; Nieger, M. Catalytic Activation of N–N Multiple Bonds: A Homogeneous Palladium Catalyst for Mechanistically Unprecedented Reduction of Azo Compounds. *Angew. Chem. Int. Ed.* **2006**, *45* (14), 2305–2308. https://doi.org/10.1002/anie.200503875.
(93) Muñiz, K.; Iglesias, A. Phenanthroline Ligands in Aryl Palladium Hydrazinato Complexes: Catalysts for Efficient Coupling of Azo Compounds with Aryl Boronic Acids. *Angew. Chem. Int. Ed.* **2007**, *46* (33), 6350–6353. https://doi.org/10.1002/anie.200700288.
(94) Sunesson, Y.; Limé, E.; Nilsson Lill, S. O.; Meadows, R. E.; Norrby, P.-O. Role of the Base in Buchwald–Hartwig Amination. *J. Org. Chem.* **2014**, *79* (24), 11961–11969. https://doi.org/10.1021/jo501817m.
(95) Brusoe, A. T.; Hartwig, J. F. Palladium-Catalyzed Arylation of Fluoroalkylamines. *J. Am. Chem. Soc.* **2015**, *137* (26), 8460–8468. https://doi.org/10.1021/jacs.5b02512.
(96) Rangarajan, T. M.; Singh, R.; Brahma, R.; Devi, K.; Singh, R. P.; Singh, R. P.; Prasad, A. K. BrettPhos Ligand Supported Palladium-Catalyzed C–O Bond Formation through an Electronic Pathway of Reductive Elimination: Fluoroalkoxylation of Activated Aryl Halides. *Chem. Eur. J.* **2014**, *20* (44), 14218–14225. https://doi.org/10.1002/chem.201404121.
(97) Gomberg, M.; Bachmann, W. E. The Synthesis of Biaryl Compounds by Means of the Diazo Reaction. *J. Am. Chem. Soc.* **1924**, *46* (10), 2339–2343. https://doi.org/10.1021/ja01675a026.
(98) Proctor, R. S. J.; Phipps, R. J. Recent Advances in Minisci-Type Reactions. *Angew. Chem. Int. Ed.* **2019**, *58* (39), 13666–13699. https://doi.org/10.1002/anie.201900977.
(99) Candish, L.; Freitag, M.; Gensch, T.; Glorius, F. Mild, Visible Light-Mediated Decarboxylation of Aryl Carboxylic Acids to Access Aryl Radicals. *Chem. Sci.* **2017**, *8* (5), 3618–3622. https://doi.org/10.1039/C6SC05533H.
(100) Peng, K.; Mawamba, V.; Schulz, E.; Löhr, M.; Hagemann, C.; Schatzschneider, U. iClick Reactions of Square-Planar Palladium(II) and Platinum(II) Azido Complexes with Electron-Poor Alkynes: Metal-Dependent Preference for N1 vs N2 Triazolate

Coordination and Kinetic Studies with ^{1}H and ^{19}F NMR Spectroscopy. *Inorg. Chem.* **2019**, *58* (17), 11508–11521. https://doi.org/10.1021/acs.inorgchem.9b01304.

(101) Tangallapally, R. P.; Yendapally, R.; Lee, R. E.; Lenaerts, A. J. M.; Lee, R. E. Synthesis and Evaluation of Cyclic Secondary Amine Substituted Phenyl and Benzyl Nitrofuranyl Amides as Novel Antituberculosis Agents. *J. Med. Chem.* **2005**, *48* (26), 8261–8269. https://doi.org/10.1021/jm050765n.

(102) Luo, C.; Guldi, D. M.; Imahori, H.; Tamaki, K.; Sakata, Y. Sequential Energy and Electron Transfer in an Artificial Reaction Center: Formation of a Long-Lived Charge-Separated State. *J. Am. Chem. Soc.* **2000**, *122* (28), 6535–6551. https://doi.org/10.1021/ja993959z.

(103) Sun, N.; Hong, L.; Huang, F.; Ren, H.; Mo, W.; Hu, B.; Shen, Z.; Hu, X. General and Efficient Synthesis of 2,3-Unsubstituted Indoles Catalyzed by Acidic Mesoporous Molecular Sieves. *Tetrahedron* **2013**, *69*, 3927–3933. https://doi.org/10.1016/j.tet.2013.03.026.

(104) Bae, S.; Jang, H.-L.; Jung, H.; Joo, J. M. Catalytic C–H Allylation and Benzylation of Pyrazoles. *J. Org. Chem.* **2015**, *80* (1), 690–697. https://doi.org/10.1021/jo5025317.

(105) Katritzky, A. R.; Wu, J.; Verin, S. V. A Convenient, One-Pot Preparative Method for Tri- and Tetrasubstituted Hydrazines from Azobenzenes and Organolithiums. *Synthesis* **1995**, *1995* (06), 651–653. https://doi.org/10.1055/s-1995-3985.

(106) McAtee, J. R.; Martin, S. E. S.; Ahneman, D. T.; Johnson, K. A.; Watson, D. A. Preparation of Allyl and Vinyl Silanes by the Palladium-Catalyzed Silylation of Terminal Olefins: A Silyl-Heck Reaction. *Angew. Chem. Int. Ed.* **2012**, *51*, 3663–3667. https://doi.org/10.1002/anie.201200060.

(107) Uehling, M. R.; King, R. P.; Krska, S. W.; Cernak, T.; Buchwald, S. L. Pharmaceutical Diversification via Palladium Oxidative Addition Complexes. *Science* **2019**, *363*, 405–408. https://doi.org/10.1126/science.aac6153.

(108) Huang, L.; Ackerman, L. K. G.; Kang, K.; Parsons, A. M.; Weix, D. J. LiCl-Accelerated Multimetallic Cross-Coupling of Aryl Chlorides with Aryl Triflates. *J. Am. Chem. Soc.* **2019**, *141* (28), 10978–10983. https://doi.org/10.1021/jacs.9b05461.

(109) Sun, R.; Qin, Y.; Nocera, D. G. General Paradigm in Photoredox Nickel-Catalyzed Cross-Coupling Allows for Light-Free Access to Reactivity. *Angew. Chem. Int. Ed.* **2020**, *59* (24), 9527–9533. https://doi.org/10.1002/anie.201916398.

(110) Konev, M. O.; McTeague, T. A.; Johannes, J. W. Nickel-Catalyzed Photoredox-Mediated Cross-Coupling of Aryl Electrophiles and Aryl Azides. *ACS Catal.* **2018**, *8* (10), 9120–9124. https://doi.org/10.1021/acscatal.8b02954.

(111) Lau, S. H.; Yu, P.; Chen, L.; Madsen-Duggan, C. B.; Williams, M. J.; Carrow, B. P. Aryl Amination Using Soluble Weak Base Enabled by a Water-Assisted Mechanism. *J. Am. Chem. Soc.* **2020**, *142* (47), 20030–20039. https://doi.org/10.1021/jacs.0c09275.

(112) Sapountzis, I.; Knochel, P. A General Amination Method Based on the Addition of Polyfunctional Arylmagnesium Reagents to Functionalized Arylazo Tosylates. *Angew. Chem. Int. Ed.* **2004**, *43* (7), 897–900. https://doi.org/10.1002/anie.200353241.

(113) Lin, Q.; Spielvogel, E. H.; Diao, T. Carbon-Centered Radical Capture at Nickel(II) Complexes: Spectroscopic Evidence, Rates, and Selectivity. *Chem* **2023**, *9* (5), 1295–1308. https://doi.org/10.1016/j.chempr.2023.02.010.

(114) Franke, M. C.; Longley, V. R.; Rafiee, M.; Stahl, S. S.; Hansen, E. C.; Weix, D. J. Zinc-Free, Scalable Reductive Cross-Electrophile Coupling Driven by Electrochemistry in an Undivided Cell. *ACS Catal.* **2022**, *12* (20), 12617–12626. https://doi.org/10.1021/acscatal.2c03033.

(115) Chi, B. K.; Widness, J. K.; Gilbert, M. M.; Salgueiro, D. C.; Garcia, K. J.; Weix, D. J. In-Situ Bromination Enables Formal Cross-Electrophile Coupling of Alcohols with Aryl and Alkenyl Halides. *ACS Catal.* **2022**, *12* (1), 580–586. https://doi.org/10.1021/acscatal.1c05208.
(116) Perkins, R. J.; Hughes, A. J.; Weix, D. J.; Hansen, E. C. Metal-Reductant-Free Electrochemical Nickel-Catalyzed Couplings of Aryl and Alkyl Bromides in Acetonitrile. *Org. Process Res. Dev.* **2019**, *23* (8), 1746–1751. https://doi.org/10.1021/acs.oprd.9b00232.
(117) Fu, J.; Lundy, W.; Chowdhury, R.; Twitty, J. C.; Dinh, L. P.; Sampson, J.; Lam, Y.; Sevov, C. S.; Watson, M. P.; Kalyani, D. Nickel-Catalyzed Electroreductive Coupling of Alkylpyridinium Salts and Aryl Halides. *ACS Catal.* **2023**, *13* (14), 9336–9345. https://doi.org/10.1021/acscatal.3c01939.
(118) Beutner, G. L.; Simmons, E. M.; Ayers, S.; Bemis, C. Y.; Goldfogel, M. J.; Joe, C. L.; Marshall, J.; Wisniewski, S. R. A Process Chemistry Benchmark for Sp^2–Sp^3 Cross Couplings. *J. Org. Chem.* **2021**, *86* (15), 10380–10396. https://doi.org/10.1021/acs.joc.1c01073.
(119) Wang, X.; Wang, S.; Xue, W.; Gong, H. Nickel-Catalyzed Reductive Coupling of Aryl Bromides with Tertiary Alkyl Halides. *J. Am. Chem. Soc.* **2015**, *137* (36), 11562–11565. https://doi.org/10.1021/jacs.5b06255.
(120) Prieto Kullmer, C. N.; Kautzky, J. A.; Krska, S. W.; Nowak, T.; Dreher, S. D.; MacMillan, D. W. C. Accelerating Reaction Generality and Mechanistic Insight through Additive Mapping. *Science* **2022**, *376* (6592), 532–539. https://doi.org/10.1126/science.abn1885.
(121) Lovering, F. Escape from Flatland 2: Complexity and Promiscuity. *Med. Chem. Commun.* **2013**, *4* (3), 515. https://doi.org/10.1039/c2md20347b.
(122) Greaves, M. E.; Johnson Humphrey, E. L. B.; Nelson, D. J. Reactions of Nickel(0) with Organochlorides, Organobromides, and Organoiodides: Mechanisms and Structure/Reactivity Relationships. *Catal. Sci. Technol.* **2021**, *11* (9), 2980–2996. https://doi.org/10.1039/D1CY00374G.
(123) Thane, T. A.; Jarvo, E. R. Ligand-Based Control of Nickel Catalysts: Switching Chemoselectivity from One-Electron to Two-Electron Pathways in Competing Reactions of 4-Halotetrahydropyrans. *Org. Lett.* **2022**, *24* (28), 5003–5008. https://doi.org/10.1021/acs.orglett.2c01335.
(124) Haibach, M. C.; Shekhar, S.; Ahmed, T. S.; Ickes, A. R. Recent Advances in Nonprecious Metal Catalysis. *Org. Process Res. Dev.* **2023**, *27* (3), 423–447. https://doi.org/10.1021/acs.oprd.2c00344.
(125) Hamby, T. B.; LaLama, M. J.; Sevov, C. S. Controlling Ni Redox States by Dynamic Ligand Exchange for Electroreductive Csp3–Csp2 Coupling. *Science* **2022**, *376* (6591), 410–416. https://doi.org/10.1126/science.abo0039.
(126) Hansen, E. C.; Pedro, D. J.; Wotal, A. C.; Gower, N. J.; Nelson, J. D.; Caron, S.; Weix, D. J. New Ligands for Nickel Catalysis from Diverse Pharmaceutical Heterocycle Libraries. *Nat. Chem.* **2016**, *8* (12), 1126–1130. https://doi.org/10.1038/nchem.2587.
(127) Kim, Y.; Iwai, T.; Fujii, S.; Ueno, K.; Sawamura, M. Dumbbell-Shaped 2,2′-Bipyridines: Controlled Metal Monochelation and Application to Ni-Catalyzed Cross-Couplings. *Chem. Eur. J.* **2021**, *27* (7), 2289–2293. https://doi.org/10.1002/chem.202004053.
(128) Tang, T.; Hazra, A.; Min, D. S.; Williams, W. L.; Jones, E.; Doyle, A. G.; Sigman, M. S. Interrogating the Mechanistic Features of Ni(I)-Mediated Aryl Iodide Oxidative

Addition Using Electroanalytical and Statistical Modeling Techniques. *J. Am. Chem. Soc.* **2023**, jacs.3c01726. https://doi.org/10.1021/jacs.3c01726.
(129) Isbrandt, E. S.; Sullivan, R. J.; Newman, S. G. High Throughput Strategies for the Discovery and Optimization of Catalytic Reactions. *Angew. Chem. Int. Ed.* **2019**, *58* (22), 7180–7191. https://doi.org/10.1002/anie.201812534.
(130) Aguirre, A. L.; Loud, N. L.; Johnson, K. A.; Weix, D. J.; Wang, Y. ChemBead Enabled High-Throughput Cross-Electrophile Coupling Reveals a New Complementary Ligand. *Chem. Eur. J.* **2021**, *27* (51), 12981–12986. https://doi.org/10.1002/chem.202102347.
(131) *Phosphine Predictor | Sigma-Aldrich*. https://www.sigmaaldrich.com/deepweb/assets/sigmaaldrich/product/documents/377/478/phosphine-predictor-br80087en-ms.pdf (accessed 2023-07-08).
(132) Zhao, S.; Gensch, T.; Murray, B.; Niemeyer, Z. L.; Sigman, M. S.; Biscoe, M. R. Enantiodivergent Pd-Catalyzed C–C Bond Formation Enabled through Ligand Parameterization. *Science* **2018**, *362* (6415), 670–674. https://doi.org/10.1126/science.aat2299.
(133) Crawford, J. M.; Gensch, T.; Sigman, M. S.; Elward, J. M.; Steves, J. E. Impact of Phosphine Featurization Methods in Process Development. *Org. Process Res. Dev.* **2022**, *26* (4), 1115–1123. https://doi.org/10.1021/acs.oprd.1c00357.
(134) Zhang, C.; Santiago, C. B.; Crawford, J. M.; Sigman, M. S. Enantioselective Dehydrogenative Heck Arylations of Trisubstituted Alkenes with Indoles to Construct Quaternary Stereocenters. *J. Am. Chem. Soc.* **2015**, *137* (50), 15668–15671. https://doi.org/10.1021/jacs.5b11335.
(135) Guo, J.-Y.; Minko, Y.; Santiago, C. B.; Sigman, M. S. Developing Comprehensive Computational Parameter Sets To Describe the Performance of Pyridine-Oxazoline and Related Ligands. *ACS Catal.* **2017**, *7* (6), 4144–4151. https://doi.org/10.1021/acscatal.7b00739.
(136) Lau, S. H.; Borden, M. A.; Steiman, T. J.; Wang, L. S.; Parasram, M.; Doyle, A. G. Ni/Photoredox-Catalyzed Enantioselective Cross-Electrophile Coupling of Styrene Oxides with Aryl Iodides. *J. Am. Chem. Soc.* **2021**, *143* (38), 15873–15881. https://doi.org/10.1021/jacs.1c08105.
(137) Frisch, M. J.; Trucks, G. W.; Schlegel, H. B.; Scuseria, G. E.; Robb, M. A.; Cheeseman, J. R.; Scalmani, G.; Barone, V.; Petersson, G. A.; Nakatsuji, H.; Li, X.; Caricato, M.; Marenich, A. V.; Bloino, J.; Janesko, B. G.; Gomperts, R.; Mennucci, B.; Hratchian, H. P.; Ortiz, J. V.; Izmaylov, A. F.; Sonnenberg, J. L.; Williams; Ding, F.; Lipparini, F.; Egidi, F.; Goings, J.; Peng, B.; Petrone, A.; Henderson, T.; Ranasinghe, D.; Zakrzewski, V. G.; Gao, J.; Rega, N.; Zheng, G.; Liang, W.; Hada, M.; Ehara, M.; Toyota, K.; Fukuda, R.; Hasegawa, J.; Ishida, M.; Nakajima, T.; Honda, Y.; Kitao, O.; Nakai, H.; Vreven, T.; Throssell, K.; Montgomery Jr., J. A.; Peralta, J. E.; Ogliaro, F.; Bearpark, M. J.; Heyd, J. J.; Brothers, E. N.; Kudin, K. N.; Staroverov, V. N.; Keith, T. A.; Kobayashi, R.; Normand, J.; Raghavachari, K.; Rendell, A. P.; Burant, J. C.; Iyengar, S. S.; Tomasi, J.; Cossi, M.; Millam, J. M.; Klene, M.; Adamo, C.; Cammi, R.; Ochterski, J. W.; Martin, R. L.; Morokuma, K.; Farkas, O.; Foresman, J. B.; Fox, D. J. Gaussian 16 Rev. C.01, 2016.
(138) Zhao, Y.; Truhlar, D. G. The M06 Suite of Density Functionals for Main Group Thermochemistry, Thermochemical Kinetics, Noncovalent Interactions, Excited States, and Transition Elements: Two New Functionals and Systematic Testing of

Four M06-Class Functionals and 12 Other Functionals. *Theor. Chem. Acc.* **2008**, *120* (1), 215–241. https://doi.org/10.1007/s00214-007-0310-x.
(139) Dunning, T. H., Jr. Gaussian Basis Sets for Use in Correlated Molecular Calculations. I. The Atoms Boron through Neon and Hydrogen. *J. Chem. Phys.* **1989**, *90* (2), 1007–1023. https://doi.org/10.1063/1.456153.
(140) Wilson, A. K.; Woon, D. E.; Peterson, K. A.; Dunning, T. H. Gaussian Basis Sets for Use in Correlated Molecular Calculations. IX. The Atoms Gallium through Krypton. *J. Chem. Phys.* **1999**, *110*, 7667–7676. https://doi.org/10.1063/1.478678.
(141) Hay, P. J.; Wadt, W. R. Ab Initio Effective Core Potentials for Molecular Calculations. Potentials for the Transition Metal Atoms Sc to Hg. *J. Chem. Phys.* **1985**, *82* (1), 270–283. https://doi.org/10.1063/1.448799.
(142) Dolg, M.; Wedig, U.; Stoll, H.; Preuss, H. Energy-adjusted Ab Initio Pseudopotentials for the First Row Transition Elements. *J. Chem. Phys.* **1987**, *86* (2), 866–872. https://doi.org/10.1063/1.452288.
(143) Marenich, A. V.; Cramer, C. J.; Truhlar, D. G. Universal Solvation Model Based on Solute Electron Density and on a Continuum Model of the Solvent Defined by the Bulk Dielectric Constant and Atomic Surface Tensions. *J. Phys. Chem. B.* **2009**, *113* (18), 6378–6396. https://doi.org/10.1021/jp810292n.
(144) Glendening, E. D.; Badenhoop, J. K.; Reed, A. E.; Carpenter, J. E.; Bohmann, J. A.; Morales, C. M.; Karafiloglou, P.; Landis, C. R.; Weinhold, F. NBO 7.0.10, 2018.
(145) Yuan, M.; Song, Z.; Badir, S. O.; Molander, G. A.; Gutierrez, O. On the Nature of C(Sp3)–C(Sp2) Bond Formation in Nickel-Catalyzed Tertiary Radical Cross-Couplings: A Case Study of Ni/Photoredox Catalytic Cross-Coupling of Alkyl Radicals and Aryl Halides. *J. Am. Chem. Soc.* **2020**, *142* (15), 7225–7234. https://doi.org/10.1021/jacs.0c02355.
(146) Newman-Stonebraker, S. H.; Smith, S. R.; Borowski, J. E.; Peters, E.; Gensch, T.; Johnson, H. C.; Sigman, M. S.; Doyle, A. G. Univariate Classification of Phosphine Ligation State and Reactivity in Cross-Coupling Catalysis. *Science* **2021**, *374* (6565), 301–308. https://doi.org/10.1126/science.abj4213.
(147) Janssen-Müller, D.; Sahoo, B.; Sun, S.; Martin, R. Tackling Remote Sp^3 C–H Functionalization via Ni-Catalyzed "Chain-walking" Reactions. *Isr. J. Chem.* **2020**, *60* (3–4), 195–206. https://doi.org/10.1002/ijch.201900072.
(148) Hansch, Corwin.; Leo, A.; Taft, R. W. A Survey of Hammett Substituent Constants and Resonance and Field Parameters. *Chem. Rev.* **1991**, *91* (2), 165–195. https://doi.org/10.1021/cr00002a004.
(149) Yamamoto, T.; Wakabayashi, S.; Osakada, K. Mechanism of C–C Coupling Reactions of Aromatic Halides, Promoted by Ni(COD)2 in the Presence of 2,2'-Bipyridine and PPh3, to Give Biaryls. *J. Organomet. Chem.* **1992**, *428* (1–2), 223–237. https://doi.org/10.1016/0022-328X(92)83232-7.
(150) Piszel, P. E.; Orzolek, B. J.; Olszewski, A. K.; Rotella, M. E.; Spiewak, A. M.; Kozlowski, M. C.; Weix, D. J. Protodemetalation of (Bipyridyl)Ni(II)–Aryl Complexes Shows Evidence for Five-, Six-, and Seven-Membered Cyclic Pathways. *J. Am. Chem. Soc.* **2023**, jacs.3c00618. https://doi.org/10.1021/jacs.3c00618.
(151) Ting, S. I.; Williams, W. L.; Doyle, A. G. Oxidative Addition of Aryl Halides to a Ni(I)-Bipyridine Complex. *J. Am. Chem. Soc.* **2022**, *144* (12), 5575–5582. https://doi.org/10.1021/jacs.2c00462.

(152) Sakai, H. A.; Liu, W.; Le, C. "Chip"; MacMillan, D. W. C. Cross-Electrophile Coupling of Unactivated Alkyl Chlorides. *J. Am. Chem. Soc.* **2020**, *142* (27), 11691–11697. https://doi.org/10.1021/jacs.0c04812.
(153) Kim, S.; Goldfogel, M. J.; Gilbert, M. M.; Weix, D. J. Nickel-Catalyzed Cross-Electrophile Coupling of Aryl Chlorides with Primary Alkyl Chlorides. *J. Am. Chem. Soc.* **2020**, *142* (22), 9902–9907. https://doi.org/10.1021/jacs.0c02673.
(154) Liao, J.; Basch, C. H.; Hoerrner, M. E.; Talley, M. R.; Boscoe, B. P.; Tucker, J. W.; Garnsey, M. R.; Watson, M. P. Deaminative Reductive Cross-Electrophile Couplings of Alkylpyridinium Salts and Aryl Bromides. *Org. Lett.* **2019**, *21* (8), 2941–2946. https://doi.org/10.1021/acs.orglett.9b01014.
(155) Gavryushin, A.; Kofink, C.; Manolikakes, G.; Knochel, P. An Efficient Negishi Cross-Coupling Reaction Catalyzed by Nickel(II) and Diethyl Phosphite. *Tetrahedron* **2006**, *62* (32), 7521–7533. https://doi.org/10.1016/j.tet.2006.03.123.
(156) Buonomo, J.; Everson, D.; Weix, D. Substituted 2,2′-Bipyridines by Nickel Catalysis: 4,4′-Di-Tert-Butyl-2,2′-Bipyridine. *Synthesis* **2013**, *45* (22), 3099–3102. https://doi.org/10.1055/s-0033-1338520.
(157) Hue, R. J.; Vatassery, R.; Mann, K. R.; Gladfelter, W. L. Zinc Oxide Nanocrystal Quenching of Emission from Electron-Rich Ruthenium-Bipyridine Complexes. *Dalton Trans.* **2015**, *44* (10), 4630–4639. https://doi.org/10.1039/C4DT03272A.
(158) Wang, H.-Y.; Tang, J.-W.; Peng, P.; Yan, H.-J.; Zhang, F.-L.; Chen, S.-X. Development of a Novel Chemoenzymatic Process for (S)-1-(Pyridin-4-Yl)-1,3-Propanediol. *Org. Process Res. Dev.* **2020**, *24* (12), 2890–2897. https://doi.org/10.1021/acs.oprd.0c00403.
(159) Duric, S.; Tzschucke, C. C. Synthesis of Unsymmetrically Substituted Bipyridines by Palladium-Catalyzed Direct C−H Arylation of Pyridine *N* -Oxides. *Org. Lett.* **2011**, *13* (9), 2310–2313. https://doi.org/10.1021/ol200565u.
(160) Tcyrulnikov, S.; Cai, Q.; Twitty, J. C.; Xu, J.; Atifi, A.; Bercher, O. P.; Yap, G. P. A.; Rosenthal, J.; Watson, M. P.; Kozlowski, M. C. Dissection of Alkylpyridinium Structures to Understand Deamination Reactions. *ACS Catal.* **2021**, *11* (14), 8456–8466. https://doi.org/10.1021/acscatal.1c01860.
(161) Dennington, R.; Keith, T. A.; Millam, J. M. GaussView, 2016.
(162) Guilian Luchini; Patterson, T.; Paton, R. DBSTEP: Release 1.0, 2021. https://doi.org/10.5281/ZENODO.4702097.
(163) Molski, M. Theoretical Modeling of Structure-Toxicity Relationship of Cyanides. *Toxicol. Lett.* **2021**, *349*, 30–39. https://doi.org/10.1016/j.toxlet.2021.05.011.
(164) Hansen, E. C.; Li, C.; Yang, S.; Pedro, D.; Weix, D. J. Coupling of Challenging Heteroaryl Halides with Alkyl Halides via Nickel-Catalyzed Cross-Electrophile Coupling. *J. Org. Chem.* **2017**, *82* (14), 7085–7092. https://doi.org/10.1021/acs.joc.7b01334.
(165) Truesdell, B. L.; Hamby, T. B.; Sevov, C. S. General C(Sp^2)–C(Sp^3) Cross-Electrophile Coupling Reactions Enabled by Overcharge Protection of Homogeneous Electrocatalysts. *J. Am. Chem. Soc.* **2020**, *142* (12), 5884–5893. https://doi.org/10.1021/jacs.0c01475.
(166) Johnson, J. B.; Rovis, T. More than Bystanders: The Effect of Olefins on Transition-Metal-Catalyzed Cross-Coupling Reactions. *Angew. Chem. Int. Ed.* **2008**, *47* (5), 840–871. https://doi.org/10.1002/anie.200700278.
(167) Huang, C.-Y. (Dennis); Doyle, A. G. Electron-Deficient Olefin Ligands Enable Generation of Quaternary Carbons by Ni-Catalyzed Cross-Coupling. *J. Am. Chem. Soc.* **2015**, *137* (17), 5638–5641. https://doi.org/10.1021/jacs.5b02503.

(168) Xu, J.; Bercher, O. P.; Watson, M. P. Overcoming the Naphthyl Requirement in Stereospecific Cross-Couplings to Form Quaternary Stereocenters. *J. Am. Chem. Soc.* **2021**, *143* (23), 8608–8613. https://doi.org/10.1021/jacs.1c03898.
(169) Lachaize, S.; Gallegos, D. C.; Antonio, J. J.; Atesin, A. C.; Ateşin, T. A.; Jones, W. D. Ortho-Fluoro Effect on the C–C Bond Activation of Benzonitrile Using Zerovalent Nickel. *Organometallics* **2023**, *42* (15), 2134–2147. https://doi.org/10.1021/acs.organomet.3c00275.
(170) Biswas, S.; Qu, B.; Desrosiers, J.-N.; Choi, Y.; Haddad, N.; Yee, N. K.; Song, J. J.; Senanayake, C. H. Nickel-Catalyzed Cross-Electrophile Reductive Couplings of Neopentyl Bromides with Aryl Bromides. *J. Org. Chem.* **2020**, *85* (12), 8214–8220. https://doi.org/10.1021/acs.joc.0c00549.
(171) Mills, L. R.; Edjoc, R. K.; Rousseaux, S. A. L. Design of an Electron-Withdrawing Benzonitrile Ligand for Ni-Catalyzed Cross-Coupling Involving Tertiary Nucleophiles. *J. Am. Chem. Soc.* **2021**, *143* (27), 10422–10428. https://doi.org/10.1021/jacs.1c05281.
(172) Ge, S.; Hartwig, J. F. Nickel-Catalyzed Asymmetric α-Arylation and Heteroarylation of Ketones with Chloroarenes: Effect of Halide on Selectivity, Oxidation State, and Room-Temperature Reactions. *J. Am. Chem. Soc.* **2011**, *133* (41), 16330–16333. https://doi.org/10.1021/ja2082087.
(173) Ge, S.; Green, R. A.; Hartwig, J. F. Controlling First-Row Catalysts: Amination of Aryl and Heteroaryl Chlorides and Bromides with Primary Aliphatic Amines Catalyzed by a BINAP-Ligated Single-Component Ni(0) Complex. *J. Am. Chem. Soc.* **2014**, *136* (4), 1617–1627. https://doi.org/10.1021/ja411911s.
(174) Green, R. A.; Hartwig, J. F. Nickel-Catalyzed Amination of Aryl Chlorides with Ammonia or Ammonium Salts. *Angew. Chem. Int. Ed.* **2015**, *54* (12), 3768–3772. https://doi.org/10.1002/anie.201500404.
(175) Nattmann, L.; Cornella, J. Ni($^{4\text{-tBu}}$Stb)$_3$: A Robust 16-Electron Ni(0) Olefin Complex for Catalysis. *Organometallics* **2020**, *39* (18), 3295–3300. https://doi.org/10.1021/acs.organomet.0c00485.
(176) Tatsumi, K.; Nakamura, A.; Komiya, S.; Yamamoto, A.; Yamamoto, T. An Associative Mechanism for Reductive Elimination of D8 NiR2(PR3)2. *J. Am. Chem. Soc.* **1984**, *106* (26), 8181–8188. https://doi.org/10.1021/ja00338a029.
(177) Jensen, A. E.; Knochel, P. Nickel-Catalyzed Cross-Coupling between Functionalized Primary or Secondary Alkylzinc Halides and Primary Alkyl Halides. *J. Org. Chem.* **2002**, *67* (1), 79–85. https://doi.org/10.1021/jo0105787.
(178) Huang, C.-Y. (Dennis); Doyle, A. G. Nickel-Catalyzed Negishi Alkylations of Styrenyl Aziridines. *J. Am. Chem. Soc.* **2012**, *134* (23), 9541–9544. https://doi.org/10.1021/ja3013825.